UNIVERSIDADE FEDERAL DE PERNAMBUCO
CENTRO DE TECNOLOGIA E GEOCIÊNCIAS
DEPARTAMENTO DE ENGENHARIA QUÍMICA
PROGRAMA DE PÓS-GRADUAÇÃO EM ENGENHARIA QUÍMICA

CAROLINE MARIA BEZERRA DE ARAUJO

WATER AND WASTEWATER TREATMENT BY RECYCLABLE AGAR-GRAPHENE OXIDE BIOCOMPOSITE HYDROGEL IN BATCH AND FIXED-BED ADSORPTION COLUMN: bench experiments and modeling for the selective removal of organic

Recife
2022

CAROLINE MARIA BEZERRA DE ARAUJO

WATER AND WASTEWATER TREATMENT BY RECYCLABLE AGAR-GRAPHENE OXIDE BIOCOMPOSITE HYDROGEL IN BATCH AND FIXED-BED ADSORPTION COLUMN: bench experiments and modeling for the selective removal of organic

Doctoral thesis presented to the Post-Graduate Program in Chemical Engineering of the Federal University of Pernambuco, as a partial requirement for obtaining the title of Doctor in Chemical Engineering.

Main Area: Chemical and Biochemical Process Engineering.

Supervisor: Prof. Dr. Marcos Gomes Ghislandi.

Supervisor: Prof. Dr. Maurício Alves da Motta Sobrinho.

Co-Supervisor: Prof. Dr. Alírio Egídio Rodrigues.

Recife

2022

Catalogação na fonte:
Bibliotecária Sandra Maria Neri Santiago, CRB-4 / 1267

A663w Araujo, Caroline Maria Bezerra de.
Water and wastewater treatment by recyclable agar-graphene oxide biocomposite hydrogel in batch and fixed-bed adsorption column: bench experiments and modeling for the selective removal of organic / Caroline Maria Bezerra de Araujo. – 2022.
173 f.: il., figs., tabs., abrev. e siglas.

Orientador: Prof. Dr. Marcos Gomes Ghislandi.
Orientador: Prof. Dr. Maurício Alves da Motta Sobrinho.
Coorientador: Prof. Dr. Alírio Egídio Rodrigues.
Tese (Doutorado) – Universidade Federal de Pernambuco. CTG. Programa de Pós-Graduação em Engenharia Química. Recife, 2022.
Inclui referências e apêndices.

1. Engenharia química. 2. Óxido de grafeno. 3. Biopolímero ágar. 4. Hidrogel biocompósito. 5. Adsorção em leito fixo. 6. Tratamento de água. 7. Efluentes têxteis. I. Ghislandi, Marcos Gomes (Orientador). II. Motta Sobrinho, Maurício Alves da (Orientador). III. Rodrigues, Alírio Egídio (Coorientador). IV. Título.

UFPE

660.2 CDD (22. ed.) BCTG/2022-415

CAROLINE MARIA BEZERRA DE ARAUJO

WATER AND WASTEWATER TREATMENT BY RECYCLABLE AGAR-GRAPHENE OXIDE BIOCOMPOSITE HYDROGEL IN BATCH AND FIXED-BED ADSORPTION COLUMN: bench experiments and modeling for the selective removal of organic

Doctoral thesis presented to the Post-Graduate Program in Chemical Engineering of the Federal University of Pernambuco, Academic Center for Technology and Geosciences, as a requirement for obtaining the title of Doctor in Chemical Engineering. Area of concentration: Chemical and Biochemical Process Engineering.

Approved in: 25 / 08 / 2022.

EXAMINATION BOARD

Participation by videoconference

_____

Profa. Dra. Diana Cristina Silva de Azevedo (External Examiner)
Universidade Federal do Ceará

Participation by videoconference

_____

Prof. Dr. Manuel Fernando Ribeiro Pereira (External Examiner)
Faculdade de Engenharia da Universidade do Porto

Participation by videoconference

_____

Prof. Dr. Mohand Benachour (Internal Examiner)
Universidade Federal de Pernambuco

Participation by videoconference

_____

Profa. Dra. Patricia Prediger (External Examiner)
Universidade Estadual de Campinas

Participation by videoconference

_____

Profa. Dra. Yêda Medeiros Bastos de Almeida (Internal Examiner)
Universidade Federal de Pernambuco

ACKNOWLEDGEMENTS

To God and to my family, because without them I would not be here today, and I would not be able to develop this research, complete this work and present this thesis to the Post-Graduation Program in Chemical Engineering of UFPE. In particular to my mother Claudia Bezerra da Costa, to my aunt Lucia Bezerra da Costa, and my grandmother Cerise Guedes Araujo (who left this world and became a star in the heavens in 2018).

To all those colleagues and friends who, in a way, contributed to my academic, professional, and personal trajectory. To all the friends of the laboratories of GPTA (UFPE), NanoA and CENAPESQ (UFRPE), LSRE/LCM (FEUP), and LGCPA (UEM). In particular, I would like to thank: Mr. Gabriel Rodrigues Bezerra da Costa, Mr. Gabriel Filipe Nascimento, Ms. Bruna Figueiredo Nascimento, Mr. Brener Gomes, Mr. Ronald Keverson, Dr. Albertina Rios, Ms. Rute Seabra, Dr. Paulo Carmo, Dr. Ronney Jose, Prof. Dr. Alexandre Ferreira, Prof. Dr. Rosângela Bergamasco, Prof. Dr. Marcelo Vieira, Dr. Gessica Wernke, Prof. Dr. Alexander Diorio, Dr. Denise Alanis, Dr. Alisson Castro, Dr. Tiago Fraga. You all were part of very remarkable and special moments of my trajectory over these years and I learned a lot from all of you!

I would also like to especially thank my supervisors: Prof. Dr. Marcos Gomes Ghislandi, Prof. Dr. Maurício Alves da Motta Sobrinho, and Prof. Dr. Alírio Egídio Rodrigues for all the support, and for guiding me throughout all these years of research, but above all, for never stopping believing in me, in my ideas and in my potential, even when I was no longer believing in myself.

To the Coordenação de Aperfeiçoamento de Pessoal de Nível Superior (CAPES) for the financial support.

To all those who were and still are part of my life, but that I could not include here in this piece of paper, but that I will always remember with affection, my sincere “thank you!”.

ABSTRACT

Due to recent advances in developing technologies for the production and processing of carbon nanomaterials, the viable application of these materials in continuous and industrial processes has become realistic. Because of their properties, graphene-based materials (GBM) have proved to be promising as adsorbents for organic contaminants in water. Thus, it is the aim of this work to develop composites using graphene oxide (GO) and the biopolymer agar, for applications in the continuous treatment of water and industrial wastewaters. Hydrogel biocomposite samples using different proportions of graphene oxide and agar biopolymer (agar-GO) were synthesized to treat water and industrial textile wastewater through fixed-bed adsorption. The hydrogels prepared using GO and agar were characterized, and measurements revealed evidence of GO interaction with the polymer that constitutes the matrix, resulting in a 3D material, with visually disordered morphology. After characterization, preliminary batch adsorption experiments were conducted to evaluate the preliminary kinetics and pH effect in the adsorption process for the anionic dyes Acid Orange 7 (AO7) and Reactive Black 5 (RB5); the cationic dyes Nile Blue A (NB), Methylene Blue (MB), Malachite Green (MG), Basic Fuchsin (BF), and Safranin-O (SO); and the anti-malaria drug Chloroquine diphosphate (CQ). Among the compounds evaluated, the hydrogel showed satisfactory results for the removal of cationic dyes and the drug. Therefore, adsorption equilibrium isotherms were obtained and fitted to Freundlich, Langmuir and Sips models, and kinetic data were adjusted to Driving Force models, and Fick's Diffusion equation. Fixed-bed experiments were carried out for the hydrogel produced with 80% of agar and 20% of GO, varying the feed flowrates in the column, and the breakthrough curves were obtained in each case. Experimental adsorption capacities values for the fixed-bed test, on a dry basis, were 226.46 $mg.g^{-1}$ (NB), 79.51 $mg.g^{-1}$ (MB), 58.25 $mg.g^{-1}$ (MG), 38.11 $mg.g^{-1}$ (BF), 100.00 $mg.g^{-1}$ (SO), and 63.00 $mg.g^{-1}$ (CQ). The column packed with the agar-GO hydrogel was tested for the treatment of both synthetic and real textile wastewater. Color and total organic carbon (TOC) were evaluated as response parameters, and there was an indication of the adsorbent selectivity for the separation of the cationic dyes present in the synthetic textile wastewater. The effluent obtained after treatment using the hydrogel indicated a decrease in the phytotoxicity of the sample, compared to the initial dye

solution, for the three plant species studied (*Cucumis sativus, Lepidium sativum*, and *Eruca sativa*). Overall, agar-GO proved to be an interesting viable alternative, since a small amount of material was used to continuously treat synthetic textile wastewater, being most of the composite biodegradable. Moreover, the material exhibited remarkable regenerative capacity - in each case, after regeneration, the breakthrough curves were superimposed - proving its effectiveness for applications in wastewater treatment.

Keywords: graphene oxide; agar biopolymer; hydrogel biocomposite; fixed-bed adsorption; water treatment; textile wastewater.

RESUMO

Devido aos avanços no desenvolvimento de tecnologias para a produção e processamento de nanomateriais de carbono, a aplicação viável desses materiais em processos contínuos e industriais tornou-se realista. Devido às suas propriedades, os materiais à base de grafeno (MBG) têm se mostrado promissores como adsorventes de contaminantes orgânicos em água. Assim, o objetivo deste trabalho é desenvolver compósitos utilizando óxido de grafeno (OG) e o biopolímero ágar para aplicações no tratamento contínuo de águas e efluentes industriais. Amostras do hidrogel biocompósito foram sintetizados utilizando diferentes proporções de óxido de grafeno e do biopolímero ágar (ágar-OG) para tratar água e efluentes têxteis industriais via adsorção em leito fixo. Os hidrogéis preparados com OG e ágar foram caracterizados, e as medições revelaram evidências de interação do OG com o polímero que constitui a matriz, resultando em um material 3D, com morfologia visualmente desordenada. Após a caracterização, experimentos preliminares de adsorção em batelada foram conduzidos para avaliar a cinética preliminar e o efeito do pH no processo de adsorção para os corantes aniônicos Laranja Ácido 7 (AO7) e Preto Reativo 5 (RB5); os corantes catiônicos Azul do Nilo A (NB), Azul de Metileno (MB), Verde Malaquita (MG), Fucsina Básica (BF) e Safranina-O (SO); e o medicamento antimalárico cloroquina difosfato (CQ). Dentre os compostos avaliados, o hidrogel apresentou resultados satisfatórios para a remoção de corantes catiônicos e do fármaco. Assim, isotermas de equilíbrio de adsorção foram obtidas e ajustadas aos modelos de Freundlich, Langmuir e Sips, e os dados cinéticos foram ajustados aos modelos de força motriz e equação de difusão de Fick. Experimentos em leito fixo foram realizados para o hidrogel produzido com 80% de ágar e 20% de OG, variando as vazões de alimentação na coluna, e as curvas de ruptura foram obtidas em cada caso. Os valores de capacidade de adsorção experimentais para os testes de leito fixo, em base seca, foram 226,46 $mg.g^{-1}$ (NB), 79,51 $mg.g^{-1}$ (MB), 58,25 $mg.g^{-1}$ (MG), 38,11 $mg.\ g^{-1}$ (BF), 100,00 $mg.g^{-1}$ (SO) e 63,00 $mg.g^{-1}$ (CQ). A coluna empacotada com o hidrogel de ágar-OG foi testada para o tratamento de efluentes têxteis sintéticos e reais. Cor e o Carbono Orgânico Total (COT) foram avaliados como parâmetros de resposta, e foram observados indícios da seletividade do adsorvente para a separação dos corantes catiônicos presentes no efluente têxtil sintético. A solução obtida após o

tratamento utilizando o hidrogel indicou uma diminuição da fitotoxicidade da amostra, em relação à solução corante inicial, para as três espécies de planta estudadas (*Cucumis sativus, Lepidium sativum* e *Eruca sativa*). No geral, o ágar-OG mostrou-se uma alternativa interessante e viável, uma vez que uma pequena quantidade de material foi utilizada para tratar continuamente efluentes têxteis sintéticos, sendo maior parte do compósito biodegradável. Além disso, o material apresentou capacidade regenerativa notória - em cada caso, após a regeneração, as curvas de ruptura ficaram sobrepostas - comprovando sua eficácia para aplicações no tratamento de efluentes.

Palavras-chave: óxido de grafeno; biopolímero ágar; hidrogel biocompósito; adsorção em leito fixo; tratamento de água; efluentes têxteis.

LIST OF ILLUSTRATIONS

Figure 1 – Flowchart diagrams illustrating the batch adsorption process (a) and the continuous adsorption process using fixed-bed (b) in a wastewater treatment plant..... 41

Figure 2 – Scheme of the mass transfer zone in a fixed-bed column for ideal and real cases..... 42

Figure 3 – Illustration of graphene nanosheets, as well as other carbon allotropes (graphite, large fullerenes, and nanotubes) below graphene structure..... 44

Figure 4 – (a) Network structure of carbon atoms in graphene nanosheet; (b) graphene oxide nanosheet, where: ● carbon atoms, ● oxygen, ● hydrogen..... 44

Figure 5 – Examples of natural and synthetic polymers commonly found in everyday life..... 48

Figure 6 – Simplified biopolymers classification diagram..... 49

Figure 7 – One of the main sources of agar, the red seaweed species *Gelidium* sp. and *Gracilaria confervoides* (a); agar biopolymer containing β-D-galactopyranose and 3,6 anhydro-α-L-galactopyranose on its chains (b)..... 50

Figure 8 – Photographs of the hydrogel produced with 80% agar and 20% GO..... 61

Figure 9 – Variation of H_2SO_4 volume in the production of graphene oxide *vs.* Removal efficiencies of the dyes MB and BB (Experimental conditions: 50 mL, initial dye concentration: 50 $mg.L^{-1}$, ~0.02g of GrO, contact time: 1 h, 250 rpm, pH =5.5, T =28 ± 3 ^{o}C)..... 63

Figure 10 – UV-Vis measurements for GO samples (a); particle size distribution from DLS analysis for samples GO-21 and GO-25 (b)..... 65

Figure 11 – XRD patterns for graphite, GO-21 and GO-25 (a); pH_{PZC} for GO-21 and GO-25 (b)..... 66

Figure 12 – Micro Raman measurements of (a) graphite powder, and (b)

GO samples……..... 67
Figure 13 – FTIR spectra of GO-21 and GO-25..... 67
Figure 14 – FTIR spectra of the hydrogels produced (left); and of pure GO (right)……..... 68
Figure 15 – Raman spectra of the hydrogels..... 70
Figure 16 – TGA results for the hydrogel samples (left); for pure GO (right)……..... 71
Figure 17 – SEM micrographs with 1000x of magnitude of pure GO (top left); pure agar (top right); and the Agar-GO aerogels samples (botton from the left to the right) with 70% Agar 30%GO, 75% Agar 25%GO, and 80% Agar 20%GO..... 72
Figure 18 – Zeta potential measurements for GO suspension and agar-GO biocomposite samples (aerogel)..... 73
Figure 19 – Chemical structure of the dyes……..…… 77
Figure 20 – Preliminary adsorption kinetics for the three hydrogel samples produced (Conditions: m_{ads}= 0.20 g (~0.004 g dry basis); V_L= 50 mL; T= 24 ^oC; 250 rpm; without pH adjustment)…….. 83
Figure 21 – Influence of the initial pH in the adsorptive capacity of Agar-GO for the removal of the dyes with C_0 = 10 $mg.L^{-1}$ (MB, MG, BF), and 20 $mg.L^{-1}$ (NB) (Experimental conditions: $V_{sol.}$ = 50 mL; T = 24 ^oC; 250 rpm; over 24h of contact time)…… 85
Figure 22 – UV-Visible scan of the dyes (left), and hypsochromic shift for NB dye at higher pH (right)…….. 86
Figure 23 – Adsorption equilibrium isotherms on a dry basis for the cationic dyes (Experimental conditions: t = 48 h; $V_{sol.}$ = 50 mL; T = 24 ^oC; 250 rpm stirring)……..…..… 87
Figure 24 – Kinetics for the cationic dyes adsorption onto the hydrogel (70%Agar 30%GO) on a dry basis (Experimental conditions: $m_{ads.}$= 0.20g hydrogel (0.00417g dry basis); $V_{sol.}$= 50 mL; T= 24 ^oC; 250 rpm; pH =8 for MB, NB, and pH~ 6 for BF and MG)…… 91
Figure 25 – Kinetics for the cationic dyes adsorption onto the hydrogel (75%Agar 25%GO) on a dry basis (Experimental conditions:

$m_{ads.}$= 0.20g hydrogel (0.00432g dry basis); $V_{sol.}$= 50 mL; T= 24 ^{o}C; 250 rpm; pH =8 for MB, NB, and pH~ 6 for BF and MG)..... 92

Figure 26 – Kinetics for the cationic dyes adsorption onto the hydrogel (80%Agar 20%GO) on a dry basis (Experimental conditions: $m_{ads.}$= 0.20g hydrogel (0.00417g dry basis); $V_{sol.}$= 50 mL; T= 24 ^{o}C; 250 rpm; pH =8 for MB, NB, and pH~ 6 for BF and MG)……. 93

Figure 27 – Proposed mechanism for the adsorption of cationic dyes on the agar-GO hydrogel biocomposite. The dye molecules are firstly attracted to the hydrogel surface (1st stage); next, the molecules diffuse into the particles to access the GO active sites (2nd stage)…….…… 96

Figure 28 – Results for the adsorptive tests comparing the removal efficiencies of the pure agar hydrogel and Agar-GO (80%Agar 20%GO) hydrogel for the 4 dyes – MB, NB, MG, BF (Experimental conditions: t = 48 h; V_L= 50 mL; m_{ads} = 0.20 g (wet hydrogel); T =24 ^{o}C; 250 rpm; pH ~6)……..…… 97

Figure 29 – FTIR spectroscopy (a) and EDS (b) of Agar-GO (80%Agar 20%GO) before and after adsorption of MB……. 97

Figure 30 – Batch adsorption/desorption cycles after regeneration with 0.30 M NaOH (Experimental conditions: $m_{ads.}$= 0.20g hydrogel (wet basis); V_L=50 mL; T =24 ^{o}C; 250 rpm)…… 99

Figure 31 – Results for the phytotoxicity assays performed using cucumber (a), cress (b) and arugula (c) seeds (Experimental conditions: number of seeds/ Petri drish = 5 (cucumber), 10 (cress and arugula); t =120 h; T =24 ^{o}C; T= 22.5 ± 2.5 °C; negative control = H_2O)…… 100

Figure 32 – Process diagram for the experimental setup of fixed-bed tests (a); detailed scheme of the packed bed column used for the breakthrough experiments (b); photograph of the experimental apparatus at FEUP laboratories (Porto, Portugal) (c)……... 105

Figure 33 – Results for tests estimating the bulk porosity using blue dextran in duplicate (Conditions: m_{bed}= 6.0g hydrogel (~0.13g dry basis); T =24 ^{o}C; Q =2.0 mL.min^{-1})…… 110

Figure 34 – Breakthrough curves for the adsorption of single MB, NB, MG, BF onto agar-GO hydrogel when Q = 2.0 mL.min^{-1} (a); breakthrough curves for the adsorption of single MB and BF onto the hydrogel, varying the flowrate (b) (Experimental conditions: m_{bed}= 6.0 g hydrogel (~0.13 g dry basis); T = 24 ^{o}C; pH=8 for MB, NB, and pH~6 for BF and MG)…… 111

Figure 35 – Batch isotherms (black dots), and the blue dot regarding the experimental values from breakthrough curves for the cationic dyes MB, NB, MG, BF (dry basis)……..… 113

Figure 36 – Results of fixed-bed regeneration and reuse for the 4 dyes – MB, NB, MG, and BF (Experimental conditions: m_{bed} = 6.0 g (0.13g on a dry basis); Q. =2.0 mL.min^{-1}; T = 24 ^{o}C; pH =8 for MB, NB, and pH~ 6 for BF and MG for the adsorption tests)… 114

Figure 37 – Experimental values and breakthrough curves predicted by the model (Experimental conditions: m_{bed}= 6.0g hydrogel (~0.13 g dry basis); Q =2.0 mL.min^{-1}; T =24^{o}C) …..…… 116

Figure 38 – Breakthrough curves for the areas of the absorption spectra in the visible region for the mix of the dyes and synthetic wastewater (a); absorption spectra of the mixture of dyes over time (b); absorption spectra of the synthetic textile wastewater over time (c) (Experimental conditions: m_{bed}= 6.0 g hydrogel (0.13g dry basis); Q =2.0 mL.min^{-1}; T =24 ^{o}C; pH=8)…..…….. 120

Figure 39 – Breakthrough curve for TOC removal from the synthetic textile wastewater using Agar-GO hydrogel……..... 122

Figure 40 – Photograph of the raw textile wastewater sample used in the fixed-bed tests (a); breakthrough curves for the areas of each absorption spectra in the visible region for the real textile wastewater (b); absorption spectra of the real textile wastewater over time (c) (Experimental conditions: m_{bed}= 6.0 g hydrogel (0.13g dry basis); Q= 2.0 mL.min^{-1}; T =24 ^{o}C)……. 124

Figure 41 – Breakthrough curves for the evolution of turbidity over time (a); breakthrough curves for the evolution of TOC over time (b) (Experimental conditions: m_{bed} = 6.0 g hydrogel (0.13 g dry basis); Q = 2.0 mL.min^{-1}; T = 24 ^{o}C)…… 125
Figure 42 – Breakthrough curves for the areas of absorption spectra in the visible region for real and synthetic textile wastewater ….. 126
Figure 43 – Process diagram depicting the experimental setup for fixed-bed adsorption experiments (a); photograph of the packed column (b)…… 133
Figure 44 – Preliminary adsorption kinetics at different initial concentrations of Chloroquine and Safranin-O (Conditions: m= 0.20 g (0.0043 g dry basis); C_0= 20 mg.L^{-1}; V= 25 mL; T= 24 ^{o}C; 250 rpm)…… 135
Figure 45 – Effect of the initial pH in the removal efficiency of Chloroquine and Safranin-O (Conditions: t = 6 h (CQ) and 24 h (SO); m= 0.20g (0.0043 g dry basis); C0= 20 mg.L^{-1}; V= 25 mL; T= 24 ^{o}C; 250 rpm)…….. 136
Figure 46 – Equilibrium adsorption isotherms for Chloroquine and Safranin-O (Conditions: t = 6 h (CQ) and 24 h (SO); C_0= 20 mg.L^{-1}; V= 25 mL; T= 24 ^{o}C; 250 rpm)…… 138
Figure 47 – Modeling of adsorption kinetics for Chloroquine and Safranin-O (Experimental conditions: m= 0.20 g (0.0043 g dry basis); C_0= 20 mg.L^{-1}; V= 25 mL; T= 24 ^{o}C; 250 rpm)…… 140
Figure 48 – Mechanism proposed for the adsorption of organic substances with basic characteristics onto the Agar-GO hydrogel composite…… 142
Figure 49 – Breakthrough curves for Chloroquine and Safranin-O at different flowrates (Conditions: m= 6 g (0.13 g dry basis); C_0= 20 mg.L^{-1}; T= 24 ^{o}C)…… 144
Figure 50 – Batch isotherms and the blue dot highlighted regarding the experimental values from breakthrough curves for the contaminants CQ and SO (dry basis)…… 145
Figure 51 – Breakthrough curves for Chloroquine and Safranin-O with the

hydrogel before and after regeneration with NaOH and reuse (Conditions: m = 6g (0.13g dry basis); C_0= 20 mg.L^{-1}; T = 24^{o}C)…….. 146

Figure 52 – Experimental values and breakthrough curves predicted by the model (Experimental conditions: m_{bed} = 6.0g hydrogel (~0.13 g dry basis); Q =2 mL.min^{-1}; T =24^{o}C)…….…… 147

Figure 53 – Competitiveness for Chloroquine and Safranin-O (Experimental conditions: t= 24 h; m= 0.20 g (0.0043 g dry basis); $C_{0\ MIX}$= 10 mg.L^{-1} for CQ and SO each in the mix; V= 25 mL; T= 24 ^{o}C; 250 rpm)……. 148

Figure 54 - Average particle size for the hydrogel samples produced …... 172

Figure 55 - Experimental values and breakthrough curve predicted for BF dye (Experimental conditions: m_{bed}= 6.0g hydrogel (~0.13 g dry basis); Q =2 mL.min^{-1}; T =24 ^{o}C)…….…… 173

LIST OF TABLES

Table 1 – Variations in H_2SO_4/H_2O ($mL_{H2SO4}.mL^{-1}_{H2O}$) proportions during GO production using 1 g of graphite, 3 g $KMnO_4$ in 3h of contact……... 57

Table 2 – Variations in Agar:GO ratios used to produce the hydrogel samples..... 60

Table 3 – Technical information of the dyes tested……..... 77

Table 4 – Conditions for the isotherm experiments..... 79

Table 5 – Adsorption isotherm parameters for the hydrogel sample 70% Agar 30% GO (on a dry basis) calculated by adjusting the experimental data…..... 88

Table 6 – Adsorption isotherm parameters for the hydrogel sample 75% Agar 25% GO (on a dry basis) calculated by adjusting the experimental data..... 88

Table 7 – Adsorption isotherm parameters for the hydrogel sample 80% Agar 20% GO (on a dry basis) calculated by adjusting the experimental data…..... 89

Table 8 – Parameters for the hydrogel samples (dry basis) calculated by adjusting the kinetic models to adsorption experimental data……. 94

Table 9 – Experimental values of the parameters from the breakthrough curves (dry basis) 111

Table 10 – Parameters predicted for the breakthrough curves (dry basis)…….. 116

Table 11 – Experimental adsorption capacities of the cationic dyes onto the agar-GO composite (dry basis) in a fixed-bed system compared to previous works..... 118

Table 12 – Breakthrough curve parameters for the mixture of dyes and synthetic wastewater……... 121

Table 13 – Characteristics of the textile wastewater before fixed-bed adsorption treatment…… 123

Table 14 – Breakthrough curve parameters of synthetic wastewater and

real textile wastewater for color removal……. 126
Table 15 – Characteristics of the adsorbates used in this work…….. 130
Table 16 – Adsorption isotherm parameters (on a dry basis) calculated by adjusting the models to the experimental data…….. 138
Table 17 – Parameters for the hydrogel (dry basis) calculated by adjusting the kinetic models to adsorption experimental data……. 140
Table 18 – Experimental values of the parameters from the breakthrough curves (dry basis)……...… 144
Table 19 – Parameters predicted for the breakthrough curves (dry basis)…….. 147

LIST OF ABBREVIATIONS AND ACRONYMS

2D	Two-dimensional
3D	Three-Dimensional
AO7	Acid Orange 7
ATR	Attenuated Total Reflectance
BB	Brilliant Blue
BF	Basic Fuchsin
BOD	Biochemical Oxygen Demand
CENAPESQ	Research Support Center of the Federal Rural University of Pernambuco
CETENE	Center for Strategic Technologies of the Northeast
COD	Chemical Oxygen Demand
CQ	Chloroquine Diphosphate
DLS	Dynamic Light Scattering
EDS	Energy Dispersive Spectroscopy
FD	Fickian Diffusion
FEUP	Faculty of Engineering of the University of Porto
FTIR	Fourier-transform infrared spectroscopy
GBM	Graphene Based Materials
GI	Germination Index
GO	Graphene Oxide
GPTA	Research Group on Environmental Technologies and Processes
GrO	Graphite Oxide
GSC	Number of Germinated seeds in the Negative Control
GSS	Number of Germinated seeds in the Sample
IC	Inorganic Carbon
ISO	International Organization for Standardization
LDF	Linear Driving Force
LGCPA	Laboratory of Environmental Management, Control and Preservation
LSRE/LCM	Associated Laboratory of Separation and Reaction

	Engineering - Laboratory of Catalysis and Materials
MB	Methylene Blue
MG	Malachite Green
MTZ	Mass Transfer Zone
MV	Methyl Violet
NanoA	Applied and Environmental Nanotechnology Group
NB	Nile Blue
PZC	Point of Zero Charge
QDF	Quadratic Driving Force
RB5	Reactive Black 5
RGI	Relative Growth Index
rGO	Reduced Graphene Oxide
RLC	Total Root Length in the Negative Control
RLS	Total Root Length in the Sample
SEM	Scanning Electron Microscopy
SO	Safranin-O
TGA	Thermogravimetric Analysis
TOC	Total Organic Carbon
TSS	Total Suspended Solids
UEM	State University of Maringá
UFPE	Federal University of Pernambuco
UFRPE	Federal Rural University of Pernambuco
UK	United Kingdom
USA	United States of America
UV-Vis.	Ultraviolet-visible
WHO	World Health Organization
WWTP	Wastewater Treatment Plant
XRD	X-ray Diffraction Analysis

LIST OF SYMBOLS

%R	Removal efficiency
θ	Diffraction angle
C_0	Initial concentration of the contaminant
C_∞	Adsorbate concentration when $t \rightarrow \infty$ (equilibrium concentration)
C_e	Adsorbate concentration in the equilibrium
C_f	Final concentration of the contaminant
C_t	Adsorbate concentration at time t
D_{ax}	Coefficient of axial dispersion
Dif	Effective homogeneous diffusivity
H_b	Fixed-bed height
I_D	Intensity of Raman “D” band
I_G	Intensity of Raman “G” band
K_F	Freundlich adsorption constant
k_h	Intraparticle mass transfer coefficient
K_L	Langmuir adsorption constant
K_S	Sips adsorption constant
m	Sips isotherm constant
m_{ads}	Adsorbent mass
n	Heterogeneity factor from Freundlich isotherm equation
P_e	Peclet number
Q	Volumetric flowrate
q^-	Average adsorbate concentration in the particle
q_0	Adsorption capacity for “cycle zero”
q_e	Adsorption capacity in the equilibrium
q_{max}	Maximum adsorption capacity from Langmuir isotherm
q_n	Adsorption capacity for “cycle n”
q_s	Maximum adsorption capacity from Sips isotherm
R	Actual particle radius
r	Radius
R^2	Coefficient of determination

T	Temperature
t	Time
t_{BR}	Breakthrough time
t_{EX}	Exhaustion time
t_f	The overall time in which $C_t \rightarrow C\infty$
t_{st}	Stoichiometric time
V	Volume of the adsorption column
v_i	Interstitial velocity of the fluid
V_L	Volume of liquid (batch adsorber)
$\bar{Y}$	Mean of experimental values
Yi	Value observed experimentally
$\hat{Y}i$	Value predicted by the model
Z	Distance from the bed entrance
ε_b	Bulk porosity
λ_{max}	Maximum wavelength
ρ_{ad}	Adsorbent density
ρ_{bed}	Bed density
χ^2	Chi-squared

CONTENTS

1	**INTRODUCTION AND OUTLINES**.....	**25**
1.1	INTRODUCTION	25
1.1.1	**Objectives**.....	**28**
1.1.1.1	Main Objective…….....	28
1.1.1.2	Specific Objectives……..…...	28
1.2	OUTLINES OF THE THESIS……..……..…	29
2	**THEORETICAL FRAMEWORK**.....	**31**
2.1	TEXTILE DYES AND WATER POLLUTION……..…….....	31
2.2	EMERGING CONTAMINANTS IN WATER……..……	34
2.3	WATER AND WASTEWATER TREATMENT……..……	36
2.3.1	**Adsorption Processes**…….....	**38**
2.3.1.1	Conventional adsorption systems for wastewater treatment..…….	39
2.4	GRAPHENE-BASED MATERIALS…….……	43
2.5	BIOPOLYMERS AND HYDROGELS……..……..	47
2.6	APPLICATIONS OF GRAPHENE-BASED MATERIALS IN WATER AND WASTEWATER TREATMENT…….....	51
3	**GRAPHENE-BASED MATERIALS PRODUCTION AND CHARACTERIZATION**……..……	**56**
3.1	METHODOLOGY	56
3.1.1	**Materials**……..……	**57**
3.1.2	**Graphene Oxide production and preliminary adsorption tests**……..	**57**
3.1.2.1	Effect of Varying H_2SO_4 Concentration in Graphite Oxidation on the Adsorption Process…….….	57
3.1.3	**Graphene Oxide characterization**…….....	**58**
3.1.4	**Agar-Graphene Oxide hydrogel production**…….....	**59**
3.1.5	**Characterization of the agar-GO biocomposite**……..……	**61**
3.2	RESULTS AND DISCUSSION.....	62
3.2.1	**Graphene Oxide Production Varying H_2SO_4 concentration**.....	**62**
3.2.2	**Graphene Oxide characterization**.....	**64**
3.2.3	**Characterization of the Agar-GO biocomposite**.....	**68**

3.3	FINAL THOUGHTS…….....	74
4	**BATCH TESTS USING AGAR-GRAPHENE OXIDE HYDROGEL SAMPLES FOR THE SELECTIVE REMOVAL OF DYES**..….....	**75**
4.1	METHODOLOGY	75
4.1.1	**Materials**	**76**
4.1.2	**Batch adsorption experiments**…….….....	**78**
4.1.2.1	Adsorption equilibrium and isotherms modeling……	79
4.1.2.2	Adsorption kinetics and modeling……	80
4.1.3	**Phytotoxicity assays**……..……..	**81**
4.2	RESULTS AND DISCUSSION…….....	83
4.2.1	**Preliminary kinetics**……	**83**
4.2.2	**Influence of the initial pH**……	**84**
4.2.3	**Adsorption equilibrium isotherms**……..……	**87**
4.2.4	**Modeling of adsorption kinetics**……	**91**
4.2.5	**Adsorption mechanism for the cationic dyes**……..…	**95**
4.2.6	**Regeneration and reuse of the adsorbent**…….	**98**
4.2.7	**Phytotoxicity before and after adsorption**…….……	**99**
4.3	FINAL THOUGHTS.....…….....	101
5	**CONTINUOUS REMOVAL OF DYES FROM WATER AND TEXTILE WASTEWATER USING AGAR-GRAPHENE OXIDE HYDROGEL IN FIXED-BED ADSORPTION COLUMN**……...	**103**
5.1	METHODOLOGY……	103
5.1.1	**Materials**……..	**104**
5.1.2	**Fixed-bed adsorption**……..…	**104**
5.1.2.1	Single-component breakthrough curves…….……	106
5.1.2.2	Fixed-bed regeneration and reuse……	108
5.1.2.3	Fixed-bed adsorption for a mixture of dyes and textile wastewater treatment……..….	108
5.2	RESULTS AND DISCUSSION…….….	109
5.2.1	**Estimating operating parameters**…….	**109**
5.2.2	**Fixed-bed adsorption for single components**……..	**110**
5.2.3	**Fixed-bed regeneration**……...	**113**

5.2.4 Modeling of the breakthrough curves..... **115**
5.2.5 Mixture of cationic dyes and synthetic textile wastewater treatment via fixed-bed adsorption..... **119**
5.2.6 Real textile wastewater treatment via fixed-bed adsorption.... **122**
5.3 FINAL THOUGHTS..... 127
6 SELECTIVE REMOVAL OF CHLOROQUINE AND SAFRANIN-O FROM WATER USING AGAR-GRAPHENE OXIDE HYDROGEL..... **128**
6.1 METHODOLOGY..... 128
6.1.1 Materials..... **129**
6.1.2 Batch adsorption experiments..... **130**
6.1.2.1 Adsorption equilibrium and isotherms modeling..... 131
6.1.2.2 Adsorption kinetics and modeling..... 131
6.1.3 Fixed-bed adsorption..... **132**
6.1.3.1 Modeling of fixed-bed breakthrough curves..... 133
6.1.4 Adsorption competitiveness in batch..... **134**
6.2 RESULTS AND DISCUSSION..... 134
6.2.1 Batch adsorption..... **134**
6.2.1.1 Preliminary kinetics..... 134
6.2.1.2 Effect of the initial pH..... 135
6.2.1.3 Adsorption equilibrium isotherms..... 136
6.2.1.4 Modeling of adsorption kinetics..... 139
6.2.2 Agar-GO adsorption mechanism..... **141**
6.2.3 Fixed-bed adsorption column..... **142**
6.2.4 Adsorption competitiveness..... **148**
6.3 FINAL THOUGHTS..... 149
7 CONCLUSIONS AND PERSPECTIVES..... **150**
7.1 CONCLUSIONS..... 150
7.2 PERSPECTIVES..... 151
REFERENCES **153**
APPENDIX A – PUBLISHED PAPERS RELATED TO THE RESEARCH REPORTED IN THIS THESIS..... **167**
APPENDIX B – BREAKTHROUGH MODELING OF BF DYE

CONSIDERING THE ABSORPTIVE CAPACITY AND EQUILIBRIUM CONCENTRATION OF THE FIXED-BED EXPERIMENT..... **172**
APPENDIX C – BREAKTHROUGH MODELING OF BF DYE CONSIDERING THE ADSORPTIVE CAPACITY AND EQUILIBRIUM CONCENTRATION OF THE FIXED-BED EXPERIMENT **173**

1 INTRODUCTION AND OUTLINES

This topic presents a general overview on graphene nanomaterials and composites and their applications in water and wastewater treatment as adsorbents to remove organic contaminants, such as dyes and pharmaceutical drugs. The aims of the work, as well as the outline of thesis are presented.

Part of the text prese nted in this main topic was published:

ARAUJO, C. M. B. *et al.* Wastewater Treatment Using Recyclable Agar-graphene Oxide Biocomposite Hydrogel in Batch and Fixed-bed Adsorption Column: Bench Experiments and Modeling for the Selective Removal of Organics. **Colloids and Surfaces A: Physicochemical and Engineering Aspects**, v. 639, p. 128357, 2022.

1.1 INTRODUCTION

Due to recent advances in developing technologies for the production and processing of carbon nanomaterials, the possibility of a viable application of these materials in continuous and industrial processes has become realistic. Compared to conventional materials, nanostructured adsorbents have exhibited higher efficiency for water treatment. Therefore, the potential for remediating environmental problems, such as water pollution, has also increased because of these nanotechnological improvements (QIN *et al.,* 2017; SADEGH *et al.,* 2017; YE *et al.,* 2017).

Graphene-based materials (GBM) exhibit unique properties, such as good chemical stability, conductivity, large theoretical surface area, and excellent recyclability potential (THAKUR; KANDASUBRAMANIAN, 2019; ABBASI *et al.,* 2021). They can also be further modified to adjust their functionality, depending on the application (JAURIS *et al.,* 2015; FRAGA *et al.,* 2019; BAPTISTTELLA *et al.,* 2021).

Because of their properties, GBM have proved to be promising as adsorbents for organic contaminants in water. Compared to conventional methods such as coagulation, flocculation and filtration, adsorption processes have been widely used for water and wastewater treatment. It is considered an efficient, economical, and easy process, especially due to the simplicity in operation (MARIN *et al.,* 2019).

The abundance of oxygen functional groups on Graphene Oxide (GO) surface has been explored in studies related to the production of a wide range of composites of macroscopic architectures, including the three-dimensional (3D) hydrogels and aerogels, and two-dimensional films and membranes (CHEN *et al.,* 2017; YE *et al.,* 2017).

Hydrogels from polysaccharides are eco-friendly materials, consisting of interconnected networks that are filled with water. Some of their properties are non-toxicity, biodegradability, and renewability. Moreover, they present low cost, simple manufacture, high adsorption capacity and ease of separation from the medium after adsorption (DUMAN *et al.,* 2020; KHALIL *et al.,* 2020). GO addition in the structure of these materials gives them properties and functions, such as increasing mechanical strength (TANG *et al.,* 2020). Because of these characteristics, graphene hydrogel adsorbents are excellent candidates as adsorbent materials, especially in dye removal.

The dyes present in industrial wastewater are complex and stable, making the wastewater challenging to treat. Because of the large volumes, complexity, and recalcitrance, wastewaters from textile industries are considered one of the main environmental polluters (SRIVASTAVA *et al.,* 2020). The release of wastewater contaminated with dyes and other organic components can cause the death of the aquatic fauna and flora due to the reduction in light penetration into the water, high toxicity, and low biodegradability of these substances (BANERJEE *et al.,* 2015; GUPTA *et al.,* 2015).

On the other hand, the presence of emerging contaminants in water is causing great environmental concern, as these compounds are not completely removed by conventional water treatment methods. A compound that has gained considerable prominence since the beginning of the Sars-Cov-2 pandemic (mainly referred to as COVID-19 pandemic) is chloroquine diphosphate (CQ). Although being a drug traditionally used to treat malaria (SCHROEDER; GERBER, 2014), with its prophylactic treatment effectiveness for COVID-19 being quite controversial, the use of this drug has been encouraged in some countries since the beginning of the pandemic. Therefore, with the increase of its production and use, metabolites of chloroquine ended up being disposed of the environment in larger quantities (DADA *et al.,* 2021; JANUÁRIO *et al.,* 2022).

Despite the World Health Organization (WHO) having concluded that chloroquine and/or hydroxychloroquine is not recommended as a prophylactic drug for the prevention or treatment of COVID-19, warning that its use can cause adverse effects, consumption of this drug in Brazil grew about 126% in 2020 (ANDRÉ, 2021; BIERNATH, 2021).

Although some applications can be found in the literature involving the use of GBM in batch adsorption systems for dye removal from water and wastewater (SARKAR *et al.,* 2020; TANG *et al.,* 2020), those focused on continuous fixed-bed processes are still little explored. Nevertheless, some results reported in previous works using this material are promising. According to Marin *et al.* (2019), GBM application in adsorption processes could present some drawbacks, regarding bed compaction and increase of the pressure in the fixed-bed column during the process. To overcome this bottleneck, supporting graphene on a higher granulometry material can be a feasible alternative, as well as the creation of structured 3D composites.

Graphene aerogels are usually derived from graphene hydrogels fabricated by chemistry assembly, polymer-induced gelation, or 3D printing, followed by freeze-drying (YE *et al.,* 2017). Chen and coworkers (2017) prepared a 3D agar/graphene oxide composite aerogel by freeze-drying the hydrogel and tested it as an adsorbent for methylene blue. Although the tests with the macrostructure have only been done in batch, Langmuir isotherm predicted the maximum adsorption capacity of 578 $mg.g^{-1}$ for the aerogel. It was also indicated that the process was endothermic and spontaneous. The aerogel produced could also be recycled, maintaining the adsorption capacity over 91% after three regeneration cycles.

Regarding real textile wastewater treatment, studies using GBM are not easily found either; some of the few works found have been recently published by the group (ARAUJO *et al.,* 2018), in which it was found that GO is a viable alternative with potential for color and turbidity removal from real textile effluents. However, only batch tests have been carried out.

The use of recyclable GO-biopolymer hydrogel for the continuous treatment of textile effluents characterizes the novelty and relevance of this work, mainly in the areas of chemical engineering, environmental and nanotechnology. Also, to date, this is the only work that uses a graphene oxide-based composite hydrogel to remove

chloroquine from water using a fixed-bed adsorption column (academic research platforms used: Science Direct and Google Scholar, July 2022).

1.1.1 Objectives

The main objective of the thesis will be approached here, as well as some of the specific objecitves related to the experiments conducted. The specific objectives will be presented each as bullet points, as follows.

1.1.1.1 Main Objective

The aim of this work is to develop composites using graphene-based material (GBM) and a biopolymer (Agar), for application in the continuous treatment of water and wastewaters. After the optimization stage regarding the nanocomposite production, the focus will be on its application for the removal of different types of organic contaminants from water – dyes of cationic and anionic nature, and the pharmaceutical drug Chloroquine - followed by the treatment of real industrial textile wastewater samples in a fixed-bed adsorption column, using Agar-GO hydrogel.

1.1.1.2 Specific Objectives

- Performing a preliminary analysis to produce graphene oxide using the modified Hummers Method.
- Production of different hydrogel samples, followed by characterization and analysis of the materials produced.
- Conducting adsorption batch tests using the hydrogels as adsorbents to evaluate the pH effect in the process, adsorption equilibrium isotherms, and kinetics for four cationic dyes: Methylene Blue (MB), Nile Blue A (NB), Malachite Green (MG) and Basic Fuchsin (BF); and two anionic dyes: Acid Orange 7 (AO7) and Reactive Black 5 (RB5).
- Evaluate the regenerative capacity of the Agar-GO samples in batch system.
- Phytotoxicity assays after treatment with the Agar-GO composite, using cucumber (*Cucumis sativus*), arugula (*Eruca vesicaria*), and watercress (*Nasturtium officinale*) as bioindicators.

- Evaluating the effect of varying the Agar/GO ratio during the adsorption tests and select the best samples for further analysis.
- To carry out adsorption tests in fixed-bed column using the best hydrogel composite for each adsorbate separately, assessing the regenerative capacity of the bed in each case.
- To test the fixed-bed column packed with the Agar-GO hydrogel for a mixture of the four cationic dyes; a synthetic textile wastewater produced based on polyacrylic fibers dyeing effluent; and a real textile wastewater sample. Color, total organic carbon (TOC) and turbidity were measured considered as response parameters.
- Conducting adsorption batch tests and fixed-bed experiments using the sample of hydrogel as adsorbent (80% Agar 20% GO), for the removal of Safranin-O (SO) and CQ.
- To perform competitive adsorption tests with SO and CQ, proposing an adsorption mechanism for Agar-GO and the organic substances in water.

1.2 OUTLINES OF THE THESIS

This work exhibits important insights into the production of a partially biodegradable GO biocomposite hydrogel, and its application in fixed-bed water and wastewater treatment. It also provides an idea about its potential for regeneration and reuse, and selectivity, indicating the possibility of recovering the organic substances.

Topic 2 – It presents the theoretical frameworks of the thesis.

Topic 3 - It exhibits the methodology and preliminary results to produce graphene oxide, varying some operating conditions; in addition to the production of Agar-GO biocomposite samples in different proportions (% of agar and GO), showing the characterization measurements for each hydrogel sample.

Topic 4 - It presents the methodology, results, and discussion of batch adsorption tests for four cationic and two anionic dyes, using the three hydrogel samples produced, in addition to regeneration and phytotoxicity tests for samples after adsorption. The adsorption mechanism was also proposed and discussed in this topic.

Topic 5 - It presents the methodology, results, and discussion of fixed-bed adsorption tests for: 4 cationic dyes (MB, NB, MG, BF) separately, a mixture of them, a synthetic textile effluent, and a real textile wastewater sample, using the hydrogel - 80 % agar 20% GO. Furthermore, tests regarding the regeneration and reuse of the bed after adsorption were included and discussed in this topic.

Topic 6 – It exhibits the methodology and results for comparative adsorptive tests performed for a cationic dye (SO) and a pharmaceutical drug (Chloroquine), using the Agar-GO hydrogel biocomposite.

Topic 7 - This topic presents the overall conclusion of the thesis, as well as the perspectives for future work.

The scientific papers (including original research, a review, and a book topic) published during the doctorate period, which composes parts of this thesis, are indicated at the beginning of each main topic. In addition, comments on these papers are detailed in Appendix A.

2 THEORETICAL FRAMEWORKS

This topic presents the theoretical framework of the thesis, which comprises subjects related to the areas of Environmental Engineering, Chemical Process Engineering, as well as Nanomaterials and Biocomposites. Among the topics discussed, it can be highlighted: the presence of dyes and emerging contaminants (pharmaceutical drugs, more specifically) in water bodies and wastewater, water and wastewater treatment processes, and adsorption systems (batch and continuous fixed-bed column). The production and applications of graphene nanomaterials, biocomposite hydrogels were also addressed, as well as the application of graphene-based materials in novel technologies for water and wastewater treatment.

Part of the text presented in this main topic was published:

FRAGA, T. J. M.; ARAUJO, C. M. B.; MOTTA SOBRINHO, M. A.; GHISLANDI, M. G. Chapter Five - The role of multifunctional nanomaterials in the remediation of textile wastewaters**. In: Sustainable Technologies for Textile Wastewater Treatments**. Woodhead Publishing, p. 95-136, 2021.

ARAUJO, C. M. B. *et al.* Nanocomposites and their employment as scavengers of water pollutants. **Journal of Chemistry and Applications**, v. 1, p. 18-31, 2019.

2.1 TEXTILE DYES AND WATER POLLUTION

The presence of dye in wastewaters of many industries, such as pulp and paper, leather, printing, food, and textile industry, originate during the coloring stages (NAYAK; PAL, 2020). The textile industry is one of the largest and oldest industries, present worldwide, due to the human need for clothing and utilitarian uses in decoration, hospital, military, and others (FUJITA, JORENTE, 2015). Its production process can be divided into two categories: spinning (normally a dry process) and wet process, involving the use of dyes (GHALY *et al.*, 2014).

Textile industry also offers numerous jobs, including many that do not require special skills, which contributes to job creation in developing countries (GHALY *et al.*, 2014). In Brazil, the textile sector is of great economic importance, as it is a strong job generator, with a large volume of production and exports. Brazil also stands out among the five largest textile producers in the world (MACHADO; PAGLIOTO; CARVALHO, 2018).

In the Northeast of Brazil, one of the main producers is the state of Pernambuco. At the Pernambuco Textile Center, 77% of its production comes from the cities of Agreste: 38.1% from the city of Santa Cruz do Capibaribe, 24.1% from Caruaru and 14.8% from the city of Toritama (PIMENTEL, 2017). Industries benefit textile materials by altering, the color and softness of the fabrics, performing bleaching, dyeing, softening, degreasing, and finishing processes (LIMA *et al.*, 2016). However, these processes demand large amounts of water, favoring the generation of huge volumes of wastewater.

Different dyes can be used during dyeing process. These are organic chemical compounds that can selectively absorb visible light. Due to this property, dyes appear colored because of the presence of chromophore groups such as nitro, nitrous, azo and carbonyl. The color of these compounds may further be enhanced and /or modified by auxochromes - ethyl, nitro, amino, sulfonic, hydroxyl, methoxy, ethoxy, chlorine and bromine groups (AYODHYA; VEERABHADRAM, 2018; MÓDENES *et al.*, 2011).

The most used dyes in the textile industries are acidic, basic, direct dyes, reactive dyes, etc., where azo dyes are the main class of dyes used in the industry. Despite the various types of classifications, dyes can be classified based on their charge after being dissolved in water. Thus, there are cationic dyes, which are basic dyes, while anionic dyes include direct, acidic, reactive, and nonionic dyes (AYODHYA; VEERABHADRAM, 2018). Some examples of cationic dyes are methylene blue (MB), Nile blue (NB), malachite green (MG), basic fuchsin (BF), Safranin-O (SO), and others. Examples of anionic dyes, on the other hand, include acid orange 7 (AO7), reactive red 198, and reactive black 5 (RB5).

All those dyes are non-biodegradable and can be carcinogenic, being also very harmful to the respiratory tract if inhaled, irritating the eyes, causing dermatitis, redness and dryness of the skin, digestive system stimulation, sleepiness, irritation of the mouth and throat if ingested, and even cause genetic mutation in human beings (NAYAK; PAL, 2020; FOROUTAN; MOHAMMADI; RAMAVANDI, 2019). To assess the acute toxicity and genotoxicity of the textile dyes Direct Black 38 and Reactive Blue 15, an ecotoxicity testing battery was performed by Oliveira *et al.* (2018). The authors observed that both dyes caused acute toxicity and genotoxicity for aquatic organisms. Direct Black 38 was considered the most toxic dye, attributed to its lethal

toxicity on *A. salina*, as well as capacity to induce DNA damage in *D. magna* and RTG-2 cells.

Nevertheless, cationic dyes might be more harmful than anionic dyes, since they present higher capacity to penetrate the cell membrane of aquatic beings, facilitated by the easy interaction with negatively charged cells membrane (ABUZERR; DARWISH; MAHVI, 2018). Cationic dyes are widely used to color different products, as they are easy to use and have durable and good adhesion to materials (NAYAK; PAL, 2020).

According to the Global Trade (2020), in 2019 the world trade of direct dyes and preparations based increased by 1% to 110K tonnes. Furthermore, China, the U.S., and India were the countries with the largest market size that year, with a combined 48% share of the global market. Japan, Brazil, Indonesia, Pakistan, Mexico, France, Canada, Germany, and the UK together accounted for 27%.

Yet, according to a market study published by Growth Market Reports the global indigo dyes market was valued at over 1,120 million US Dollars in 2020. In addition, it is expected to grow at a rate of 5% by 2028 (Growth Market Reports, 2021).

In addition to the presence of various types of dyes, gum, pectin, soap, and detergent, NaOH, carbonates, sulfides and chlorides are also present in this effluent, which can hamper the process of removing each of the contaminants, and the proper treatment of industrial wastewater. These wastewaters present as a main characteristic an intense color, being toxic to aquatic life (ABER, SHEYDAEI, 2012).

The most common sources of wastewater generated by the textile industries come from the washing, bleaching, dyeing, and finishing steps. Wastewater from dyeing steps contain large quantities of stable substances and chemicals difficult to degrade (ABER, SHEYDAEI, 2012). This is because during dyeing processes not all dyes applied to the fabrics are fixed. According to Gupta *et al.* (2015), 93% of water consumed in the textile industries comes out as colored effluent (mostly due to the dyes), containing high concentration of organic compounds and heavy metals.

2.2 EMERGING CONTAMINANTS IN WATER

The presence of emerging environmental pollutants in water bodies is causing concern in society, as well as in the scientific field. The contaminants known as "emerging" can be represented by a great variety of chemical compounds detected in the environment. Despite the presence of those pollutants in the environment not being recent, they became more relevant during the last decades (especially for the scientific community) due to the development of more sensitive analytical technologies that revealed the presence of emerging substances in soil, air, and water (RAMÍREZ-MALULE; QUINONES-MURILLO; MANOTAS-DUQUE, 2020; VIOTTI *et al.,* 2019).

These compounds usually come from common anthropogenic activities such as domestic, agricultural, healthcare, and industrial processes. They can be hormones and steroids, hygiene and personal care products, surfactants, pesticides, fertilizers, microplastics, trace metals, pharmaceuticals, among others. Because of their presence in the environment, emerging contaminants can affect the living organisms causing endocrine disruption, mutagenesis, congenital disorders, as well as carcinogenesis (RAMÍREZ-MALULE; QUINONES-MURILLO; MANOTAS-DUQUE, 2020).

Among these contaminants, pharmaceutical drugs (veterinary and human) stand out, as they have been extensively used on medicine during the last decades. That concern is caused because of their high resistance towards biodegradation, toxicity accumulation and promotion of antibiotic-resistant microbial growth (HIEW *et al.,* 2019).

Investigations regarding the occurrence of drugs in the aquatic bodies have been carried out, and these investigations found out the presence of the micropollutants, in which the molecules have low biodegradability (VIOTTI *et al.,* 2019). The main sources of pharmaceutical wastes are the wastewaters from municipal areas, pharmaceutical industries, and hospitals. The presence of these pollutants in the environment can potentially interfere in the aquatic ecosystem and endanger human health as well (HIEW *et al.,* 2019).

According to a literature review conducted by Ramírez-Malule, Quinones-Murillo and Manotas-Duque (2020), Brazil is one of the countries that provided the

largest number of publications reporting studies related to emerging contaminants between the years of 2000 and 2019, along with the United States of America (USA), China, Spain, Italy, Canada, Germany, France, the United Kingdom (UK) and India. This reinforces the idea of how relevant this topic is, both in Brazil and in several other major countries in the world.

Those emerging compounds are not completely removed by conventional water and wastewater treatment processes. Therefore, there is a need for developing effective methods to properly treat wastewater, aiming to regulate their concentration in the environment (HIEW *et al.,* 2019; VIOTTI *et al.,* 2019). Some recent works have presented studies focusing on the application of adsorptive processes to remove these contaminants.

Wernke *et al.* (2021) tested three carbon-based adsorbents to remove the cephalexin antibiotic from water: carbon with silver and copper oxide nanoparticles supported in activated carbon (CA-NPsAg/CuO); silver and copper oxide nanoparticles supported in graphene (OGR-NPsAg/CuO) and GO impregnated with silver and copper oxide nanoparticles supported in activated carbon (CA-OGR-NPsAg/CuO). As a result, the authors obtained, in each case, maximum adsorption capacity values of 756.8 $mg.g^{-1}$, 557.7 $mg.g^{-1}$, and 95.82 $mg.g^{-1}$ for CA-OGR-NPsAg/CuO, CA-NPsAg/CuO, and OGR-NPsAg/CuO, respectively.

Due to the recent COVID-19 pandemic situation that humanity is facing since the early months of 2020, anti-malaria drugs, such as hydroxychloroquine and chloroquine (CQ) has been widely used (especially in the first year of the pandemic) in some countries like Brazil, to try to control the infection caused by SARS-CoV-2. However, according to the World Health Organization (WHO) (2021), the efficacy of those drugs was not scientifically proven as a prophylactic drug for COVID-19. Nevertheless, the large increase in CQ consumption also increased the discharge of the anti-malaria drugs and their metabolites in the environment.

Hydroxychloroquine, Chloroquine, and their metabolites end up going to wastewater treatment plants and the aquatic environment, becoming a source of pollution, being identified as potentially persistent and bioaccumulative, posing serious risk to aquatic organisms. Bioassays using Daphnia magna and Chlorella vulgaris suggested that CQ has harmful potential to aquatic beings. Besides the

binding of CQ with DNA and inhibition of the metabolic functions, interfere with hemoglobin, it can cause cell death (SAIM; BEHIRA, 2021).

In the face of it, Januário *et al.* (2021) produced a novel adsorbent by combining babassu coconut activated carbon and graphene oxide to remove CQ and dipyrone. The authors noted that the process was endothermic and the maximum adsorption capacities of CQ and dipyrone at 318 K were 37.65 and 62.43 $mg.g^{-1}$, respectively.

For the aforementioned works, it was noted that, in both cases, adsorbents prepared using graphene-based nanomaterials in their composition were used, showing promising results in the removal of emerging contaminants from water.

2.3 WATER AND WASTEWATER TREATMENT

Water contamination is a global environmental problem. Depending on its origin, wastewater can be classified as industrial, domestic, or municipal, and storm water. The discharge of untreated industrial wastewater in the environment is a major concern in society. Wastewaters generated in pharmaceutical industries present a mixture of organic compounds whose effects can cause exerting endocrine disrupting, developing antibiotic resistant microbes, even cause extinction of some biota. In addition, there is a chance of these compounds be transformed into metabolites with even higher toxicity levels. Wastewater streams are main reservoirs of many types of emerging contaminants (RAMÍREZ-MALULE; QUINONES-MURILLO; MANOTAS-DUQUE, 2020).

On the other hand, high water consumption in textile companies has led to the treatment and reuse of the industrial wastewater produced. Textile wastewater characteristics are heterogeneous, and the variability of parameters, such as turbidity, color, Chemical Oxygen Demand (COD), Biochemical Oxygen Demand (BOD), Total Suspended Solids (TSS), and pH, can be linked with the raw materials used during the process. Besides dyes, different substances such as salts, heavy metals, bleaching, surfactants, and smoothing and dispersing agents could also be traced in textile wastewater, which makes the treatment process more complex and costly (ARAUJO *et al.,* 2020; HASSANZADEH *et al.,* 2017).

Thus, a large amount of research has been done to find sustainable and effective treatment processes. In this regard, the main technologies applied to deal with this problem involving separation methods include filtration, coagulation-flocculation, ion exchange, and adsorption. Among the commonly applied treatment options, coagulation-flocculation is a physicochemical method that is still considered an effective and low-cost pretreatment before proceeding with other separation processes. However, that requires a significant amount of chemicals, generating high quantities of sludge (ANASTOPOULOS *et al.,* 2018; ARAUJO *et al.,* 2020).

Choosing the most appropriate technology for industrial wastewater treatment depends on the analysis of the type and characteristics of the contaminants. Textile wastewater treatment typically encompasses physical, chemical, and biological processes where various primary, secondary, and tertiary treatment processes have been used for this purpose. However, these treatments are often not effective in removing all contaminants (ABER, SHEYDAEI, 2012; GHALY *et al.*, 2014).

Regarding emerging contaminants, Ramirez-Malule, Quinones-Murillo, and Manotas-Duque (2020) highlight that the conventional wastewater treatment plants are also not capable of fully remove these contaminants from water and wastewaters. Consequently, they stay in water and end up being discharged into water bodies, posing risks to aquatic fauna.

Primary, secondary, and tertiary treatment processes are commonly applied to treat those effluents, including coagulation-flocculation, sedimentation, aeration ponds, activated sludge and filtration (ABER, SHEYDAEI, 2012; SHI, *et al.*, 2014). Some disadvantages related to conventional treatments include the creation of short circuits (preferred pathways), as well as the difficulty in controlling flake formation during coagulation-flocculation. Sludges formed because of primary and secondary treatment processes also pose a problem regarding waste management and disposal (CESTARI, *et al.*, 2012; GHALY *et al.*, 2014).

Thus, in addition to conventional methods, different technologies, such as adsorption processes, have been applied to wastewater treatment (ARAUJO *et al.,* 2018). The employment of nanocomposites in wastewater treatment by separation processes is wide for adsorption and filtration techniques. Several types of nanosorbents have been synthesized and investigated in laboratory assays by researchers from every part of the world.

The aim is to develop profitable nanocomposites that might be used as substitutes of conventional adsorbents, as activated carbons, despite the high cost of these novel materials becomes challenging when it comes to large-scale production. Regarding filtration techniques, the use of nanomaterials takes place mostly in the impregnation of the surfaces of polymeric films that constitute the membranes. Moreover, the dispersion of the nanomaterials throughout polymeric matrices is difficult since interactions of different natures interfere in their adhesion. Furthermore, in most of the cases, it becomes necessary to investigate the reactant to provide functional groups to ease the dispersion and adhesion to the polymeric film, which increases the production cost of the membrane.

2.3.1 Adsorption Processes

The methods employed for color removal in textile effluents vary according to their effectiveness, costs, and environmental impacts. Adsorption processes are known as efficient for the removal of a wide range of pollutants, cost-effective, simple design, and ease of operation (WERNKE *et al.,* 2021). Successful adsorption of water pollutants also offers their recovery. Additionally, it should be noted that the regeneration of adsorbents for subsequent treatment cycles is gaining importance, since it minimizes treatment costs (ANASTOPOULOS *et al.,* 2018). Adsorption occurs when the contaminant molecules in aqueous phase reaches the surface of the adsorbent, remaining there either because of chemical and/ or physical forces.

Numerous adsorbents, such as vegetable fibers, fruit peels, clays, activated carbon, carbon nanotubes and graphene-based materials (GBM) have been studied for adsorption application in the removal of organic pollutants from water (LI *et al.*, 2013). Due to the smaller particle size, and higher surface area, clay minerals have shown promising adsorption potential. Therefore, some nanosized clay minerals have been studied and applied as adsorbents for water and wastewater treatment, such as halloysite. The use of halloysite for environmental remediation gained attention during the last decade, and that can be attributed to the better knowledge and understanding of the structure and reactivity of halloysite, which highlighted its unique features such as morphology, chemical composition, and structural arrangement of functional groups (ANASTOPOULOS *et al.,* 2018).

Among the many types of adsorbents, several studies report adsorption of emerging contaminants, dyes, and textile wastewater in activated carbon, which is one of the most widely used and studied adsorbents for this purpose. However, the high costs for obtaining this product, coupled with its low regenerative capacity, have motivated the search for new adsorbents (BAPTISTTELLA *et al.*, 2018).

Adsorbents made from biomass have attracted great attention, mainly due to their biodegradability and biocompatibility. However, a disadvantage of conventional biosorbents is the difficulty of separation and recovery. In addition, their relatively low dye adsorptive capabilities limit practical applications of biosorbents in the treatment of textile wastewater (SHI *et al.*, 2014).

On the other hand, there are graphene nanomaterials. These are carbonaceous materials, and their structures and electronic properties make them interact strongly with organic molecules through hydrogen bonds, π-π stacking, electrostatic forces, van der Waals forces and hydrophobic interactions. Their nanometric structures also give them some advantages, such as rapid equilibrium rates, high adsorption capacity and effectiveness over a wide pH range (LI *et al.*, 2013). Through the surface area premise, graphene, which theoretically presents almost twice the surface area of activated carbons, when well developed, can provide a good alternative for water and wastewater treatment (UPADHYAY; SOIN; ROY, 2014). A topic talking specifically about graphene will be presented later.

2.3.1.1 Conventional adsorption systems for wastewater treatment

Adsorption is usually performed in batch (non-continuous process) or column (continuous process). Figure 1 a and b depict, respectively, the flowchart diagrams of wastewater treatment plants (WWTP) using batch adsorption process and fixed-bed continuous adsorption process. The choice of the system depends on factors such as: the volume of the fluid to be processed, its composition, as well as the regeneration conditions of the adsorbent. Adsorption isotherms are important in the preliminary analysis of the adsorbent, as they give an indication of the removal efficiency of a certain compound, as well as the maximum amount that can be adsorbed per unit. However, such experiments are limited to the treatment of small

volumes of effluent, in addition to not providing data for the exact size of continuous treatment systems (NASCIMENTO *et al.,* 2014).

The most common application of batch adsorption is in laboratory scale due to the simplicity of operation and low cost. In this case, the adsorbent and the fluid are in contact from the beginning to the end of the experiment, being possible to obtain both kinetic parameters and isotherms. On the other hand, operations involving adsorption columns are mostly used when working on industrial scale. In this case, the apparatus should be designed a little more carefully, and in the case of the specifically fixed-bed, porous brackets at the end of the column should be included to prevent bed movement (REYNOLDS; RICHARDS, 1995).

Fixed-bed systems are usually more economical, and are widely applied in several fields, such as clarification of vegetable and mineral oils, protein purification (RIOS *et al.,* 2020 a), and removal of organic pollutants from industrial wastewater (ARAUJO *et al.,* 2020). This type of system is one of the most effective configurations to treat large volumes of effluents and adsorption-desorption cycles, allowing a more efficient use of the adsorbent.

As shown in Figure 1b, the fixed-bed system consists of a column where particles of the adsorbent are placed in contact with the fluid, using pumping, which can be done with upward or downward flow. Thus, the amount of adsorbate in the liquid and solid phases changes over time and space. The concentration of the solution increases through the column, as the adsorbent retains the adsorbate, until the adsorbent saturates, and the effluent concentration is equal to the feed concentration (NASCIMENTO *et al.,* 2014).

Figure 1 – Flowchart diagrams illustrating the batch adsorption process (a) and the continuous adsorption process using fixed-bed (b) in a wastewater treatment plant.

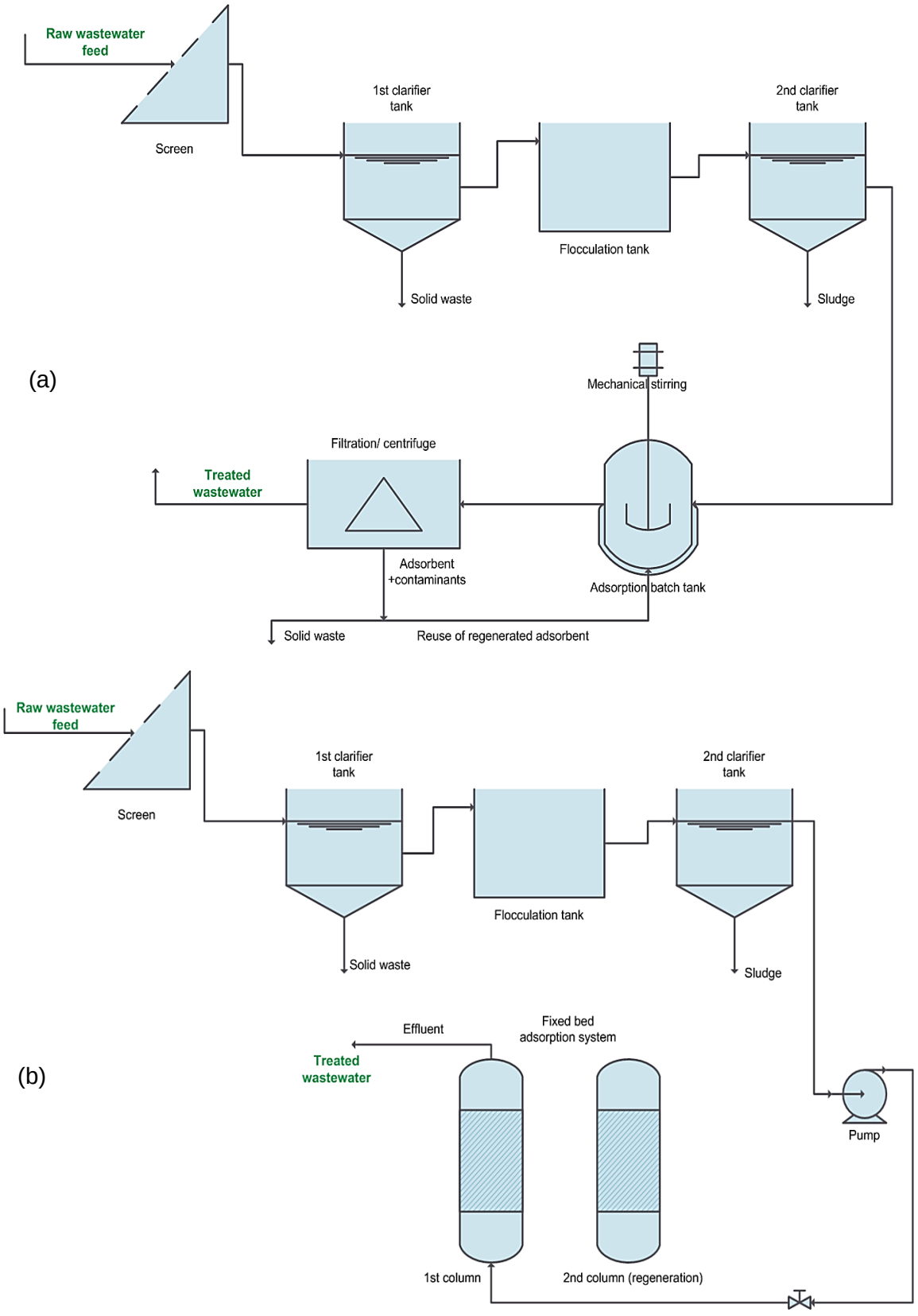

Source: The Author (2022)

The study of adsorption columns in fixed-bed systems is firstly performed in laboratory, by obtaining the breakthrough curves – see Figure 2. The performance of the column is related to the length and shape of the mass transfer zone (MTZ), which can be considered as a region within the column in which the adsorbate concentration ranges from 90% to 5% of the initial value. That is the region where most of the mass transfer takes place. In the ideal case, the adsorbent at the beginning of the column would receive a high amount of sorbate - this would be the region with the greatest mass transfer - and MTZ would not exist as the equilibrium is immediately established, triggering an immediate increase in the effluent concentration.

Nevertheless, in a real system, it takes time for the MTZ to be established, because of the resistance to mass transfer. Therefore, the curve exhibits another profile, as shown in the Figure 2. The more open the shape of the curve, the greater the resistance to mass transfer. Parameters such as the mechanism of adsorption, adsorption isotherm, volumetric flow rate, concentration of solute in the feed, and height of the bed contribute to the shape of the curve (NASCIMENTO *et al.,* 2014).

Then, experimental data can be described by mathematical models that predict large-scale column operation. In this study, the breakthrough curve is important as it gives an indication of the breakthrough point, i.e., the point in time when the effluent concentration exceeds the maximum allowable discharge concentration of a specific substance (MOHAN *et al.*, 2017).

Figure 2 - Scheme of the mass transfer zone in a fixed-bed column for ideal and real cases.

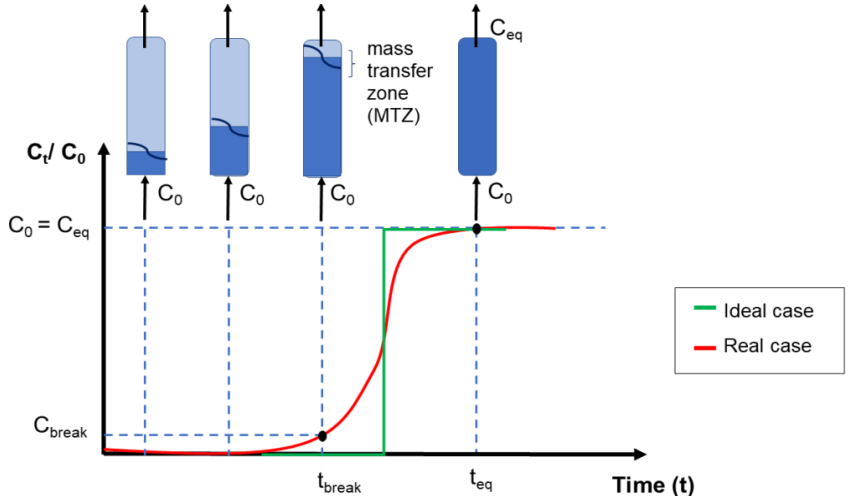

Source: The Author (2022)

For dye removal and treatment of textile wastewater via adsorption, a fixed-bed column is generally preferable to batch processes since the former can process large amounts of effluents under continuous adsorption /desorption cycles. To design an adsorption column, it is necessary to proceed with the prior evaluation of the economic conditions for the operation. Modeling and simulation techniques are useful for predicting the ideal condition for column adsorption (OOI *et al.,* 2016). Although several studies have recently reported the use of GBM for dye removal in aqueous media by adsorption, most of these consider only batch processes, being the application in continuous systems not very common.

A proposed alternative for GBM applications as adsorbents in continuous systems would be to use graphene (or GO) in its three-dimensional (3D) form (CHEN *et al*., 2017), as it will be discussed later.

2.4 GRAPHENE-BASED MATERIALS

Over the last couple of years, the scientific and commercial interests in graphene and its derivatives have increased considerably, especially due to GBM unique properties. Graphene-based nanomaterials have a high theoretical specific surface area (up to 2630 $m^2.g^{-1}$), great regeneration capacity, as well as exceptional electrical properties, being considered promising materials for the removal of contaminants. Graphene can be defined as a two-dimensional (2D) material formed by a hexagonal network of carbon atoms linked together by sp^2 bonds, presenting unique electronic, chemical, and mechanical properties. It is considered two-dimensional because it exhibits one dimension in the nanoscale order, and two other dimensions usually larger than the nanoscale (ISO, 2017; NOVOSELOV *et al.,* 2004).

Graphene is also considered the precursor of graphene family nanomaterials and other families of carbon nano-allotropes, including graphite, large fullerenes, and nanotubes, as depicted in Figure 3 (CHEN *et al.,* 2017; SUAREZ-IGLESIAS *et al.,* 2016). Structurally, it is analogous to the honeycomb structure, where each carbon atom forms three bonds with its first neighbors, as detailed in Figure 4 a (JAURIS *et al.,* 2015; JUNGES; JAURIS; ROSSATO, 2015; SHI, *et al.*, 2014).

Figure 3 – Illustration of graphene nanosheets, as well as other carbon allotropes (graphite, large fullerenes, and nanotubes) below graphene structure.

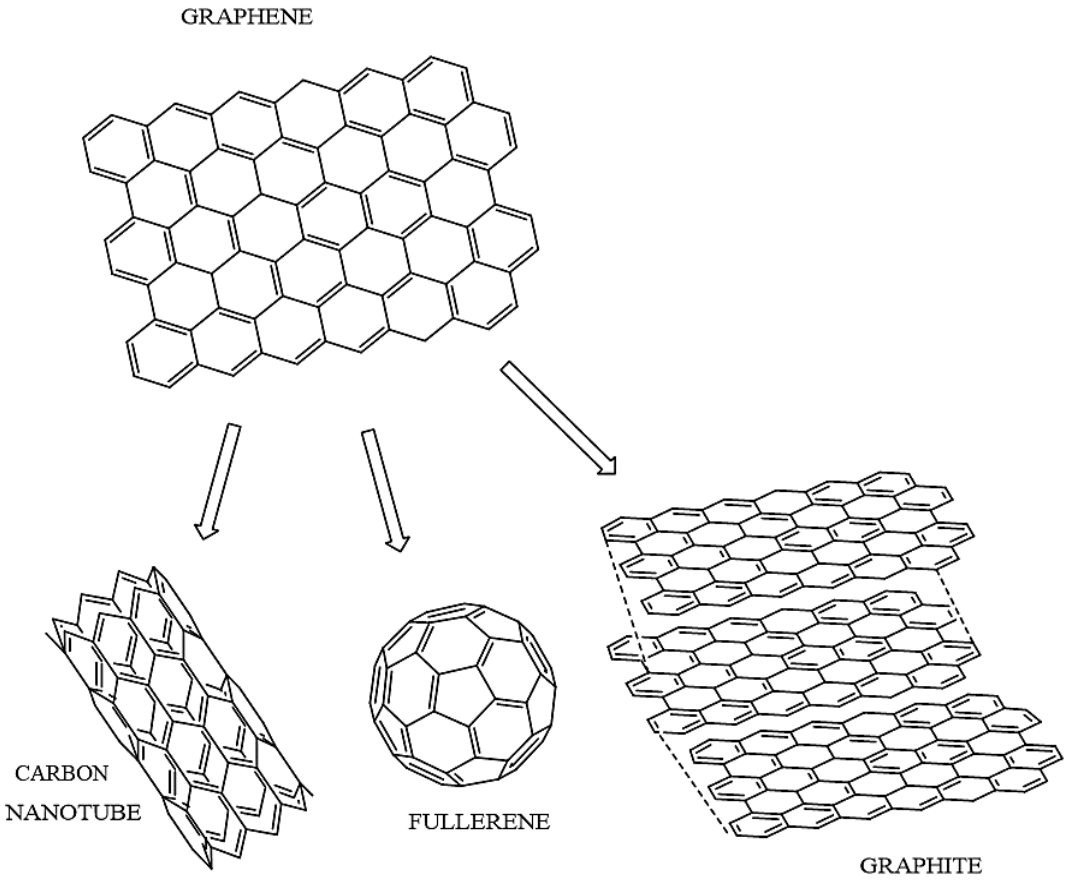

Source: The Author (2022)

Figure 4 – (a) Network structure of carbon atoms in graphene nanosheet; (b) graphene oxide nanosheet, where: ● carbon atoms, ● oxygen, ● hydrogen.

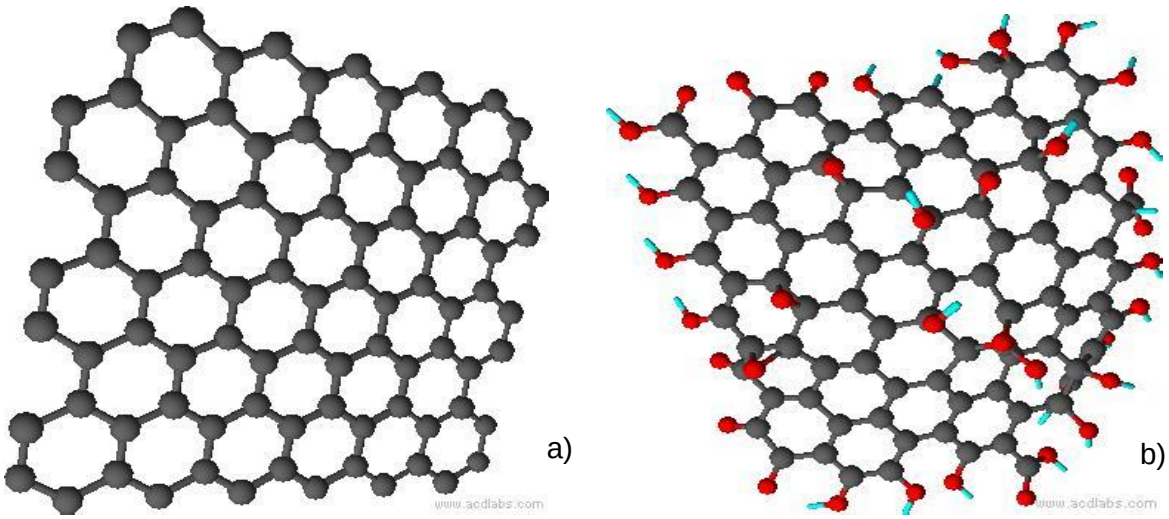

Source: The Author (2022)

Graphene's exceptional properties have attracted applications in the areas of nanoelectronics, photocatalysis/photodegradation and may also be incorporated into other materials on a macroscopic scale. In photocatalytic and adsorption processes, GBM have been promising, mainly because of its high specific area, as well as good optical transmittance and high intrinsic electronic mobility (GORGOLIS; GALIOTIS, 2017; JUNGES; JAURIS; ROSSATO, 2015; YANG *et al*., 2016).

According to Atchudan *et al.* (2016), GBM's hexagonal structure can provide a building support for the growth and anchoring of other hexagonal nanostructures such as ZnO, TiO_2 and SnO_2. GO, specifically, with various oxygenated groups on its surface, has excellent dispersibility, offering several opportunities for the manufacture of hybrid composites.

Because of the many ways to produce GBM, the literature lacked standards to properly stablish the properties of graphene and its derivatives. However, in 2017, the International Organization for Standardization (ISO) stablished quality parameters for graphene through ISO TS 80004/2017, in which graphene is classified as a nanomaterial with carbonaceous hexagonal lattice in form of nanosheets with a stacking of up to 10 nanolayers (FRAGA *et al.,* 2020; ISO, 2017).

Regarding the different ways of synthesizing GBM, as it usually happens to new materials intended for large-scale applications, the development of methods for mass production and processing of nano graphene materials has become a priority. As graphite basically consists of several stacked layers of numerous graphene sheets bonded together by Van der Waals bonds, it is in principle possible to produce graphene from high purity graphite if these bonds are broken by means of a top-down approach. It is important to bear in mind that top-down methods start from larger materials that are further decomposed into nanostructures. The bottom-up methods, on the other side, start from atoms and molecules and end up grouped into larger particles (GREWE; MEGGOUH; TÜYSÜZ, 2016).

Although the pioneering approach proposed by Novoselov *et al.* (2004), who won the Nobel Prize in Physics in 2010 for the production of graphene via micromechanical graphite exfoliation, lead to a high-quality material, this technique presents low productivity and is not considered suitable for large scale production. There are also some studies involving the production of GBM via electrochemistry. In this case, the electrochemical oxidation of the graphite proceeds. Such method has

as its main advantage that it almost completely avoids the use of hazardous materials. In addition, by controlling the electrode potential, the thickness of the GO sheets can be easily controlled (ASSIS FILHO *et al.,* 2018; SHAMAILA *et al.*, 2016).

Nowadays, one of the ways that provides higher graphene production depends on the conversion of graphite into graphite oxide via chemical reactions (CHOWDHURY; BALASUBRAMANIAN, 2014). From the beginning of its preparation in the 19th century, graphite oxide has been produced by Brodie, Staudenmaier and later by Hummers (HUMMERS; OFFEMAN, 1958). Such methods involve the oxidation of graphite in the presence of strong acids and oxidants, where the oxidation level changes according to the method and reaction conditions (CHOWDHURY; BALASUBRAMANIAN, 2014).

Graphite oxide can be defined as a structure composed of several layers of strongly hydrophilic graphene oxide sheets. Thus, graphite oxide can be completely exfoliated to produce aqueous colloidal suspensions of GO sheets (see Figure 2.4b) via sonication, or intense stirring of the mixture over a long period of time (ARAUJO *et al.,* 2018 a, b).

The most widespread and applied chemical method for obtaining GO is Hummers, followed by sonication. In this method, the oxidation of graphite is done by rigorously treating an equal mass of graphite in a H_2SO_4 concentrated solution, containing three equal masses of $KMnO_4$ and half mass of $NaNO_3$ (HUMMERS, 1957; HUMMERS; OFFEMAN, 1958). The Hummers Method is more advantageous compared to others, due to its high efficiency and satisfactory safety during synthesis (CHEN *et al.*, 2013). Despite the not so recent discovery, the behavior of GO is not yet fully understood, being that considered a non-stoichiometric compound, since it is possible the presence of keto, epoxide, peroxide, hydroxyl, and carboxyl groups on its surface (MACEDO, 2011).

Several studies have employed modified versions of the Hummers Method, making minor changes, mostly regarding the dosage of reagents, reaction time, as well as the types of oxidants and graphite used (ARAUJO *et al.,* 2018 a, b; SHAMAILA *et al.*, 2016). In addition to modifications made regarding the required acid volume, the number of steps and the conditions under which the reaction takes place (SHAHRIARY; ATHAWALE, 2014). A study by Chen *et al.* (2013) presented a version of the Hummers method without using $NaNO_3$. As a result, graphene oxide

production was quite like the one prepared by the traditional Hummers method. Such modification did not decrease product yield and eliminated the production of toxic gases NO_2 e N_2O_4.

In general, it is considered that graphene oxide itself is usually prepared by exfoliating graphite oxide in distilled water with sonication. After producing the oxide by the chemical route, the implementation of techniques aiming at converting graphene oxide to reduced graphene oxide (rGO) is continued. The obtained rGO tends to present properties very similar to those of graphene, although it can usually present a certain degree of lattice disorder, caused by several defects in the hexagonal network, and some functional groups resist the reduction (SUAREZ-IGLESIAS *et al.,* 2016; SHAHRIARY; ATHAWALE, 2014).

The use and application of graphene-based materials specifically for wastewater treatment, will be presented in the following topics.

2.5 BIOPOLYMERS AND HYDROGELS

Nanocomposites can be defined as hybrid materials consisting of a polymer matrix reinforced with a nano-scale filler, which must have at least one nanometric dimension. Polymer nanocomposites have emerged as they normally exhibit exceptional physiochemical properties. These materials were first developed by Toyota research group which has bestowed new dimensions by inclusion of organic and inorganic nanofiller owing to the numerous applications (RHIM, 2011; SHARMA *et al.,* 2018).

The fabrication of polymer nanocomposite has been facilitated by using sonication, however the weight % on the mixture, as well as size and shape of the nanomaterial are important parameters. Depending on the nanomaterial, different methods can be used to functionalize its surface, so that a more uniform dispersion is obtained. Many processing methods have been discussed for the synthesis of nanocomposites based on polymers, which relies on the type of polymer, its molecular weight, the solvent used, as well as the size of the nanomaterial incorporated. In general, the unification of polymer nanocomposite requires good homogeneous dispersion, as when the nanoparticles encounter the matrix, they might stack, forming agglomerates (SHARMA *et al.,* 2018). Regarding their nature,

polymers can be classified as natural (also called biopolymers, they come from living beings) or synthetic (obtained by chemical reactions in the laboratory). There are natural organic and natural inorganic polymers. Figure 5 shows examples of natural and synthetic polymers commonly found in everyday life.

Figure 5 – Examples of natural and synthetic polymers commonly found in everyday life

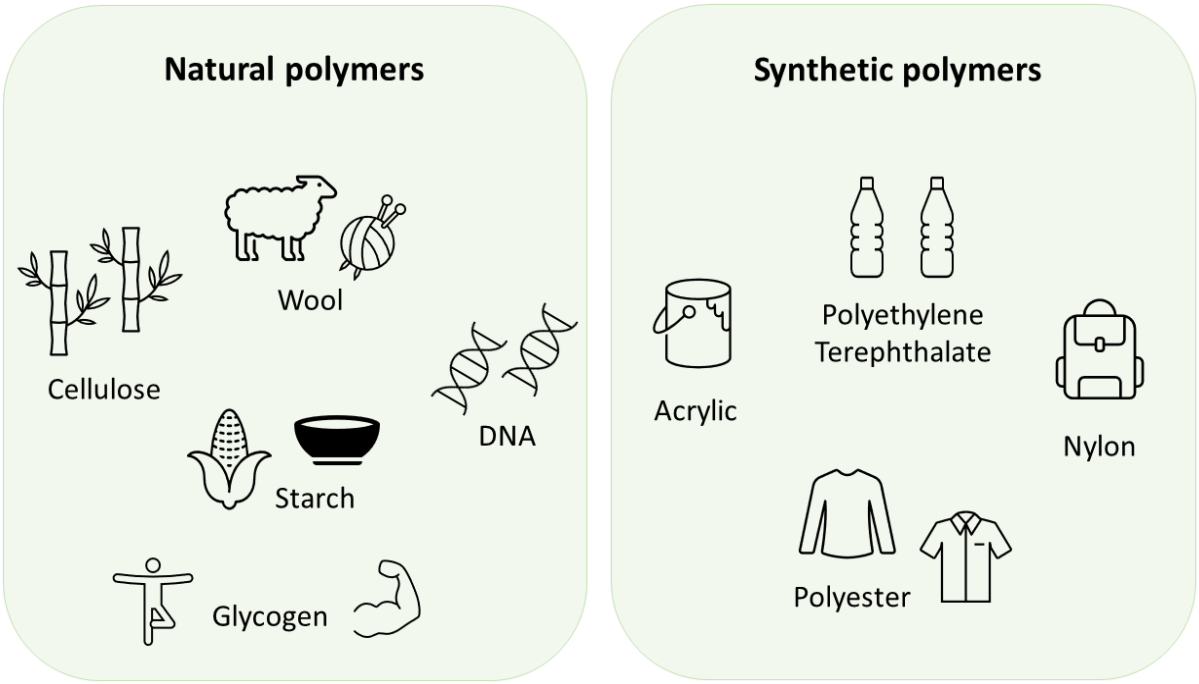

Source: The Author (2022)

As well-known, biomaterials are present on the planet in great amounts, being one of the renewable resources, with environmentally friendly characteristics. Biopolymers are originated from living organisms, polynucleotides, polysaccharides, and biomass production, and can be applied as an alternative to substitute many other thermoplastics. These materials exhibit interesting benefits, such as biocompatibility, nontoxicity, and biodegradability (SHARMA *et al.,* 2018; SRIVASTAVA *et al.,* 2020). Figure 6 exhibits a brief classification of biopolymers, including biodegradable and non-degradable thermoplastics.

Figure 6 – Simplified biopolymers classification diagram.

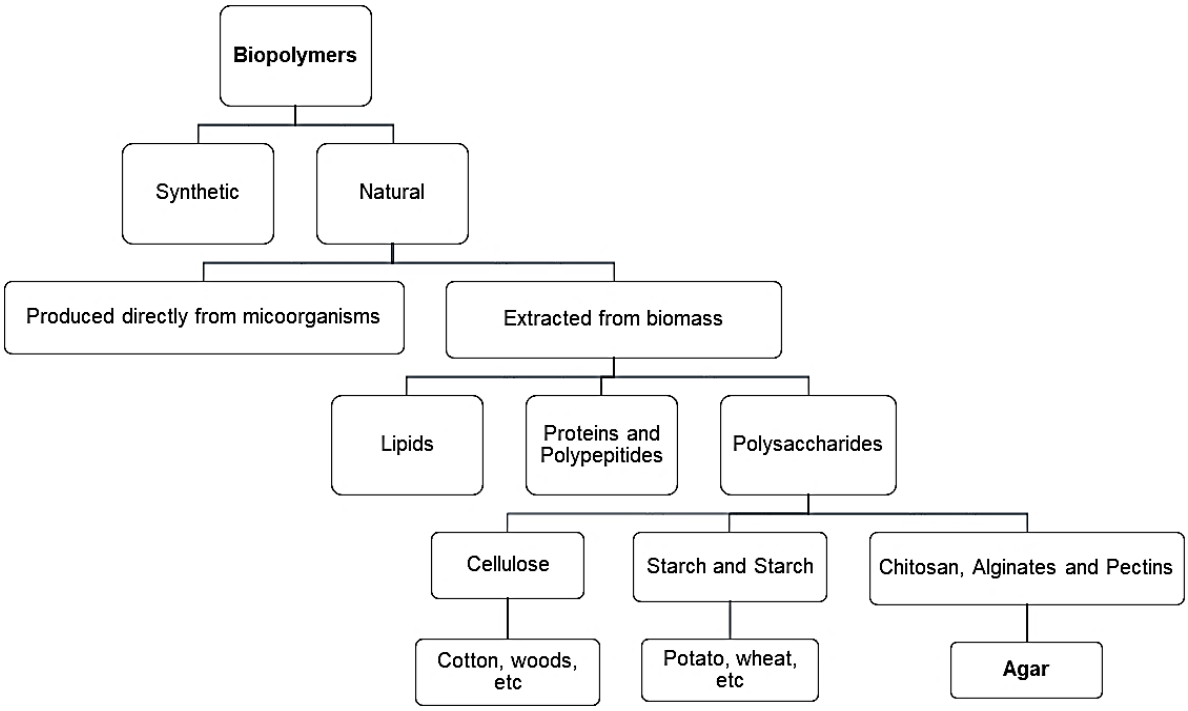

Source: adapted from Sharma *et al.* (2018).

One of the most common approaches for the fabrication of natural nanocomposites (also called bionanocomposites) consists of incorporating an inorganic matrix with the biopolymers. That can be performed to enhance their adsorptive properties. Recently, different research has focused on the development of new polymeric adsorption matrixes. These novel materials are versatile, as they can provide an economical and efficient option for industrial applications (SRIVASTAVA *et al.,* 2020).

Thus, the hydrogels are emerging as efficient adsorbents for the removal of organic and inorganic aqueous pollutants. They are hydrophilic, insoluble, cross-linked polymers with high swelling capacity, being able to absorb large volumes of water inside its 3D reticulated networks. Hydrogels can be synthesized via chemical route, when the polymer chains are bonded via covalent bonds; and via physical route, in which non-covalent bonding exist between the molecules and polymeric chains. The physical route normally involves mild conditions compared to chemical processes (SINHA; CHAKMA, 2019).

Normally, nanoparticles and different chemical catalysts can be incorporated in the hydrogels for diverse applications, including biomedical engineering, food, and

agricultural engineering, as well as water treatment. Hydrogels offer flexibility in terms of modifications of surface characteristics - charge, functionality, large area, controllable pore structure, interesting acid/base properties, and hydrophilicity (SINHA; CHAKMA, 2019).

Zheng, Zhu, and Wang (2014) produced granular composite hydrogels via in-situ polymerization using the biopolymer chitosan, acrylic acid and itaconic acid as the monomers, and attapulgite as the inorganic component. The resulting hydrogel was used for the adsorption of MG dye, and it was observed that the introduction of only 5 wt% of attapulgite into the hydrogel improved the adsorption capacity and could also be regenerated/ reused for several times.

Among the biopolymers, agar is a natural biopolymer consisting of a mixture of natural polysaccharides (agarose and agaropectin) normally derived from red seaweeds of the class *Rhodophyceae* – see Figure 7. The main components of the chains are β-D-galactopyranose and 3,6 anhydro-α-L-galactopyranose. Agar becomes soluble in near-boiling water and upon cooling, the polymeric chains self-assemble into helical fibers, which aggregate forming a hydrogel (GARRIDO *et al.,* 2016). It is essential for many activities, including food production, preparation of solid plate media, and electrophoretic gels for use in life science assays (SASUGA *et al.,* 2018).

Figure 7 – One of the main sources of agar, the red seaweed species *Gelidium* sp. and *Gracilaria confervoides* (a); agar biopolymer containing β-D-galactopyranose and 3,6 anhydro-α-L-galactopyranose on its chains (b).

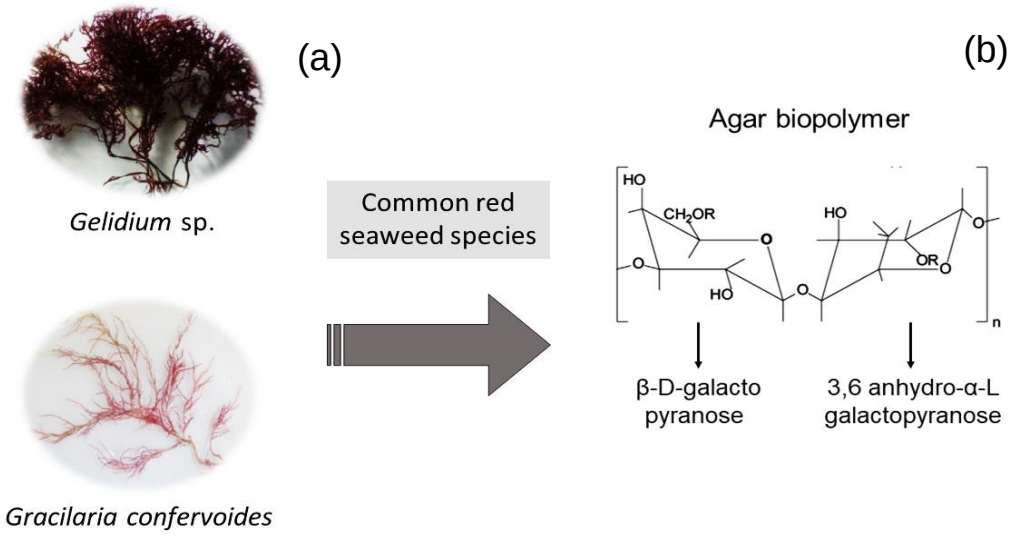

Source: adapted from Ismail, Alotaibi, El-Sheekh (2020)

The red algal *Gelidium* are currently exploited worldwide for the extraction of agar and agarose, being the most important source of raw material, although other algae such as *Gracilaria* and *Pterocladia* have also been explored for agar production (GARRIDO *et al.,* 2016). Even though the agar extracted from *Gelidium* represents approximately 1.6% of the world phycocolloid production, its properties, such as high gelling strength and low gelling temperatures makes it difficult to be replaced by other species of seaweed (SANTOS; MELO, 2018). According to Ferdouse *et al.* (2018), in 2015 the seaweed production was over 30 million tones, and the leading countries were Chile, China and Norway (mainly brown and red types) for wild species; and China, Indonesia, the Republic of Korea and the Philippines for cultured species.

Agar have been used to obtain composites as well, especially in studies regarding nanocomposite films. Rhim (2011) worked on the production of Agar/clay nanocomposite films with different amount of the nanoclay - 0, 2.5, 5, 10, 15, and 20 g clay/100 g agar. Characterization results revealed that even at low level of nanoclay addition, the properties of the materials were greatly influenced with the nanoclay content.

Agar-soy protein biocomposite films were processed by Garrido *et al.* (2016), obtaining transparent and homogeneous films. The conformational changes occurred during the extrusion process and the effect of agar on the final properties were analyzed. In overall, the good compatibility between agar and soy protein was confirmed by scanning electron microscopy (SEM) micrography.

Previous studies have evaluated agar in both powdered and hydrogel/aerogel forms as an adsorbent for MB dye. Chen *et al.* (2017) have also tested a 3D agar/GO composite aerogel (80 w% agar, 20 w% GO) regarding its adsorption capacity of methylene blue in batch mode. In that occasion, the aerogel exhibited a maximum adsorption capacity of 578 mg g^{-1}, predicted by the Langmuir isotherm.

2.6 APPLICATIONS OF GRAPHENE-BASED MATERIALS IN WATER AND WASTEWATER TREATMENT

The processes commonly applied for water treatment and purification are often not able to remove certain types of contaminants such as drugs and some

organic compounds (JAURIS *et al.,* 2015; UPADHYAY; SOIN; ROY, 2014). The rapid development of nanotechnology has also been reflected in water and wastewater treatment. In this context, graphene and its nanomaterials have shown themselves as effective in water treatment, due to their good chemical stability, low density, and structural diversity (GREWE; MEGGOUH; TÜYSÜZ, 2016; UPADHYAY; SOIN; ROY, 2014). For methylene blue removal using GO, Peng *et al.* (2016) used amorphous graphite, not often used for GO production. In the study, the experimental adsorption capacity of the dye in GO was 2255.35 $mg.g^{-1}$.

Shi *et al.* (2014) also studied the adsorption of methylene blue on a magnetic cellulose-graphene oxide composite. They found out that the cellulose -GO compound was very stable and could be easily recycled. The adsorption efficiency in this case was over 89% even after being recycled five times.

Graphene nanocomposites with magnetic materials, such as Fe_3O_4, have been explored to remove pollutants from water. Fe_3O_4 is one of the most widely used materials for water purification due to its great biocompatibility, ensuring the safety as well as magnetic properties, which makes it easy to collect after treatment. Thus, after adsorption, the Fe_3O_4-graphene can be easily separated using a magnetic field (UPADHYAY; SOIN; ROY, 2014).

According to recent studies carried out by the research group (ARAUJO *et al*., 2018 a, b; FRAGA *et al*., 2018; SILVA *et al.*, 2021), graphene-based materials are potential adsorbents, effective in removing textile dyes from water. Moreover, in these studies, the potential of GBM in the removal of color and turbidity from real textile effluent samples was observed, which reinforces the potential of a possible application of these materials as adsorbents in industrial scale.

Although many previous works presented batch tests using various types of GBM as adsorbents for dye removal from aqueous medium, the difficulty of applying these materials for continuous adsorption systems still represents a bottleneck. Because they are extremely light and thin, GBM are easily carried out and difficult to be separated during recycling, which is an obstacle to industrial scale application. Therefore, a support material is generally required to immobilize GBM in a fixed-bed adsorption column (GONG *et al.,* 2015).

Direct application of GO as a filter layer to a compacted sand column is one of the options employed to improve the filtration of contaminants, providing a convenient and economical method for effluent treatment in a fixed-bed column. Dong *et al*. (2016) evaluated the potential of GO directly applied in a filter for the removal of Levofloxacin and Pb (II) in aqueous solution. The removal of contaminants was high for all conditions tested in single and mixed solution systems.

Another alternative would be to apply graphene (or GO) as a three-dimensional (3D) structure for packaging in adsorption column using graphene hydrogels and aerogels (CHEN *et al.,* 2017). Aerogels are porous materials that exhibit high porosity and surface area with large pore volumes. They are generally prepared from molecular precursors by sol-gel methods, followed by supercritical or freeze-drying to remove solvents and replace them with air. They have high porosity, low density, low thermal conductivity, and dielectric constant. They can be applied in catalytic and adsorption processes and many other areas (GORGOLIS; GALIOTIS, 2017).

Aerogels can also be obtained by freeze-drying previously prepared hydrogels. Graphene hydrogels can be prepared by adding the nanomaterial to a polymer solution, followed by free radical polymerization to chemically cross-link the main polymer component around the nanocomposite. In some cases, simple homogenization of the precursor materials causes gelation, leading to hydrogels with interesting properties including injectability and self-healing (ULLAH *et al.*, 2015).

Liu *et al.* (2012) synthesized an aerogel from GO suspension by centrifugal vacuum drying method, and then used it for adsorptive removal of MB and methyl violet (MV) dyes. The adsorption tests showed that 99.1% of MB and 98.8% of MV were removed and steady state was reached in just 2 min. The gel exhibited adsorptive capacity of 397 and 467 mg g^{-1} for MB and MV, respectively, demonstrating the high capacity of GO sponges in dye removal.

However, although some 3D GBM have already been tested directly for the removal of dyes in aqueous media, the nanometric size, high dispersion, and stability of the nanosheets make the release of this material into the aquatic environment a potential secondary contamination risk. Therefore, there is still a need to make these gels more resistant, especially when considering a practical application on a large scale (CHEN *et al.,* 2017; DONG *et al*., 2016).

Previous studies have shown 3D GBM composites with some coagulant agents and polymers, to increase the nanocomposite strength. As an example, Chen *et al.* (2017) produced a 3D agar-GO aerogel composite via freeze drying. The adsorptive capacity of the material was tested for MB dye and a maximum adsorption capacity near 580 $mg.g^{-1}$ was observed. The use of agar, as well as increasing the mechanical strength, also preserves the reusability potential of the material, as it maintained over 91% of adsorption capacity after the 4^{th} adsorption-desorption cycle.

In general, among the literature works which based their study on the application of GBM in continuous fixed-bed processes for water decontamination, it is worth mentioning some recent research published over the last six years - academic research platforms used: Science Direct and Google Scholar (July 2022):

a) Adsorption of heavy metals (Cr(VI), As(III), Cd(II), and Pb(II)) in groundwater using sand columns enriched with GO in lab-scale (ABBASI *et al.,* 2021).
b) Synthesis of a magnetic porous reduced GO via in situ chemical co-precipitation of Fe (III) and GO and its use as an adsorbent for the removal of triclosan by conducting with continuous flow fixed column (LI *et al.,* 2020).
c) Glyphosate removal from contaminated water using GO-$MnFe_2O_4$ nanocomposite supported on vegetal activated carbon as adsorbent in a fixed-bed column (MARIN *et al.,* 2019).
d) Synthesis of a graphene-based monolith by chemical reduction of GO using magnesium ascorbyl phosphate, and application as an adsorbent for Bisphenol A removal in a fixed-bed system (FANG *et al.,* 2018).
e) Pb(II) removal from aqueous solution using GO decorated by MgO nanocubes as adsorbent in a continuous up flow fixed-bed column study (MOHAN *et al.,* 2017).
f) Study of a laboratory-scale fixed-bed column containing a GO-polylysine aerogel as adsorbent for Cr(VI) removal (SINGH *et al.,* 2017).

As seen from the previous works, some of the GBM adsorbents produced for applications in fixed-bed adsorption were supported on sand (ABBASI *et al.,* 2021) or on activated carbon (MARIN *et al.,* 2019). Other experiments were performed by freeze-drying the composites and using them for packing the adsorption columns

(FANG *et al.,* 2018; LI *et al.,* 2020; SINGH *et al.,* 2017). In the present work, the prepared nano-biocomposite was used without the need for lyophilization, being therefore an easier method (and with fewer steps) for its application as an adsorbent in a fixed-bed column. The hydrogel production method will be detailed in the next topic.

3 GRAPHENE-BASED MATERIALS PRODUCTION AND CHARACTERIZATION

In this topic, different samples of graphene-based materials (including graphene oxide and agar-graphene oxide composites) were produced from the variation of operational parameters in the reaction medium during the syntheses. After, characterization analyzes were performed to compare the morphologies and physical-chemical properties, including Raman spectroscopy, Fourier-transform infrared (FTIR) spectroscopy, thermogravimetric analysis (TGA), Scanning electron microscopy (SEM), as well as Zeta Potential measurements. All characterization analyzes conducted were important to access the properties of the nanomaterials produced via the proposed synthesis methods, and to prove their quality. Preliminary batch adsorption tests were also performed for the GO samples produced.

Parts of this main topic have been published:

NASCIMENTO, G. F. O.; COSTA, G. R. B.; ARAUJO, C. M. B. *et al.* Graphene-based materials production and application in textile wastewater treatment: color removal and phytotoxicity using *Lactuca sativa* as bioindicator. **Journal of Environmental Science and Health, Part A**, v. 55, n. 1, p. 97-106, 2020.

ARAUJO, C. M. B. *et al.* Wastewater Treatment Using Recyclable Agar-graphene Oxide Biocomposite Hydrogel in Batch and Fixed-bed Adsorption Column: Bench Experiments and Modeling for the Selective Removal of Organics. **Colloids and Surfaces A: Physicochemical and Engineering Aspects**, v. 639, p. 128357, 2022.

3.1 METHODOLOGY

Graphene oxide aqueous suspensions, as well as the Agar-GO biocomposite samples were produced in the Laboratories of the Research Group on Environmental Technologies and Processes (GPTA), located at the Federal University of Pernambuco (UFPE, Brazil). Part of the hydrogel processing and posterior characterization were conducted in the laboratories of the Research Support Center (CENAPESQ), and the Applied and Environmental Nanotechnology Group (NanoA), both located at the Federal Rural University of Pernambuco (UFRPE, Brazil).

3.1.1 Materials

GO was produced using analytical grade graphite powder (Synth, Brazil), $KMnO_4$ (Química Moderna, Brazil), and H_2SO_4 (AnalaR NORMAPUR VWR Chemicals, France). Agar-GO hydrogel samples were synthesized using the analytical grade agar powder for laboratory and industrial use, acquired from Anidrol (Brazil), and used without further purification.

3.1.2 Graphene Oxide production and preliminary adsorption tests

GO production, via the modified Hummers and Offeman method (HUMMERS; OFFEMAN, 1958) was done following previous studies by Araujo et al. (2018) using for each sample: 1 g of pure graphite, 3 g $KMnO_4$, about 200 mL of distilled H_2O and 10 mL of H_2O_2 (33% w/w) to finish the oxidation reaction after 3 h of contact. Each sample was synthesized using different ratios of H_2SO_4 and distilled water so that the total volume in the reaction medium remained 25 mL – see Table 1.

Table 1 - Variations in H_2SO_4 /H_2O ($mL_{H2SO4}.mL^{-1}_{H2O}$) proportions during GO production using 1 g of graphite, 3 g $KMnO_4$ in 3 h of contact.

Sample	H_2SO_4 volume (mL)	H_2O volume (mL)
GO-25	25	0
GO-23	23	2
GO-22	22	3
GO-21	21	4
GO-20	20	5

Source: The Author (2022)

After synthesis, the samples were sealed and stored in amber flasks. All assays were performed in replicate.

3.1.2.1 Effect of Varying H_2SO_4 Concentration in Graphite Oxidation on the Adsorption Process

Studying the effects of varying the acid concentration used during graphite oxidation in the dye adsorption process, 1 mL of each graphite oxide (GrO) sample

produced was used (~0.02 g.mL^{-1} each suspension), together with 50 mL of the respective dye solution with an initial concentration of 50 mg.L^{-1} (pH = 5.5). The dye solutions were produced from stock solutions (1000 mg.L^{-1}) prepared for each one of the dyes studied - methylene blue (MB) and brilliant blue (BB). In this case, it was decided to use the samples before the ultrasonic exfoliation process, to carry out the preliminary adsorptive tests, since the separation of the nanomaterial after adsorption is easier for GrO than for GO.

The flasks containing the solutions were placed under constant stirring (250 rpm) for 1 h at room temperature (28 ± 3 °C) to ensure the equilibrium was reached. After 1 h of contact, separation of the supernatant was done by centrifugation for 10 min at 4000 rpm. The initial and final concentrations were measured and recorded using a UV-Vis spectrophotometer.

It should be noted that the same test was developed under the same conditions for MB and BB dyes. The aim was to investigate the behavior of the GBM produced to adsorb both cationic (MB) and anionic (BB) dyes dispersed in water, since real textile wastewater samples usually contains dyes of different natures, along with many other organic and inorganic components. The removal efficiencies were calculated according to Equation 1, in which C_0 and C_f are the initial and final concentrations of the dye, respectively.

$$\%R = \frac{(C_0 - C_f)}{C_0}.100 \quad (1)$$

3.1.3 Graphene Oxide characterization

Characteristics of the graphene oxide samples produced (GO-21 and GO-25) were observed applying different techniques, such as X-ray diffraction (XRD); ultraviolet-visible (UV-Vis) spectroscopy; dynamic light scattering (DLS); pH at the point of zero charge (pH_{PZC}); Fourier transform infrared spectroscopy and micro-Raman spectroscopy.

XRD of graphite powder and GO samples were performed using a X-ray diffractometer (Rigaku, model: Ultima), with diffraction angle (2θ) ranging from 5º–50º. XRD analyses were performed in the Center for Strategic Technologies of the Northeast (CETENE), Brazil. DLS measurements for nanoparticle size analysis were

performed using the GBM samples dispersed in water (Malvern Panalytical, mastersizer 2000 - Hydro 2000MU), with size range from 0.020 to 2000.000 µm.

UV-vis spectra were obtained by diluting graphene oxide suspensions in water and scanning them in a UV-visible spectrophotometer (Genesys 10 uv – Thermo Scientific, wavelength: 200–800 nm). pH_{PZC} were measured based on the experiment of 11 points. Thus, pH solutions of 1, 2, 3, 4, 5, 6, 8, 9, 10, 11, 12 were prepared using NaOH and HCl solutions, 6 $mol.L^{-1}$ each. Then, 2.5 mL of the respective GO sample were placed into 100mL Erlenmeyer flasks containing 50 mL of aqueous solution with pH values adjusted. The flasks were transferred to a MARCONI MA-420 shaker for 24 h under constant stirring at 50 rpm. The final pH values were determined using a bench pH meter (PHTEK, PHS-3B). The DLS, pH_{PZC} and UV-Vis analysis were performed in the laboratories of the Center for Technologies and Geosciences, located in the Federal University of Pernambuco, Brazil.

Micro Raman spectroscopy was proceeded in a Senterra Raman Scope system with a 532 nm wavelength incident laser (laser power 20 kW), in a range between 800 and 2700 cm^{-1}. FTIR spectra were obtained using a PerkinElmer spectrum two spectrometer, ranging from 650 to 4000 cm^{-1}. Both analyzes were conducted at the laboratory facilities of the Civil Police Criminalistics Institute, in the state of Pernambuco (Brazil).

3.1.4 Agar-Graphene Oxide hydrogel production

To produce the agar-GO hydrogels, firstly, graphene oxide was synthesized by the modified Hummers method proposed using 25 mL of concentrated H_2SO_4 (GO-25). It was chosen to use the GO produced with sulfuric acid P.A., because although the other samples need a smaller amount of acid during synthesis, the dilution of the acid is a laborious process that involves some risks for production in larger quantities, representing therefore one more step in the process. After completing the oxidation of pristine graphite as described previously, graphite oxide suspension was washed with distilled water, and sonicated for 1h to obtain GO suspension (ARAUJO *et al.*, 2018).

Thereafter, 0.30 g of agar was diluted in 20 mL of deionized water. The solution was placed under constant stirring on a magnetic hot plate stirrer at T ~85 °C

for 20 min. Then, a volume of GO suspension prepared (10 $g.L^{-1}$) was added to the system under constant stirring and maintained for approximately 5 min for homogenization. The hydrogel formed was placed in a Petri dish until cooling, and total gelification was observed. Agar is a biopolymer that easily gelifies at 24 ^{o}C.

Subsequently, the hydrogel was cut into smaller pieces with the aid of a spatula, obtaining an average particle size for the composites of approximately 0.30 (± 0.01) cm. The excess humidity was removed using qualitative paper filter, and the samples were stored inside sealed glass flasks in the fridge. The average particle size distribution was performed (see Appendix B), since the particles size significantly influences mass transfer during the batch, as well as and continuous adsorption processes. Agar:GO ratios used to produce the samples are exhibited in Table 2.

Table 2 - Variations in Agar:GO ratios used to produce the hydrogel samples.

Sample	**GO percent (%Weight)**	**Agar percent (%Weight)**
80%Agar20%GO	20%	80%
75%Agar25%GO	25%	75%
70%Agar30%GO	30%	70%

Source: The Author (2022)

Figure 8 exhibits some photographs of a hydrogel sample produced in laboratory. As can be seen, the sample has a brownish color, similar to pure graphene oxide, however, with a gelatinous texture due to the agar added in its composition. It is worth mentioning that the samples produced with 70%, 75% and 80% agar were all visually and texturally similar to the one shown in the photo.

Figure 8 – Photographs of the hydrogel produced with 80% agar and 20% GO

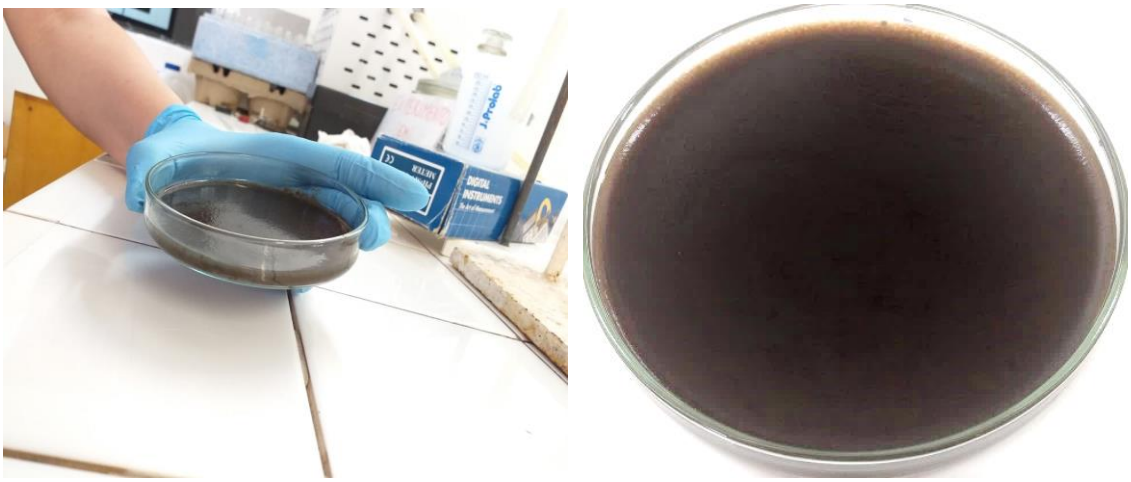

Source: The Author (2022)

3.1.5 Characterization of the agar-GO biocomposite

To perform the characterization measurements, flasks containing the Agar-GO hydrogels were placed in an ultra-freezer (Sanyo, MDF U33V) at -80 °C for 24 h. Thereafter, the samples were placed in a freeze dryer (Martin Christ, ALPHA 1-4 LD PLUS) for 48 h. These equipment are in the laboratories of the Research Support Center, located at the UFRPE. The composite hydrogel was previously packed in 2 mL disposable Eppendorf. After freezing, the samples were lyophilized to remove all water, where the frozen samples were kept under a high vacuum. This process was chosen because it allows the sublimation of water without causing changes/ damages to the material's structure (CHEN *et al.*, 2017).

Raman spectroscopy analysis, Fourier transform infrared spectroscopy, thermogravimetric analysis, and the Scanning electron microscopy images of the sample were determined. SEM micrographs were obtained using the TESCAN VEGA3 (TESCAN ANALYTICS) scanning electron microscope, to observe the surface structure of the material produced (Agar-GO) and the samples of agar and the GO used as precursors for the hydrogel production. A concentrated GO solution was placed in a petri dish and dried for 24 h at 65 °C in a hot air oven. The resulting compact film was analyzed in SEM.

FTIR analyzes of vibrational spectroscopy were performed in the medium infrared region on the Shimadzu spectrophotometer (IR Prestige-21), with coupled

attenuated total reflectance (ATR) accessory, in the following conditions: Region 4000-600 cm^{-1}, 4 cm^{-1} of resolution, accumulations: 20. TGA measurements were recorded in a Thermobalance (TGA Q50), using a heating ramp of 10 °C.min^{-1}, from 25 to 900 °C with a flow rate of 25 mL.min^{-1} of N_2. Raman spectroscopy analyzes were performed in the inVia Raman microscope (Renishaw) with Ar laser (20-580 mW).

Surface charge of the dispersed agar-GO (aerogel powder) samples and the precursor GO suspension were determined using a zeta potential analyzer (Delsa Nano C Particle Analyzer, Beckman Coulter) in a pH range from 2 – 10 at 25 ^oC. HCl and NaOH stock solutions (0.30 mol.L^{-1}) were used to adjust the pH values.

3.2 RESULTS AND DISCUSSION

Results regarding the production and characterization of GO, as well as the production and characterization of agar-GO nano-biocomposites will be addressed and discussed in this section.

3.2.1 Graphene Oxide Production Varying H_2SO_4 concentration

Results of the adsorption tests for the graphite oxide samples produced with different concentrations of H_2SO_4 are shown in Figure 9. It is observed that as the acid concentration decreases, the adsorption of BB is favored, while MB adsorption is disadvantaged by excessively decreasing the acid concentration. This occurs because the acid is involved with the formation of oxygen groups on the materials surface during the oxidation, allowing the penetration $KMnO_4$ into the graphite layers more effectively (CHEN *et al.,* 2013). These groups support the interaction between GrO and MB due to the negative density of the adsorbent and the cationic characteristic of the dye, so that adsorption occurs both via electrostatic interactions with the oxygenated groups on the GrO surface and by π-π interactions between the aromatic rings (YAN *et al.,* 2014).

Figure 9 – Variation of H_2SO_4 volume in the production of graphene oxide *vs.* Removal efficiencies of the dyes MB and BB (Experimental conditions: 50 mL, initial dye concentration: 50 $mg.L^{-1}$, ~0.02g of GrO, contact time: 1 h, 250 rpm, pH = 5.5, T = 28 ± 3 °C).

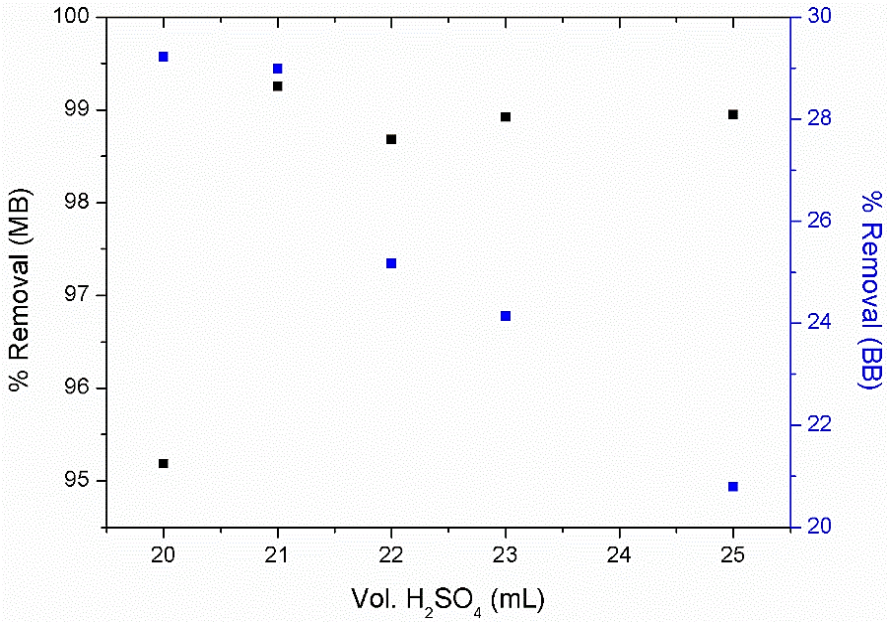

Source: The Author (2022)

Apparently, a decrease in the amount of acid during GrO production leads to a lower degree of graphite oxidation, decreasing the number of functional groups on the surface of the material. This, on the other side, enables a better interaction of the material with anionic dyes, such as BB dye, via π-π interactions of the aromatic rings present in both the adsorbent and adsorbate structures (FRAGA *et al.,* 2018).

Yan *et al.* (2014) prepared and analyzed several GO samples with different degrees of oxidation using the modified Hummers method, varying the $KMnO_4$ dosage and oxidation time. When analyzing the effects of the oxidation degree on MB adsorption, it was observed that the adsorptive capacities increased exponentially with the increase of the degree of oxidation of the sample. The explanation would be related to the increase in the degree of exfoliation of graphitic layers, caused by the energetic oxidation, as well as the production of a larger number of active sites. The characteristics of GO-MB interaction gradually change from parallel stacking of MB molecule in the graphenic plane through the

hydrophobic π-π interactions, to the vertical position by means of electrostatic interaction, as there is an increase in the oxidation degree.

Araujo *et al.* (2018) were able to decrease the volume of H_2SO_4 from 25 mL to 23 mL without considerable reduction of MB adsorption. This research, on the other hand, demonstrates that the best experimental point (GO-21) was able not only to maintain the high MB percentage removal (99%) but also to increase BB removal by 21% to 29%. Therefore, the sample prepared with 21 mL H_2SO_4 will be used in subsequent tests. Important characterizations will also be presented for this sample.

Overall, a decrease in the amount of acid causes a reduction in costs with production process, making the material less aggressive to the environment, without making it lose the ability to adsorb the dyes. However, it is observed that sample GO-20 shows a more pronounced decrease in the percentage removal of MB, while there is a slight increase in the BB removal efficiency. H_2SO_4 provides the energic medium necessary for graphite oxidation to occur. Thus, it is believed that a greater decrease in the acid concentration tends to affect even more its effectiveness as adsorbent by the decrease in the amount of graphite that becomes GrO.

Although the sample GO-21 exhibited the best results in terms of removal efficiency of the dyes, it was chosen to use GO-25 to produce the biocomposite (agar-GO). Even though GO-21 needs a smaller amount of sulfuric acid during synthesis, the dilution of the acid is a laborious process that involves some risks for production in larger quantities, representing one more step in the process.

3.2.2 Graphene Oxide characterization

The optical absorption spectra of GO-21 and GO-25 suspensions are exhibited in Figure 10 a. In general, it is possible to see in the samples the presence of prominent absorption peaks in ~230 nm, attributed to π-π* transition of the C-C bonds of the aromatic rings; and a shoulder in 296 nm, associated with the n-π transition of the C=O bonds on the surface of GO samples (GURUNATHAN; HAN; KIM, 2013b; MEHL *et al.,* 2014). DLS measurements were performed in aqueous solution to estimate GO lateral sizes. It was found that the average particle sizes of GO-21 and GO-25 were respectively ~26 μm and ~32 μm - see Figure 10 b. DLS measurements could contribute to show that when comparing both samples (GO-21 and GO-25), the results were almost the same, indicating that the sample produced

with less H_2SO_4 presents similar characteristics to the one produced with more concentrated acid (GURUNATHAN *et al.,* 2013a; GURUNATHAN; HAN; KIM, 2013b).

Figure 10 – UV-Vis measurements for GO samples (a); particle size distribution from DLS analysis for samples GO-21 and GO-25 (b).

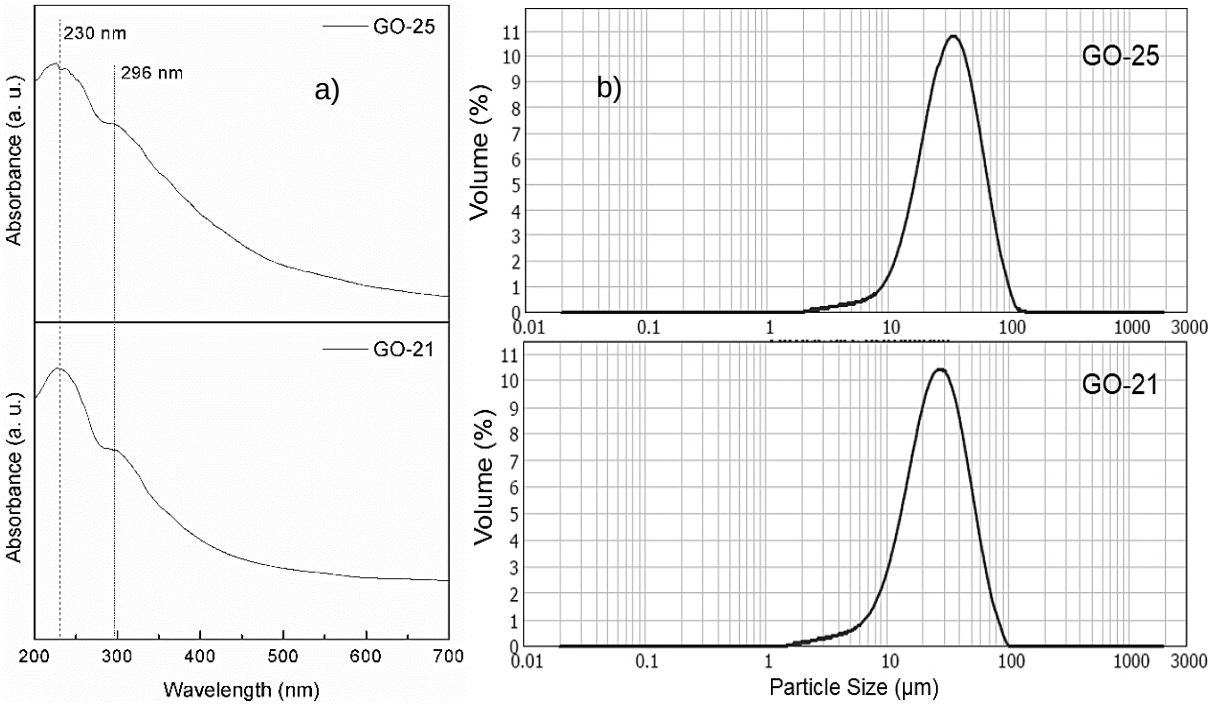

Source: The Author (2022)

Crystalline structures of the GO samples and pristine graphite were characterized by XRD. Graphite powder exhibited a main basal diffraction (002) peak located at approximately 2θ = 26°, as the diffraction peaks of GO-21 and GO-25 appear at the lower angles of 7.7° and 8.6°, respectively. Thus, it can be verified an increase in the interlayering spacing in both cases, as the 2θ values decreased from 26º to below 10º (Figure 11 a). The increase in d-spacing is related to the formation of oxygen functional groups between the graphitic layers, indicating the successful oxidation of graphite (GURUNATHAN *et al.,* 2013a; MEHL *et al.,* 2014).

The pH values at the Point of Zero Charges for both samples were determined. As it can be observed in Figure 11 b, it is possible to see the formation of a well-defined plateau near the final pH 2.5. Therefore, pH_{PZC} values were 2.64

and 2.37 for samples GO-21 and GO-25, respectively. For pH values over the pH_{PZC}, adsorption of cationic dyes is favored.

Tabrizi and Zamani (2016) evaluated the application of GO aerogels as adsorbents to remove Pb (II) from water. Performing the Zeta Potential measurements for GO colloidal suspension, the authors observed that the isoelectric point of the particles was approximatelly 2.4, which is similar to the results found in the present work.

Figure 11 - XRD patterns for graphite, samples GO-21 and GO-25 (a); pH_{PZC} for the samples GO-21 and GO-25 (b).

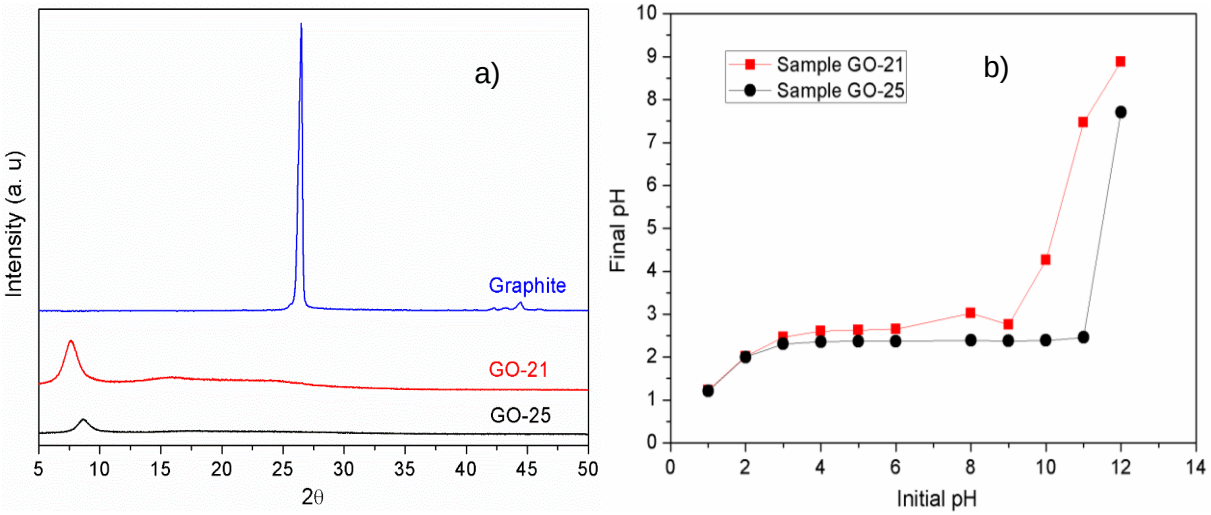

Source: The Author (2022)

Raman spectra of graphite, GO-21 and GO-25 in Figure 12 (a) and (b) exhibited D band at approximately 1350 cm^{-1} and G band at 1600 cm^{-1}. The D/G peak intensity ratio, known as I_D/I_G, usually indicates the lattice disorder of graphitic and graphene-based materials. Therefore, I_D/I_G values were estimated to be ~1.20 and ~1.60 for samples GO-21 and GO-25, respectively, indicating as expected, an overall increase in defects after oxidation. These defects arise from the disruption of the carbon basal plane structure by the introduction of functional groups due to oxidation (TIWARI *et al.,* 2013; ZHAO *et al.,* 2017). Comparing the graphite to GO spectra, it can be observed an increase in the D band intensity for both GO-21 and GO-25, being this increase more pronounced for the sample produced using more sulfuric acid.

Figure 12 – Raman measurements of (a) graphite powder, and (b) GO samples.

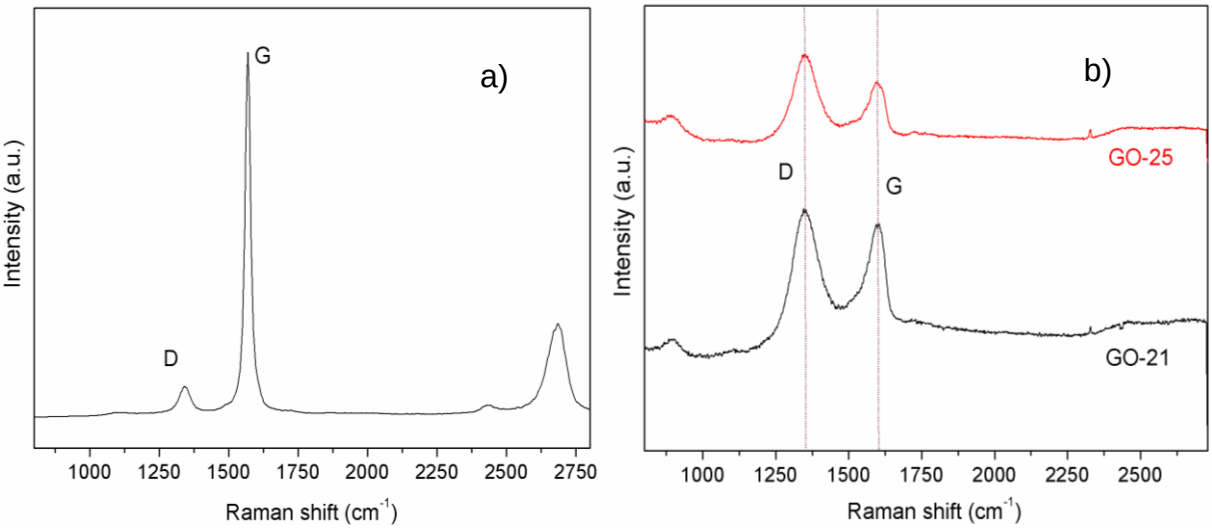

Source: The Author (2022)

FTIR spectra exhibited in Figure 13 shows the vibration modes of GO-21 and GO-25. The bands located in 3350 cm^{-1} are assigned to O–H stretching vibrations from hydroxyl groups on GO surface and water adsorbed. The absorption bands at 1725 cm^{-1} are the characteristic band of C=O groups. Bands near 1600 cm^{-1} are associated with the skeletal vibrations of C=C from unoxidized graphite. The shoulders at ~1400 cm^{-1} might be attributed to O-H or C-H. The bands at 1170 and 1050 cm^{-1} are assigned to C-O-C and C–O bonds, respectively (SARKER *et al.,* 2018; TIWARI *et al.,* 2013).

Figure 13 – FTIR spectra of GO-21 and GO-25.

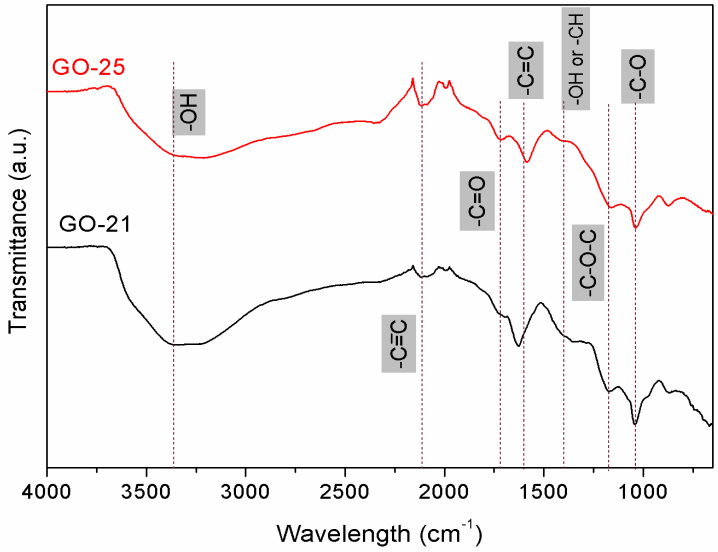

Source: The Author (2022)

3.2.3 Characterization of the Agar-GO biocomposite

In the composite, agar was used to build the 3D microstructure, reinforcing the stabilizing of graphene oxide nanosheets. It was choosen because this polymer is nontoxic and biodegradable with numerous oxygen functional groups. According to Chen *et al.* (2017), it is suposed that, as the hydrogel is forming, the oxygen groups existing on both agar and GO surface might react via dehydration reaction and interact via hydrogen bonding.

From Figure 14, the reactions to synthesize the composite do not appear to affect GO properties, as it is interpreted from the FTIR curves. It is possible to observe the maintenance of the bands corresponding to the chemical bonds related to GO oxygenated groups, and as more agar is added into the system, some peaks appear, while others lose intensity in the spectra. That might indicate that GO and agar are successfully compounded into composite aerogels.

Figure 14 – FTIR spectra of the hydrogels produced (left); and of pure GO (right).

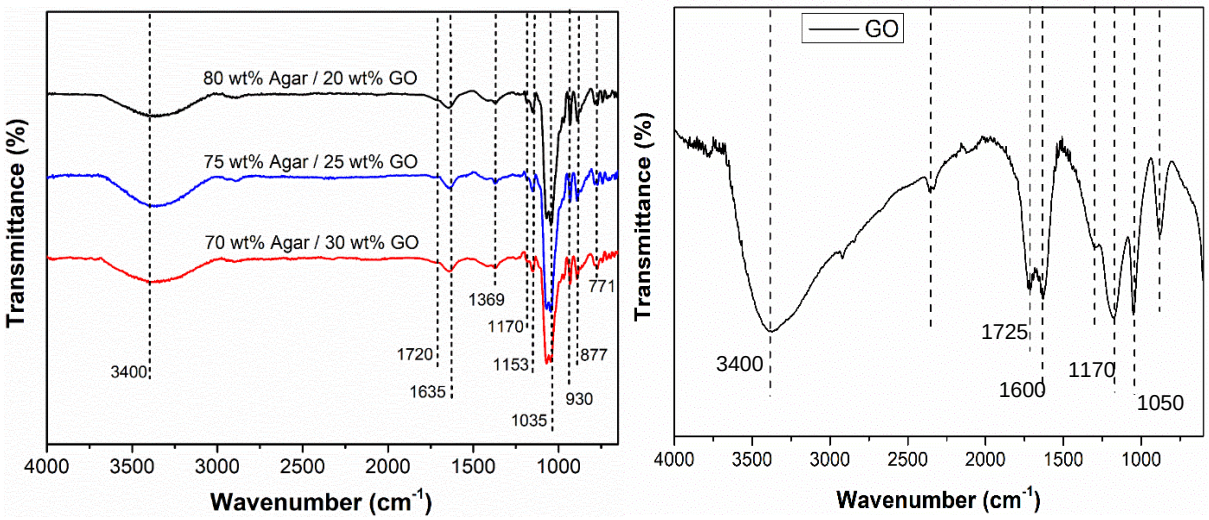

Source: The Author (2022)

The broad band at 3400 cm^{-1}, exhibited in all samples, might correspond to the hydroxyl group (O-H) stretching of agar participating in the hydrogen bonding in inter and intramolecular bond formation. However, broad bands between 2900 cm^{-1} and 3700 cm^{-1} are also related to the absorption peaks corresponding, respectively, to -C-H and -O-H stretches due to the adsorbed water over the GO surface. The smaller

peaks around 2922 cm^{-1} observed in samples with 70, 75 and 80% of agar are assigned to CH_2 stretching, being found in pure agar samples (LI *et al.,* 2020).

The band at approximately 1710 cm^{-1}, related to the vibration of the bonds in the carboxylic groups existing in both materials. The band at 1635 cm^{-1} assigned to C=O stretching, is also characteristic of pure agar (as it is the characteristic absorption band of polysaccharides), due to stretching vibration of the conjugated peptide bond formed by amine (-NH) and acetone (-CO) groups. The intense bands at ~1035 cm^{-1} observed in all samples, can be related to stretching vibrations of the C-O bonds, specific for epoxide moieties (-C-O-C) in GO samples; and/or correspond to CH_2 scissoring observed in pure agar. Bands at 1066 cm^{-1} are attributed to ester sulfate link vibrations or 3,6-anhydrogalactose bridges. Bands at 1170 cm^{-1}, which corresponds to ester sulfate, are observed in all samples. A characteristic band at 930 cm^{-1} is due to the 3,6-anhydro-α-L-galactopyranose unit in pure agar, being observed in the samples with more agar content. Another typical absorption band of agar is observed at ~877 cm^{-1}, attributed to C-H of β-galactose. The bands at 1150 cm^{-1} are also attributed to ester sulfate link vibrations (GARRIDO *et al.,* 2016; HSIEH, S. *et al.,* 2010; SELVALAKSHMI *et al.,* 2017).

Therefore, shifts in the positions as well as changes in the band's intensity, absence and appearance of new bands could be attributed to the interactions of GO with the polymer matrix, confirming the complex formation between the polymer and the GBM.

From the results of the Raman spectroscopy in Figure 15, it is evident the presence of 2 characteristic bands: G band at ~1590 cm^{-1}, related to the vibration of the sp^2 carbon basal plane, while the D band at ~1350 cm^{-1}, being usually related to defects in the GO sheet. The ratio of D to G band intensities usually is used to evaluate the lattice disorder of carbon-based materials (ARAUJO *et al.,* 2018).

Figure 15 - Raman spectra of the hydrogels.

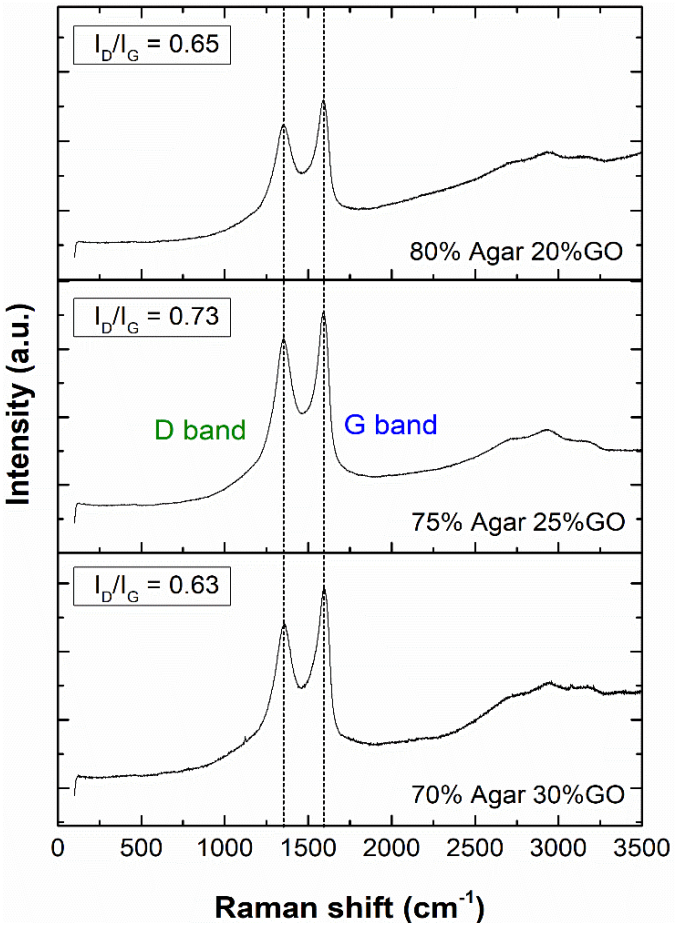

Source: The Author (2022)

From the Raman spectra, it is noted that in general, as more agar is added into the sample, the I_D/I_G ratio decreases from values over 1.20 (in the original GO sample) to values below 0.75. It is worth mentioning that the I_D/I_G ratio gives an idea of the lattice disorder of the material, which is used as an indicative for GBM characterization. For GO samples, this number is normally found between 0.9 – 1.2 (data observed from previous works published by this research group); as for pristine graphite, it is usually bellow 0.4 (ARAUJO *et al.,* 2018, 2020).

TGA curves in Figure 16 exhibit apparent differences between GO and agar-GO. This is because of the polymeric matrix, which in all cases constitute more than 50wt.% of the composite. Both GO and the hydrogel samples presented a significant amount of water, increasing the loss of mass at temperatures close to 100 °C. There are also substantial losses from 200-300 °C, which is when the bonds with the oxygenated groups are broken. On the composite, from 400 °C onwards, the mass

loss continues almost linearly, probably because of the thermal degradation of agar. The remaining mass is due to graphene, which remains stable above 800 °C (WANG *et al.,* 2021).

It is worth mentioning that, in general, the mass of each agar-GO sample reduces to less than 10%, while the GO only reduces to 88% approximately. This occurs because the density of lyophilized graphene-based hydrogels can be extremely small, as reported by Hu *et al.* (2013); therefore, the mass used to perform the analyzes on the microbalance was much smaller, compared to that of the GO compacts.

Figure 16 – TGA results for the hydrogel samples (left); for pure GO (right).

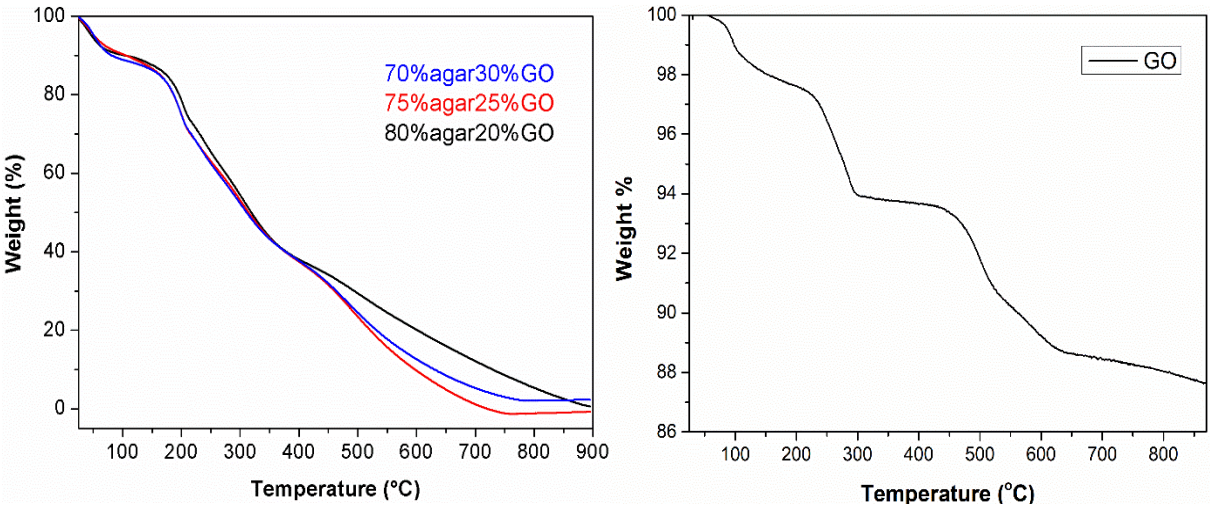

Source: The Author (2022)

From previous works, graphene oxide usually exhibits a rapid weight loss at ~200 ºC, which can be attributed to the removal of different oxygen functional groups present on GO surface. On the other hand, from previous works, it is known that agar has only one major weight loss occuring from 250-350 ºC, assigned to agar decomposition (CHEN *et al.,* 2017).

It is possible to compare the morphology of the samples by analyzing the SEM micrographs Figure 17. For the compacts of GO, it can be seen the slightly undulated arrangement of multilayer compact sheets.

Figure 17 – SEM micrographs with 1000x of magnitude of pure GO (top left); pure agar (top right); and the Agar-GO aerogels samples (botton from the left to the right) with 70% Agar 30%GO, 75% Agar 25%GO, and 80% Agar 20%GO.

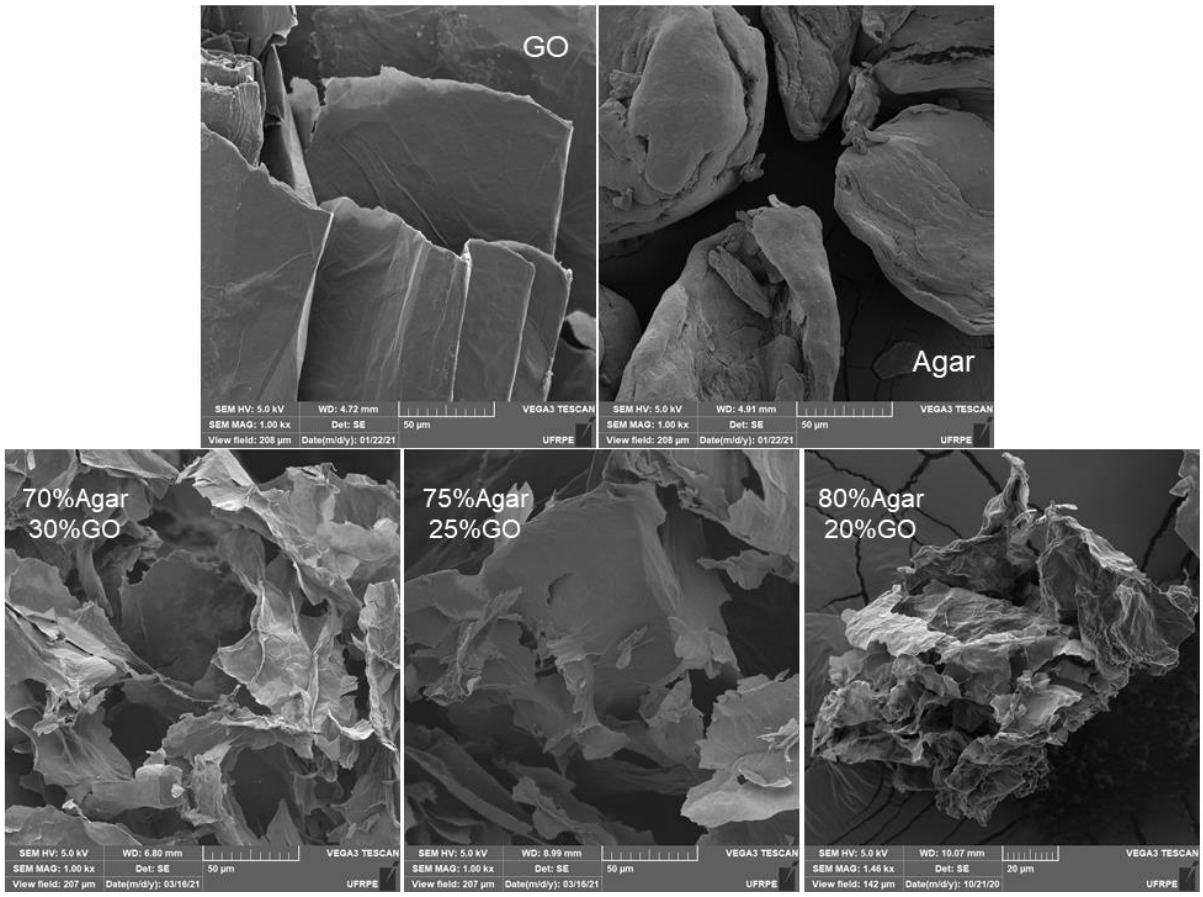

Source: The Author (2022)

On the other side, the organization of pure agar resembles round forms, which will act as the polymeric matrix and provide mechanical stability for the Agar-GO composites seeds. While in the agar-GO composites, there is evidence of wrapped thinner GO sheets, which interacted with the polymer that constitutes the matrix, resulting in airy 3D disordered porous microstructures. That characteristic seems to be more evident for the sample with more agar content (80% agar 20%GO). Chen *et al.* (2017) noted that the Agar-GO aerogels tend to form a 3D porous microstructure consisting of randomly oriented GO nanosheets, confirming the results observed in this work.

The zeta potential measurements of GO suspension and the biocomposite samples are depicted in Figure 18. Overall, for all the samples analyzed, it can be noted the presence of only negative charges in the pH range studied. It was verified

that both GO and agar-GO isoelectric points are below pH = 2. That indicates the surface charges of graphene oxide, as well as the biocomposites are negatively charged at pH ≥2, and adsorption of cationic pollutants can be favored through electrostatic interactions (JANUÁRIO *et al.*, 2022). In addition, the highest negative charge density (-46.80 mV) was observed at pH = 8 for GO.

Evaluating the adsorptive removal of cationic dyes from water using GO, Konicki *et al.* (2017) observed, during the zeta potential measurements, that the surface charge of GO was also negative over the pH range studied - pH from 1.7 to 12.2.

Figure 18 – Zeta potential measurements for GO suspension and agar-GO biocomposite samples (aerogel).

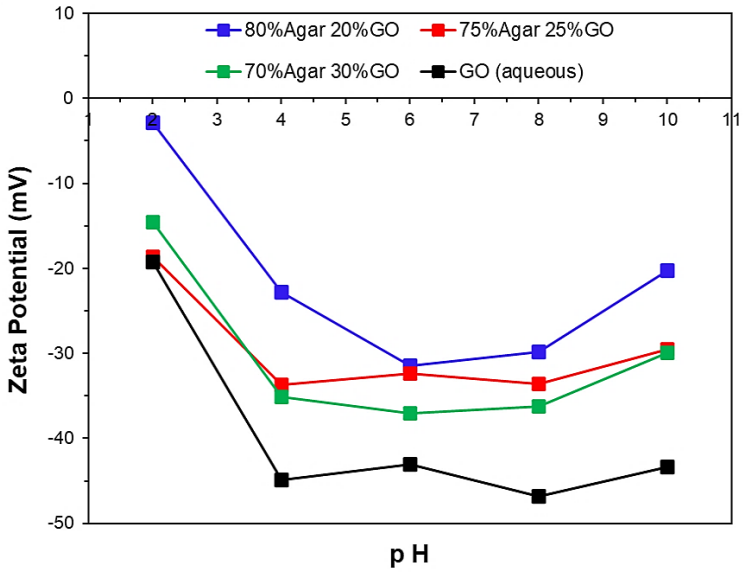

Source: The Author (2022)

These results are also in agreement with what was presented in Figure 11 b, in which the value obtained for the pH_{PZC} of GO-25 sample was 2.37, indicating that the material has a high density of negative charges on its surface.

From the Zeta Potential results, there are indications that the composites developed are likely to be more attracted to compounds with cationic characteristics since the surface of the composites present high negative surface charges.

3.3 FINAL THOUGHTS

It was noted that a small decrease in the amount of acid during GrO production, to a certain extent, led to a lower degree of graphite oxidation, decreasing the number of functional groups on the surface of the material. This, on the other side, enabled a better interaction of the material with anionic dyes, such as BB, via π-π interactions of the aromatic rings. The characterization analyzes of the GO samples (GO-21 and GO-25) revealed that graphite oxidation did indeed occur in both samples. This shows the possibility of reducing the amount of acid used during the synthesis of the material and yet the medium remains favorable for the reaction to occur. Characterization measurements of the biocomposites synthesized using graphene oxide and agar in different proportions revealed evidence of GO interaction with the polymeric matrix, resulting in 3D materials, with visually disordered morphologies for the lyophilized hydrogels. Also, the FTIR spectra indicated that a variety of oxygen functional groups were present in all hydrogel samples produced. Moreover, Zeta potential measurements revealed that the surface of the biocomposites produced, as well as the GO suspension, were negatively charged within a pH rage varying from 2 to 10, which could be an indication that the biocomposites are likely to be more attracted to compounds with cationic nature.

4 BATCH TESTS USING AGAR-GRAPHENE OXIDE HYDROGEL SAMPLES FOR THE SELECTIVE REMOVAL OF DYES

Hydrogel biocomposite samples were synthesized using graphene oxide and agar biopolymer (Agar-GO) to be tested as adsorbents for cationic and anionic dyes. Batch experiments were conducted to evaluate the pH effect in the adsorption process, adsorption isotherms, and kinetics for four cationic dyes – Nile Blue A (NB), Methylene Blue (MB), Malachite Green (MG) and Basic Fuchsin (BF) - and two anionic dyes - Reactive Black 5 (RB5) and Acid Orange 7 (AO7). Adsorption equilibrium isotherms were fitted to Freundlich, Langmuir and Sips models, and kinetic data were adjusted to Driving Force models, and Fick's Diffusion equation. Five cycles of the adsorbents regeneration and reuse were carried out using NaOH solution, and phytotoxicity assays were performed for each dye solution before and after adsorption. The effluent obtained after treatment via adsorption with the hydrogel indicated a decrease in the phytotoxicity, compared to the initial dye solution, for the three plant species studied - *Cucumis sativus, Lepidium sativum*, and *Eruca sativa*. Agar-GO proved to be a viable alternative, as the material also exhibited remarkable regenerative capacity, proving its effectiveness for applications in water and wastewater treatment.

Part of this main topic has been published:

ARAUJO, C. M. B. *et al.* Wastewater Treatment Using Recyclable Agar-graphene Oxide Biocomposite Hydrogel in Batch and Fixed-bed Adsorption Column: Bench Experiments and Modeling for the Selective Removal of Organics. **Colloids and Surfaces A: Physicochemical and Engineering Aspects**, v. 639, p. 128357, 2022.

4.1 METHODOLOGY

Graphene oxide aqueous suspension was produced in the Laboratories of the Research Group on Environmental Technologies and Processes (GPTA), located at the Federal University of Pernambuco (UFPE, Brazil). All batch experiments described in this topic were performed in the Laboratory of Separation and Reaction Engineering - Laboratory of Catalysis and Materials (Associated Laboratory LSRE-LCM), at the Faculty of Engineering of the University of Porto (FEUP, Portugal).

4.1.1 Materials

GO was produced using analytical grade graphite powder (Synth, Brazil), $KMnO_4$ (Química Moderna, Brazil), and H_2SO_4 (AnalaR NORMAPUR VWR Chemicals, France). Agar-GO hydrogel samples were synthesized using the analytical grade agar powder for laboratory and industrial use, acquired from Anidrol (Brazil), and used without further purification. The methodologies involving the synthesis of GO, as well as the production process of the hydrogels, are described in detail in Topic 3.

For the batch adsorption tests, the dyes used - MB, NB, MG, BF, AO7 and RB5 - were purchased from Merck (Germany) and used without further purification. Stock solutions (1000 $mg.L^{-1}$) of each dye were prepared by dissolving a certain amount of the dye in deionized water, and kept in sealed glass flasks covered in aluminum foil.

Figure 19 exhibits the chemical structure of both anionic and cationic dyes used. Table 3 shows some technical information of the dyes. HCl 1 $mol.L^{-1}$ and NaOH 1 $mol.L^{-1}$ (PanReac AppliChem, Portugal) were used for pH adjustment.

Figure 19 - Chemical structure of the dyes

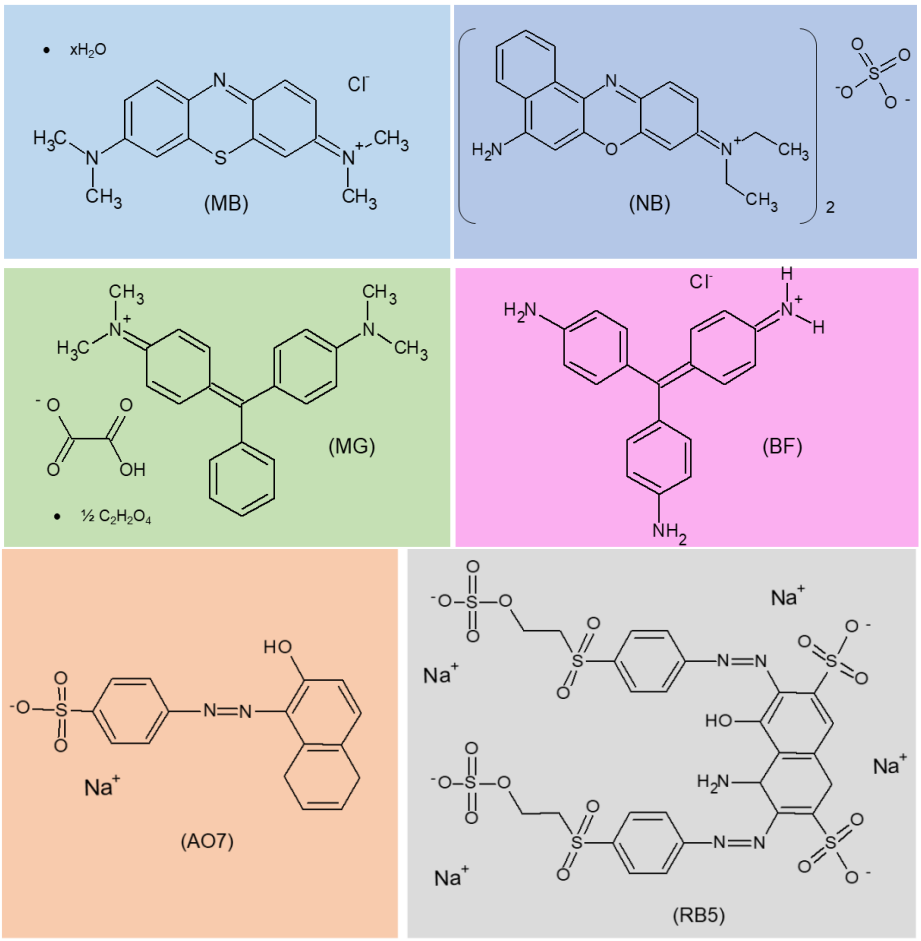

Source: The Author (2022)

Table 3 - Technical information of the dyes tested.

Dye	Alternative name	Chemical formula	Molecular weight ($g.mol^{-1}$)	λ_{max} (nm)	CAS number	Color Index
Methylene Blue	Basic Blue 9	$C_{16}H_{18}ClN_3S \cdot xH_2O$	319.85	663	122965-43-9	52015
Nile Blue A	Basic Blue 12	$2C_{20}H_{20}N_3O \cdot SO_4$	732.85	635	3625-57-8	51180
Basic Fuchsin	Basic Red 9	$C_{19}H_{17}N_3 \cdot HCl$	323.82	541	569-61-9	42500
Malachite Green	Basic Green 4	$C_{23}H_{25}N_2 \cdot C_2HO_4 \cdot 0.5C_2H_2O_4$	463.50	617	2437-29-8	42000
Acid Orange 7	Orange II	$C_{16}H_{11}N_2NaO_4S$	350.32	485	633-96-5	15510
Reactive Black 5	Remazol Black B	$C_{26}H_{21}N_5Na_4O_{19}S_6$	991.82	597	17095-24-8	20505

Source: The Author (2022)

4.1.2 Batch adsorption experiments

Batch adsorption tests were carried out using the samples produced with 80w% agar and 20w% GO, 75w% agar and 25w% GO, 70w% agar and 30w% GO, as adsorbents. The hydrogel samples were tested for all the cationic and anionic dyes in replicate. Before proceeding with the batch tests, UV-Visible scan (Spectroquant Prove 300) of the dyes were obtained at different pH values, as well as each respective calibration curve. The final and initial concentrations were determined in a UV-Vis spectrophotometer according to the λ_{max} values presented in Table 3.

Preliminary kinetic experiments were carried out to verify the time in which the batch adsorption systems reached equilibrium. To perform the batch experiments, aliquots of 50 mL of each dye solution (with pH previously adjusted when necessary) and initial concentrations of 50 $mg.L^{-1}$ for RB5, 30 $mg.L^{-1}$ for AO7, 20 $mg.L^{-1}$ for NB, 10 $mg.L^{-1}$ for MB, MG, and BF, were added to flasks containing 0.20 g of the wet agar-GO hydrogel, which is equivalent to approximately 0.0043 g of adsorbent on a dry basis. The sealed flasks were placed under constant stirring of 250 rpm at 24 °C. The overall contact time was 48 h for BR5, AO7, MB and NB, and 24 h for MG and BF to ensure the equilibrium was reached (CHEN *et al.,* 2017). The supernatant solution was analyzed after 1-2 min decantation, without filtration or centrifugation.

To obtain the dye concentration, a UV-Visible spectrophotometer (Jasco 7800) was used. To evaluate the effect of changing the initial pH of the dye solutions, adsorption tests were done in that conditions, varying the pH in each case. The initial pH values of the solutions were adjusted using 1 $mol.L^{-1}$ NaOH and HCl solutions.

For the regeneration and reuse of the adsorbent, 1 g of the wet agar-GO hydrogel was added into 50 mL of the respective dye solution and placed under constant stirring at 24 ^{o}C. The final concentration was recorded, and the adsorbent was separated by decantation. After that, for the desorption tests, the adsorbent used was added into 50 mL of 0.30 M NaOH for 2 h and 250 rpm stirring. Samples were washed 5 times with deionized water after desorption to remove the residual NaOH, so that pH =7. The relative adsorption capacity q_n/ q_0 was calculated for each cycle (n) (CHEN *et al.,* 2017).

4.1.2.1 Adsorption equilibrium and isotherms modeling

Equilibrium adsorption isotherms were obtained for the 3 hydrogel samples at 24°C. Tests were conducted at 24 °C, and the initial pH was adjusted according to the best conditions after evaluating the effect of the initial pH. Initial pH values were adjusted using NaOH and HCl solutions and a bench pH meter. The isotherms were built by ranging the mass of the hydrogels, keeping constant the initial concentration and volume of dye solutions. Tests were proceeded using sealed glass flasks under constant stirring (250 rpm). The conditions for the isotherm experiments are exhibited in Table 4.

Table 4 – Conditions for the isotherm experiments.

Dye	Contact time (h)	Initial pH	Initial concentration ($mg.L^{-1}$)	Wet agar-GO mass (g)
Methylene Blue	48	8	10	0.05, 0.1, 0.2, 0.3, 0.5, 0.8
Nile Blue A	48	8	20	0.05, 0.1, 0.2, 0.3, 0.5, 0.8
Basic Fuchsin	24	6	10	0.05, 0.1, 0.2, 0.3, 0.5, 0.8
Malachite Green	24	6	10	0.05, 0.1, 0.2, 0.3, 0.5, 0.8

Source: The Author (2022)

Using the experimental data, the adsorption capacity in batch could be calculated by Equation 2, in which q is the amount of dye adsorbed in mg per g of adsorbent; C_0 and C_f are the initial and final concentrations of the dye solution, $mg.L^{-1}$; m_{ads} is the adsorbent mass in g, and V_L is the volume of the solution in L.

$$q = \frac{(C_0 - C_f).V_L}{m_{ads}} \quad (2)$$

Adsorption equilibrium data obtained experimentally for each dye were fitted to the isotherms of Langmuir (Equation 3), Freundlich (Equation 4) and Sips (Equation 5) in the non-linear format of each model (ABBASI *et al.*, 2021).

$$q_e = \frac{q_{max}.K_L.C_e}{1+K_L.C_e} \quad (3)$$

$$q_e = K_F.C_e^{1/n} \quad (4)$$

$$q_e = \frac{q_s.K_s.C_e^m}{1+K_s.C_e^m} \quad (5)$$

From the equations, q_e represents the amount of dye adsorbed when the equilibrium is reached ($mg.g^{-1}$), C_e is the dye concentration in the equilibrium ($mg.L^{-1}$). K_F ($mg^{1-(1/n)}.(g^{-1}).L^{1/n}$) is the Freundlich adsorption constant, and *n* is the heterogeneity factor. K_L is the Langmuir adsorption constant ($L.mg^{-1}$), and q_m is the maximum adsorption capacity ($mg.g^{-1}$) predicted by the model. K_S $(L.mg^{-1})^m$ and *m* are the Sips adsorption constants, in which q_s is the maximum adsorption capacity ($mg.g^{-1}$) predicted by the Sips isotherm.

4.1.2.2 Adsorption kinetics and modeling

Preliminary batch kinetic tests were carried out to verify the time in which the adsorption systems reached equilibrium, and which systems have greater adsorptive capacities under the studied conditions.

To perform the experiments, aliquots of 50 mL of each dye solution, with initial concentrations of 30 $mg{\cdot}L^{-1}$ AO7, 50 $mg{\cdot}L^{-1}$ RB5, 20 $mg{\cdot}L^{-1}$ NB, and 10 $mg{\cdot}L^{-1}$ MB, MG and BF were added to flasks containing 0.20 g of the respective hydrogel samples. The sealed flasks were placed under constant stirring of 250 rpm at 24°C without pH correction. Aliquots of the supernatant were taken, and the respective concentrations were estimated at each time interval.

To find out the adsorption kinetic parameters, tests were repeated under the same conditions adjusting the pH according to the results from the experiments evaluating the effect of the initial pH.

The experimental data obtained during the batch kinetic experiments were modeled following a phenomenological approach. Therefore, the diffusivity parameters were obtained by solving a system of differential equations. Equation 6 represents the mass balance in a batch adsorption tank. The initial condition is t =0 → C =C_0 → $\bar{q}$ =0. Equation 7 is regarding the Linear Driving Force (LDF), and Equation 8 is the Quadratic Driving Force (QDF) expressions.

$$V_L.\frac{dC}{dt} + m_{ads}.\frac{d\bar{q}}{dt} = 0 \quad (6)$$

$$\frac{d\bar{q}}{dt} = k_h(q_e - \bar{q}) \quad (7)$$

$$\frac{d\bar{q}}{dt} = k_h\frac{(q_e{}^2 - \bar{q}^{\,2})}{2\bar{q}} \quad (8)$$

With $\bar{q}$ being the average adsorbate concentration in the particle; q_e the adsorbed concentration in equilibrium with the fluid concentration at a given instant – it can be obtained from the isotherm model; and k_h the intraparticle mass transfer coefficient. Using k_h, the effective homogeneous diffusivity (*Dif*) can be estimated, with *R* as the particle radius (RIOS *et al.*, 2020). *Dif* value is given by Equation 9 for LDF model, and Equation 10 for QDF model (SIRCAR; HUFTON, 2000).

$$D_{if\ LDF} = \frac{k_h.R^2}{15} \tag{9}$$

$$D_{if\ QDF} = \frac{k_h.R^2}{9.14} \tag{10}$$

Another method for obtaining the diffusivity inside the particle is through the Fickian Diffusion (FD) model, which consists of doing the mass balance for a control volume inside the particle (Equation 11). The boundary conditions are r =0 → ∂q/ ∂r =0; r =R → q =q*; and the initial condition is t =0 → q(r) =0.

$$\frac{\partial q}{\partial t} = \frac{D_{if}}{r^2}.\frac{\partial}{\partial r}\left[r^2.\left(\frac{\partial q}{\partial r}\right)\right] \tag{11}$$

In general, the driving force models describe the mass transfer inside the adsorbent, and besides the ease of finding the solution numerically, these models require less computational effort, compared to FD model (PEEL; BENEDEK, 1981; RIOS *et al.*, 2020; RODRIGUES; SILVA, 2016; SIRCAR; HUFTON, 2000).

The quality of the kinetic models fitting to the experimental data was analyzed using coefficient of determination (R^2), calculated by Equation 12.

$$R^2 = 1 - \frac{\sum_{i=1}^{N}(Yi - \hat{Y}_i)^2}{\sum_{i=1}^{N}(Yi - \bar{Y})^2} \tag{12}$$

Being N the total number of experimental points, Yi the value observed experimentally, $\hat{Y}$i the value predicted by the model, and $\bar{Y}$ the mean of experimental values (ANDRADE *et al.*, 2020).

4.1.3 Phytotoxicity assays

The knowledge of toxic effects of pollutants is a key requirement for environmental risk assessments, especially for processes involving the use of nanomaterials, which in turn may represent a source of secondary contamination in water and wastewaters (MAÑAS; DE LAS HERAS, 2018).

Therefore, to assess whether the graphene oxide present in the hydrogel is leached during adsorption, possibly affecting water quality in the water bodies, phytotoxicity tests were carried out. For the assays, three types of vegetable seeds were used: cucumber (*Cucumis sativus*), cress (*Lepidium sativum*), and arugula (*Eruca sativa*). The methodology used for the tests was based on Mendes *et al.* (2016), Gerber *et al.* (2017) and Baptisttella *et al.* (2020). The bioassays were conducted for the cationic dyes (MB, NB, MG, and BF) before and after the batch adsorption tests.

Firstly, adsorption tests were proceeded for the initial dye concentrations of 20 $mg{\cdot}L^{-1}$ NB, and 10 $mg{\cdot}L^{-1}$ MB, MG, and BF, using 50 mL of each dye solution and 0.20 g of the wet hydrogel produced with 80% Agar and 20%GO. The flasks were placed under constant stirring of 250 rpm at 24°C for 48 h. The supernatants were collected after 1-2 min decantation.

Therefore, Petri dishes were lined at their base and sides with qualitative filter paper, and 5 cucumber seeds were placed spaced apart on each dish. For the tests with watercress and arugula seeds, 10 seeds were placed on each respective dish. 4 mL of each dye solution, before and after treatment; as well as the negative control (distilled H_2O), and positive control ($Al_2(SO_4)_3$) were placed in different petri dishes. Assays were done in replicate. Each petri dish was placed in an incubator wrapped in foil to prevent humidity loss, where they were stored for 120 h at 22.5 ± 2.5 °C, protected from light. After 5 days, the dishes were taken from the incubator and the roots sizes of the germinated seed were measured using a transparent ruler, and the number of germinated seeds were counted. It was assumed the negative control was valid only when the percentage of germination was ≥90% (SOBRERO; RONCO, 2004).

From the results, the relative growth index (RGI) was estimated by Equation 13, and the germination index (GI) by Equation 14. From the equations, the total root length in the sample is RLS, the total root length in the negative control is RLC, the number of germinated seeds in the sample is GSS and the number of germinated seeds in the negative control is GSC (BAPTISTTELLA *et al.*, 2020).

$$RGI = \frac{RLS}{RLC} \tag{13}$$

$$GI = RGI.\frac{GSS}{GSC}.100\% \tag{14}$$

4.2 RESULTS AND DISCUSSION

Results regarding the application of agar-GO nano-biocomposites as adsorbents to remove cationic and anionic dyes in batch process will be addressed and discussed in this section.

4.2.1 Preliminary kinetics

The results obtained for the preliminary adsorption kinetics of the six dyes, using the three hydrogel samples produced, are shown in Figure 20. In the figure it is possible to see, in each case, the evolution of the adsorptive capacity with time. It is also noted that the anionic dyes (AO7 and RB5) showed much lower adsorptive capacities when compared to the values obtained for the cationic dyes NB, MB, MG, and BF.

Figure 20 – Preliminary adsorption kinetics for the three hydrogel samples produced (Conditions: m_{ads}= 0.20 g (~0.004 g dry basis); V_L= 50 mL; T= 24 ºC; 250 rpm; without pH adjustment).

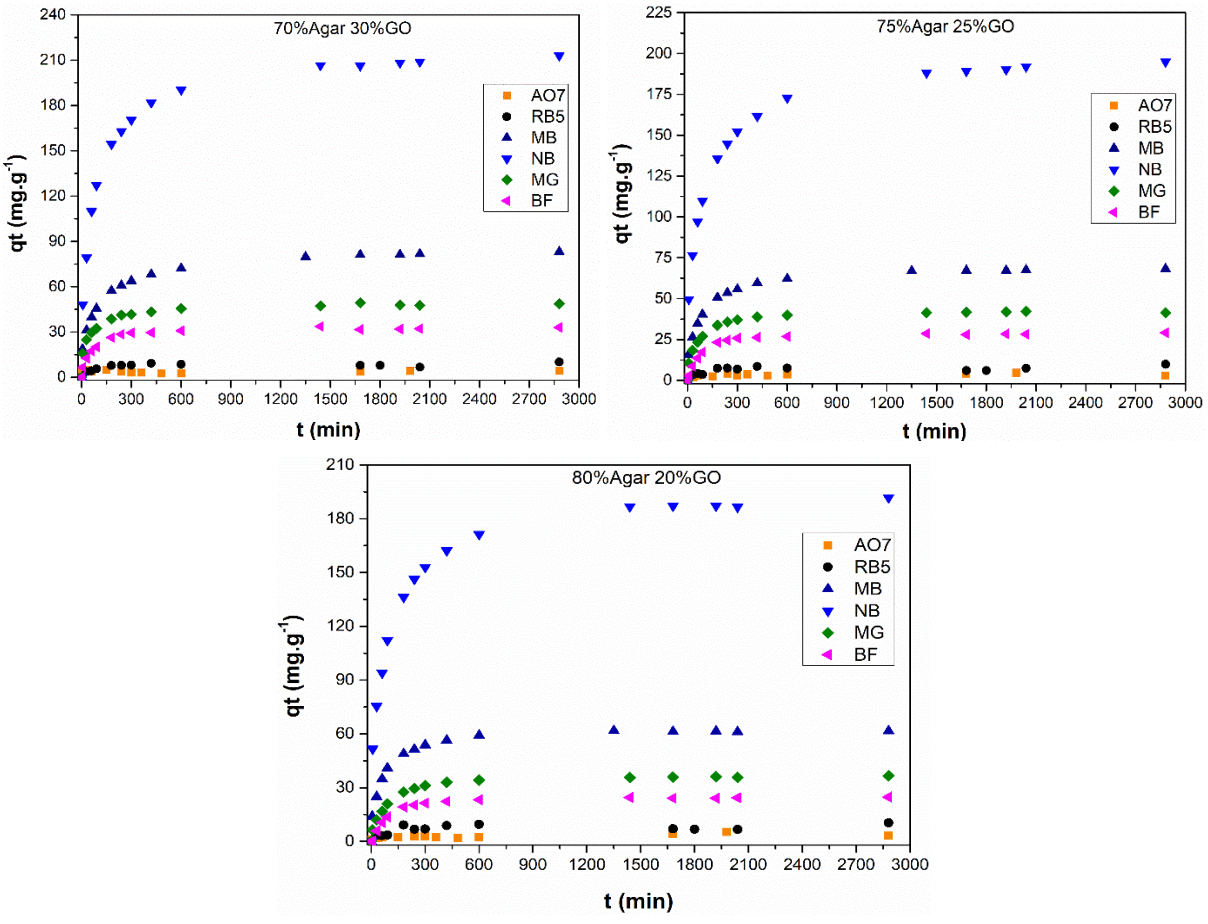

Source: The Author (2022)

By analyzing and comparing the results of the three hydrogel samples, it is noted that the greater the amount of GO in the composite, the greater the adsorption capacity achieved for the cationic dyes when reaching equilibrium. This difference is even more expressive in the case of the sample produced with 70% agar and 30% GO. Regarding the anionic dyes, there is almost no difference between samples.

From the graphs, it is also noted that for MG and BF, the adsorption capacity values increase faster within the first 300 min of the experiment, and from there, q_t becomes slower, until it reaches equilibrium. On the other side, for MB and NB, the adsorption capacities increase rapidly in the first 600 min, and from that point, the increases become smoother, tending to the equilibrium. In general, it was observed that 24 h was sufficient to guarantee a steady state for MG and BF, and 48h was enough time to guarantee the equilibrium of adsorption for NB and MB.

Similar behavior was noticed by Duman and coworkers for MB adsorption by agar/κ-carrageenan hydrogel. In their experiments, the adsorption by the hydrogel demonstrated a rapid increase during the first 210 min. That was attributed to the presence of many adsorption sites on the adsorbent, then gradually decreased. In that occasion, the equilibrium was also ensured within 48 h (DUMAN *et al.,* 2020).

4.2.2 Influence of the initial pH

Results to assess the influence of varying the initial pH of the dye solutions are shown in Figure 21. In this case, it is essential to mention that the pH range used in each case was different, being some of them larger and others more restricted. The dyes BF and MG, for example, which exhibit similar structures, have strong pH dependence (ADEYI *et al.,* 2020). Das et al. say that depending on pH, the dye salt and its carbinol form are interconvertible between them, and the MG aqueous solutions does not show any color at extremely high pH. This effect can be easily re-converted by decreasing the pH (DAS *et al.,* 2009).

The same effect could be observed for BF experimentally. For the NB, it was noticed that there was a shift in its characteristic wavelength for extremely high pH, as exhibited in Figure 22. This phenomenon is known as hypsochromic shift and consists of the peak's shift to a shorter wavelength, caused by the removal of conjugation or a change in the polarity of the solvent.

It is observed that the three Agar-GO samples tested showed similar behavior for all dyes evaluated. Analyzing the results obtained for both anionic dyes indeed, the adsorptive capacities obtained within the evaluated pH range presented very low values, especially when compared to the values obtained for the cationic dyes. There is only a slight increase in q_e when the pH goes from 4 to 2. However, working conditions where pH =2 can be challenging from an operational point of view.

Figure 21 - Influence of the initial pH in the adsorptive capacity of Agar-GO for the removal of the dyes with C_0 = 10 mg.L^{-1} (MB, MG, BF), and 20 mg.L^{-1} (NB) (Experimental conditions: $V_{sol.}$ = 50 mL; T = 24 ^{o}C; 250 rpm; over 24h of contact time).

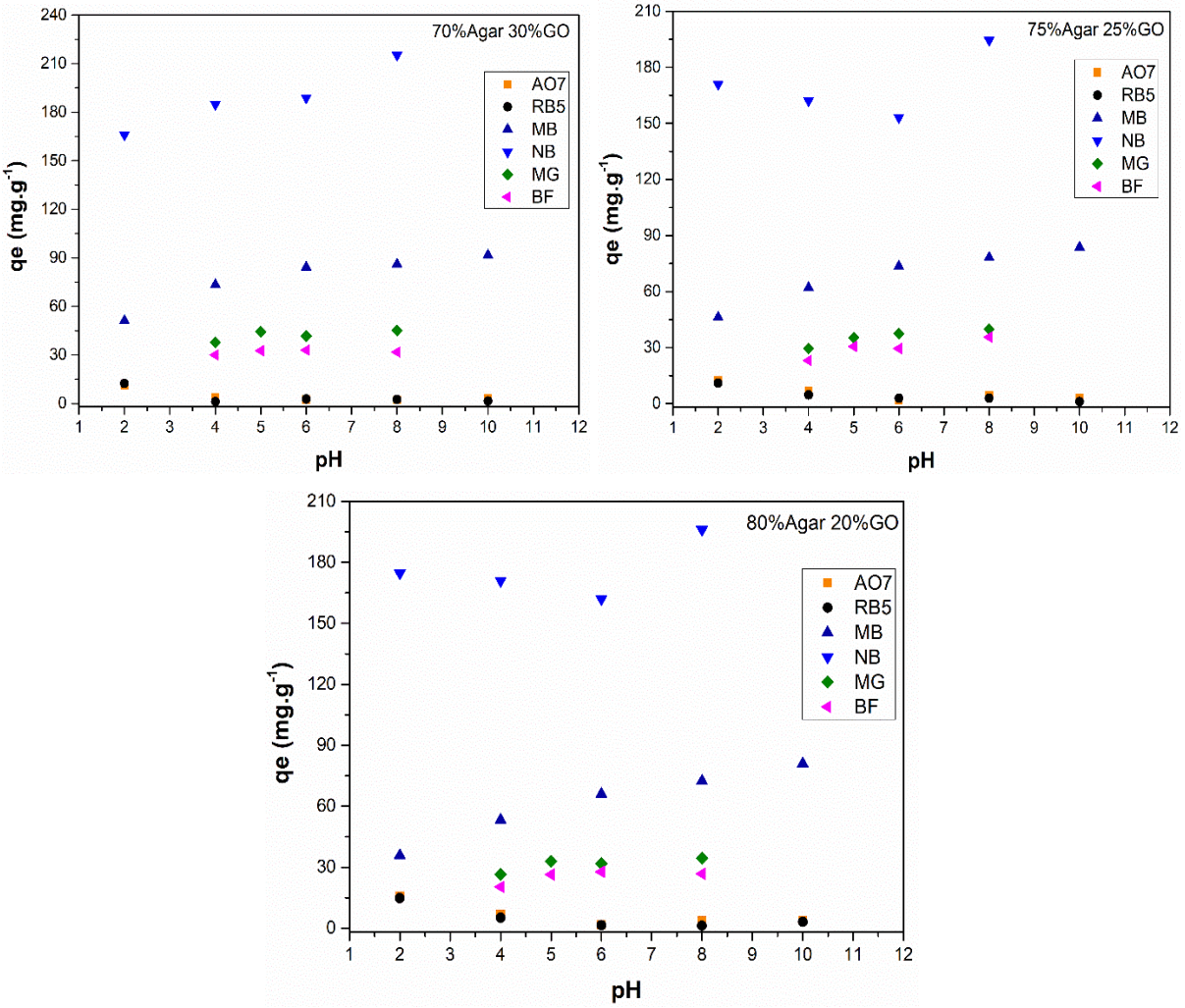

Source: The Author (2022)

Figure 22 - UV-Visible scan of the dyes (left), and hypsochromic shift for NB dye at higher pH (right).

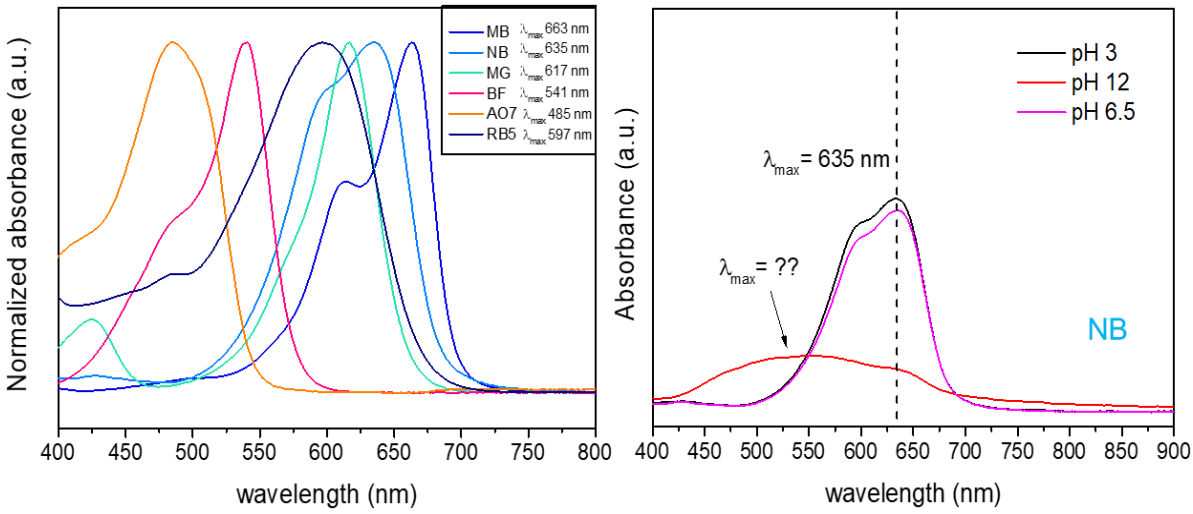

Source: The Author (2022)

Figure 21 also shows practically no change in adsorptive capacity when varying the pH of BF and MG solutions within the studied range. Studying the production and application of granular composite hydrogels via in-situ polymerization using chitosan and other components, Zheng, Zhu, and Wang (2014) suggested that, even varying the initial pH of the MG solution, the carboxylic groups present in the polymer matrix were dissociated during the adsorption. Thus, a constant adsorption capacity was noted when the initial pH ranged from 4 to 8.

Adeyi *et al.* (2020) also did not find significant changes in MG adsorption by ranging the pH of dye solution, inferring that MG adsorption is attributed to electrostatic forces and other interactions, such as hydrophobic interactions.

Overall, it was observed that the adsorptive capacity grows gradually, as the pH increases for MB dye. This behavior was previously observed by Chen *et al.* (2017) when analyzing the effect of the initial pH on the adsorption of methylene blue by graphene-based materials. While for the NB, the effect of the pH change was more significantly noticed when the value is increased from 6 to 8. That could be related to the adsorbent charge and molecular charge of adsorbate.

Therefore, in subsequent tests, it was decided to work with pH = 8 for methylene blue and Nile blue A solutions; while for malachite green and basic fuchsin, tests were proceeded without adjusting the initial pH. Since the preliminary

kinetics tests and the pH study with the anionic dyes did not show satisfactory results regarding the adsorption capacity, it was decided to proceed with the batch adsorption study only for the cationic dyes from now on.

4.2.3 Adsorption equilibrium isotherms

Figure 23 depicts the adsorption equilibrium isotherms obtained experimentally for the cationic dyes. Results for the respective adjustments to Langmuir, Freundlich, and Sips isotherms are also shown in Figure 23, for each hydrogel sample. The fitting of the isotherms parameters for modeling the equilibrium data were analyzed using non-linear data regression. Data regarding the non-linear modeling are presented in Tables 5, 6, and 7.

Figure 23 - Adsorption equilibrium isotherms on a dry basis for the cationic dyes (Experimental conditions: t = 48 h; $V_{sol.}$ = 50 mL; T = 24 ºC; 250 rpm stirring).

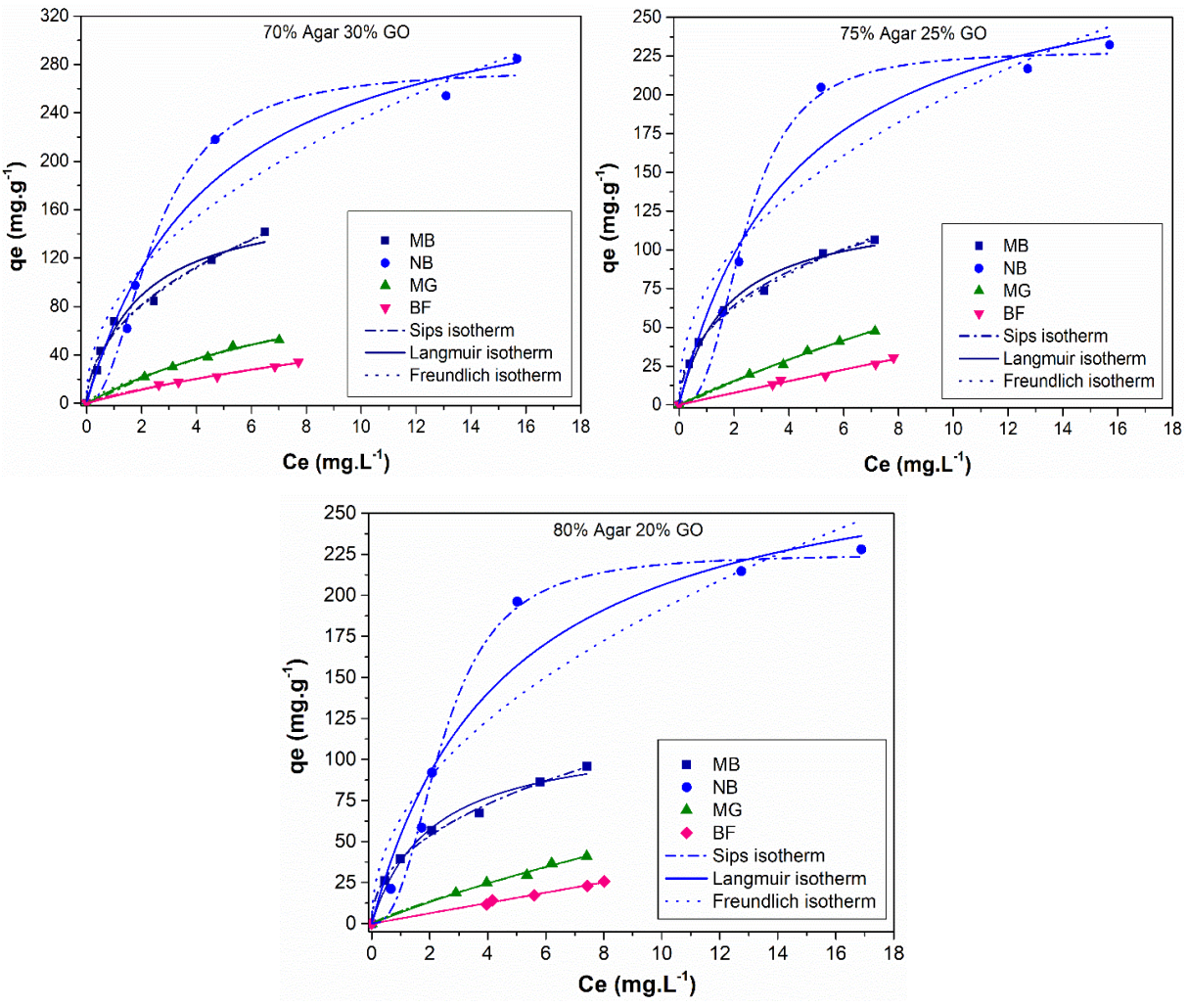

Source: The Author (2022)

Table 5 - Adsorption isotherm parameters for the hydrogel sample 70% Agar 30% GO (on a dry basis) calculated by adjusting the experimental data.

Isotherm	Parameters	MB		NB		MG		BF	
		Result	Std. Error	Result	Std. Error	Result	Std. Error	Result	Std. Error
Experimental	$q_{max}(mg.g^{-1})$	141.48	-	284.69	-	52.29	-	34.00	-
Freundlich	K_F ($mg^{1-(1/n)}$. (g^{-1}). $L^{1/n}$)	57.68	3.39	81.11	19.53	13.32	1.25	6.89	0.45
	n	2.10	0.17	2.17	0.47	1.39	0.11	1.29	0.06
	Reduced-χ^2	41.82	-	$1.1\ 10^3$	-	3.07	-	0.48	-
	Adjusted-R^2	0.98	-	0.92	-	0.99	-	0.99	-
Langmuir	$q_{max}(mg.g^{-1})$	170.85	15.90	362.75	42.19	135.92	21.97	110.49	23.64
	$K_L(L.mg^{-1})$	0.55	0.14	0.22	0.07	0.09	0.02	0.06	0.02
	Reduced-χ^2	73.25	-	533.71	-	2.10	-	0.83	-
	Adjusted-R^2	0.97	-	0.96	-	0.99	-	0.99	-
Sips	q_S ($mg.g^{-1}$)	708.87	$2.2\ 10^3$	273.74	12.70	93.76	40.78	1000.0	$2.1\ 10^4$
	K_S $(L.mg^{-1})^m$	0.09	0.31	0.15	0.04	0.12	0.03	$6.9\ 10^{-3}$	0.15
	m	0.54	0.24	2.09	0.38	1.23	0.38	0.79	0.42
	Reduced-χ^2	51.33	-	163.12	-	2.48	-	0.68	-
	Adjusted-R^2	0.98	-	0.99	-	0.99	-	0.98	-

Source: The Author (2022)

Table 6 - Adsorption isotherm parameters for the hydrogel sample 75% Agar 25% GO (on a dry basis) calculated by adjusting the experimental data.

Isotherm	Parameters	MB		NB		MG		BF	
		Result	Std. Error	Result	Std. Error	Result	Std. Error	Result	Std. Error
Experimental	$q_{max}(mg.g^{-1})$	106.32	-	232.26	-	47.59	-	30.37	-
Freundlich	K_F ($mg^{1-(1/n)}$. (g^{-1}). $L^{1/n}$)	46.15	1.63	74.09	20.31	8.57	0.81	4.07	0.71
	n	2.30	0.12	2.31	0.62	1.14	0.07	1.04	0.10
	Reduced-χ^2	8.82	-	$1.0\ 10^3$	-	1.58	-	1.61	-
	Adjusted-R^2	0.99	-	0.89	-	0.99	-	0.99	-
Langmuir	$q_{max}(mg.g^{-1})$	128.10	7.93	301.45	41.57	278.00	116.58	803.77	$2.9\ 10^3$
	$K_L(L.mg^{-1})$	0.57	0.10	0.24	0.09	0.03	0.01	$4.8\ 10^{-3}$	0.02
	Reduced-χ^2	22.16	-	557.94	-	1.46	-	1.66	-
	Adjusted-R^2	0.98	-	0.94	-	0.99	-	0.99	-
Sips	q_S ($mg.g^{-1}$)	261.74	143.50	228.21	6.27	153.21	200.03	500.0	$1.3\ 10^4$
	K_S $(L.mg^{-1})^m$	0.22	0.14	0.10	0.03	0.05	0.05	$8.0\ 10^{-3}$	0.20
	m	0.59	0.12	2.63	0.37	1.13	0.43	1.00	1.12
	Reduced-χ^2	7.65	-	57.58	-	1.88	-	2.23	-
	Adjusted-R^2	0.99	-	0.99	-	0.99	-	0.98	-

Source: The Author (2022)

Table 7 - Adsorption isotherm parameters for the hydrogel sample 80% Agar 20% GO (on a dry basis) calculated by adjusting the experimental data.

Isotherm	Parameters	MB		NB		MG		BF	
		Result	Std. Error	Result	Std. Error	Result	Std. Error	Result	Std. Error
Experimental	$q_{max}(mg.g^{-1})$	95.71	-	228.04	-	41.04	-	25.72	-
Freundlich	K_F ($mg^{1-(1/n)}$. (g^{-1}). $L^{1/n}$)	39.24	1.06	63.98	16.76	7.61	0.82	3.18	0.44
	n	2.25	0.09	2.10	0.48	1.19	0.09	1.00	0.07
	Reduced-χ^2	3.42	-	$1.1\ 10^3$	-	1.34	-	0.63	-
	Adjusted-R^2	0.99	-	0.88	-	0.99	-	0.99	-
Langmuir	$q_{max}(mg.g^{-1})$	116.57	8.56	299.57	38.60	194.83	77.86	$5.3\ 10^3$	$1.1\ 10^5$
	$K_L(L.mg^{-1})$	0.48	0.10	0.22	0.08	0.04	0.02	$6.0\ 10^{-4}$	0.01
	Reduced-χ^2	21.72	-	493.13	-	1.43	-	0.64	-
	Adjusted-R^2	0.98	-	0.95	-	0.99	-	0.99	-
Sips	q_S ($mg.g^{-1}$)	$1.2\ 10^3$	$5.2\ 10^3$	225.36	7.41	$8.8\ 10^3$	$1.8\ 10^6$	$2.6\ 10^3$	$3.9\ 10^5$
	K_S ($L.mg^{-1})^m$	0.03	0.15	0.11	0.03	$8.6\ 10^{-4}$	0.17	$1.2\ 10^{-3}$	0.17
	m	0.47	0.11	2.81	0.39	0.85	0.58	1.00	1.04
	Reduced-χ^2	4.35	-	34.76	-	1.82	-	0.86	-
	Adjusted-R^2	0.99	-	0.99	-	0.99	-	0.99	-

Source: The Author (2022)

Overall, the highest values of adsorption capacity were exhibited for NB, followed by MB, MG, and BF. In general, all the isotherms exhibited an increase in the adsorption capacity, as the equilibrium concentration gradually increased. Considering that the hydrogels produced consists of approximately 98% humidity, the maximum adsorption capacities values, obtained experimentally, were for the hydrogel sample with 70% Agar and 30% GO (on a dry basis).

Studying the sono-assisted adsorption of MB and NB by a magnetic composite synthesized from date stones (Phoenix dactylifera) and nanoparticles of cobalt in ferrite ($AC/CoFe_2O_4$), Foroutan and coworkers (2019) also noted that the adsorption process for these compounds was favorable. However, only for higher pH values the maximum adsorption capacity (86.24 $mg.g^{-1}$ for NB, and 87.48 $mg.g^{-1}$ for MB) was reached. Even so, these values are lower compared to those found in the present work.

On the other hand, MB and MG adsorption on perlite and alginate-coated perlite beads, evaluated by Parlayici, reported adsorption capacities for MB equal to

6.65 $mg.g^{-1}$ and 104.2 $mg.g^{-1}$ for perlite and alginate-coated perlite, respectively. As for MG, the adsorption capacities achieved were 3.87 $mg.g^{-1}$ for perlite and 74.63 $mg.g^{-1}$ for the alginate-coated perlite (PARLAYICI, 2019).

Siddiqui and coworkers observed experimental q_e values near 110 $mg.g^{-1}$, and a maximum adsorption capacity, predicted by the Langmuir model, of 184 $mg.g^{-1}$ at 30 ^oC when investigating NB adsorption onto the MoO_3/polypyrrole nanocomposite (SIDDIQUI; KHAN; ALAM KHAN, 2019). These values are lower than the present work (on a dry basis) for NB dye, under similar conditions.

For all the hydrogel samples studied, the graphs in Figure 23 and the Tables show that NB equilibrium data better adjusted to the Sips isotherm. In this case, the compatibility of Sips isotherm indicates the combined features of Freundlich and Langmuir equations (NAYAK; PAL, 2020). Investigating the use of overripe Abelmoschus esculentus seeds as an adsorbent to remove NB from aqueous medium, Nayak and Pal found that indeed, the adsorption isotherm that better represented the equilibrium process was Sips model.

Overall, by evaluating and comparing the adjusted-R^2 values, all the experimental data seem to have adjusted well to the Sips model. However, except for NB, the standard error values were very high - sometimes they were even higher than those predicted for the variables. Thus, it is inferred the data showed better adjustment to the Freundlich isotherm for MB, MG, and BF dyes. Freundlich parameter n indicates the type of isotherm. Therefore, if $n > 1$ adsorption is favorable, and if $n < 1$ the process it is unfavorable. In all cases, n values were above 1, confirming the spontaneous nature of the adsorption (AL-GOUTI; DA'ANA, 2020).

In Figure 23, it is noted that the isotherms of the MG and BF dyes have formats that resemble linear isotherms, which are the simplest adsorption case where the amount adsorbed is directly proportional to the solute concentration in the mobile phase (RANA *et al.,* 2019). This can also be observed in the values of n obtained for the Freundlich model - in all cases, the values were very close to 1, especially for the BF dye. From the Freundlich equation, when $n \rightarrow 1$, the isotherm tends to be $q_e = K_F.C_e$, which indicates a straight line.

From the Tables, it is noted that MB also demonstrated a satisfactory fit to the Langmuir model. Chen and coworkers (2017) produced an Agar-GO aerogel by

vacuum freeze-drying, for the adsorptive removal of MB dye. They observed that the adsorption isotherm data were best fitted to Freundlich model, although the R^2 values for Langmuir and Freundlich isotherms were quite close to each other, being both over 0.98. Thus, the results found in the present work are in agreement with the literature.

4.2.4 Modeling of adsorption kinetics

Adsorption kinetic curves are depicted in Figures 24, 25 and 26 for the cationic dye's adsorption using the hydrogel samples - 70%Agar 30%GO, 75%Agar 25%GO, and 80%Agar 20%GO.

Figure 24 - Kinetics for the cationic dyes adsorption onto the hydrogel (70%Agar 30%GO) on a dry basis (Experimental conditions: $m_{ads.}$= 0.20 g hydrogel (0.00417g dry basis); $V_{sol.}$= 50 mL; T= 24 ºC; 250 rpm; pH =8 for MB, NB, and pH~ 6 for BF and MG).

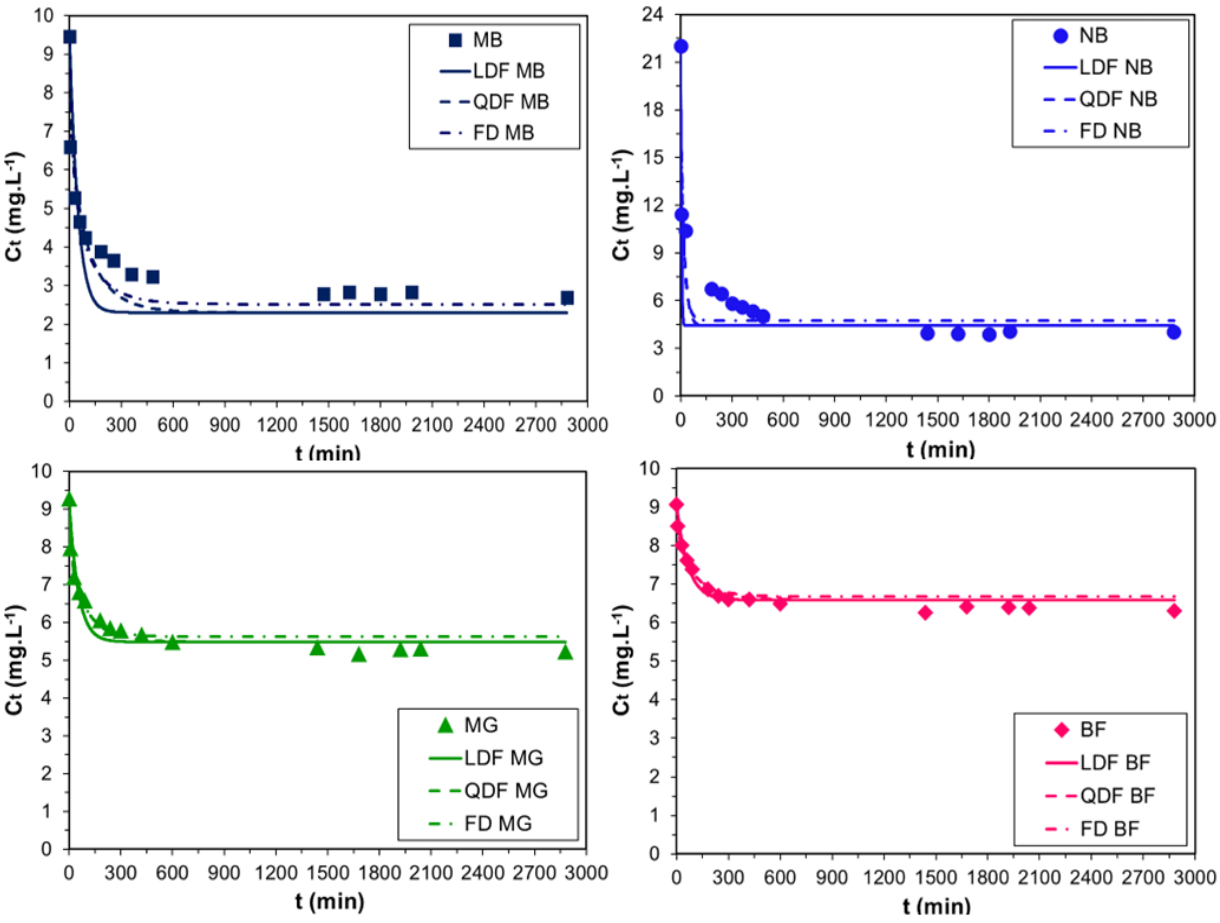

Source: The Author (2022)

Figure 25 - Kinetics for the cationic dyes adsorption onto the hydrogel (75%Agar 25%GO) on a dry basis (Experimental conditions: $m_{ads.}$= 0.20 g hydrogel (0.00432g dry basis); $V_{sol.}$= 50 mL; T= 24 ^{o}C; 250 rpm; pH =8 for MB, NB, and pH~ 6 for BF and MG).

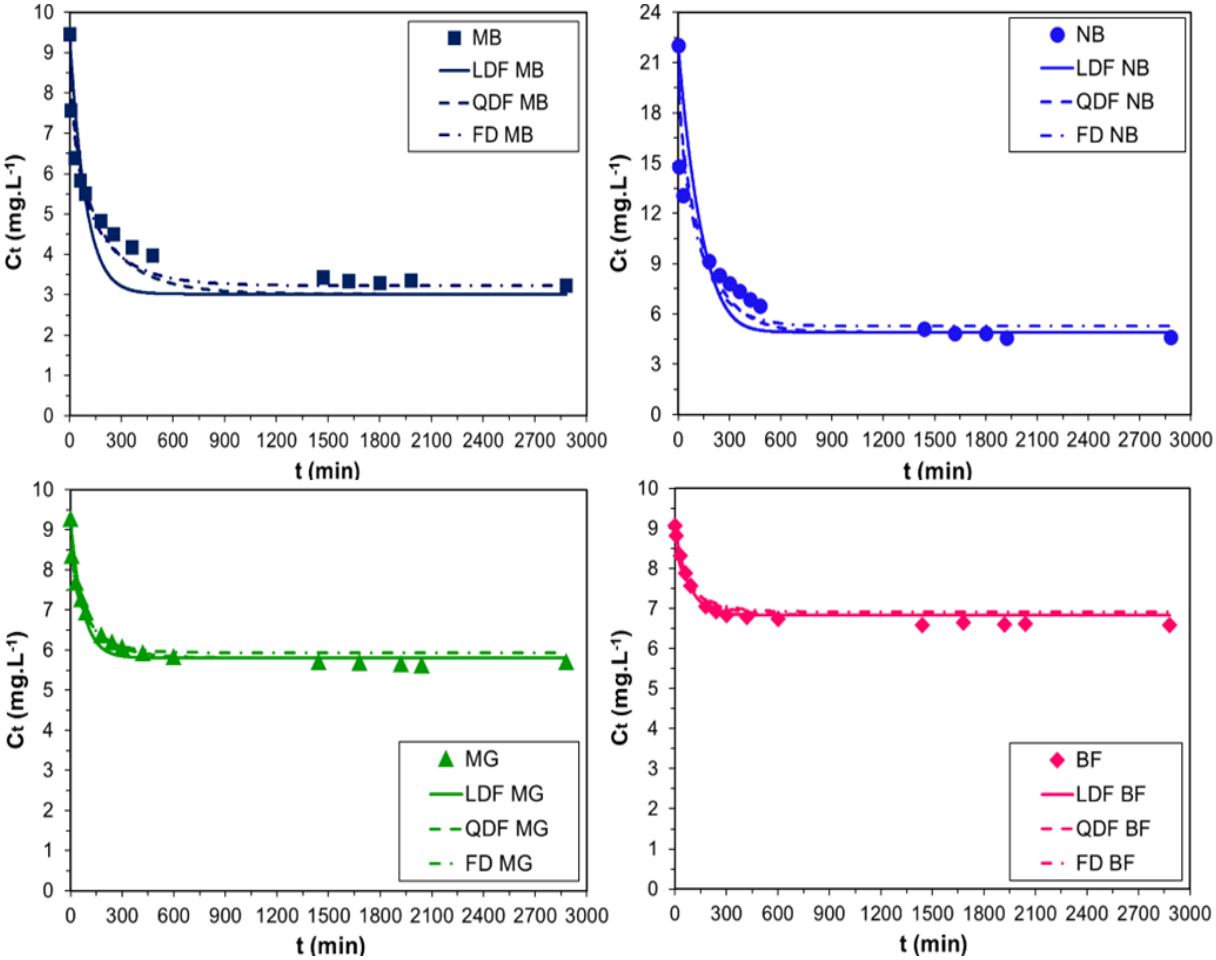

Source: The Author (2022)

Figure 26 - Kinetics for the cationic dyes adsorption onto the hydrogel (80%Agar 20%GO) on a dry basis (Experimental conditions: $m_{ads.}$= 0.20 g hydrogel (0.00435g dry basis); $V_{sol.}$= 50 mL; T= 24 ^{o}C; 250 rpm; pH =8 for MB, NB, and pH~ 6 for BF and MG).

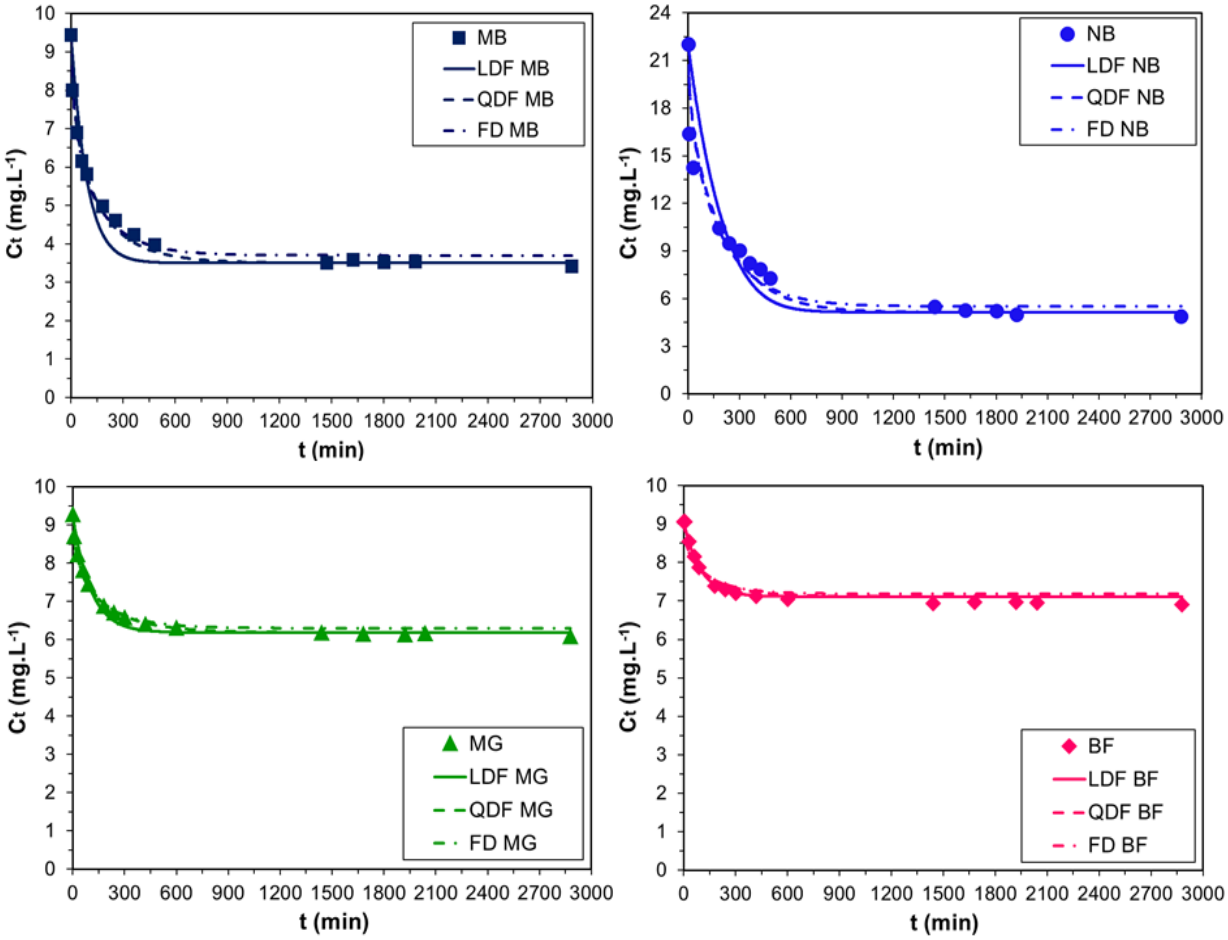

Source: The Author (2022)

The respective modeling parameters are exhibited in Table 8. For MG and BF, the dye concentration decreased faster in the first 300 min of the experiment, and from there, the decrease becomes slower, until it reaches equilibrium. On the other side, for MB and NB, the dye concentration decreases rapidly in the first 480 min, and from that point, the decay becomes smoother, tending to the equilibrium. The observed behavior explained above is in accordance with the linear driving force model, i.e., the adsorption rate decreases as the driving force decreases.

Table 8 - Parameters for the hydrogel samples (dry basis) calculated by adjusting the kinetic models to adsorption experimental data.

Hydrogel	Model	Parameters	Results			
			MB	NB	MG	BF
80% Agar 20% GO	LDF	k_{hLDF} (min^{-1})	$6.90\ 10^{-3}$	$4.30\ 10^{-3}$	$6.80\ 10^{-3}$	$8.10\ 10^{-3}$
		Dif_{LDF} ($m^2.min^{-1}$)	$1.04\ 10^{-9}$	$6.45\ 10^{-10}$	$1.01\ 10^{-9}$	$1.22\ 10^{-9}$
		R^2	0.91	0.81	0.98	0.98
	QDF	k_{hQDF} (min^{-1})	$2.60\ 10^{-3}$	$2.40\ 10^{-3}$	$2.90\ 10^{-3}$	$3.80\ 10^{-3}$
		Dif_{QDF} ($m^2.min^{-1}$)	$6.40\ 10^{-10}$	$5.91\ 10^{-10}$	$7.14\ 10^{-10}$	$9.35\ 10^{-10}$
		R^2	0.99	0.93	0.99	0.95
	FD	Dif_{FD} ($m^2.min^{-1}$)	$8.80\ 10^{-10}$	$7.40\ 10^{-10}$	$9.50\ 10^{-10}$	$1.20\ 10^{-9}$
		R^2	0.99	0.92	0.99	0.93
75% Agar 25% GO	LDF	k_{hLDF} (min^{-1})	$6.40\ 10^{-3}$	$6.20\ 10^{-3}$	$9.50\ 10^{-3}$	$9.70\ 10^{-3}$
		Dif_{LDF} ($m^2.min^{-1}$)	$9.60\ 10^{-10}$	$9.30\ 10^{-10}$	$1.43\ 10^{-9}$	$1.45\ 10^{-9}$
		R^2	0.80	0.72	0.95	0.97
	QDF	k_{hQDF} (min^{-1})	$2.10\ 10^{-3}$	$3.30\ 10^{-3}$	$4.00\ 10^{-3}$	$4.60\ 10^{-3}$
		Dif_{QDF} ($m^2.min^{-1}$)	$5.17\ 10^{-10}$	$8.12\ 10^{-10}$	$9.85\ 10^{-10}$	$1.13\ 10^{-9}$
		R^2	0.95	0.89	0.99	0.95
	FD	Dif_{FD} ($m^2.min^{-1}$)	$7.60\ 10^{-10}$	$1.10\ 10^{-9}$	$1.40\ 10^{-9}$	$1.40\ 10^{-9}$
		R^2	0.96	0.88	0.98	0.92
70% Agar 30% GO	LDF	k_{hLDF} (min^{-1})	$9.80\ 10^{-3}$	0.13	$1.30\ 10^{-2}$	$1.20\ 10^{-2}$
		Dif_{LDF} ($m^2.min^{-1}$)	$1.47\ 10^{-9}$	$1.95\ 10^{-8}$	$1.95\ 10^{-9}$	$1.80\ 10^{-9}$
		R^2	0.71	0.84	0.91	0.96
	QDF	k_{hQDF} (min^{-1})	$2.80\ 10^{-3}$	$1.90\ 10^{-2}$	$5.30\ 10^{-3}$	$5.40\ 10^{-3}$
		Dif_{QDF} ($m^2.min^{-1}$)	$6.89\ 10^{-10}$	$4.68\ 10^{-9}$	$1.30\ 10^{-9}$	$1.33\ 10^{-9}$
		R^2	0.88	0.88	0.97	0.97
	FD	Dif_{FD} ($m^2.min^{-1}$)	$1.10\ 10^{-9}$	$6.30\ 10^{-9}$	$1.80\ 10^{-9}$	$1.70\ 10^{-9}$
		R^2	0.91	0.89	0.95	0.94

Source: The Author (2022)

From Table 8, the models fit satisfactorily to the experimental data. Evaluating the coefficients of determination for the hydrogel sample 80%Agar 20%GO, the values presented were above 0.90, except for the regression of the LDF model to the data obtained for NB, in which R^2 =0.80. LDF showed the best fit for the kinetic data of BF dye. In contrast, for MB and NB, the best adjustments were for the QDF and FD models. All models fitted well with the data obtained for MG dye, since $R^2 \geq 0.98$.

The effective diffusivity values estimated for each case indicated that the adsorption of basic fuchsin and malachite green reached the equilibrium faster than NB and MB (RIOS *et al.,* 2020).

4.2.5 Adsorption mechanism for the cationic dyes

Because it is considered a mass transfer process, adsorption can be characterized by the following consecutive steps: bulk diffusion, film diffusion, intraparticle diffusion, and finally the attachment by adsorption (LI *et al.*, 2020). As depicted in the SEM micrographs (Topic 3), the biocomposite structure has a great amount of interspaces and channels, which indicates that the dyes molecules can be adsorbed through pore diffusion mass transfer (LI *et al.*, 2021).

Batch adsorption kinetics study of MB dye using an agar-graphene oxide aerogel, carried out by Chen and coworkers (2017), suggested that MB diffusion limited the adsorption rate onto the agar-GO aerogel. The authors presumed the adsorption mechanism was based on the electrostatic interactions between the cationic dye and the composite aerogel. They propose that the process was divided in two stages, being the first one related to external diffusion, in which the adsorption rate is higher due to the availability of large active sites on the materials surface (film diffusion); the second one is a slower adsorption stage, controlled by diffusion inside the adsorbent particle (pore diffusion).

The removal mechanism proposed for this work can be visualized in Figure 27, in which the green lines in the 3D composite indicate the agar polymer helical structure involving the GO nano sheets. Firstly, dye molecules interact with the active sites on the hydrogel surface; then, the molecules start diffusing into the pores to access the more GO active sites (slower stage). Interactions at GO active sites can occur through hydrogen bonding, electrostatic attractions, or π-π conjugation interactions (LI *et al.*, 2021).

Figure 27 - Proposed mechanism for the adsorption of cationic dyes on the agar-GO hydrogel biocomposite. The dye molecules are firstly attracted to the hydrogel surface (1st stage); next, the molecules diffuse into the particles to access the GO active sites (2nd stage).

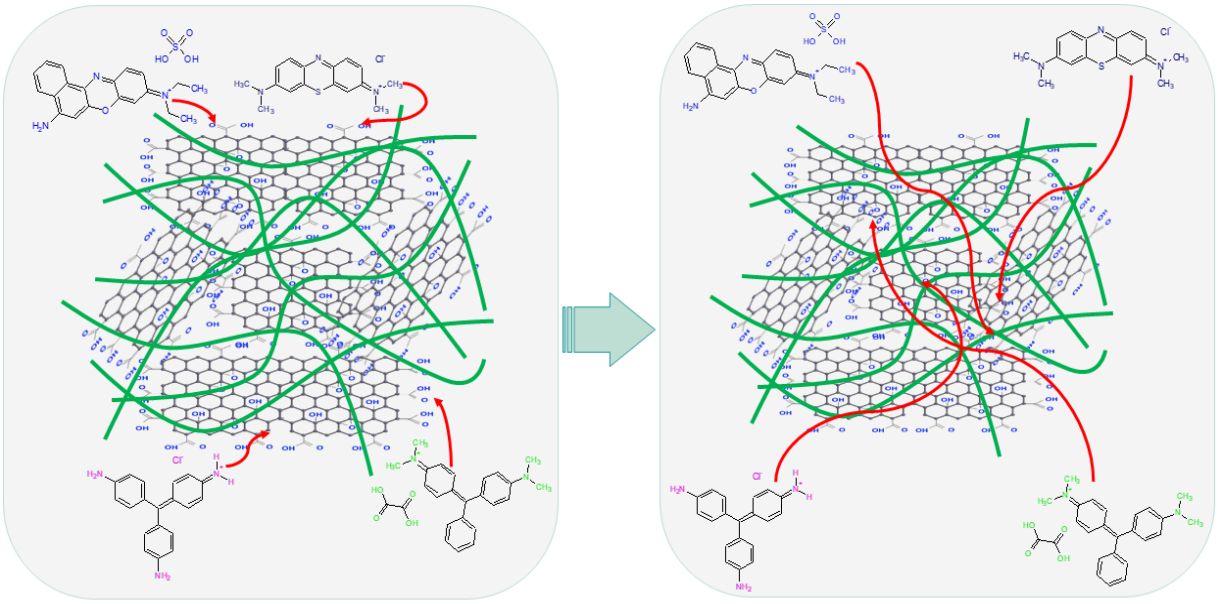

Source: The Author (2022)

Although some pure agar aerogels have been used in previous works to remove dyes from water, the adsorption capacity of these materials is still not quite satisfactory (HUANG *et al.*, 2020). Thus, performing adsorptive tests for the four dyes with Agar-GO (80%Agar 20%GO) and pure agar hydrogels under the same conditions of the batch tests (Figure 28), it was observed that the removal efficiencies were more than double for Agar-GO, as compared to pure agar. Therefore, although the cationic dyes might also interact with the hydroxyl groups present in the agarose and agaropectin chains of agar (SAMIEY; ASHOORI, 2012), it is suggested that the main responsible for adsorbing the dyes in the composite are the active sites present in GO (TANG *et al.*, 2020). The fact that the adsorptive capacity of the dyes increases as the percentage of GO in the composite increases, as it could be seen in the batch tests, also supports this hypothesis.

Figure 28 - Results for the adsorptive tests comparing the removal efficiencies of the pure agar hydrogel and Agar-GO (80%Agar 20%GO) hydrogel for the 4 dyes – MB, NB, MG, BF (experimental conditions: t =48 h; V_L= 50 mL; m_{ads} =0.20g (wet hydrogel); T =24 ºC; 250 rpm; pH ~6)

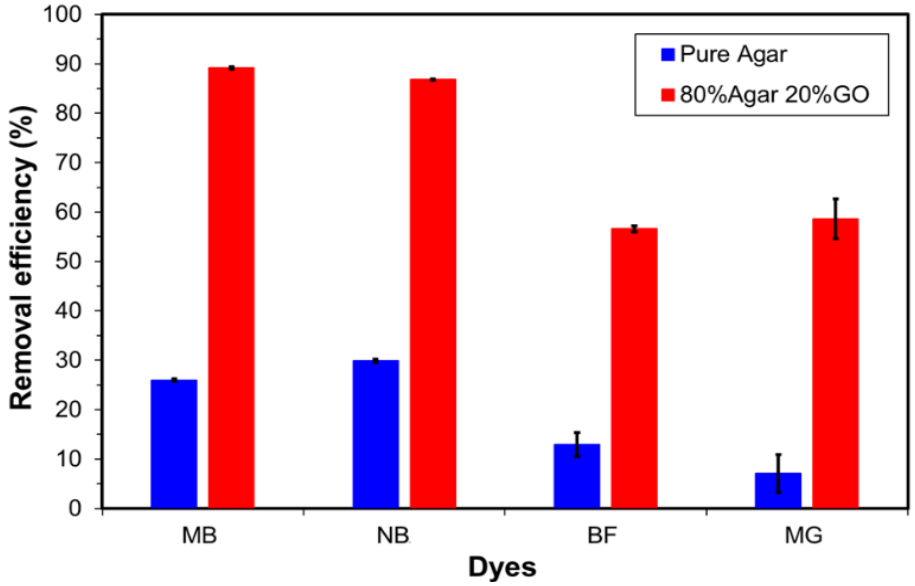

Source: The Author (2022)

FTIR and energy dispersive spectroscopy (EDS) measurements of the hydrogel before and after adsorption with one of the studied dyes (methylene blue) were also performed. Results of both analyses corroborate the explanation given in the proposed mechanism, as can be seen in the Figure 29.

Figure 29 - FTIR spectroscopy (a) and EDS (b) of Agar-GO (80%Agar 20%GO) before and after adsorption of MB

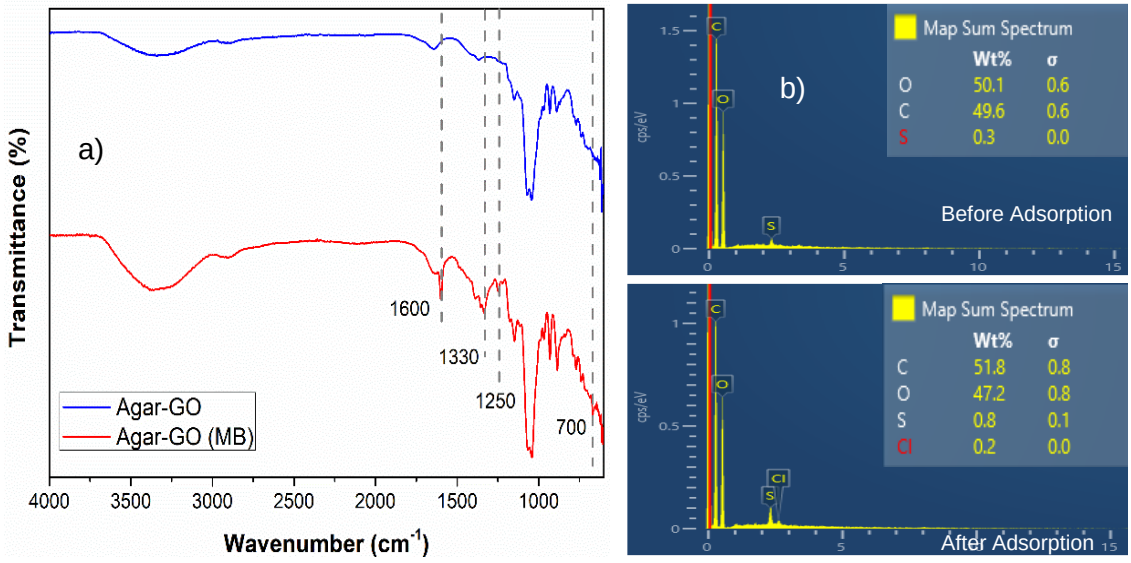

Source: The Author (2022)

Figure 29 a, exhibits the maintenance of the bands related to the Agar-GO biocomposite for the samples before and after MB adsorption. However, in the sample after MB adsorption, it occurs the appearance of bands at: 1600 cm^{-1} ascribed to C=C stretching and N-H bending; 1330 cm^{-1} attributed to S=O stretching; 1250 cm^{-1} due to C-N stretching, and at 700 cm^{-1} observed in benzene derivatives. Observing the chemical structure of MB dye in Figure 19 it can be assumed that these new bands are related to the adsorption of the dye on the surface of the composite material.

The EDS analysis, in Figure 29 b, indicates that after adsorption of MB there is an increase in the wt.% of Sulfur. This finding agrees with the presence of these elements in the structure of MB, confirming it´s loading on the hydrogel, which is composed basically of C and O elements. The residual amount of S in the pristine hydrogel might be from the sulfuric acid which was used for the initial oxidation of graphite during GO preparation.

4.2.6 Regeneration and reuse of the adsorbent

Five adsorption–desorption batch cycles were completed during the agar-GO hydrogel regeneration and reused, as depicted in Figure 30. The adsorption capacity increased after the 1st regeneration, especially for MG and BF, preserving nearly the same values after that, even at the end of the last cycle. This may have been caused by the possible presence of sodium hydroxide ions remaining in the material, even after successive washes. In this case, washing the material after regeneration may have interfered with the results, since the same behavior was not observed when the washing was done continuously in fixed-bed, as it will be detailed in the next topic (Topic 5). In addition, the presence of foreign ions may affect the process, competing or favoring the adsorption.

Figure 30 – Batch adsorption/desorption cycles after regeneration with 0.30 M NaOH (Experimental conditions: $m_{ads.}$= 0.20g hydrogel (wet basis); V_L=50 mL; T =24 ºC; 250 rpm).

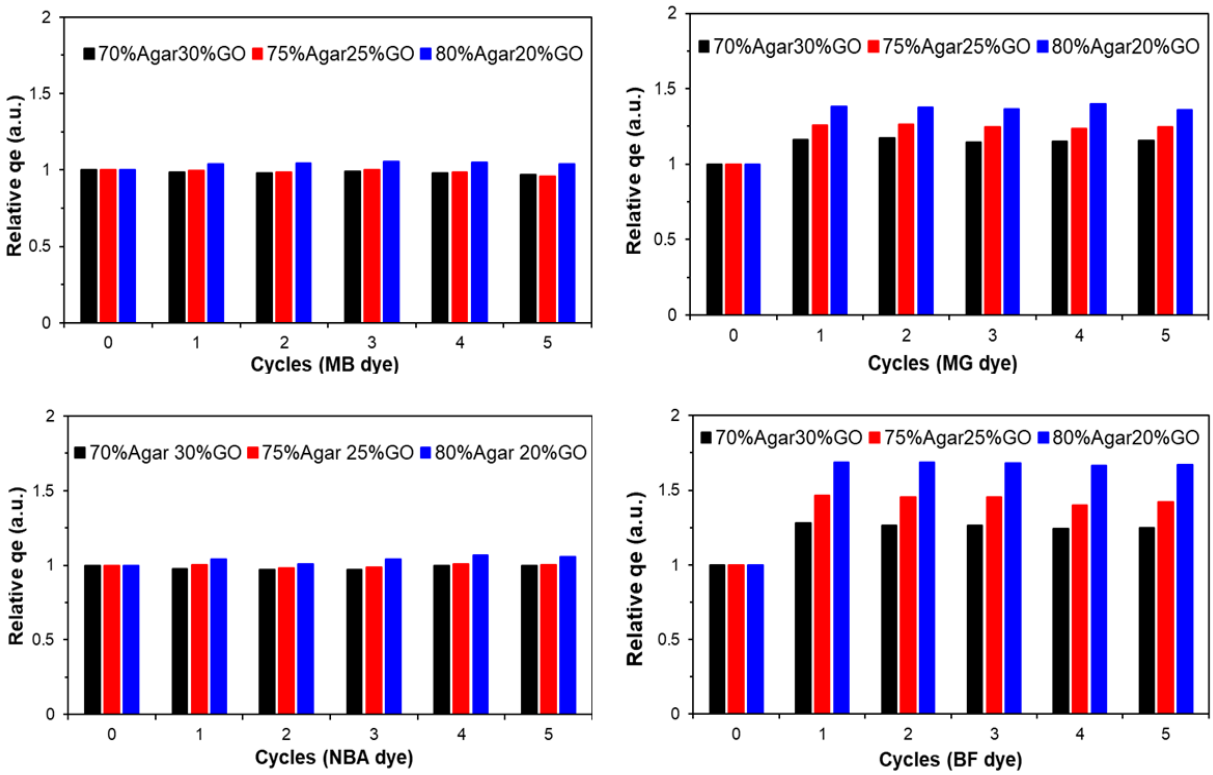

Source: The Author (2022)

Studying the removal of triclosan from aqueous medium using magnetic porous reduced GO as adsorbent, Li and coworkers (2020) noted that the nanocomposite could be satisfactorily regenerated for up to five adsorption-desorption cycles.

In addition, Fang *et al.* (2018) also found promising results regarding the regeneration and reuse of magnesium ascorbyl phosphate graphene-based monolith produced for bisphenol A adsorption. Even after five cycles of regeneration, the adsorption capacity of the material still maintained 88%, indicating a promissing potential for regeneration and reuse of the GBM produced.

4.2.7 Phytotoxicity before and after adsorption

Results in terms of relative growth index and germination index obtained with the phytotoxicity tests using cucumber, arugula and cress seeds are shown in Figure 31.

Regarding the positive control, seeds with irregular root development were noticed, as it was already expected. In the assays performed with the positive control, irregularities regarding defective primary root (atrophied, necrosed or absent), were observed. According to Mañas and De las Heras (2018) an irregular seedling would not be able to develop in a normal plant when grown in soil under favorable conditions, as it present irreparably defective essential structures.

Figure 31 – Results for the phytotoxicity assays performed using cucumber (a), cress (b) and arugula (c) seeds (Experimental conditions: number of seeds/ Petri drish.= 5 (cucumber), 10 (cress and arugula); t =120 h; T =24 ºC; T= 22.5 ± 2.5 °C; negative control = H_2O).

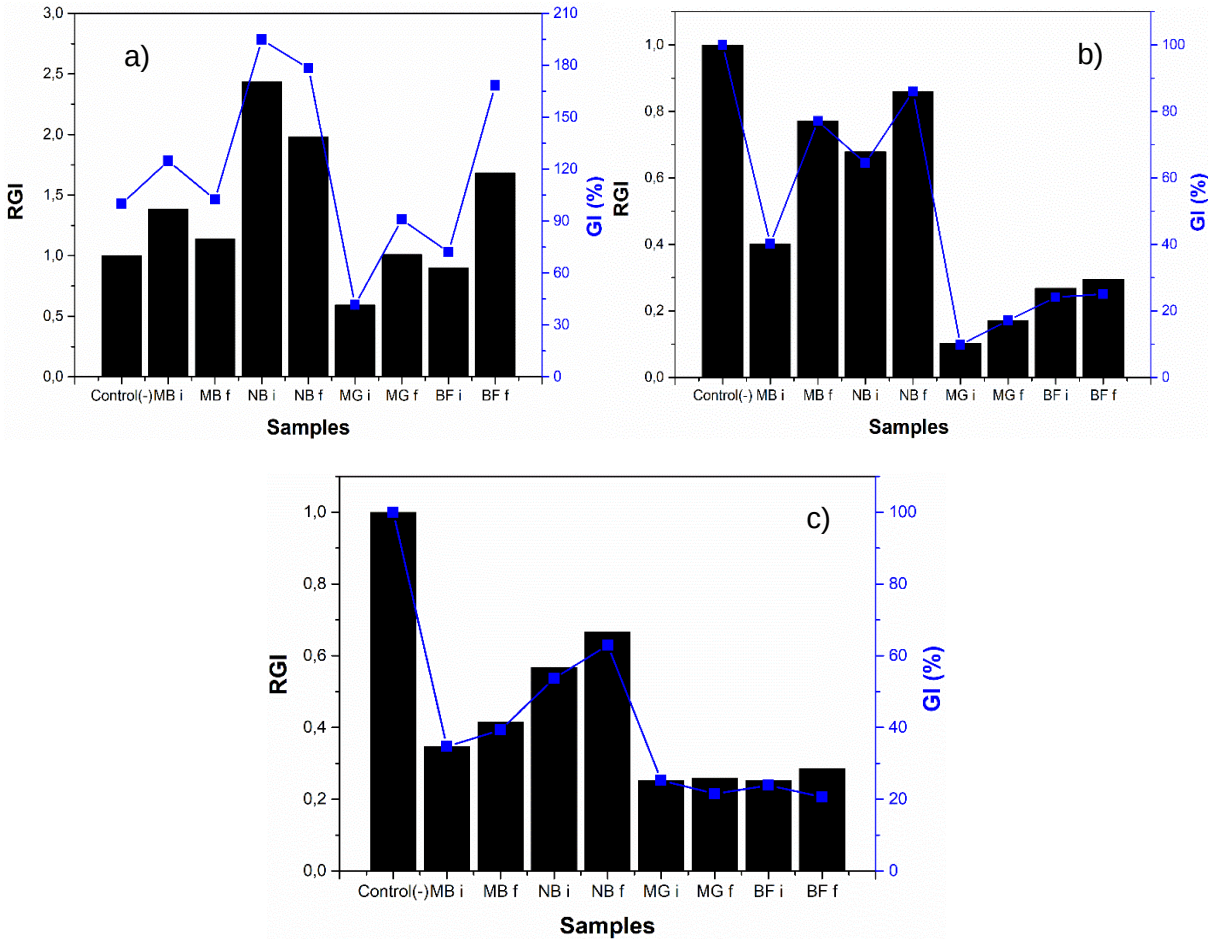

Source: The Author (2022)

There are not clear and official statements, however, according to Mañas and De las Heras (2018), GI values equal to or higher than 80% indicate that phytotoxic substances are found at very low concentrations in the sample (or even indicate their absence). On the other hand, GI values below or equal to 50% possibly indicate the

strong presence of phytotoxic substances. Values between 50 and 80% might indicate a moderate presence of phytotoxicity. Therefore, it can be assumed that a GI values under 50% implies the phytotoxicity of the sample.

Thus, according to Figure 31 a, it is noted that the samples after adsorption with the hydrogel, studied with cucumber seeds, had very low or moderate phytotoxic substances, since GI was over 50%. Although the samples studied with cress (Figure 31 b) and arugula (Figure 31 c) seeds presented phytotoxic substances specially for MG and BF, since GI was under 50% in both cases, it is noted that there are no indications of increase in the phytotoxicity of the solution of any of the dyes studied after the adsorption with the Agar-GO biocomposite (using hydrogel produced with 80% of agar and 20% of GO).

Such results may indicate that, in fact, the composite hydrogel would not represent a source of secondary contamination for the aqueous medium, despite the fact that pure GO can affect plant growth and development. Although, it is important to highlight that the potential phytotoxic effects of graphene-based materials depend on many factors, such as the plant species, exposure concentration and time of exposure (WANG *et al.,* 2019).

In this case, probably, besides GO not being so easily detached from the composite in aqueous medium, even if some amount of GO has leached into the medium, the concentration was so residual that it did not affect root growth, compared to the solution before adsorption.

4.3 FINAL THOUGHTS

Three hydrogel samples prepared using graphene oxide and agar were tested as adsorbents for the removal of anionic and cationic dyes from water. Preliminary kinetic tests indicated that the hydrogels tested were efficient in removing cationic dyes, however, there was practically no significant removal of anionic dyes. Batch experiments showed practically no change in adsorptive capacity when varying the pH of BF and MG solutions. For MB the adsorptive capacity increases gradually, and for the NB, the change is noticed more significantly when pH is increased from 6 to 8. MB, MG, and BF isotherms were best fitted to Freundlich model, and NB isotherm fitted Sips model. Kinetic data were satisfactorily adjusted to LDF, QDF, and Fick’s

Diffusion equations. The maximum experimental adsorption capacities, on a dry basis, were obtained for the sample produced with 70% of Agar and 30% of GO, being 141.48 $mg.g^{-1}$ (MB), 284.69 $mg.g^{-1}$ (NB), 52.29 $mg.g^{-1}$ (MG), and 34.00 $mg.g^{-1}$ (BF). The hydrogels also demonstrated a good regenerative potential, and a decrease in the phytotoxicity effects of the effluents was observed after adsorption. Thus, after the proposed treatment, the composite hydrogel produced would not represent a source of secondary contamination for the aqueous medium.

5 CONTINUOUS REMOVAL OF DYES FROM WATER AND TEXTILE WASTEWATER USING AGAR-GRAPHENE OXIDE HYDROGEL IN FIXED-BED ADSORPTION COLUMN

Hydrogel biocomposite using graphene oxide and agar biopolymer was synthesized to treat textile wastewater through fixed-bed adsorption. Fixed-bed experiments were carried out, and the adsorption capacities obtained (single-component) for the cationic dyes on a dry basis were 226.46 $mg.g^{-1}$ (NB), 79.51 $mg.g^{-1}$ (MB), 58.25 $mg.g^{-1}$ (MG), 38.11 $mg.g^{-1}$ (BF). LDF model was fitted with the experimental breakthrough curves. The column packed with the agar-GO hydrogel was tested for the treatment of synthetic textile wastewater, as well as a real textile wastewater sample. Color and total organic carbon (TOC) were evaluated and there was an indication of the adsorbent selectivity for the separation of the dyes, which can facilitate the cationic dyes recovery. Agar-GO proved to be a viable and eco-friendly alternative, since a small amount of material was used to treat over 6 L of the synthetic wastewater, being most of the composite biodegradable, as it was made up of 80% agar biopolymer. Moreover, the material exhibited remarkable regenerative capacity of the bed, proving its effectiveness for applications in industrial textile wastewater treatment.

Part of this main topic has been published:

DE ARAUJO, C. M. B. *et al.* Wastewater Treatment Using Recyclable Agar-graphene Oxide Biocomposite Hydrogel in Batch and Fixed-bed Adsorption Column: Bench Experiments and Modeling for the Selective Removal of Organics. **Colloids and Surfaces A: Physicochemical and Engineering Aspects**, v. 639, p. 128357, 2022.

5.1 METHODOLOGY

Graphene oxide aqueous suspension was produced in the Laboratories of the Research Group on Environmental Technologies and Processes (GPTA), located at the Federal University of Pernambuco (UFPE, Brazil). All the fixed-bed adsorption experiments described in this topic were performed in the Laboratory of Separation and Reaction Engineering - Laboratory of Catalysis and Materials (Associated Laboratory LSRE-LCM), at the Faculty of Engineering of the University of Porto (FEUP, Portugal).

5.1.1 Materials

Breakthrough experiments were conducted in a borosilicate glass column packed with the agar-GO biocomposite hydrogel prepared with 80% of Agar and 20% of graphene oxide, as it was the sample that presented a higher mechanical resistance during the batch tests. The column (GE Healthcare, XK 16/20) inner diameter was 1.6 cm, with a total height of 20 cm (adjustable). For packing the column, 6.0 g of wet hydrogel was used (equivalent to 0.1304 g of adsorbent on a dry basis), and the bed height was 7.0 cm. The packaging was carried out with the column partially filled with water to prevent the hydrogel from drying out, and the bed was compacted naturally by gravity.

5.1.2 Fixed-bed adsorption

Before starting the adsorption tests, water was pumped through the system for ~20 min, to remove air bubbles and check for leaks. The flowchart diagram of the fixed-bed experiments is given in Figure 32 a, and Figure 32 b exhibits a detailed scheme of the column used during the experiments. Figure 32 c shows a photograph of the experimental apparatus.

Figure 32 - Process diagram for the experimental setup of fixed-bed tests (a); detailed scheme of the packed bed column used for the breakthrough experiments (b); photograph of the experimental apparatus at FEUP laboratories (Porto, Portugal) (c).

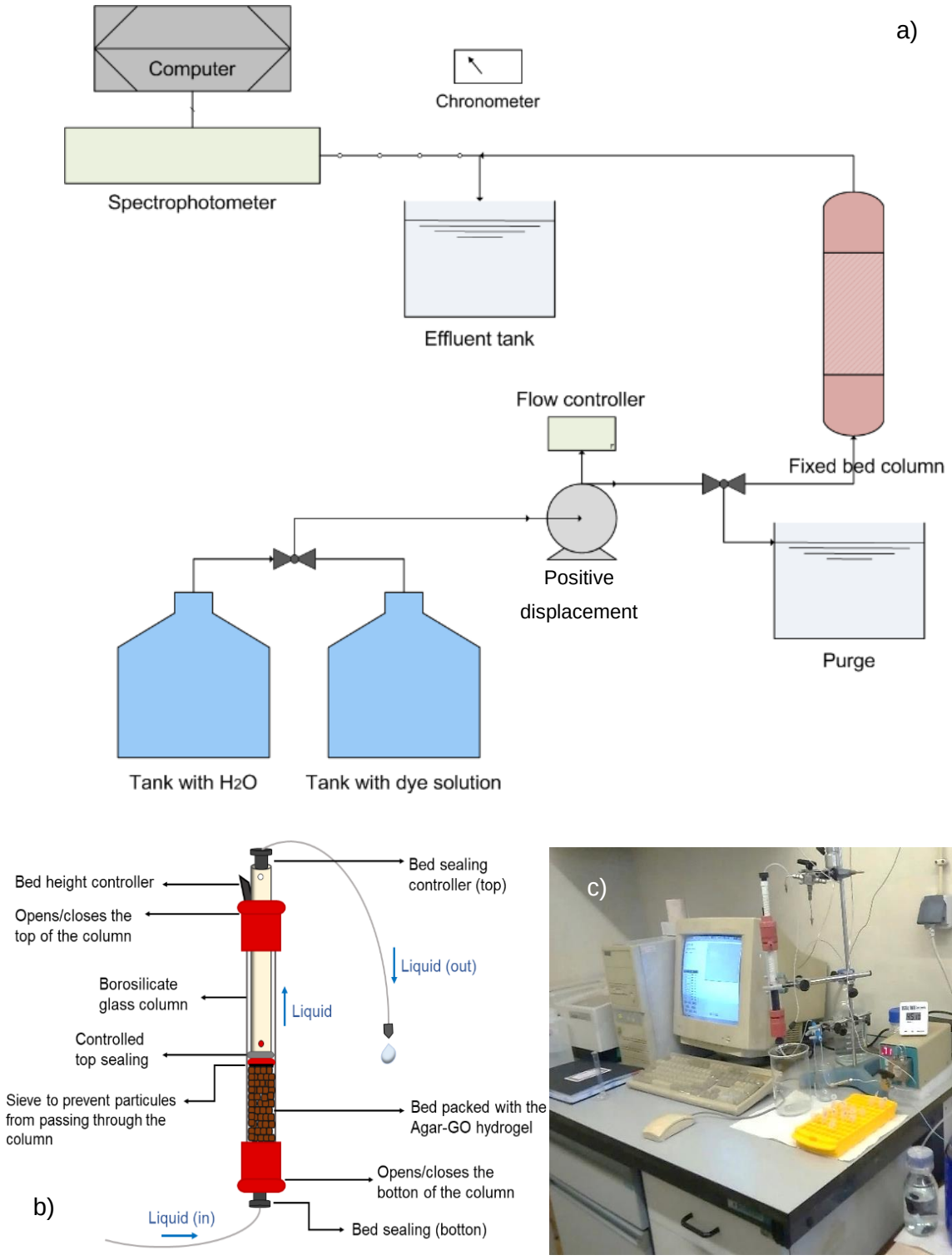

Source: The Author (2022)

As it can be seen, the system has a positive displacement pump, and in the suction line, there is a valve that allows changing the supply between the two tanks. At the beginning of each experiment, the feed and regeneration solutions were purged before the column inlet to reduce the dead volume. The fluid was pumped to the adsorption columns in an upward flow. The samples were collected manually at the top of the column at given time intervals.

Some operational parameters that describe the behavior of the breakthrough curve, such as the bed density (ρ_{bed}) and the adsorbent density (ρ_{ad}) were estimated experimentally by pycnometry. To estimate the bed porosity (bulk porosity, ε_b), blue dextran (Merck, molecular weight: 2000000 g.mol^{-1}) was used as a tracer.

5.1.2.1 Single-component breakthrough curves

Fixed-bed experiments were carried out for diluted solutions of each dye. The average flow rate was 2.0 mL.min^{-1} in each case, with a feed concentration of 20 mg L^{-1} for NB and 10 mg L^{-1} for MB, BF and MG. Tests were also carried out with a volumetric flow rate of 4.0 mL.min^{-1} for MB and BF, to verify how the increase in flowrate affects the adsorption of dyes with different structures - BF and MG dyes have more similar molecular structures between them, compared to MB and NB. The initial pH was adjusted to 8.0 for MB and NB solutions, and the experiments were conducted at 24 ºC.

The breakthrough curves were obtained from the fixed-bed experiments, and it was possible to estimate the breakthrough times, t_{BR}; the exhaustion times t_{EX}; the stoichiometric times, t_{st}; and the adsorption capacities, q_e. The breakthrough time and the exhaustion time were the times in which C_t/C_0 = 0.05 and C_t/C_0 = 0.95, respectively. t_{st} is given by Equation 15, q_e is given by Equation 16, and the removal efficiency of the column was calculated using Equation 17.

$$t_{st} = \int_0^{\infty}(1 - \frac{C}{C\infty})dt \quad (15)$$

$$q_e = \frac{C\infty.Q.\left[\int_0^{\infty}(1-\frac{C}{C\infty})dt\right]-\varepsilon.V.C\infty}{m} \quad (16)$$

$$\%R = \frac{\int_0^{\infty}(1-\frac{C_t}{C\infty})dt}{tf}.100\% \quad (17)$$

Being C∞ the equilibrium concentration, and C_0 =C∞; Q the constant inlet flow rate; ε the column bulk porosity; V the volume of the column, and m is the mass of adsorbent in the fixed-bed column (RIOS *et al.*, 2020). Moreover, t_f in Equation 17 is the overall time in which $C_t \rightarrow C\infty$ (DOTTO *et al.*, 2015).

Regarding the modeling of the breakthrough curves, the experiments were simulated by a model comprising a mass balance, linear driving force model (LDF) to describe the mass transfer, and the corresponding boundary and initial conditions.

Following the phenomenological approach, the mass balance for the adsorbate in fixed-bed is given by Equation 18. It considers convection flow, axial dispersion, accumulation in the fluid, as well as the rate of adsorption onto the adsorbent.

$$D_{ax}\frac{\partial^2 C}{\partial z^2} - v_i\frac{\partial C}{\partial z} - \frac{\partial C}{\partial t} - \frac{(1-\varepsilon_b)}{\varepsilon_b}\frac{\partial q}{\partial t} = 0 \quad (18)$$

Where C is the concentration of adsorbate in the fluid phase ($mg.L^{-1}$), q is the amount of dye in the solid phase ($mg.g^{-1}$), z is the distance from the bed entrance (m), t is the time (min), ε_b is the bed porosity, and D_{ax} is the coefficient of axial dispersion. Equation 19 gives the relationship between D_{ax} and Peclet number (*Pe*).

$$Pe = \frac{v_i H_b}{D_{ax}} \quad (19)$$

In which H_b is the bed height (m), and v_i is the interstitial velocity of the fluid ($m.min^{-1}$). For the modeling, it was considered that the mass balance to the particle was described by the Linear Driving Force equation (Equation 7), using the data estimated during batch tests as a starting point for making the adjustments. The isotherm parameters were obtained from the fit of equilibrium experimental data to the isotherm's models - Freundlich model was used for MB, MG, and BF, as Sips model for NB dye. It was assumed that for t= 0 → C_0= q_0= 0, and the boundary conditions were:

$$z = H_b \rightarrow \frac{\partial C}{\partial z} = 0 \quad (20)$$

$$z = 0 \rightarrow D_{ax}\frac{\partial C}{\partial z} = v_i(C - C_\infty) \quad (21)$$

The values of the coefficients of determination were estimated using the Equation 12 given in Topic 4.

5.1.2.2 Fixed-bed regeneration and reuse

Column regeneration and reuse are key factors for the feasible application of adsorption in industrial processes (DOTTO *et al.*, 2015). Therefore, the regeneration of the column was done by feeding the system with 0.30 M NaOH, applying the same flowrate and temperature (24 ^{o}C) used for the adsorption tests. After desorption, the feed (NaOH) has been switched, using the valves to purge the basic regeneration solution, and the system was continually washed with deionized water until pH =7.

This process was done at least 3 times for each system with the respective dyes studied.

5.1.2.3 Fixed-bed adsorption for a mixture of dyes and textile wastewater treatment

Dynamic experiments were also conducted for a mixture of the four dyes (~12.5 g of dyes per L of water, pH =8.0), a synthetic textile wastewater sample produced in the laboratory, and a real textile wastewater sample collected in textile finishing industry (Portugal). After collection, the raw wastewater was kept in a freezer at a temperature close to 0 °C, without any chemicals addition to try to preserve its original characteristics and to avoid rapid degradation. The raw wastewater sample was used in full concentration during the tests. The average flow rate of 2.0 mL.min^{-1} was applied for the bench tests.

Wastewater characterizations were carried out based on the methodology proposed by the Standard Methods for the Examination of Water and Wastewater. Measurements of the initial temperature, pH, color, turbidity, conductivity, Total Organic Carbon (TOC), and Inorganic Carbon (IC) contents were performed for the real wastewater sample.

For synthetic wastewater production, the dye solutions were prepared with distilled water, and mixed. Then, the mixture of the dyes had its temperature raised to 60 ^{o}C, when the dispersing, lubricating agents and Na_2SO_4 were gradually added, with the system under constant magnetic stirring at 350 rpm for 20 min. Then, the temperature was raised to ~100 ^{o}C for 1h. Thereafter, the solution gradually cooled at room temperature (24 ^{o}C) (CHAUDHARY; GUPTA; GUPTA, 2017; SÁ LUÍS, 2009). Before proceeding with fixed-bed experiments, the pH was corrected to 8.0.

The change in color due to adsorption was verified by scanning the samples in the visible region (400–700 nm). This quantification was performed by numerically calculating the areas under each spectral curve over time (O. SALOMÓN *et al.*, 2020). The change in color, TOC and turbidity were response parameters for the tests with real textile wastewater. Color and TOC were response parameter for the tests with the synthetic wastewater as well.

5.2 RESULTS AND DISCUSSION

Results regarding the application of agar-GO nano-biocomposites as adsorbents to remove the cationic dyes (sinlge component and mixture), as well as synthetic and real textile wastewater samples, in fixed-bed process will be addressed and discussed in this section.

5.2.1 Estimating operating parameters

The operational parameters that described the behavior of the breakthrough curve were estimated by pycnometry for the hydrogel sample produced with 80% of Agar and 20% of GO. Thus, the value obtained for bed density was 0.373 $g.cm^{-3}$, and the adsorbent density was 1.011 $g.cm^{-3}$, very close to the density of liquid water (approximately 1 $g.cm^{-3}$). This was already expected since the hydrogel is composed of about 98% water.

Bulk porosity was estimated using blue dextran as a tracer, as well as the Peclet number and coefficient of axial dispersion. The result is shown in Figure 33.

Figure 33 – Results for tests estimating the bulk porosity using blue dextran in duplicate (Conditions: m_{bed}= 6.0g hydrogel (~0.13g dry basis); T =24 ºC; Q =2.0 mL.min^{-1})

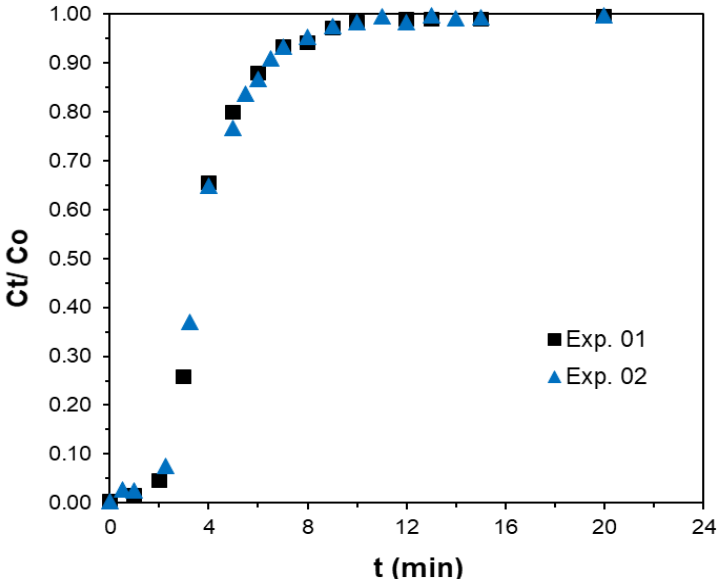

Source: The Author (2022)

In this case, the average value of ε_b was 0.585, Pe number was 7.62, and D_{ax} was 1.56 10^{-4} m^2.min^{-1}. As it can be seen in the experiment carried out in duplicate, the passage time of the tracer through the column is quite small, compared to the total times of the experiments carried out with the cationic dyes (approximately 24 h), as will be detailed in the following topics.

5.2.2 Fixed-bed adsorption for single components

Breakthrough curves for each cationic dye tested when the volumetric flowrate was 2.0 mL.min^{-1}, using the hydrogel, are exhibited in Figure 34 a; as the breakthrough curves for the adsorption of single MB and BF onto the hydrogel, varying the volumetric flowrates are shown in Figure 34 b. Values of breakthrough time and exhaustion time were estimated, depicted in Table 9, along with other experimental parameters.

Figure 34 - Breakthrough curves for the adsorption of single MB, NB, MG, BF onto agar-GO hydrogel when Q = 2.0 mL.min^{-1} (a); breakthrough curves for the adsorption of single MB and BF onto the hydrogel, varying the flowrate (b) (Experimental conditions: m_{bed}= 6.0 g hydrogel (~0.13 g dry basis); T = 24 ^{o}C; pH=8 for MB, NB, and pH~6 for BF and MG).

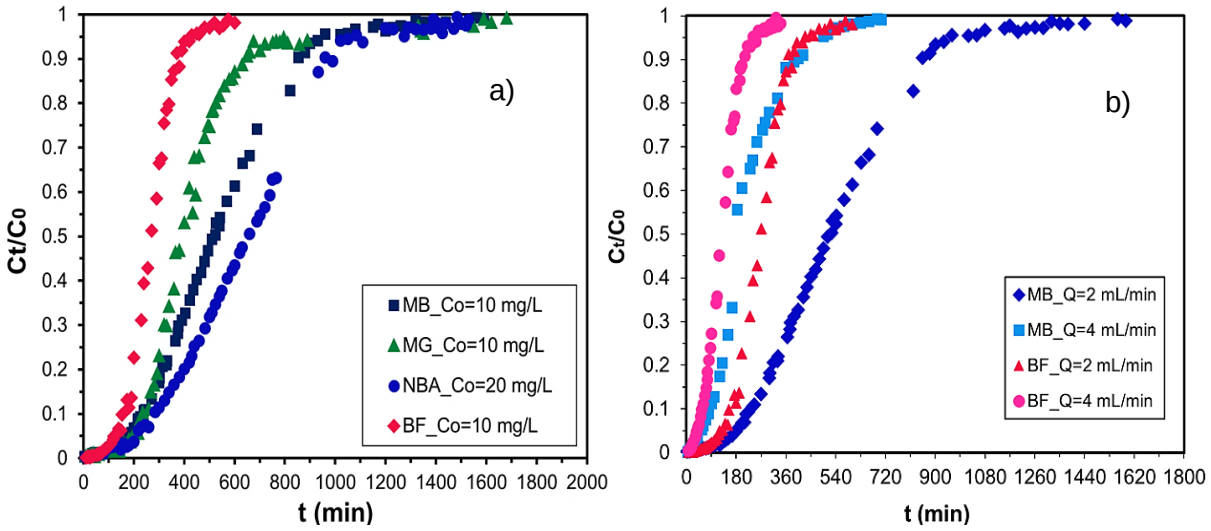

Source: The Author (2022)

Table 9 - Experimental values of the parameters from the breakthrough curves (dry basis)

Dye	Q (mL.min^{-1})	t_{BR} (min)	t_{EX} (min)	$t_{f\ Total}$ (min)	t_{st} (min)	Removal efficiency (%)	q_e fixed-bed (mg.g^{-1})
MB	2	182	945	1590	549.40	34.55	79.51
	4	52	489	705	220.06	31.21	62.65
BF	2	122	428	600	272.09	45.35	38.11
	4	37	239	340	131.67	38.73	35.34
MG	2	197	1015	1680	447.95	26.66	58.25
NB	2	209	1145	1530	656.20	42.89	226.46

Source: The Author (2022)

Breakthrough times for the average flowrate of 2.0 mL.min^{-1} ranged from 3 - 3.5 h for MB, MG, and NB, while for BF it was near 2 h. Nevertheless, tests carried out under the same experimental conditions when the flowrate was higher (4.0 mL.min^{-1}), showed t_{BR} values almost 3 times smaller compared to the lowest flowrate.

All breakthrough curves in Figure 34 present a symmetric S-shape, being the basic fuchsin curves the most S-shaped ones. Dispersion effects are also observed in the breakthrough curves. Dispersion effects happen for several reasons, such as axial dispersion, mass transfer resistances, the non-ideal packing of the column, and the fluid distribution throughout the column (DELGADO, 2006).

From Table 9, for tests with lower flow rate, the adsorbed quantities of dye from the breakthrough curves onto the agar-GO hydrogel (dry basis) were 79.51 mg g^{-1} for MB, 226.46 mg g^{-1} for NB, 58.25 mg g^{-1} for MG, and 38.11 mg g^{-1} for BF. The higher value was obtained for Nile blue A, followed by methylene blue, malachite green and basic fuchsin, in this respective order. These values were already expected, following the adsorption equilibrium isotherms.

Breakthrough curves can be affected by various parameters, including the inlet flow rate. When increasing the volumetric flow rate, in general, there was a small decrease in the removal efficiencies of the respective dyes, MB and BF. It was also notorious the decrease in the values of adsorptive capacities when the flow rate was increased from 2.0 to 4.0 $mL.min^{-1}$. Indeed, by increasing the flowrate, one can expect two outcomes, if the system is under external mass transfer control, the breakthrough time should then increase, since the film will be reduced by increasing the flowrate. On the opposite, one can increase the internal mass transfer resistance by not giving enough contact time between the adsorbate and the adsorbent, which seems to be the case.

By evaluating the fixed-bed adsorption of MB by ultrasonic surface modified chitin supported on sand, Dotto and coworkers (2015) observed that at lowest flow rates, the residence time in the bed was sufficient to guarantee the diffusion of the dye in the adsorbent structure. On the other hand, by increasing the flowrate, the residence time was not sufficient leading to a kinetically controlled process.

Comparing the adsorption capacities in Table 9 when Q =2.0 $mL.min^{-1}$, for MB and NB, the values from the isotherms in batch and those from fixed-bed experiments exhibited errors below 20% in between them. The same was not observed when comparing batch and fixed-bed values of q_e for MG and BF, as the errors were >20%. That can be justified by the fact that the feed concentrations in fixed-bed (C_e) were outside of the concentration interval studied in the batch experiments, as exhibited in Figure 35. This explains why q_e was higher in the

adsorption column experiments for MG and BF. Furthermore, these differences could be attributed to the sum of small experimental errors, that due to the long experimental times, become more significant (RIOS *et al.*, 2020).

Figure 35 - Batch isotherms (black dots), and the blue dot regarding the experimental values from breakthrough curves for the cationic dyes MB, NB, MG, BF (dry basis).

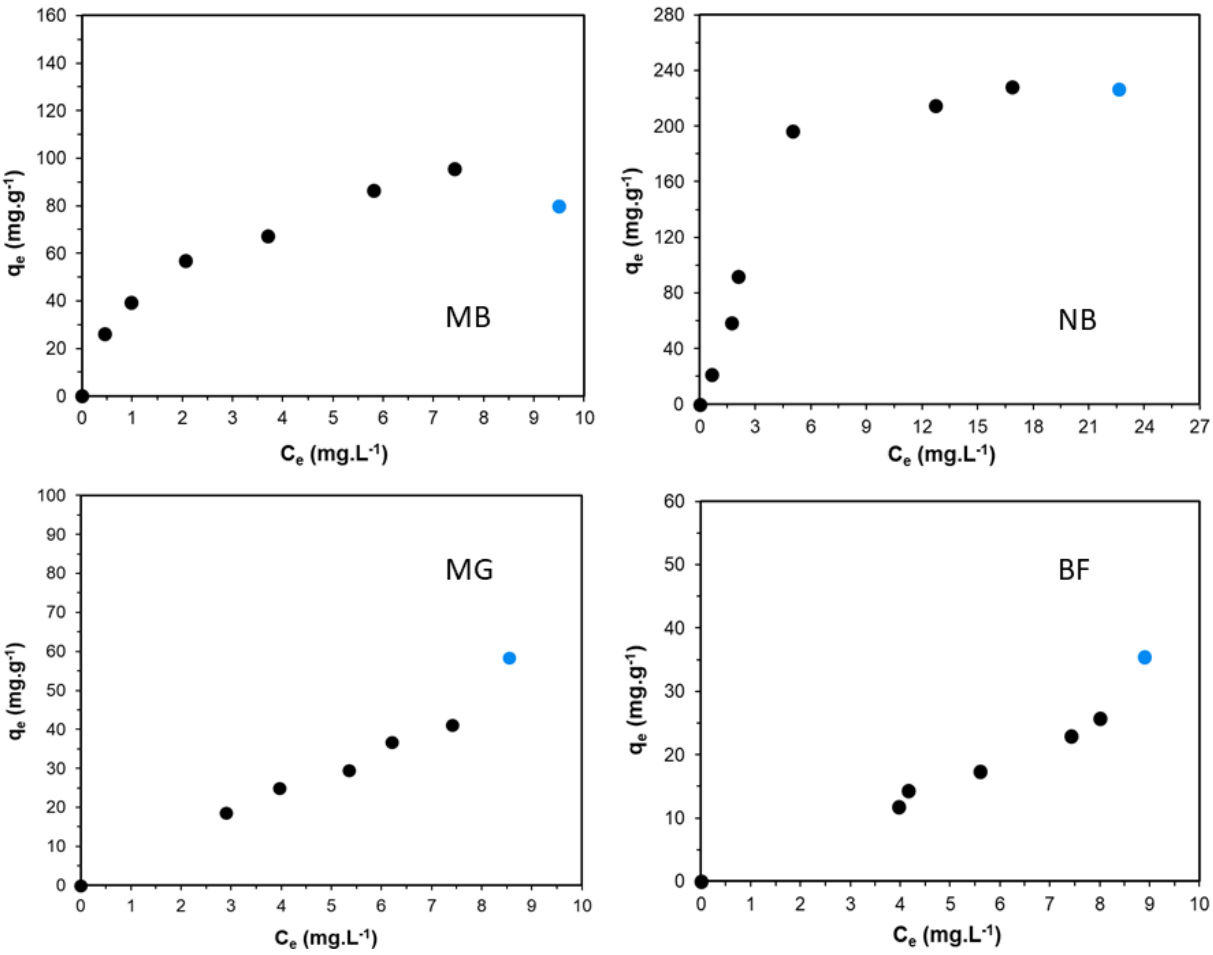

Source: The Author (2022)

5.2.3 Fixed-bed regeneration

The regeneration and reuse of the adsorbent is necessary for a successful adsorption process, which is essential for the industrial applications. According to Mohan *et al.* (2017), the adsorbent regeneration reduces the operational cost of the adsorption plant. Therefore, Figure 36 depicts the results of fixed-bed regeneration and reuse for the dyes MB, NB, MG, and BF. The regeneration experiments were carried out similarly to fixed-bed adsorption tests but using 0.30 M NaOH as the

regenerative solution. Deionized water was used in abundance to wash the bed and neutralize the pH continuously. As it can be seen, the results indicate the system exhibit good regenerative performance, since for each system, the curves were all superimposed on each other.

Figure 36 - Results of fixed-bed regeneration and reuse for the 4 dyes – MB, NB, MG, and BF. (Experimental conditions: m_{bed} = 6.0 g (0.13g on a dry basis); $Q_.$ =2.0 mL.min^{-1}; T = 24 ^{o}C; pH =8 for MB, NB, and pH~ 6 for BF and MG for the adsorption tests)

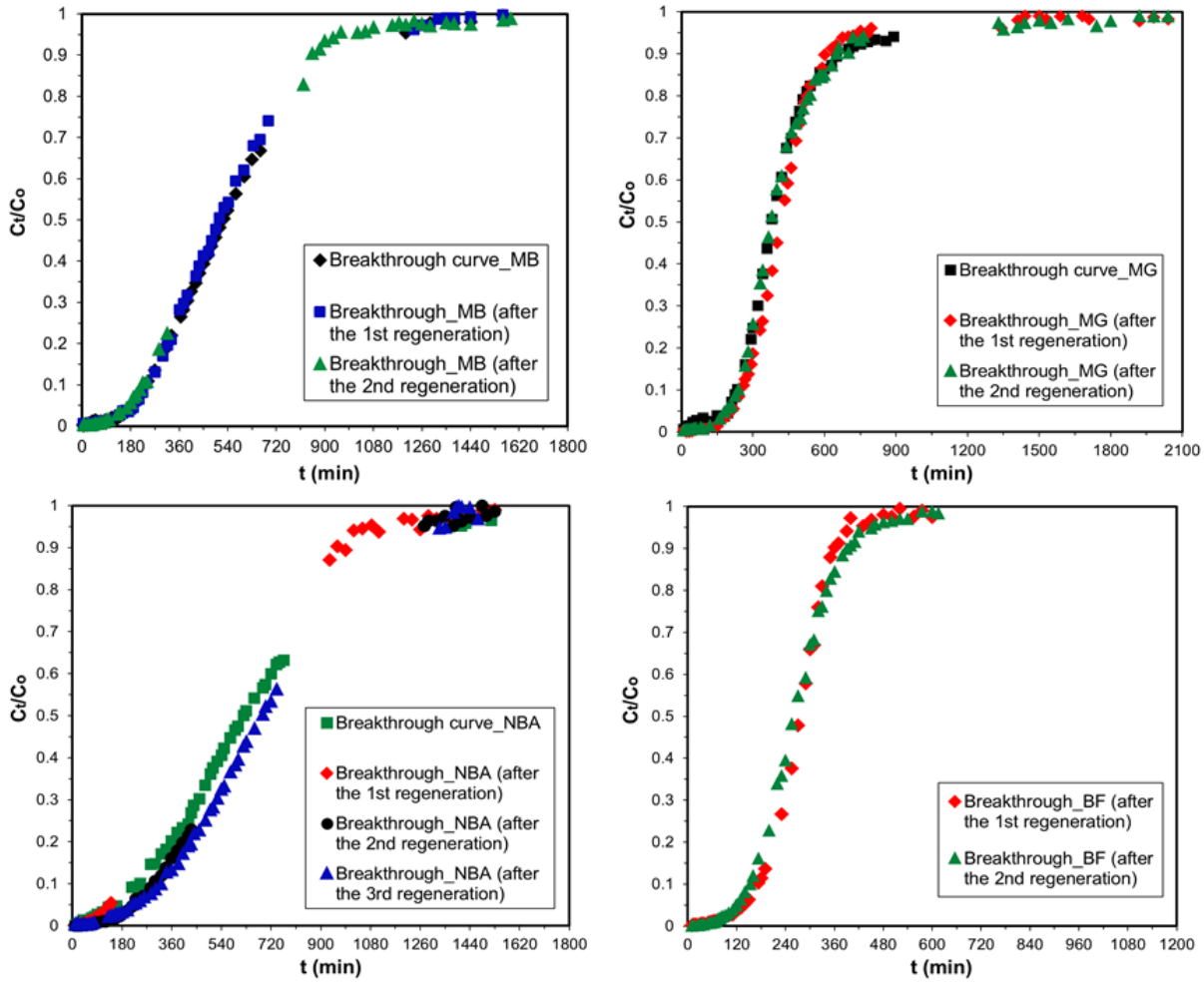

Source: The Author (2022)

It is essential to observe from Figure 36 that when the adsorbent is regenerated and reused, the breakthrough curves obtained, under the same conditions, did not show significant changes, remaining virtually constant, with similar values and shape. That corroborates with the idea that washing the material after

regeneration in batch mode might have interfered with the results for the reuse obtained in that case.

Evaluating the the removal of Pb (II) from water using GO decorated by MgO nanocubes in a fixed-bed adsorption column, Mohan *et al.* (2017) observed that for the three adsorption-desorption cycles with 0.1 M HCl, the regeneration efficiency was 97%. This reinforces the fact that GBM and its derivatives have remarkable regenerative potential, which represents a competitive advantage over other adsorbent materials.

5.2.4 Modeling of the breakthrough curves

Regarding the modeling of the breakthrough curves, LDF model for mass transfer was coupled to the mass balance, and results obtained after solving the system of equations numerically are depicted in Table 10 and Figure 37. As seen, the model exhibited a good prediction of the experimental data, being adequate to represent the experimental breakthrough curves. R^2 values were 0.98 for MB, 0.99 for NB, and 0.94 for MG. The least suitable fit to the model was presented for BF dye (R^2 = 0.88).

In addition to the sum of small experimental errors that become more significant because of the long experimental times, the observed deviation between experimental values and simulation for basic fuchsin (reflected in the coefficient of determination below 0.90) may be related to the condition that the modeling of breakthrough curves was proceeded based on the parameters from modeling of batch equilibrium data. As the equilibrium concentration was outside of the concentration interval used in batch tests, this difference was more significantly reflected in the fixed-bed parameters of BF dye - see Table 9.

To illustrate that, Appendix C presents the breakthrough modeling for BF, considering the adsorption capacity, as well as the equilibrium concentration of the fixed-bed experiment. Thus, in this case, keeping the other parameters constant (k_h, *Pe*, D_{ax}), the R^2 value rised from 0.88 to 0.94. Comparing the estimated values (Freundlich model) of the adsorptive capacities when C_e =9.28 mg.L^{-1} with the value obtained experimentally in fixed-bed test, the relative error (%) decreases from

23.43% to 12.88% when the fixed-bed experimental point is included in the batch isotherm.

Figure 37 - Experimental values and breakthrough curves predicted by the model (Experimental conditions: m_{bed}= 6.0g hydrogel (~0.13 g dry basis); Q =2.0 mL.min^{-1}; T =24ºC)

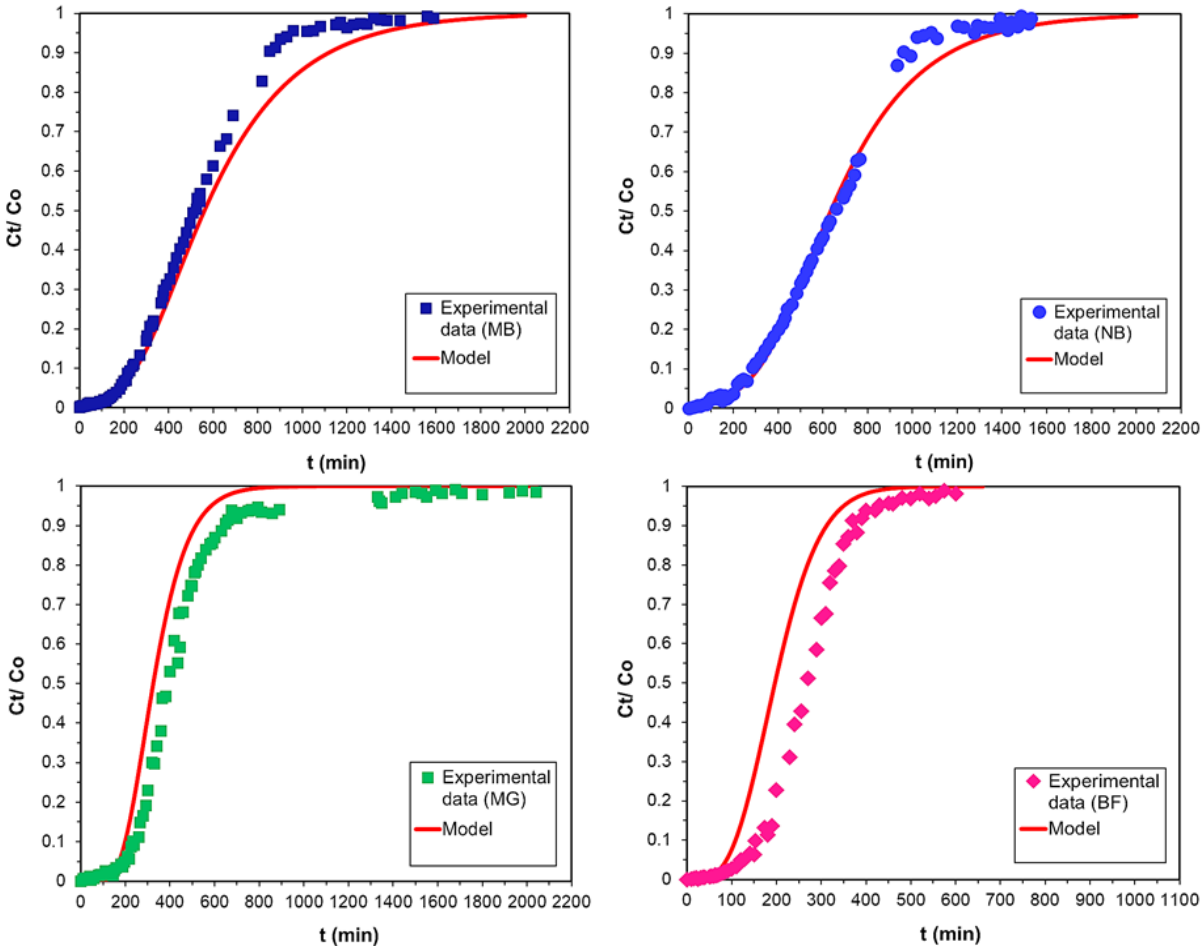

Source: The Author (2022)

Table 10 - Parameters predicted for the breakthrough curves (dry basis).

Parameters	Results			
	MB	NB	MG	BF
k_h (min^{-1})	3.70 10^{-3}	4.30 10^{-3}	5.20 10^{-2}	7.50 10^{-2}
D_{ax} (m^2.min^{-1})	9.20 10^{-5}	2.5 10^{-4}	6.50 10^{-5}	1.56 10^{-5}
Pe	12.93	4.76	18.31	76.28
R^2	0.98	0.99	0.94	0.88

Source: The Author (2022)

Observing the parameters in Table 10, it is indicated by the k_h values estimated that the adsorption of BF and MG reached the equilibrium faster than MB and NB. The same behavior was noted when modeling kinetic data in batch. The highest Peclet number (*Pe)* was obtained for BF (*Pe* =76.28), and the lowest value was for NB (*Pe* =4.76). In fact, the S-shaped breakthrough curves for MB, MG, and NB dyes were more inclined compared to the curve for BF, which in turn revealed a higher estimated *Pe* number. This can indicate the predominance of advective transport in the system (NASCIMENTO *et al.*, 2021).

Experimental values of adsorption capacity in the equilibrium, obtained on a dry basis, were compared with q_e values reported in previous works using different adsorbents, as shown in Table 11. It must be mentioned that the chemical groups on the materials surface, the surface area, morphological structure of the adsorbents, and pH should be considered, as these are essential parameters (PARLAYICI, 2019). Data revealed that, in general, the synthesized hydrogel using agar-GO demonstrated high adsorption capacities in fixed-bed system, being effective in removing the cationic dyes from water.

Table 11 - Experimental adsorption capacities of the cationic dyes onto the agar-GO composite (dry basis) in a fixed-bed system compared to previous works.

Adsorbent	Dye	$m_{ads.}$ (g)	Bed height (cm)	$C_{0\ dye}$ ($mg.L^{-1}$)	Q_0 ($mL.min^{-1}$)	q_e ($mg.g^{-1}$)	Reference
Unmodified citrus peels encapsulated with calcium alginate	MB	4.00	3.5	200	2.0	31.45	(AICHOUR *et al.*, 2019)
Ultrasonic surface modified chitin supported on sand	MB	5.0 g USM-chitin, 180.0g sand	25.0	50	10.0	51.80	(DOTTO, G. L. *et al.*, 2015)
Shaped MCM-41	MB	-	2.8	10	1.8	55.00	(RIOS *et al.*, 2020)
NaOH-modified rice husk	MG	-	4.5	50	5.0	57.61	(CHOWDHURY; SAHA, 2014)
Poly(Acrylonitrile Co-Acrylic Acid) Modified with Thiourea	MB	-	6.0	50	5.0	26.50	(ADEYI *et al.*, 2020)*
	MG					24.00	
Wastes from the Pacara Earpod tree	BF	28.00	25.0	200	20.0	124.50	(O. SALOMÓN *et al.*, 2020)
Ironwood seeds	BF	29.00	25.0	200	20.0	76.50	
Agar-GO composite hydrogel	MB	0.13	7.0	10	2.0	79.51	*This work*
	NB			20		226.46	
	MG			10		58.25	
	BF			10		38.11	

Source: The Author (2022)

* Simultaneous adsorption of MG and MB dyes binary mixture.

5.2.5 Mixture of cationic dyes and synthetic textile wastewater treatment via fixed-bed adsorption

Figure 38 a depicts the breakthrough curves for the areas below each absorption spectra in the visible region, for the mix of the dyes and the synthetic textile wastewater, as well as the respective absorption spectra for each case over time (Figures 38 b and c). The increase in $A_{Total(t)}/A_{Total0}$ follows the growth in the peaks of the absorption spectra as time increases. The breakthrough time for the mixture of dyes was about 1.75 h and is probably ascribed to the fact that basic fuchsin starts to leave the system earlier than the other dyes, as seen in the individual continuous tests with each dye.

The absorption spectra allow to observe the same behavior, and after BF, malachite green also begins to leave the column gradually. After 11.5 h, it is noticed that the MB and NB dyes start to leave the column in higher quantity. The formation of small "steps" is seen in the breakthrough curve for the mixture, indicating the beginning of the dye output according to the greater or lesser affinity of the dyes with the adsorbent.

Figure 38 - Breakthrough curves for the areas of the absorption spectra in the visible region for the mix of the dyes and synthetic wastewater (a); absorption spectra of the mixture of dyes over time (b); absorption spectra of the synthetic textile wastewater over time (c) (Experimental conditions: m_{bed}= 6.0 g hydrogel (0.13g dry basis); Q =2.0 mL.min^{-1}; T =24 ºC; pH=8).

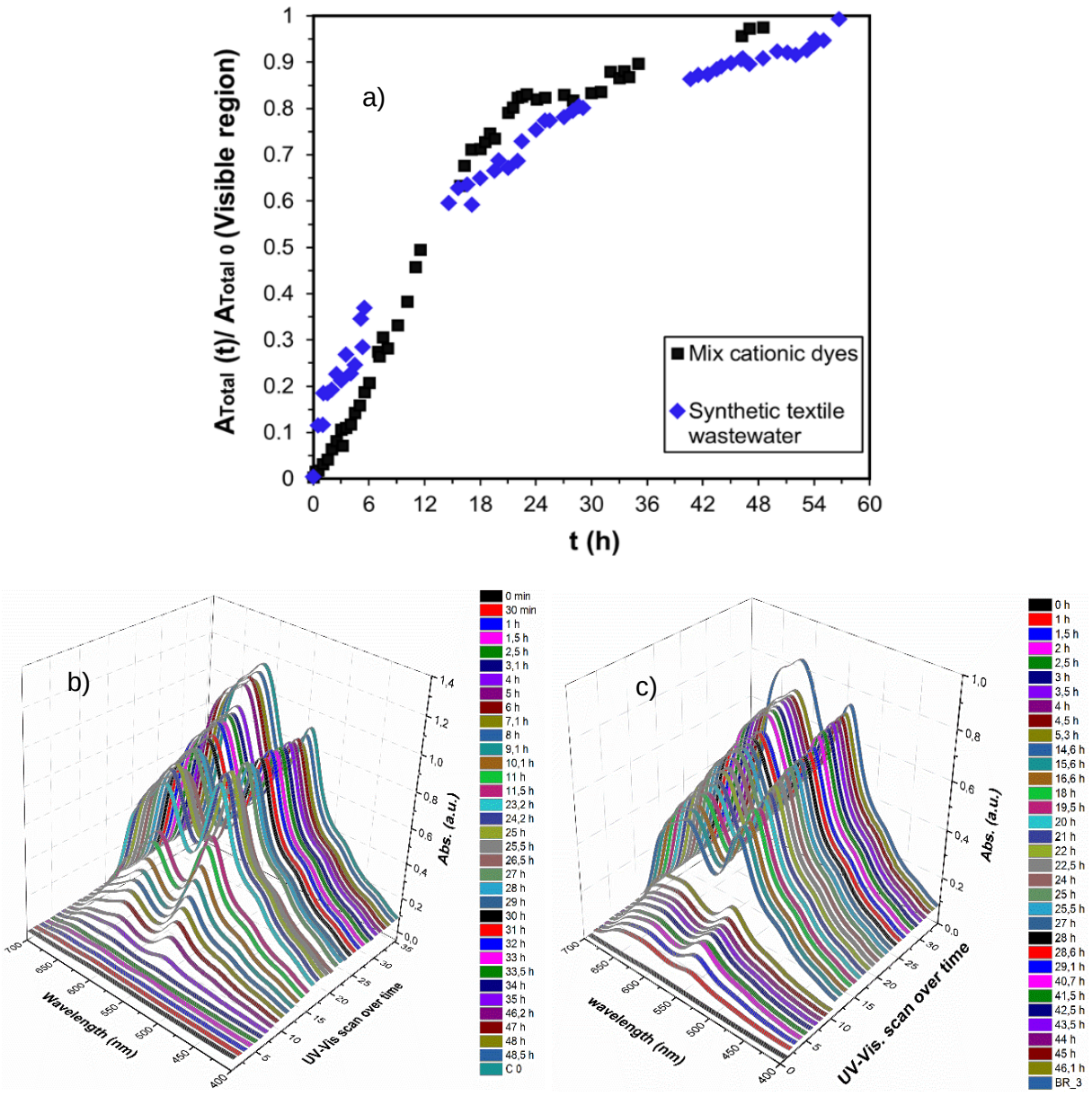

Source: The Author (2022)

The total time of the experiment was also much higher than single solute adsorption, being over 48 h, with an exhaustion time of 46.2 h (see Table 12). As reported by Walker and Weatherley (2000), the reduction in the fixed-bed efficiency

is expected in multi-solute adsorption systems, being attributed to the occurrence of competitive adsorption.

Table 12 - Breakthrough curve parameters for the mixture of dyes and synthetic wastewater

Sample	**t_{BR} (h)**	**t_{EX} (h)**	**$t_{f\ Total}$ (h)**	**Total volume of wastewater (L)**
Dyes mixture	1.75	46.20	48.50	5.82
Synthetic textile wastewater	0.21	54.10	56.70	6.80

Source: The Author (2022)

The formation of "steps" in the breakthrough curve was also observed analyzing the produced textile wastewater. There was a considerable decrease in the t_{BT} value, which reduced more than eight times as compared to the system with only a mixing of dyes in water. Besides different types of dyes, the textile wastewater produced has significant loads of other organic compounds (dispersing and lubricant agents) and can act as colorless agents affecting adsorption. Some of these colorless compounds can likely interfere, hampering the adsorption of the dyes, forming the first “steps” in the curves more rapidly. The exhaustion time also increased to 54.1 h.

In Figure 39, the breakthrough curve of TOC evolution over time is exhibited. The increase in $TOC_{(t)}$ /TOC_0 is fast, being over 0.87 in the first 30 min of the test; and bed exhaustion was observed in less than 2 h, quite different behavior from what was observed for color removal. As the textile wastewater produced has greater amounts of other organic compounds (compared to the dyes), these colorless compounds start to come out right at the beginning of the treatment, probably because most of them are not adsorbed by the biocomposite hydrogel. That is an indication of the adsorbent selectivity to separate the dyes.

Figure 39 - Breakthrough curve for TOC removal from the synthetic textile wastewater using Agar-GO hydrogel

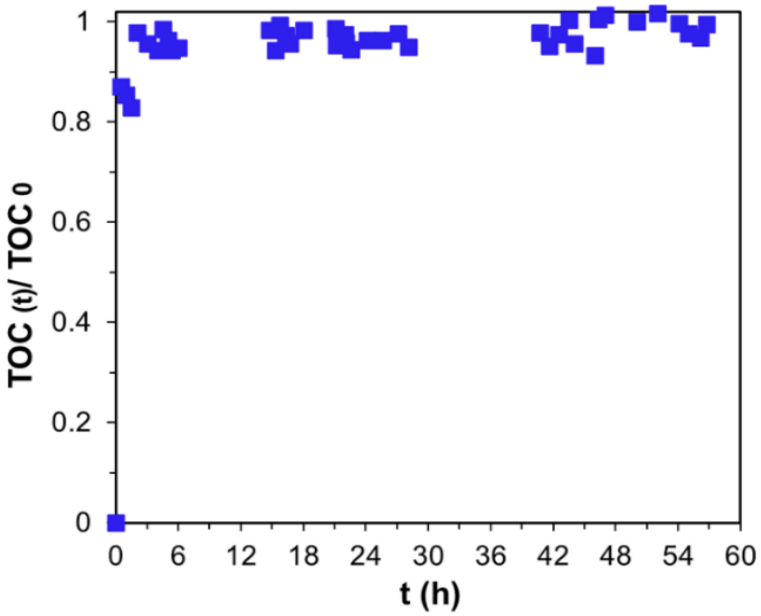

Source: The Author (2022)

According to Tang *et al.* (2020), agar/reduced GO composite was indeed capable of selectively adsorbing organic dyes. In this case, the selectivity could be ascribed to charge complementarity as the anionic groups on the biocomposite surface strongly attract the cationic groups in the dyes. Therefore, the dyes in wastewater could be partially recovered after adsorption/desorption treatment, with the possibility of returning to the coloring stage in a textile mill.

5.2.6 Real textile wastewater treatment via fixed-bed adsorption

Table 13 shows some characteristics of the raw wastewater from the textile mill, and the same wastewater after filtration using paper filter. Overall, the values found for the parameters regarding the real effluent agree with what was observed in previous works (ARAUJO *et al.,* 2020; HAYAT *et al.,* 2015). However, the value obtained for TOC was slightly lower than that observed by Biswas, Ray and Majumder (2020).

It is worth mentioning that that these parameters are influenced by the type of treatment used and the stage of the process the effluent is collected in the industrial wastewater treatment plant.

Table 13 - Characteristics of the textile wastewater before fixed-bed adsorption treatment

Parameters	**Raw textile wastewater**	**Filtered textile wastewater**	**Reference for raw wastewater**
pH	7.83	7.94	Araujo et al. (2020), Hayat et al. (2015)
Turbidity (NTU)	148.95	45.52	Hayat et al. (2015)
Conductivity (mS/cm)	7.25	7.10	Araujo et al. (2020), Hayat et al. (2015)
Color (nm)	236.23	154.44	-
TOC (mg/L)	175.20	127.50	Biswas, Ray, Majumder (2020)
IC (mg/L)	153.45	149.80	-

Source: The Author (2022)

The raw wastewater presented an intense red-brownish color to the naked eye, as exhibited in Figure 40 a. Figure 40 b depicts the breakthrough curves for the areas below each absorption spectra in the visible region, for the real textile wastewater, as well as the respective absorption spectra for each case over time (Figure 40 c). Figure 41 shows the breakthrough curves for the evolution of turbidity and TOC over time.

Figure 40 - Photograph of the raw textile wastewater sample used in the fixed-bed tests (a); breakthrough curves for the areas of each absorption spectra in the visible region for the real textile wastewater (b); absorption spectra of the real textile wastewater over time (c) (Experimental conditions: m_{bed}= 6.0 g hydrogel (0.13g dry basis); Q= 2.0 mL.min^{-1}; T =24 ^{o}C).

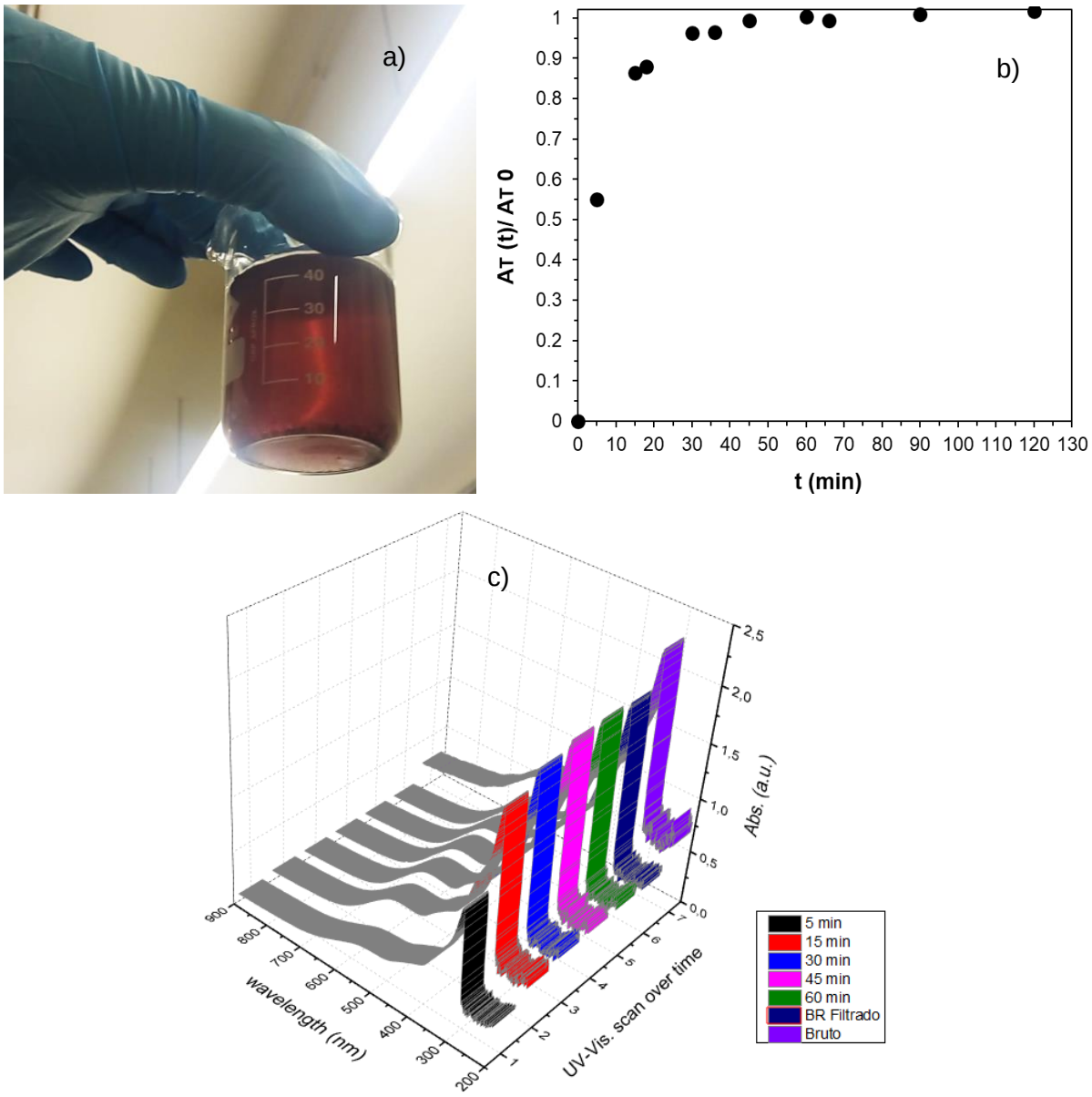

Source: The Author (2022)

Figure 41 – Breakthrough curves for the evolution of turbidity over time (a); breakthrough curves for the evolution of TOC over time (b) (Experimental conditions: m_{bed} = 6.0 g hydrogel (0.13 g dry basis); Q = 2.0 mL.min^{-1}; T = 24 ^{o}C)

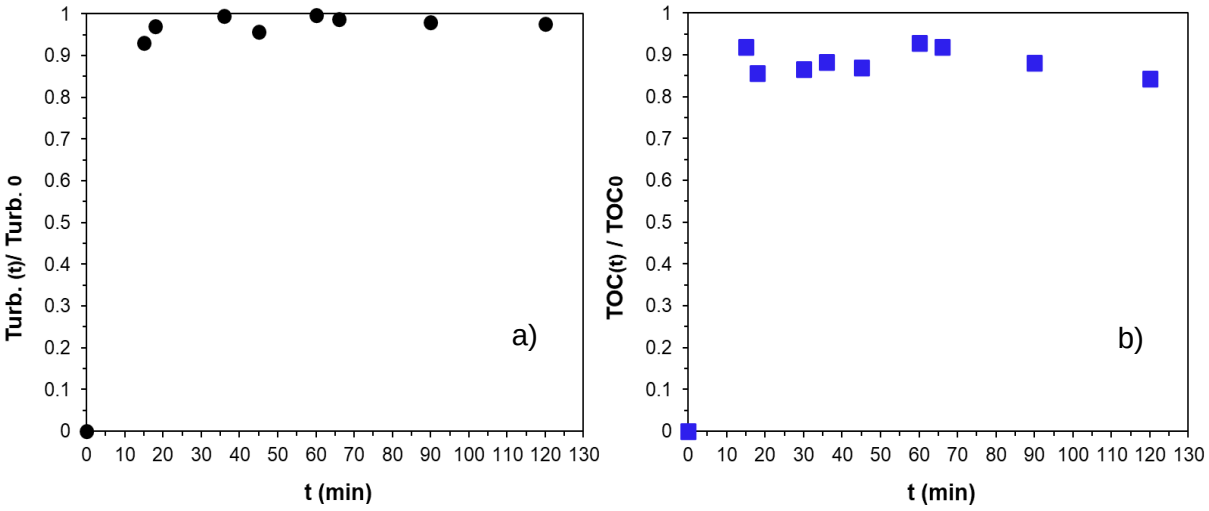

Source: The Author (2022)

From Figure 40 b it is observed that in about 30 min of the experiment the exhaustion time had already been reached. Breakthrough time (t_{BT}) occurred in less than 5 min of experiment. From the curves obtained in Figure 41, it was observed that both the breakthrough curve for TOC and for Turbidity presented behaviors similar to what is observed in Figure 40 b, since in less than 30 min t_{EX} had already been reached in both cases.

This can be attributed to the fact that most of the dyes present in the effluent are anionic (direct and reactive), since this effluent did not come from the dyeing of polyacrylic fibers (which in turn uses cationic dyes in the dyeing process). As previously discussed, the active sites of the biocomposite have a greater affinity for cationic substances, where interactions occur more easily on the surface of the adsorbent material. This, once again, indicates that indeed, the developed hydrogel selectively removes cationic dyes present in textile effluents. These cationic substances could even be fully recovered from industrial wastewaters, since the biocomposite produced has a remarkable capacity for regeneration and use.

For comparison purposes, Table 14 shows the parameters of the fixed-bed adsorption tests for both the synthetic and real textile wastewater. Figure 42 depicts the respective breakthrough curves obtained. Comparing the data from both

experiments, it is noted that while the t_{EX} value for the real wastewater is 30 min, the exhaustion time for the synthetic wastewater was over 54 h.

A great difference was also noticed between the total volumes of wastewater through the system. For the real textile wastewater, less than 250 mL of effluent were obtained at the end of the experiment with the fixed-bed column; for the synthetic wastewater, it was possible to obtain almost 7 L of effluent at the end of the process. Comparing the breakthrough curves in Figure 42, it is clear that, in fact, the proposed system was not efficient to treat the real wastewater sample, for the reasons already mentioned.

Table 14 - Breakthrough curve parameters of synthetic wastewater and real textile wastewater for color removal

Textile wastewater	**Dye type**	**t_{BR} (h)**	**t_{EX} (h)**	**t_{Total} (h)**	**Total volume of wastewater (L)**
Synthetic	Cationic	0.21	54.1	56.7	6.80
Real (raw)	Anionic	< 0.10	0.50	2.00	0.24

Source: The Author (2022)

Figure 42 – Breakthrough curves for the areas of absorption spectra in the visible region for real and synthetic textile wastewater

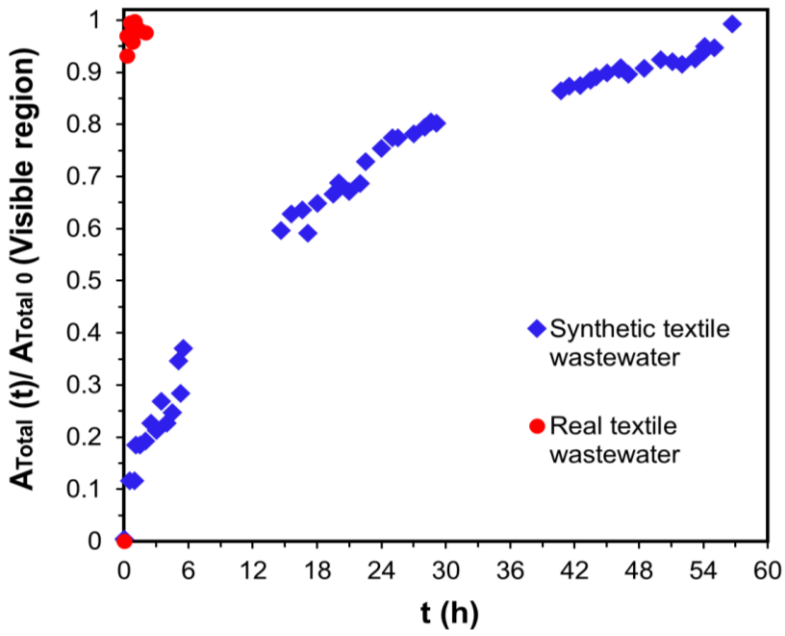

Source: The Author (2022)

In general, the results shed light on the practical use and viable application of graphene-based materials for the continuous treatment of water and industrial wastewater. Agar-GO hydrogel proved to be a feasible, economical, and environmentally friendly alternative since a small amount of material - 0.025 g of GO and 0.100 g of agar - is necessary to form the 6.00 g of hydrogel used to pack the column. Moreover, most of the material is of biodegradable nature, and it also showed remarkable regenerative and reuse capacity, proving its effectiveness and efficiency for application in industrial textile wastewater treatment.

The difficulty in separating the GO nanosheets from water did not represent a problem during the use of the hydrogel, which was exceptional for using the nanocomposite in the column. That also possibly reduces the risk of GO being leached by water during the process, which could represent a source of secondary contamination for water bodies.

5.3 FINAL THOUGHTS

Fixed-bed experiments using the hydrogel produced with 80% Agar and 20% GO indicated that the adsorption capacities of each dye separately, on a dry basis, were 79.51 $mg.g^{-1}$ (MB), 226.46 $mg.g^{-1}$ (NB), 58.25 $mg.g^{-1}$ (MG), and 38.11 $mg.g^{-1}$ (BF), demonstrating good regenerative potential. LDF model was fitted with the experimental data of breakthrough curves. The column packed with the agar-GO hydrogel was tested for the treatment of synthetic textile wastewater, and there was an indication of the adsorbent selectivity for the dye's separation. Agar-GO proved to be a viable, economical, and eco-friendly exciting alternative, since a small amount of adsorbent was used to continuously treat textile wastewater, being most of the composite biodegradable. Furthermore, the novel material showed remarkable regenerative capacity, proving its effectiveness and efficiency for wastewater treatment.

6 SELECTIVE REMOVAL OF CHLOROQUINE AND SAFRANIN-O FROM WATER USING AGAR-GRAPHENE OXIDE HYDROGEL

Chloroquine diphosphate, a drug normally used to treat malaria, has gained a lot of attention since the beginning of the COVID-19 pandemic, and its consumption has increased significantly in countries like Brazil, even after its proven controversial effectiveness to treat the disease. In this topic, Chloroquine (CQ), and the cationic dye Safranin-O (SO) were removed from water using the agar-graphene oxide (Agar-GO) hydrogel, produced via simple one-step jellification process. Batch experiments were performed, with adsorption isotherms satisfactorily fitting (R^2> 0.98) Sips (SO) and Freundlich (CQ) isotherms. Driving force models and Fick's diffusion equation were applied to the modeling of kinetic data, and a satisfactory fit was obtained. Adsorption competitiveness tests carried out in batch indicated that competitive adsorption occurs when both components are mixed in water solution - the adsorptive capacities dropped ~10 $mg.g^{-1}$ for each component, remaining 41 $mg.g^{-1}$ for SO and 31 $mg.g^{-1}$ for CQ. Fixed-bed breakthrough curves obtained in an adsorption column showed adsorption capacities over 63 $mg.g^{-1}$ and 100 $mg.g^{-1}$ for CQ and SO, respectively, also exhibiting outstanding regenerative potentials. Overall, the biocomposite produced using graphene oxide proved to be a viable and environmentally friendly alternative to continuously remove both contaminants from water.

Part of this main topic has been published:

DE ARAUJO, C. M. B. *et al.* Continuous removal of pharmaceutical drug Chloroquine and Safranin-O dye from water using agar-graphene oxide hydrogel: selective adsorption in batch and fixed-bed experiments. **Environmental Research**, v.216, p. 114425, 2022.

6.1 METHODOLOGY

Graphene oxide aqueous suspension was produced in the Laboratories of the Research Group on Environmental Technologies and Processes (GPTA), located at the Federal University of Pernambuco (UFPE, Brazil). All the adsorption experiments (both batch and fixed-bed) described in this topic were performed at the Laboratory of Environmental Management, Control and Preservation (LGCPA), in the

Department of Chemical Engineering at the State University of Maringá (UEM, Brazil).

6.1.1 Materials

GO preparation was performed using analytical grade graphite powder (Synth, Brazil), $KMnO_4$ (Química Moderna, Brazil), and H_2SO_4 (AnalaR NORMAPUR VWR Chemicals, France). The Agar-GO hydrogel (80% agar 20% GO) synthesis was performed using the analytical grade agar powder for laboratory and industrial use, obtained from Anidrol (Brazil), used without further purification. The methodologies involving the synthesis of GO, as well as the production process of the hydrogels, are described in detail in Topic 3.

Safranin-O (certified by the Biological Stain Commission) was obtained from Inlab (Brazil), and chloroquine diphosphate was purchased from a local drugstore (Farmácia Catanduvas, Brazil). Both analytical grade compounds were used without purification. 0.3 $mol.L^{-1}$ solutions of HCl and NaOH were used for pH adjustment.

Stock solutions of SO and CQ were prepared by dissolving each compound in distilled water to a volume up to 1000 mL. The working solutions used in the experiments were prepared by diluting the respective stock solutions with deionized water to the required concentrations (5, 10, and 20 $mg.L^{-1}$). Table 15 exhibits some characteristics regarding SO and CQ.

Table 15 - Characteristics of the adsorbates used in this work.

Name	**Chloroquine diphosphate**	**Safranin-O**
Synonyms	N4-(7-Chloro-4-quinolinyl)-N1,N1-dimethyl-1,4-pentanediamine diphosphate salt, N4-(7-chloroquinolin-4-yl)-N1,N1-diethylpentane-1,4-diamine diphosphate	Basic Red 2, Gossypimine, Cotton Red, 3,7-diamino-2,8-dimethyl-5 phenylphenazonium chloride
Molecular structure	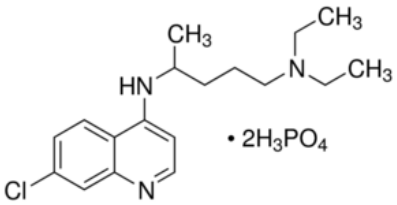	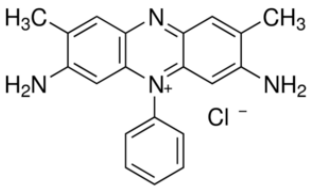
Molecular formula	$C_{18}H_{26}ClN_3 \cdot 2H_3PO_4$	$C_{20}H_{19}ClN_4$
Maximum wavelength (λ_{max} nm)	343	518
Molecular weight (g.mol^{-1})	515.86	350.84
CAS Number	50-63-5	477-73-6

Source: The Author (2022)

6.1.2 Batch adsorption experiments

Batch adsorption experiments were performed using a mass of the wet hydrogel with 25 mL solutions of SO and CQ, 20 mg.L^{-1} each, in separate sealed flasks. The flasks were then placed in a shaker for constant stirring at 250 rpm and T = 25 ^{o}C. After the specified contact time, the samples were removed from agitation and the supernatant was collected after decanting the hydrogel, and the final and initial concentrations were determined in a UV-Vis spectrophotometer according to the λ_{max} values presented in Table 15.

Preliminary adsorption kinetic experiments were carried out in order to verify, for different initial concentrations of adsorbates (5, 10, and 20 mg.L^{-1}) and a fixed mass of wet hydrogel (0.20 g), the time needed for the systems to reach equilibrium of adsorption. The adsorption capacity, q, was calculated using Equation 1.

Thereafter, the effect of changing the initial pH of CQ and SO solutions was evaluated in terms of removal efficiency in batch, %R (Equation 1 – Topic 3). The initial pH values of the solutions were adjusted using 0.30 mol.L^{-1} NaOH and HCl solutions.

6.1.2.1 Adsorption equilibrium and isotherms modeling

Adsorption isotherms of Chloroquine diphosphate and Safranin-O were obtained by adding 25 mL of the specified adsorbate solution (20 mg.L^{-1}) into flasks containing a specific mass of wet agar-GO. In each case, 0.10, 0.20, 0.50, 0.80, and 1.00 g of the hydrogel were weighted and used for the tests. Experiments were conducted in the natural pH of the adsorbates. The flasks were placed under constant stirring at 24 ^{o}C for 6 h (CQ) and 24 h (SO), to ensure the equilibrium was reached.

Using experimental data, the adsorption behaviors of the organic contaminants were evaluated using Langmuir (Equation 3), Freundlich (Equation 4) and Sips (Equation 5) adsorption isotherm models.

6.1.2.2 Adsorption kinetics and modeling

Kinetic experiments were conducted by placing 0.20 g of the wet agar-GO biocomposite into 25 mL of each CQ and SO solutions at an initial concentration of 20 mg.L^{-1}. Experiments were conducted in the natural pH of the adsorbates. Samples were taken and the concentrations were estimated at different time intervals in the range of 0 to 6 h for chloroquine, and from 0 to 24 h for Safranin-O. Studying the adsorption kinetics is important to determine and understand the rate-limiting mechanism of both adsorbates on the hydrogel of agar-GO.

The mass balance in a batch adsorption tank is given by Equation 6. The model was fit to the experimental data by applying the driving force models and Fick's equation, and the parameters were obtained by solving a system of differential equations. The Linear Driving Force (LDF) and Quadratic Driving Force (QDF) models are given by Equations 7 and 8, respectively. The effective homogeneous diffusivity (Dif) was estimated by Equation 9 for LDF model, and Equation 10 for QDF model, with R referring to the particle radius (RIOS *et al.,* 2020).

The diffusivity inside the particle was directly estimated using the Fick's Diffusion (FD) equation, doing the mass balance for a control volume inside the spherical particle (Equation 11).

6.1.3 Fixed-bed adsorption

Fixed-bed experiments were carried out for diluted solutions of CQ and SO, with an inlet concentration of 20 mg L^{-1}. The average flow rates in each case were around 2.0 $mL.min^{-1}$ and 4.0 $mL.min^{-1}$, to analyze the effect of the flowrate in the adsorption of both organic substances. Experiments were conducted at 24 ^{o}C with initial pH = 7.

Breakthrough curves were obtained using a borosilicate glass column packed with the biocomposite hydrogel. The process diagram of the fixed-bed experiments is given in Figure 43 a. The column used was purchased by the LGCPA (UEM) from GE Healthcare - XK 16/20, inner diameter 1.6 cm, total height 20 cm adjustable (Figure 43 b). 6.0 g of wet hydrogel was used for packing the column (~0.13 g of adsorbent on a dry basis), which was equivalent to a bed height of approximately 7.0 cm. The bed was compacted naturally by gravity and particle diameter was ~3 mm. Before starting the column adsorption, water was pumped through the system, using a peristaltic pump, for a few minutes, to prevent leaks and eliminate possible air bubbles. The fluid was pumped to the adsorption column in an upward flow, and samples were collected manually over time at the top of the column.

Figure 43 - Process diagram depicting the experimental setup for fixed-bed adsorption experiments (a); photograph of the packed column (b).

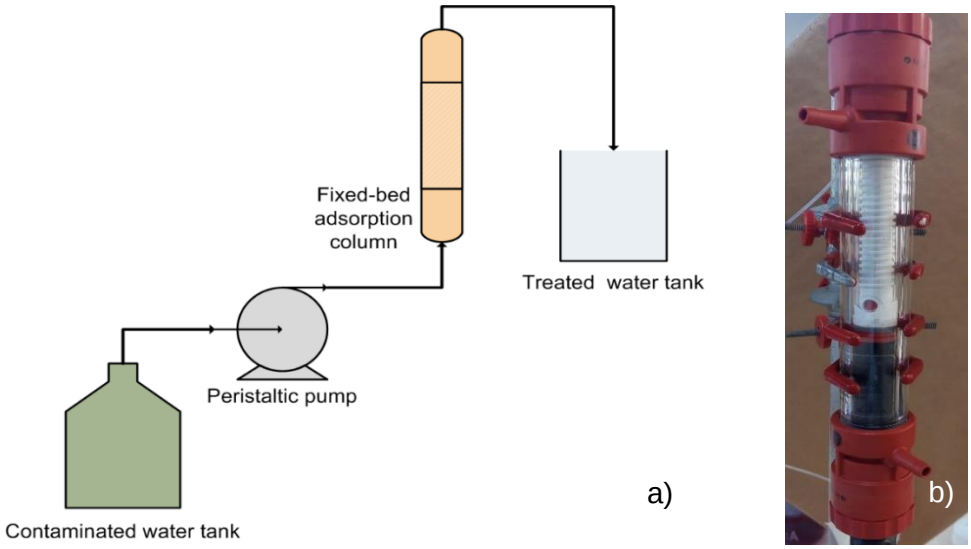

Source: The Author (2022)

Bed regeneration was performed by feeding the system with 0.30 M NaOH, applying the same flowrate and temperature used for the respective adsorption test. After desorption, the feed (NaOH solution) has been switched, and the system was continually washed with deionized water until pH =7.

From the breakthrough curves, the breakthrough time (t_{BR}), exhaustion time (t_{EX}), stoichiometric time (t_{st}), and the adsorption capacities (q_e) were estimated. It is worth mentioning that the breakthrough time and the exhaustion time were considered the times in which $C_t/C_0 = 0.05$ and $C_t/C_0 = 0.95$, respectively. t_{st} is given by Equation 15, q_e is given by Equation 16, and the removal efficiency of the column was calculated using Equation 17 (DOTTO *et al.,* 2015; RIOS *et al.,* 2020).

6.1.3.1 Modeling of fixed-bed breakthrough curves

Modeling of the breakthrough curves was performed similarly to what was proposed in Topic 5. Therefore, the experiments were simulated by a model comprising a mass balance, linear driving force model (LDF) to describe the mass transfer, as well as the corresponding boundary and initial conditions.

The mass balance for the adsorbate in fixed-bed is given by Equation 18. It considers convection flow, axial dispersion, accumulation in the fluid, as well as the

rate of adsorption onto the adsorbent. The relationship between D_{ax} and Peclet number (*Pe*) was given by Equation 19.

For the modeling, it was considered that the mass balance to the particle was described by the Linear Driving Force (LDF) equation (Equation 7). The isotherm parameters were obtained from the fit of equilibrium experimental data to the isotherm's models – Freundlich isotherm model for CQ and Sips model for SO dye.

The values of the coefficients of determination were estimated using the Equation 12 given in Topic 4.

6.1.4 Adsorption competitiveness in batch

Experiments regarding adsorption competitiveness were carried out by following the same procedure as the single-component experiments. In this case, the concentration of each component in the mixture was approximately 10 $mg.L^{-1}$, and pH = 7, approximately. Results were compared with those from single-component adsorption in terms of the equilibrium adsorption capacity (q_e), and removal efficiencies (%R).

6.2 RESULTS AND DISCUSSION

Results regarding the application of agar-GO nano-biocomposites as adsorbents to remove Safranin-O and Chloroquine diphosphate from water will be addressed and discussed in this section.

6.2.1 Batch adsorption

Results regarding the application of agar-GO nano-biocomposites to remove Safranin-O and Chloroquine diphosphate from water, in batch adsorption process will be addressed and discussed in this section.

6.2.1.1 Preliminary kinetics

Batch adsorption kinetics, obtained experimentally for CQ and SO at different initial concentrations, are exhibited in Figure 44. Overall, for CQ, the adsorptions capacities increased faster within the first 60 min of the experiment. From there, the

equilibrium is reached in approximately 120 min for all concentrations studied. On the other hand, for SO, the adsorptions capacities increased faster within the first 90 min of the experiment. From there, the equilibrium was reached within 120 min when the initial concentration was 5 $mg.L^{-1}$, and within 1200 min for the initial concentrations over 10 $mg.L^{-1}$.

Figure 44 - Preliminary adsorption kinetics at different initial concentrations of Chloroquine and Safranin-O (Conditions: m= 0.20 g (0.0043 g dry basis); C_0= 20 $mg.L^{-1}$; V= 25 mL; T= 24 ^oC; 250 rpm).

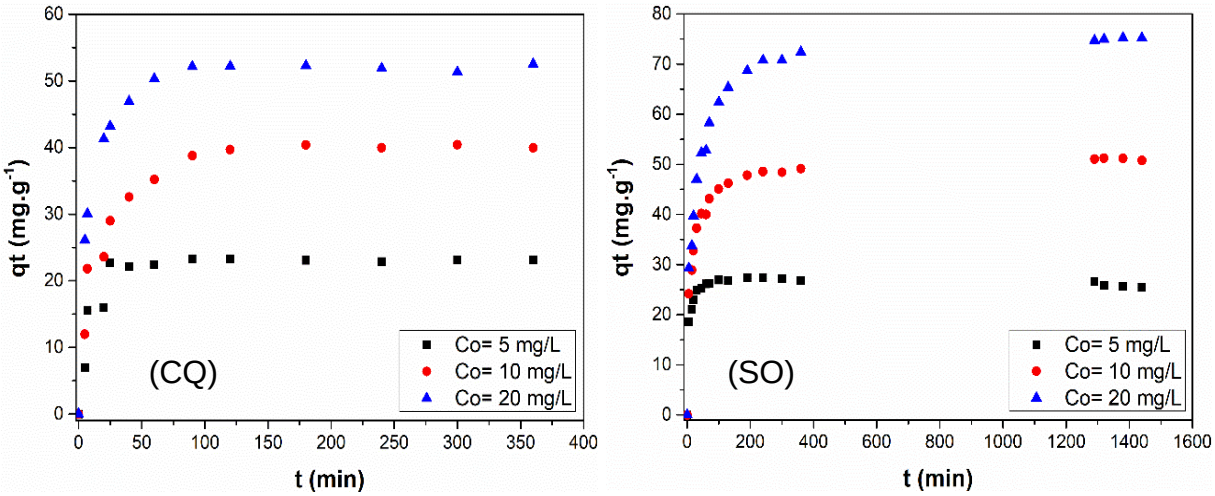

Source: The Author (2022)

A similar behavior was observed in Topic 4 for the results of preliminary adsorption kinetics for the cationic dyes MB, NB, MG, and BF. It was noted that long contact times of 24 h, and up to 48 h for some dyes, were necessary to ensure that equilibrium was reached indeed.

6.2.1.2 Effect of the initial pH

The influence of changing the initial pH of the solutions is depicted in Figure 45. It must be mentioned that the pH range used in each case was different, as the effect of protonation in Chloroquine when pH > 8 causes its concentration to be read at a much lower value than corresponds to reality.

Figure 45 - Effect of the initial pH in the removal efficiency of Chloroquine and Safranin-O (Conditions: t = 6 h (CQ) and 24 h (SO); m= 0.20g (0.0043 g dry basis); C0= 20 mg.L^{-1}; V= 25 mL; T= 24 ºC; 250 rpm).

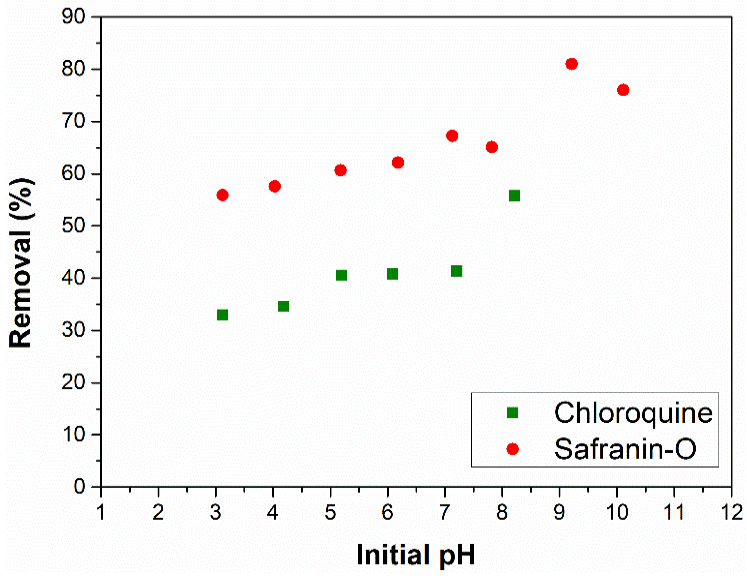

Source: The Author (2022)

Figure 45 shows that removal efficiency grows gradually, as the pH increases for both components, being more evident when the pH goes from 7 to 8 for CQ, and from 8 to 9 for SO (ADEYI *et al.,* 2020). This behavior was previously observed when analyzing the effect of the initial pH on the adsorption of methylene blue by graphene-based materials (CHEN *et al.,* 2017). That could be related to the adsorbent charge and molecular charge of adsorbate.

As SO is a cationic dye and CQ is a weak base, the great quantity of H^+ in the medium will compete with SO and CQ for the adsorption sites in acid medium, causing electrostatic repulsion, decreasing the adsorption capacity. Therefore, the H^+ competition will be less significant when the pH increases and oxygen groups of Agar-GO deprotonate, increasing the electrostatic attraction and the adsorption capacity (CHEN *et al.,* 2017).

6.2.1.3 Adsorption equilibrium isotherms

Experimental equilibrium data, and the results for the adjustments to Langmuir, Freundlich, and Sips adsorption isotherms are depicted in Figure 46. The

higher Agar-GO adsorption capacity was exhibited for the cationic dye SO, followed by CQ. In general, the isotherms exhibited an increase in the adsorption capacity, as the equilibrium concentration gradually increased. In the present work, the maximum adsorption capacities values on a dry basis, obtained experimentally, were 52.78 $mg \cdot g^{-1}$ for CQ, and 85.83 $mg \cdot g^{-1}$ for SO.

Evaluating the chloroquine adsorption by plantain peel activated carbon-supported zinc oxide nanocomposite, Dada *et al.* (2021) observed the maximum adsorption capacity of 50.51 $mg.g^{-1}$ at 303 K, very similar to what was found in the present work. When studying the adsorptive removal of chloroquine using an adsorbent synthesized through the combination of babassu coconut activated carbon and graphene oxide, Januário and coworkers (2022) found a maximum adsorption capacity value for CQ of 37.65 $mg.g^{-1}$.

Nehaba *et al.* (2019) used tea waste and active carbon manufactured from dates' stone as adsorbents to remove Safranin-O. In their study, the authors found maximum adsorption capacity values of 14.81 $mg.g^{-1}$ and 20.04 $mg.g^{-1}$ for tea waste and the activated carbon, respectively.

Overall, the values found in those previous works for the adsorption capacities at the equilibrium were lower than the obtained in the present work, using the Agar-GO hydrogel as adsorbent, considering both adsorbates analyzed (SO and CQ). On the other hand, Debnath and coworkers (2017) produced a chitosan composite crosslinked with graphene oxide for the removal of SO by ultrasonic adsorption from water. In the adsorption equilibrium study, the authors observed the maximum adsorption capacity of 279.6 $mg.g^{-1}$ at 298 K, predicted by the Langmuir equation.

Figure 46 - Equilibrium adsorption isotherms for Chloroquine and Safranin-O (Conditions: t = 6 h (CQ) and 24 h (SO); C_0= 20 mg.L^{-1}; V= 25 mL; T= 24 ºC; 250 rpm).

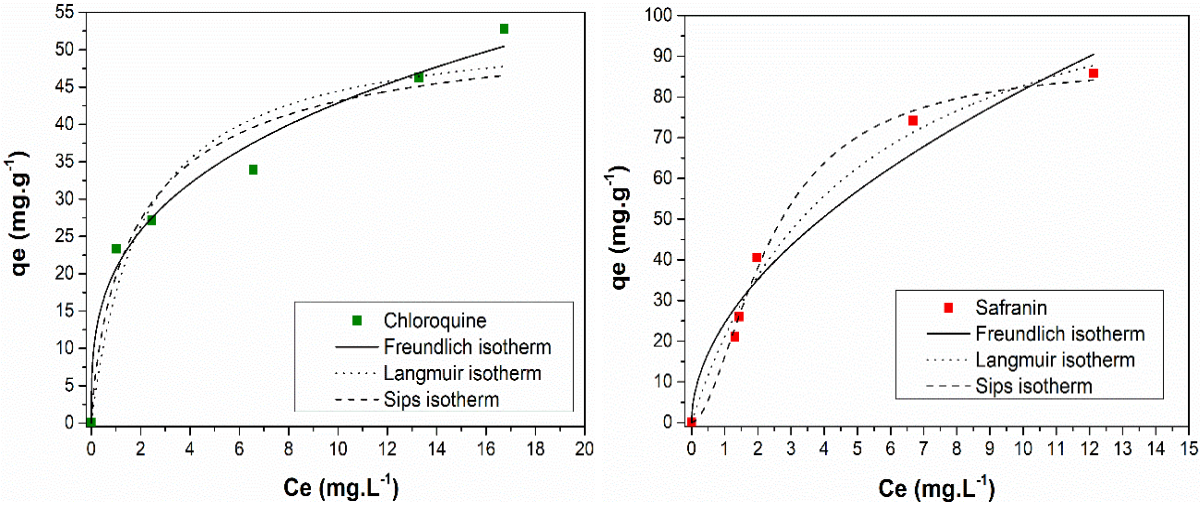

Source: The Author (2022)

Table 16 - Adsorption isotherm parameters (on a dry basis) calculated by adjusting the models to the experimental data.

Model	Parameters	Chloroquine		Safranin-O	
		Result	Std. Error	Result	Std. Error
Freundlich	K_F (mg$^{1-(1/n)}$. (g^{-1}). L$^{1/n}$)	20.68	1.75	24.45	3.65
	n	3.16	0.36	1.91	0.26
	Reduced χ^2	6.21	-	45.02	-
	Adjusted R^2	0.98	-	0.96	-
Langmuir	q_{mL} (mg.g^{-1})	53.66	5.73	122.50	10.65
	K_L(L.mg^{-1})	0.48	0.20	0.21	0.04
	Reduced χ^2	26.73	-	17.0	-
	Adjusted R^2	0.92	-	0.98	-
Sips	q_{mS} (mg.g^{-1})	55.0	25.21	88.91	5.78
	K_S (L.mg^{-1})^m	0.56	0.35	0.22	0.03
	m	0.81	0.77	1.76	0.35
	Reduced χ^2	29.73	-	7.79	-
	Adjusted R^2	0.91	-	0.99	-

Source: The Author (2022)

The fitting of the isotherm's parameters was performed using non-linear data regression. Data regarding the non-linear modeling are presented in Table 16. As

observed, SO equilibrium data better adjusted to the Sips isotherm (R^2 = 0.99), although values of coefficient of determination over 0.95 were observed for all isotherm models used. The compatibility of Sips isotherm demonstrates the combined features of Langmuir and Freundlich models. The Freundlich isotherm model was better fit to CQ equilibrium data, as the R^2 value in this case was 0.98, which indicates the adsorptive process of the organic compound occurs in multilayers. For CQ, the other isotherm models showed R^2 values below 0.95.

Evaluating the removal of SO by ultrasonic adsorption from aqueous solution, Debnath *et al*. (2017) produced a Chitosan composite crosslinked with GO. In their study, the Redlich Peterson isotherm model described the adsorption with more resemblance to the Langmuir isotherm than Freundlich.

Dada *et al.* (2021) studied the chloroquine adsorption by plantain peel activated carbon-supported zinc oxide nanocomposite. However, in this case, the authors noted that Langmuir and Temkin isotherms were better adjusted to the experimental equilibrium data, exhibiting coefficients of determination over 0.99.

6.2.1.4 Modeling of adsorption kinetics

Adsorption kinetic data are depicted in Figure 47 for the adsorption of both CQ and SO, and the respective modeling parameters are exhibited in Table 17. For the cationic dye SO, the initial concentration decreased faster in the first 5 h of the experiment, then the decrease was slowed, until the equilibrium was reached. Although, for CQ, the initial concentration of the pharmaceutical drug decreased faster in the first 1 h and 30 min, tending to the equilibrium after that. Therefore, CQ take less time to reach equilibrium compared to SO. It was observed that 24 h was sufficient to guarantee a steady state for the dye, and 6 h was sufficient to guarantee the equilibrium of adsorption for the drug. From the graphs, it is seen that the adsorption rate decreased as the driving force decreased. The same kinetic behavior was observed in previous works for the adsorption of cationic dyes (ARAUJO *et al.,* 2022; DUMAN *et al.,* 2020).

From Table 17, parameters for the hydrogel calculated by adjusting the kinetic models (LDF, QDF and FD) to adsorption experimental data are given on a dry basis. Analyzing the coefficients of determination for the adsorption of Chloroquine, the

values presented were above 0.90, and QDF and FD models showed the best fit to the kinetic data. Regarding the R^2 values for the adsorption of Safranin-O, except for the regression of the LDF model to the data obtained, in which R^2 = 0.88, QDF and FD models showed a good fit to the kinetic data (R^2 = 0.97). Comparing the effective diffusivity values, it is indicated that indeed, the adsorption of CQ reached the equilibrium faster than SO.

Table 17 - Parameters for the hydrogel (dry basis) calculated by adjusting the kinetic models to adsorption experimental data.

Model	Parameters	Results	
		Chloroquine	Safranin-O
LDF	k_{hLDF} (min^{-1})	0.12	$2.50\ 10^{-2}$
	Dif_{LDF} ($m^2.min^{-1}$)	$1.80\ 10^{-8}$	$3.75\ 10^{-9}$
	R^2	0.94	0.88
QDF	k_{hQDF} (min^{-1})	$5.90\ 10^{-2}$	$1.10\ 10^{-2}$
	Dif_{QDF} ($m^2.min^{-1}$)	$1.45\ 10^{-8}$	$2.71\ 10^{-9}$
	R^2	0.95	0.97
FD	Dif_{FD} ($m^2.min^{-1}$)	$1.80\ 10^{-8}$	$3.30\ 10^{-9}$
	R^2	0.91	0.97

Source: The Author (2022)

Figure 47 - Modeling of adsorption kinetics for Chloroquine and Safranin-O (Experimental conditions: m= 0.20 g (0.0043 g dry basis); C_0= 20 $mg.L^{-1}$; V= 25 mL; T= 24 ºC; 250 rpm).

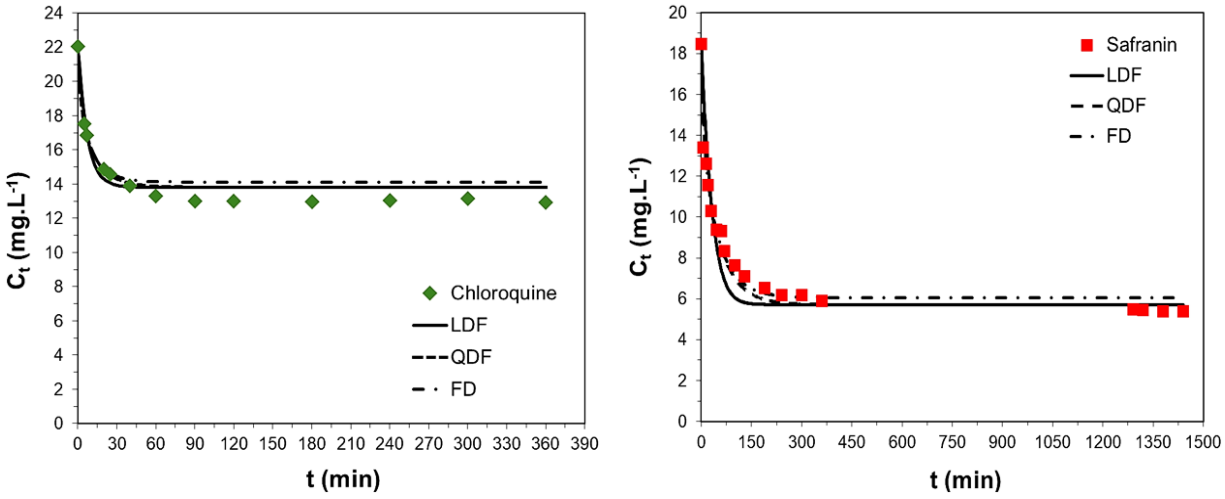

Source: The Author (2022)

6.2.2 Agar-GO adsorption mechanism

The removal mechanism proposed is presented in Figure 48, where the blue lines in the Agar-GO composite indicate the polymer helical structure wrapping GO nano sheets. As shown in the SEM micrographs (Topic 3), the Agar-GO aerogel structure presents many interspaces and channels, indicating that the adsorption of adsorbate molecules can occur through pore diffusion mass transfer. Thus, it is proposed that the adsorption mechanism is based on the electrostatic interactions between the cationic structures in CQ and SO molecules, and the composite.

As mentioned, Safranin-O is a basic dye, as well as MB, NB, MG, and BF dyes. Chloroquine, in turn, is considered a weak base, having 1 or 2 protonated Nitrogen in its structure, depending on the pH of the medium. In fact, Chloroquine is a diprotic weak base that can exist in both protonated and unprotonated forms (AL-BARI, 2014). Therefore, the compounds (SO and CQ) have in common the fact that both have some "basic" characteristic.

Figure 48 - Mechanism proposed for the adsorption of organic substances with basic characteristics onto the Agar-GO hydrogel composite

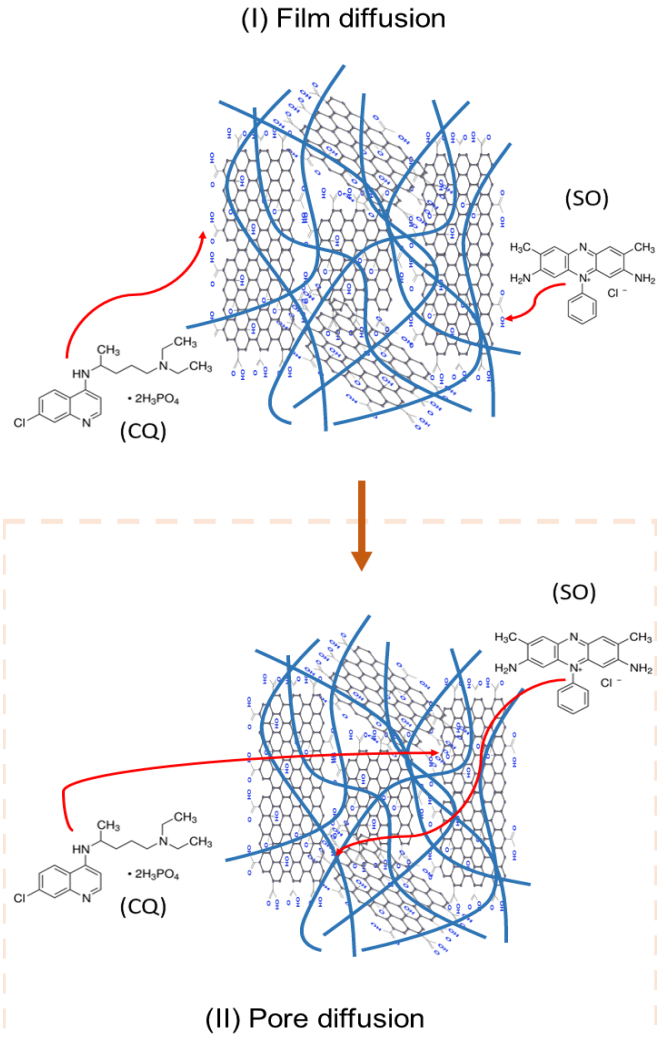

Source: The Author (2022)

In Figure 48, firstly, the adsorbates interact with the active sites on the adsorbent surface. Then, the molecules diffuse into the composite pores to access the more GO active sites (slower/ limiting step). As explained in Topic 4, the interactions between GO active sites and the molecules might occur through electrostatic attractions, hydrogen bonding, or π-π conjugation interactions.

6.2.3 Fixed-bed adsorption column

Breakthrough curves for each contaminant, using the agar-GO hydrogel packed bed, are exhibited in Figure 49 for different volumetric flowrates. Overall, the breakthrough curves present a S-shape, except for the curve for SO at a higher flowrate condition. Dispersion effects are observed in the breakthrough curves, and that probably occur because of the non-ideal packing of the column, axial dispersion, mass transfer resistances, as well as the fluid distribution throughout the column.

Breakthrough times and exhaustion times were estimated and can be found in Table 18. Breakthrough times for Chloroquine were equal to 91 min (2.0 $mL.min^{-1}$) and 21 min (4.3 $mL.min^{-1}$); and for Safranin-O t_B were equal to 75 min (2.0 $mL.min^{-1}$) and 9 min (4.5 $mL.min^{-1}$). Furthermore, by increasing the flowrate, if the system is under internal mass transfer resistance (which seems to be the case here), when the contact time between the adsorbate and the adsorbent decreases, the t_B also decreases (DOTTO *et al.,* 2015). That corroborates with the theory that pore diffusion is the controlling/ limiting step during the adsorption process.

Glyphosate removal from water using a composite of GO and $MnFe_2O_4$ nanoparticle supported on activated carbon was investigated by (MARIN *et al.,* 2019) in a fixed-bed adsorption system. The authors observed that although the increase in flowrate helps to reduce the external mass transfer resistance in the liquid film, very high flowrates greatly reduce the adsorbent/adsorbate contact time inside the column, which can negatively influence the contaminant removal process.

On the other hand, the experimental data in Table 18 demonstrate that for each adsorbate, tests with different flow rates exhibited approximately the same values for the respective adsorption capacities on a dry basis (66.15 $mg.g^{-1}$ and 63.89 $mg.g^{-1}$ for CQ; 101.52 $mg.g^{-1}$ and 100.64 $mg.g^{-1}$ for SO). Similar values of removal efficiencies were observed as well, for each adsorbate, even when changing the flow rates.

Zaka and coworkers (2021) evaluated the efficiency of reduced graphene oxide magnetite to remove the anti-inflammatory drugs Sodium diclofenac and Aspirin from wastewater. In addition to batch experiments, the authors also performed fixed-bed adsorption tests using the nanocomposite produced, where they found adsorption capacity values equal to 5.249 $mg.g^{-1}$ (Sodium diclofenac) and

23.59 mg.g^{-1} (Aspirin), predicted by the Thomas model (ZAKA; IBRAHIM; KHAMIS, 2021).

Figure 49 - Breakthrough curves for Chloroquine and Safranin-O at different flowrates (Conditions: m= 6 g (0.13 g dry basis); C_0= 20 mg.L^{-1}; T= 24 ^{o}C).

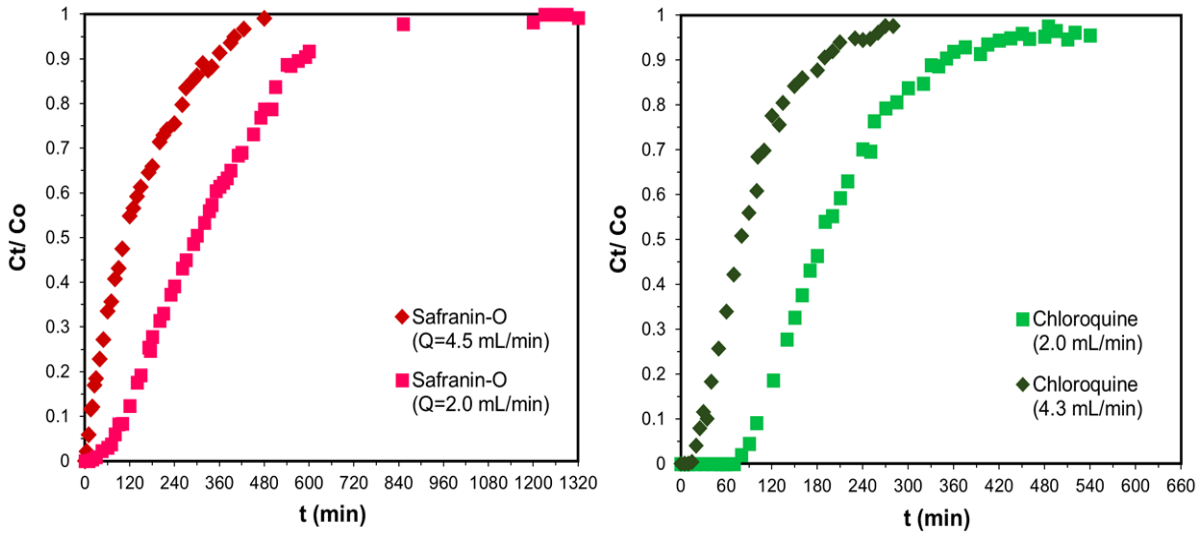

Source: The Author (2022)

Table 18 - Experimental values of the parameters from the breakthrough curves (dry basis).

Contaminant	Q (mL.min^{-1})	t_{BR} (min)	t_{EX} (min)	$t_{f\ Total}$ (min)	t_{st} (min)	%R	q_e fixed-bed (mg.g^{-1})
Chloroquine (CQ)	2.0	91	435	540	211.66	39.20	66.15
	4.3	21	230	280	94.91	33.90	63.89
Safranin-O (SO)	2.0	75	737	1230	336.50	27.36	101.52
	4.5	9	402	480	146.30	30.48	100.64

Source: The Author (2022)

Comparing the adsorption capacities values from the fixed-bed experiments with the q_e from the isotherms in batch, the errors were >10%. That could be attributed to the fact that the feed concentration (which is also the equilibrium concentration, C_e) was outside of the concentration interval used to plot the isotherms (See Figure 50). Although, the sum of small experimental errors, through

the long experimental hours must also have contributed to make this difference more significant (RIOS *et al.,* 2020).

Figure 50 – Batch isotherms and the blue dot highlighted regarding the experimental values from breakthrough curves for the contaminants CQ and SO (dry basis)

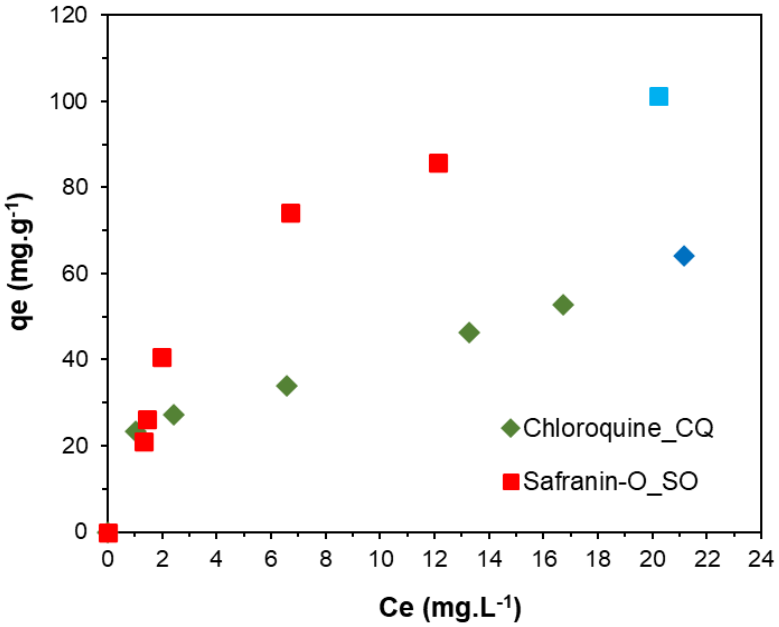

Source: The Author (2022)

When the adsorbent is regenerated and reused using 0.30 M NaOH, the breakthrough curves obtained, under the same conditions, did not show significant changes, remaining virtually constant, with similar experimental points and shape, as shown in Figure 51. This behavior was also observed for the breakthrough curves obtained for the cationic dyes in Topic 5.

Graphene-based materials such as composites and those obtained after the functionalization of GO also showed remarkable potential for regeneration and reuse (after adsorption) in previous works. Studying the adsorptive removal of methylene blue dye using the amino-iron oxide functionalized graphene oxide as adsorbent, (FRAGA *et al.,* 2019) noted that the adsorbent maintained its removal rate over 95% even after 10 adsorption-desorption cycles.

Figure 51 - Breakthrough curves for Chloroquine and Safranin-O with the hydrogel before and after regeneration with NaOH and reuse (Conditions: m= 6 g (0.13 g dry basis); C_0= 20 mg.L^{-1}; T= 24 ºC).

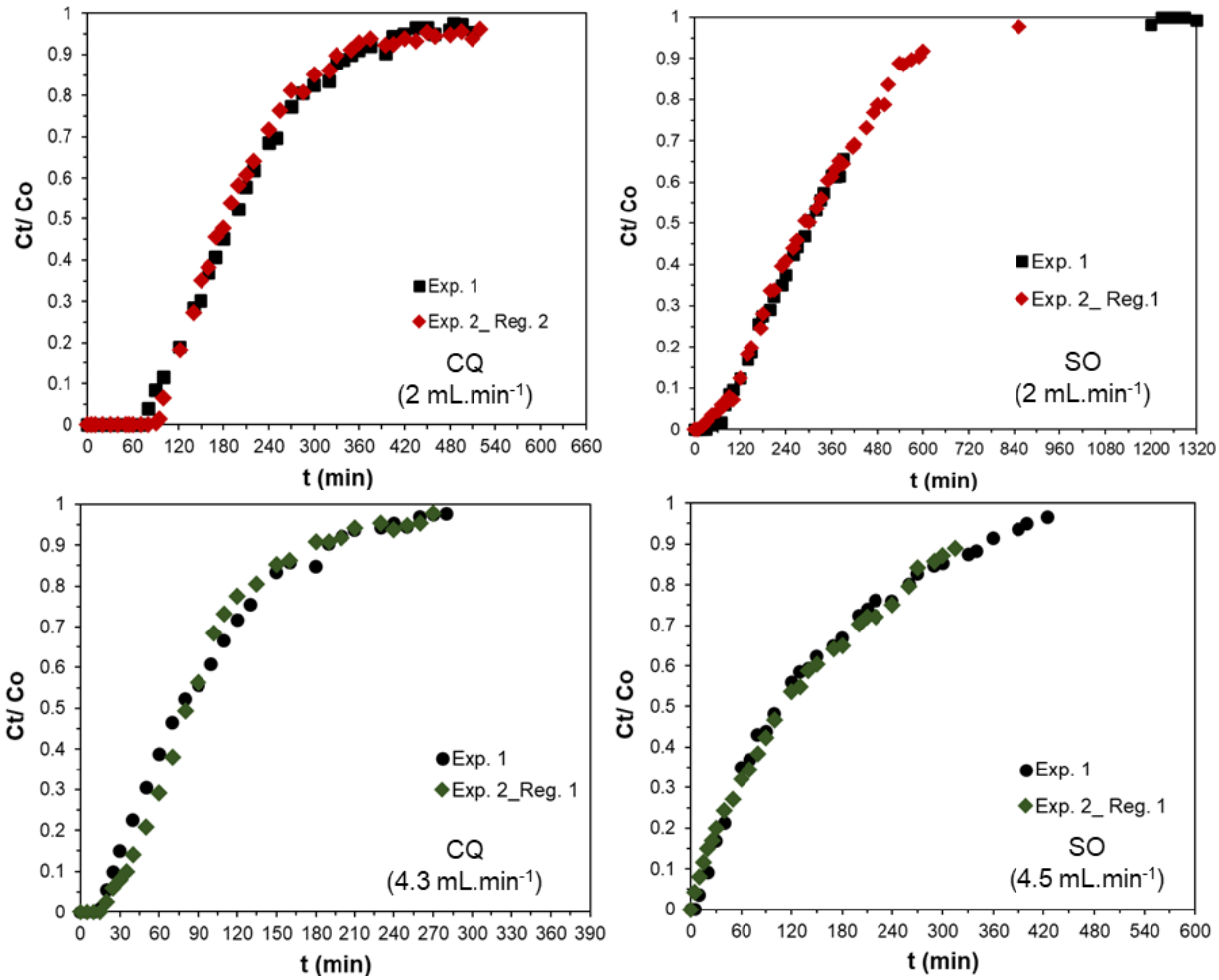

Source: The Author (2022)

Regarding the modeling of the breakthrough curves, LDF model for mass transfer was coupled to the mass balance, and the results obtained after solving the system of differential equations numerically are exhibited in Table 19 and depicted in Figure 52. Similar to what was observed in Topic 5 for the modeling of the breakthrough curves obtained for the cationic dyes MB, NB, MG and BF, the LDF model also exhibited a good prediction of the experimental data, being adequate to represent the experimental curves. R^2 values were 0.90 and 0.93 for the modeling of CQ and SO breakthrough curves, respectively.

Figure 52 - Experimental values and breakthrough curves predicted by the model (Experimental conditions: m_{bed}= 6.0g hydrogel (~0.13 g dry basis); Q =2 mL.min^{-1}; T =24ºC)

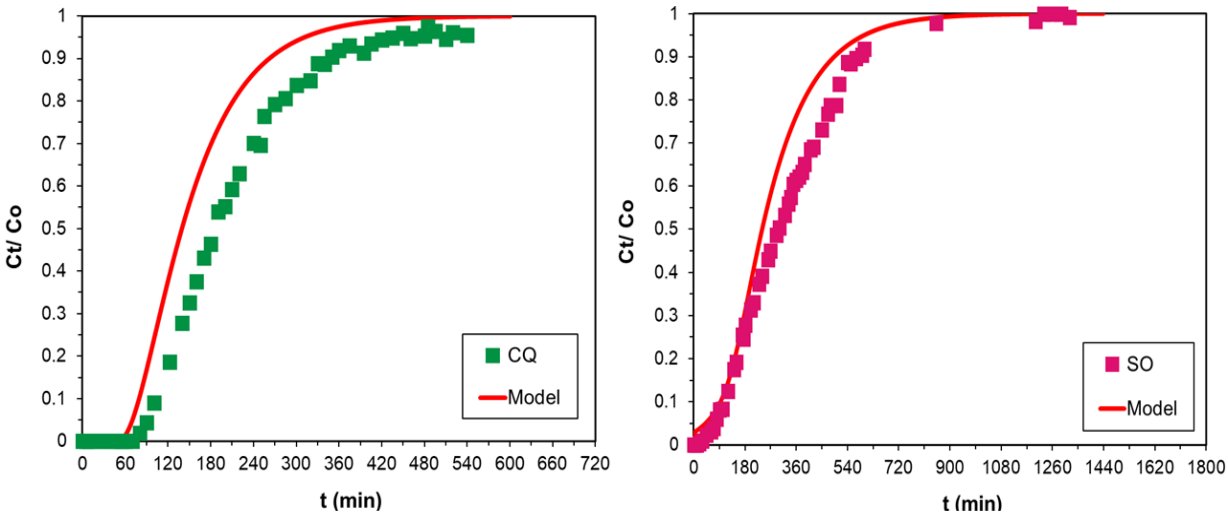

Source: The Author (2022)

Table 19 - Parameters predicted for the breakthrough curves (dry basis).

Parameters	Results	
	CQ	SO
k_h (min^{-1})	2.20 10^{-2}	6.90 10^{-3}
D_{ax} (m^2.min^{-1})	1.60 10^{-4}	2.80 10^{-4}
Pe	7.44	4.25
R^2	0.90	0.93

Source: The Author (2022)

Observing the parameters in Table 19, it is indicated by the k_h values estimated that the adsorption of CQ reached the equilibrium faster than SO. The same behavior was noted when modeling kinetic data in batch. Peclet number obtained for CQ breakthrough curve was very close to the estimated value using blue dextran as a tracer (*Pe* = 7.62 – See Topic 5). On the other hand, Peclet number estimated for SO breakthrough curve was very close to those obtained for NB dye (*Pe* = 4.76). That results might indicate the predominance of advective transport in the continuous system (NASCIMENTO *et al.*, 2021).

6.2.4 Adsorption competitiveness

Studying the adsorption competitiveness in batch (Figure 53) the maximum adsorption capacities and the removal efficiency of both organic contaminants under binary conditions were lower than those under single-component conditions. According to the results, compared to the single-component adsorption isotherm, the reduction rates (%) of maximum adsorption capacity in the binary adsorption system were around 19% for SO and 22% for CQ. As the reduction rates considering the removal efficiency in the binary adsorption system were around 20% for SO and 26% for CQ.

These results indicate that the adsorption of both CQ and SO onto agar-GO was almost equally affected by the competitive adsorption (PARK *et al.,* 2015). Bai *et al.* (2020) studied the simultaneous adsorption of two cationic dyes (methylene blue and neutral red) using a composite of alginate hybridized with graphene oxide in both single and binary systems. The authors noted that in a single solute the dyes were adsorbed by the composites due to hydrogen bonding, electrostatic attraction, and π−π interaction. Although, competitive adsorption of both dyes was observed in the binary system, and the authors ascribed that to the structure formulas and molecular sizes of the dyes.

Figure 53 - Competitiveness for Chloroquine and Safranin-O (Experimental conditions: t= 24 h; m= 0.20 g (0.0043 g dry basis); $C_{0\ MIX}$= 10 mg.L^{-1} for CQ and SO each in the mix; V= 25 mL; T= 24 ºC; 250 rpm).

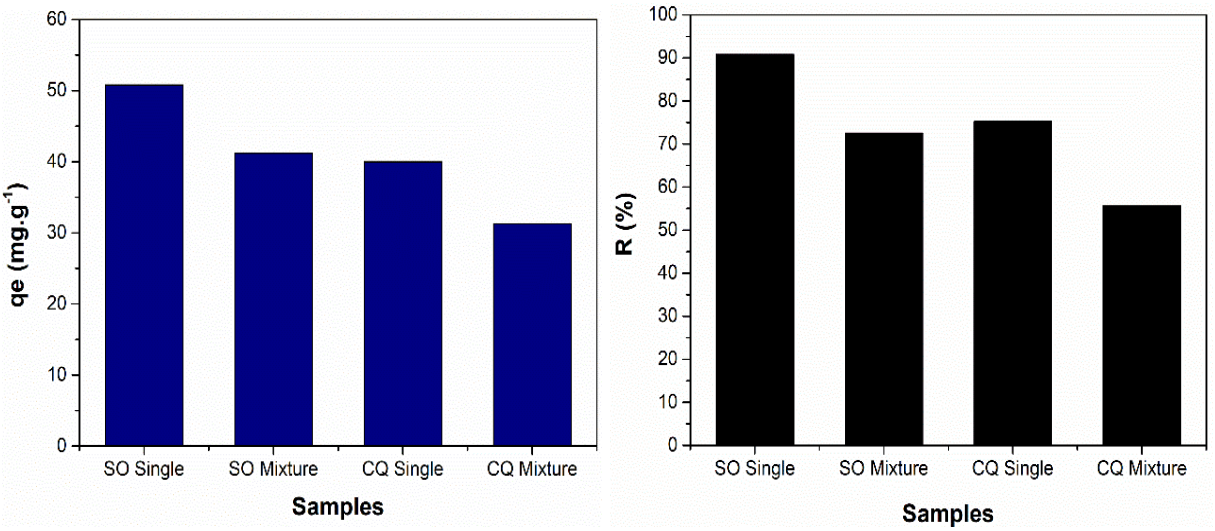

Source: The Author (2022)

6.3 FINAL THOUGHTS

Agar-GO hydrogel was used as adsorbent to remove the cationic dye Safranin-O and the pharmaceutical drug Chloroquine, and the competitiveness of the adsorption using the biocomposite was tested. From the batch experiments, the adsorption isotherms satisfactorily fitted (R^2 >0.98) Sips (Safranin-O) and Freundlich (Chloroquine) isotherms. Driving force models and Fick's diffusion equation were applied to the modeling of kinetic data, and a satisfactory fit was obtained in both cases. Adsorption competitiveness carried out in batch indicated that competitive adsorption occurs when both components were mixed in water, as the adsorptive capacities dropped approximately 10 $mg.g^{-1}$ for each component, remaining 41 $mg.g^{-1}$ for safranin-O and 31 $mg.g^{-1}$ for chloroquine. Fixed-bed breakthrough curves obtained in an adsorption column showed adsorption capacities over 63 $mg.g^{-1}$ and 100 $mg.g^{-1}$ for chloroquine and Safranin-O, respectively, also exhibiting outstanding regenerative potentials. Overall, the biocomposite produced using GO proved to be a viable and environmentally friendly alternative to continuously remove emergent contaminants from water.

7 CONCLUSIONS AND PERSPECTIVES

This topic presents the overall conclusions of the thesis, focused on the development of hydrogel biocomposites using graphene oxide and the biopolymer agar, for applications in the continuous treatment of water and industrial wastewaters, through fixed-bed adsorption. In addition to the general conclusion, this topic also presents some perspectives for future works that may be explored beyond the subject studied.

7.1 CONCLUSIONS

Studying the GO production, it was noticed that decreasing, up to a certain extent, the amount of acid during GrO production promoted to a lower degree of graphite oxidation, which enabled a better interaction of the material with anionic dyes via π-π interactions. However, satisfatory oxidation still occurs, showing the possibility of reducing the amount of acid used during the synthesis. Characterizations of three biocomposite (Agar-GO) hydrogels synthesized in different proportions evidenced GO interaction with the polymeric matrix, resulting in 3D materials, with visually disordered morphologies, and a variety of oxygen functional groups.

Preliminary batch kinetic tests indicated that the hydrogels were efficient in removing cationic dyes, but the same was not observed for the anionic dyes. MB, MG, and BF isotherms were best fitted to Freundlich model, and NB isotherm fitted Sips model. Kinetic data were satisfactorily adjusted to LDF, QDF, and Fick's Diffusion equations. The maximum experimental adsorption capacities, on a dry basis, were obtained for the sample produced with 70% of Agar and 30% of GO, being 141.48 $mg.g^{-1}$ (MB), 284.69 $mg.g^{-1}$ (NB), 52.29 $mg.g^{-1}$ (MG), and 34.00 $mg.g^{-1}$ (BF). Fixed-bed experiments were performed for the sample produced with 80% of Agar and 20% of GO, since it presented a higher mechanical resistance during the tests; and the adsorption capacities obtained, on a dry basis, were 79.51 $mg.g^{-1}$ (MB), 226.46 $mg.g^{-1}$ (NB), 58.25 $mg.g^{-1}$ (MG), and 38.11 $mg.g^{-1}$ (BF), also demonstrating good regenerative potential. The column packed with the hydrogel was tested for the treatment of synthetic textile wastewater, and there was an indication of the adsorbent "preference" for the separation of cationic dyes.

In addition, the hydrogel was tested as adsorbent to remove Safranin-O and the pharmaceutical drug Chloroquine, and the adsorption competitiveness for the dye and the drug using the biocomposite as adsorbent was tested. From the batch experiments, the adsorption isotherms satisfactorily fitted Sips (SO) and Freundlich (CQ) isotherms. Driving force models and Fick's diffusion equation were applied to the modeling of kinetic data, and a satisfactory fit was obtained in both cases. Tests regarding adsorption competitiveness carried out in batch indicated that competitive adsorption occurs when both components were mixed in water, as the adsorptive capacities dropped approximately 10 $mg.g^{-1}$ for each component, remaining 41 $mg.g^{-1}$ for SO and 31 $mg.g^{-1}$ for CQ. Finally, fixed-bed breakthrough curves obtained in an adsorption column showed adsorption capacities over 63 $mg.g^{-1}$ and 100 $mg.g^{-1}$ for CQ and SO, respectively.

Overall, the agar-GO hydrogels exhibited a remarkable regenerative capacity in all experiments performed - both in batch and fixed-bed, also with the cationic dyes and the pharmaceutical drug tested. The novel material synthesized proved to be a viable, economical, and environmentally friendly alternative, since most of the composite is biodegradable, and a small amount of adsorbent was used to continuously treat wastewater. Moreover, a decrease in the phytotoxicity effects of the effluent was observed after adsorption; thus, the composite produced would not represent a source of secondary contamination for the aqueous medium.

7.2 PERSPECTIVES

Although the Agar-GO hydrogel has shown satisfactory results for the removal of organic compounds with cationic or weak base characteristics in aqueous media, it would be interesting to test the removal of other types of contaminants with a positive charge, such as heavy metal ions. A study was carried out in the laboratory for the removal of Cd^{2+}, Pb^{2+} and Ni^{2+} using Agar-GO, however, due to the difficulty of accessing the equipment for quantification, it was only possible to perform a few preliminary tests. However, there is the perpective of obtaining promising results in this area.

In addition, there is also the possibility of testing other types of graphene-based materials during composite synthesis, such as reduced graphene oxide, or

functionalized GO. This could be done to expand the range of contaminants that can be adsorbed by the developed material.

Since the material developed showed mechanical stability for tests in fixed-bed, a possibility for future work could also involve testing the material as an adsorbent in other types of continuous systems - simulated moving bed (SMB), for example. The influence of sonication on the adsorption of cationic dyes and pharmaceuticals can also be explored using the hydrogel as adsorbent.

REFERENCES

ABBASI, M.; SAFARI, E.; BAGHDADI, M.; JANMOHAMMADI, M. Enhanced adsorption of heavy metals in groundwater using sand columns enriched with graphene oxide: Lab-scale experiments and process modeling. **Journal of Water Process Engineering**, v. 40, p. 101961, 2021.

ABER, S.; SHEYDAEI, M. Removal of COD from industrial effluent containing indigo dye using adsorption method by activated carbon cloth: optimization, kinetic, and isotherm studies. **CLEAN–Soil, Air, Water**, v. 40, n. 1, p. 87-94, 2012.

ABOUBARAKA, A. E.; ABOELFETOH, E. F.; EBEID, E. Z. M. Coagulation effectiveness of graphene oxide for the removal of turbidity from raw surface water. **Chemosphere**, v. 181, p. 738-746, 2017.

ABUZERR, S.; DARWISH, M.; MAHVI, A. H. Simultaneous removal of cationic methylene blue and anionic reactive red 198 dyes using magnetic activated carbon nanoparticles: equilibrium, and kinetics analysis. **Water Science and Technology**, v. 2017, n. 2, p. 534-545, 2018.

ADEYI, A. A.; JAMIL, S. N. A. M.; ABDULLAH, L. C.; CHOONG, T. S. Y.; LAU, K. L.; ALIAS, N. H. Simultaneous adsorption of malachite green and methylene blue dyes in a fixed-bed column using poly (acrylonitrile-co-acrylic acid) modified with thiourea. **Molecules**, v. 25, n. 11, p. 2650, 2020.

AICHOUR, A.; ZAGHOUANE-BOUDIAF, H.; ZUKI, F. B. M.; AROUA, M. K.; IBBORA, C. V. Low-cost, biodegradable and highly effective adsorbents for batch and column fixed bed adsorption processes of methylene blue. **Journal of Environmental Chemical Engineering**, v. 7, n. 5, p. 103409, 2019.

AL-BARI, A. A. Chloroquine analogues in drug discovery: New directions of uses, mechanisms of actions and toxic manifestations from malaria to multifarious diseases. **Journal of Antimicrobial Chemotherapy**, v. 70, n. 6, p. 1608–1621, 2014.

ALFONSO-GORDILLO, G.; FLORES-ORTIZ, C. M.; MORALES-BARRERA, L.; CRISTIANI-URBINA, E. Biodegradation of methyl tertiary butyl ether (MTBE) by a microbial consortium in a continuous up-flow packed-bed biofilm reactor: kinetic study, metabolite identification and toxicity bioassays. **PloS one**, v. 11, n. 12, p. e0167494, 2016.

AMERICAN PUBLIC HEALTH ASSOCIATION. A. P. H. A. Water Environment Federation (1999) Standard methods for the examination of water and wastewater. **Standard Methods**.

ANASTOPOULOS, I.; MITTAL, A.; USMAN, M.; MITTAL, J.; YU, G.; NÚÑEZ-DELGADO, A.; KORNAROS, M. A review on halloysite-based adsorbents to remove pollutants in water and wastewater. **Journal of Molecular Liquids**, v. 269, p. 855-868, 2018.

DE ANDRADE, J. R.; OLIVEIRA, M. F.; CANEVESI, R. L. S.; LANDERS, R.; DA SILVA, M. G. C.; VIEIRA, M. G. A. Comparative adsorption of diclofenac sodium and losartan potassium in organophilic clay-packed fixed-bed: X-ray photoelectron spectroscopy characterization, experimental tests and theoretical study on DFT-based chemical descriptors. **Journal of Molecular Liquids**, v. 312, p. 113427, 2020.

ANDRÉ, N. Venda de ivermectina cresce 857% no último ano. **CNN Brasil. Retrieved September**, v. 23, p. 2021, 2021.

ARAUJO, C. M. B.; ASSIS FILHO, R. B.; BAPTISTTELLA, A. M. S.; NASCIMENTO, G. F. O.; COSTA, G. R. B.; CARVALHO, M. N.; GHISLANDI, M. G.; MOTTA SOBRINHO, M. A. Systematic study of graphene oxide production using factorial design techniques and its application to the adsorptive removal of methylene blue dye in aqueous medium. **Materials Research Express**, v. 5, 2018.

ARAÚJO, C. M. B.; NASCIMENTO, G. F. O., COSTA, G. R. B.; BAPTISTTELLA, A. M.; FRAGA, T. J.; ASSIS FILHO, R. B.; GHISLANDI, M. G.; MOTTA SOBRINHO, M. A. Real textile wastewater treatment using nano graphene-based materials: optimum pH, dosage, and kinetics for colour and turbidity removal. **The Canadian Journal of Chemical Engineering**, v. 98, n. 6, p. 1429-1440, 2020.

ARAUJO, C. M. B.; NASCIMENTO, G. F. O.; COSTA, G. R. B.; SILVA, K. S.; BAPTISTTELLA, A. M. S.; GHISLANDI, M. G.; MOTTA SOBRINHO, M. A. Adsorptive removal of dye from real textile wastewater using graphene oxide produced via modifications of hummers method. **Chemical Engineering Communications**, p. 1-13, 2018.

ASSIS FILHO, R. B.; ARAUJO, C. M. B., BAPTISTTELLA, A. M. S.; BATISTA, E. B.; BARATA, R. A.; GHISLANDI, M. G.; MOTTA SOBRINHO, M. A. Environmentally friendly route for graphene oxide production via electrochemical synthesis focused on the adsorptive removal of dyes from water. **Environmental Technology**, n. just-accepted, p. 1-43, 2019.

ATCHUDAN, R.; EDISON, T. N. J. I.; PERUMAL, S.; KARTHIKEYAN, D.; LEE, Y. R. Facile synthesis of zinc oxide nanoparticles decorated graphene oxide composite via simple solvothermal route and their photocatalytic activity on methylene blue degradation. **Journal of Photochemistry and Photobiology B: Biology**, v. 162, p. 500-510, 2016.

AYODHYA, D.; VEERABHADRAM, G. A review on recent advances in photodegradation of dyes using doped and heterojunction-based semiconductor metal sulfide nanostructures for environmental protection. **Materials today energy**, v. 9, p. 83-113, 2018.

BAI, H.; CHEN, J.; WANG, Z.; WANG, L.; LAMY, E. Simultaneous removal of organic dyes from aqueous solutions by renewable alginate hybridized with graphene oxide. **Journal of Chemical & Engineering Data**, v. 65, n. 9, p. 4443-4451, 2020.

BANERJEE, P.; SAU, S.; DAS, P.; MUKHOPADHAYAY, A. Optimization and modelling of synthetic azo dye wastewater treatment using graphene oxide

nanoplatelets: characterization toxicity evaluation and optimization using artificial neural network. **Ecotoxicology and environmental safety**, v. 119, p. 47-57, 2015.

BAPTISTTELLA, A. M. S.; ARAUJO, A. A. D.; BARRETO, M. C.; MADEIRA, V. S.; MOTTA SOBRINHO, M. A. The use of metal hydroxide sludge (in natura and calcined) for the adsorption of brilliant blue dye in aqueous solution. **Environmental technology**, p. 1-14, 2018.

BAPTISTTELLA, A. M. S.; ARAUJO, C. M. B.; DA SILVA, M. P.; NASCIMENTO, G. F. O. D.; COSTA, G. R. B.; DO NASCIMENTO, B. F.; GHISLANDI, M. G.; MOTTA SOBRINHO, M. A. Magnetic Fe3O4-graphene oxide nanocomposite–synthesis and practical application for the heterogeneous photo-Fenton degradation of different dyes in water. **Separation Science and Technology**, v. 56, n. 2, p. 425-438, 2021.

BIERNATH, A. “Kit covid é kit ilusão”: os dados que apontam riscos e falta de eficácia de tratamento precoce. **UOL VivaBem**, p. 1–20, 2021.

BISWAS, B.; RAY, S. K.; MAJUMDER, C. Total organic carbon (TOC) removal from textile wastewater by electro-coagulation: Prediction by response surface modeling (RSM). **J. Indian Chem. Soc.**, v. 97, n. 12b, p. 2720-2724, 2020.

BRASIL. Ministério do Meio Ambiente. Resolução nº 430, de 16 de maio de 2011. Conselho Nacional do Meio Ambiente (CONAMA), Brasília, DF, 2011.

BUSTOS-RAMÍREZ, K.; BARRERA-DIAZ, C. E.; DE ICAZA-HERRERA, M.; MARTINEZ-HERNANDEZ, A. L.; NATIVIDAD-RANGEL, R.; VELASCO-SANTOS, C. 4-chlorophenol removal from water using graphite and graphene oxides as photocatalysts. **Journal of Environmental Health Science and Engineering**, v. 13, n. 1, p. 33, 2015.

CESTARI, J. L.; MATSUMOTO, T.; DALL'AGLIO SOBRINHO, M.; LIBÂNIO, M. Avaliação hidrodinâmica de unidade piloto de floculação mecanizada. **Engenharia Sanitária e Ambiental**, p. 95-106, 2012.

CHAUDHARY, H.; GUPTA, D.; GUPTA, C. The Journal of The Textile Institute Multifunctional dyeing and finishing of polyester with Sericin and Basic dyes Multifunctional dyeing and finishing of polyester with Sericin and Basic dyes. **The Journal of The Textile institute**, v. 108, n. 3, p. 314–324, 2017.

CHEN, J.; YAO, B.; LI, C.; SHI, G. An improved Hummers method for eco-friendly synthesis of graphene oxide. **Carbon**, v. 64, p. 225-229, 2013.

CHEN, L.; LI, Y.; DU, Q.; WANG, Z.; XIA, Y.; YEDINAK, E.; LOU, J.; CI, L. High performance agar/graphene oxide composite aerogel for methylene blue removal. **Carbohydrate polymers**, v. 155, p. 345-353, 2017.

CHOWDHURY, S.; BALASUBRAMANIAN, R. Recent advances in the use of graphene-family nanoadsorbents for removal of toxic pollutants from wastewater. **Advances in colloid and interface science**, v. 204, p. 35-56, 2014.

CHOWDHURY, S.; SAHA, P. D. Effect of Hydrothermal Carbonization Reaction Parameters on. **Environmental Progress & Sustainable Energy**, v. 33, n. 3, p. 676–680, 2014.

DADA, A. O.; INYINBOR, A. A.; BELLO, O. S.; TOKULA, B. E. Novel plantain peel activated carbon–supported zinc oxide nanocomposites (PPAC-ZnO-NC) for adsorption of chloroquine synthetic pharmaceutical used for COVID-19 treatment. **Biomass Conversion and Biorefinery**, p. 1-13, 2021.

DAS, A.; PAL, A.; SAHA, S.; MAJI, S. K. Behaviour of fixed-bed column for the adsorption of malachite green on surfactant-modified alumina. **Journal of Environmental Science and Health Part A**, v. 44, n. 3, p. 265-272, 2009.

DEBNATH, S.; PARASHAR, K.; PILLAY, K. Ultrasound assisted adsorptive removal of hazardous dye Safranin O from aqueous solution using crosslinked graphene oxide-chitosan (GO[sbnd]CH) composite and optimization by response surface methodology (RSM) approach. **Carbohydrate Polymers**, v. 175, p. 509–517, 2017.

DELGADO, J. M. P. Q. A critical review of dispersion in packed beds. **Heat and Mass Transfer/Waerme- und Stoffuebertragung**, v. 42, n. 4, p. 279–310, 2006.

DONG, S.; SUN, Y.; WU, J.; WU, B.; CREAMER, A. E.; GAO, B. Graphene oxide as filter media to remove levofloxacin and lead from aqueous solution. **Chemosphere**, v. 150, p. 759-764, 2016.

DOTTO, G. L.; DOS SANTOS, J. N.; ROSA, R.; PINTO, L. A. A.; PAVAN, F. A.; LIMA, E. C. Fixed bed adsorption of Methylene Blue by ultrasonic surface modified chitin supported on sand. **Chemical Engineering Research and Design**, v. 100, p. 302-310, 2015.

DUMAN, O.; POLAT, T. G.; DIKER, C. Ö.; TUNÇ, S. Agar/κ-carrageenan composite hydrogel adsorbent for the removal of Methylene Blue from water. **International journal of biological macromolecules**, v. 160, p. 823-835, 2020.

FANG, Z.; HU, Y.; WU, X.; QIN, Y.; CHENG, J.; CHEN, Y.; TAN, P.; LI, H. A novel magnesium ascorbyl phosphate graphene-based monolith and its superior adsorption capability for bisphenol A. **Chemical Engineering Journal**, v. 334, p. 948-956, 2018.

FERDOUSE, F.; HOLDT, S. L.; SMITH, R.; MURÚA, P.; YANG, Z. The global status of seaweed production, trade and utilization. **Globefish Research Programme**, v. 124, p. I, 2018.

FOROUTAN, R.; MOHAMMADI, R.; RAMAVANDI, B. Elimination performance of methylene blue, methyl violet, and Nile blue from aqueous media using AC/CoFe2O4 as a recyclable magnetic composite. **Environmental Science and Pollution Research**, v. 26, n. 19, p. 19523–19539, 2019.

FRAGA, T. J. M.; LIMA, L. E. M.; SOUZA, Z. S. B.; CARVALHO, M. N.; LUNA FREIRE, E. M. P.; GHISLANDI, M. G.; MOTTA SOBRINHO, M. A. Amino-Fe_3O_4-

functionalized graphene oxide as a novel adsorbent of Methylene Blue: kinetics, equilibrium, and recyclability aspects. **Environmental Science and Pollution Research**, p. 1-10, 2018.

FRAGA, T. J. M.; MOTTA SOBRINHO, M. A.; CARVALHO, M. N.; GHISLANDI, M. G. State of the art: synthesis and characterization of functionalized graphene nanomaterials. **Nano Express**, v. 1, n. 2, p. 022002, 2020.

FUJITA, R. M. L.; JORENTE, M. J. V. A Indústria Têxtil no Brasil: uma perspectiva histórica e cultural. **Moda Palavra e-periódico**, v. 8, n. 15, p. 153-174, 2015.

GARRIDO, T.; ETXABIDE, A.; GUERRERO, P.; DE LA CABA, K. Characterization of agar/soy protein biocomposite films: Effect of agar on the extruded pellets and compression moulded films. **Carbohydrate polymers**, v. 151, p. 408-416, 2016.

GERBER, M. D.; LUCIA JR, T.; CORREA, L.; NETO, J. E. P.; CORREA, É. K. Phytotoxicity of effluents from swine slaughterhouses using lettuce and cucumber seeds as bioindicators. **Science of the Total Environment**, v. 592, p. 86-90, 2017.

GHALY, A. E., ANANTHASHANKAR, R.; ALHATTAB, M. V. V. R.; RAMAKRISHNAN, V. V. Production, characterization and treatment of textile effluents: a critical review. **J Chem Eng Process Technol,** v. 5, n. 1, p. 1-18, 2014.

GLOBAL TRADE. Global Direct Dye Market Decreased by -3.6% to $1.9B in 2019. Published in: July 30th, 2020. Available at: https://www.globaltrademag.com/global-direct-dye-market-decreased-by-3-6-to-1-9b-in-2019-2/. Access in: 12th October 2022.

GONG, J. L.; ZHANG, Y. L.; JIANG, Y.; ZENG, G. M.; CUI, Z. H.; LIU, K.; DENG, C. H.; NIU, Q. Y.; DENG J. H.; HUAN, S. Y. Continuous adsorption of Pb (II) and methylene blue by engineered graphite oxide coated sand in fixed-bed column. **Applied Surface Science**, v. 330, p. 148-157, 2015.

GORGOLIS, G.; GALIOTIS, C. Graphene aerogels: a review. **2D Materials**, v. 4, n. 3, p. 032001, 2017.

GREWE, T; MEGGOUH, M.; TÜYSÜZ, H. Nanocatalysts for solar water splitting and a perspective on hydrogen economy. **Chemistry–An Asian Journal**, v. 11, n. 1, p. 22-42, 2016.

GROWTH MARKET REPORTS. Global Indigo Dyes Market Expected to Reach USD 1,639 Million by 2028. Published in: December 3rd, 2021. Available at: https://growthmarketreports.com/press-release/global-indigo-dyes-market-expected-to-reach-usd-1639-million-by-2028. Access in: 12th October 2022.

GUPTA, V. K.; KHAMPARIA, S.; TYAGI, I.; JASPAL, D.; MALVIYA, A. Decolorization of mixture of dyes: a critical review. **Global Journal of Environmental Science and Management**, v. 1, n. 1, p. 71-94, 2015.

GURUNATHAN, S.; HAN, J. W.; EPPAKAYALA, V.; KIM, J. H. Green synthesis of graphene and its cytotoxic effects in human breast cancer cells. **International journal of nanomedicine**, v. 8, p. 1015, 2013 a.

GURUNATHAN, S.; HAN, J. W.; KIM, J. H. Green chemistry approach for the synthesis of biocompatible graphene. **International journal of nanomedicine**, v. 8, p. 2719, 2013 b.

HAYAT, H.; MAHMOOD, Q.; PERVEZ, A.; BHATTI, Z. A.; BAIG, S. A. Comparative decolorization of dyes in textile wastewater using biological and chemical treatment. **Separation and Purification Technology**, v. 154, p. 149-153, 2015.

HASSANZADEH, E.; FARHADIAN, M.; RAZMJOU, A.; ASKARI, N. An efficient wastewater treatment approach for a real woolen textile industry using a chemical assisted NF membrane process. **Environmental nanotechnology, monitoring & management**, v. 8, p. 92-96, 2017.

HIEW, B. Y. Z.; LEE, L. Y.; LEE, X. J.; GAN, S.; THANGALAZHY-GOPAKUMAR, S.; LIM, S. S.; PAN, G. T.; YANG, T. C. K. Adsorptive removal of diclofenac by graphene oxide: Optimization, equilibrium, kinetic and thermodynamic studies. **Journal of the Taiwan Institute of Chemical Engineers**, v. 98, p. 150-162, 2019.

HSIEH, S.; HUANG, B. Y.; HSIEH, S. L.; WU, C. C.; WU, C. H.; LIN, P. Y.; HUANG, Y. S.; CHANG, C. W. Green fabrication of agar-conjugated Fe3O4 magnetic nanoparticles. **Nanotechnology**, v. 21, n. 44, p. 445601, 2010.

HUANG, D.; QUAN, Q.; ZHENG, Y.; TANG, W.; ZHANG, Z.; QIANG, X. Dual-network design to enhance the properties of agar aerogel adsorbent by incorporating in situ ion cross-linked alginate. **Environmental Chemistry Letters**, v. 18, n. 1, p. 251-255, 2020.

HU, H; ZHAO, Z.; WAN, W.: GOGOTSI, Y.; QIU, J. Ultralight and highly compressible graphene aerogels. **Advanced materials,** v. 25, n. 15, p. 2219-2223, 2013.

HUMMERS Jr, W. S.; OFFEMAN, R. E. Preparation of graphitic oxide. **Journal of the American Chemical Society**, v. 80, n. 6, p. 1339-1339, 1958.

International Organization for Standardization - ISO. **ISO/TS 80004-13 2017 Nanotechnologies - Vocabulary - Part 13: Graphene and Related Two-Dimensional (2D) Materials**. 1st ed. Geneva, 2017.

ISMAIL, M. M.; ALOTAIBI, B. S.; EL-SHEEKH, M. M. Therapeutic uses of red macroalgae. **Molecules**, v. 25, n. 19, p. 4411, 2020.

JANUÁRIO, E. F. D.; FACHINA, Y. J.; WERNKE, G.; DEMITI, G. M. M.; BELTRAN, L. B.; BERGAMASCO, R.; VIEIRA, A. M. S. Application of activated carbon functionalized with graphene oxide for efficient removal of COVID-19 treatment-related pharmaceuticals from water. **Chemosphere**, v. 289, p. 133213, 2022.

JAURIS, I. M.; SHOPF, P. F.; DOS SANTOS, C. L.; FAGAN, S. B.; DA SILVA, I. Z. Adsorção do fármaco nimesulida em nanoestruturas de carbono. **Disciplinarum Scientia| Naturais e Tecnológicas**, v. 16, n. 2, p. 245-256, 2015.

JUNGES, T. A.; JAURIS, I. M.; ROSSATO, J. Adsorção de diazepam com óxido de grafeno: uma abordagem de primeiros princípios. **Disciplinarum Scientia| Naturais e Tecnológicas**, v. 16, n. 2, p. 151-160, 2015.

KHALIL, A.; ALI, N.; KHAN, A.; ASIRI, A. M.; KAMAL, T. Catalytic potential of cobalt oxide and agar nanocomposite hydrogel for the chemical reduction of organic pollutants. **International Journal of Biological Macromolecules**, v. 164, p. 2922-2930, 2020.

KONICKI, W.; ALEKSANDRZAK, M.; MIJOWSKA, E. Equilibrium, kinetic and thermodynamic studies on adsorption of cationic dyes from aqueous solutions using graphene oxide. **Chemical Engineering Research and Design**, v. 123, p. 35-49, 2017.

LEMUS, L. M. R.; AZAMAR-BARRIOS, J. A.; ORTIZ-VAZQUEZ, E.; QUINTANA-OWEN, P.; FREILE-PELEGRIN, Y.; PERERA, F. G.; MADERA-SANTANA, T. J. Development and physical characterization of novel bio-nanocomposite films based on reduced graphene oxide, agar and melipona honey. **Carbohydrate Polymer Technologies and Applications**, v. 2, p. 100133, 2021.

LI, K.; YAN, J.; ZHOU, Y.; LI, B.; LI, X. β-cyclodextrin and magnetic graphene oxide modified porous composite hydrogel as a superabsorbent for adsorption cationic dyes: Adsorption performance, adsorption mechanism and hydrogel column process investigates. **Journal of Molecular Liquids**, v. 335, p. 116291, 2021.

LI, Y.; DU, Q.; LIU, T.; PENG, X.; WANG, J.; SUN, J.; XIA, L. Comparative study of methylene blue dye adsorption onto activated carbon, graphene oxide, and carbon nanotubes. **Chemical Engineering Research and Design**, v. 91, n. 2, p. 361-368, 2013.

LI, Y.; DU, Q.; LIU, T.; SUN, J.; JIAO, Y.; XIA, Y.; ZHU, H. Equilibrium, kinetic and thermodynamic studies on the adsorption of phenol onto graphene. **Materials Research Bulletin**, v. 47, n. 8, p. 1898-1904, 2012.

LI, Y.; LIU, S.; WANG, C.; YING, Z.; HUO, M.; YANG, W. Effective column adsorption of triclosan from pure water and wastewater treatment plant effluent by using magnetic porous reduced graphene oxide. **Journal of hazardous materials**, v. 386, p. 121942, 2020.

LIMA, L. R. D.; SAMPAIO, Y. D. S. B.; FREITAS, M. A. L. D.; LAGIOIA, U. C. T. Um Estudo Inferencial dos Custos Ambientais e das Estações de Tratamento de Água nas Lavanderias do Pólo de Confecções do Agreste de Pernambuco. **SOCIEDADE, CONTABILIDADE E GESTÃO**, v. 11, n. 3, 2016.

LIU, F.; CHUNG, S.; OH, G.; SEO, T. S. Three-dimensional graphene oxide nanostructure for fast and efficient water-soluble dye removal. **ACS applied**

materials & interfaces, v. 4, n. 2, p. 922-927, 2012.

LOFRUMENTO, C.; ARCI, F.; CARLESI, S.; RICCI, M.; CASTELLUCCI, E.; BECUCCI, M. Safranin-O dye in the ground state. A study by density functional theory, Raman, SERS and infrared spectroscopy. **Spectrochimica Acta Part A: Molecular and Biomolecular Spectroscopy**, v. 137, p. 677-684, 2015.

MACEDO, Nadia G. **Estudo e desenvolvimento de grafite como agente anti-chama para PVC.** Dissertação de Mestrado. Ribeirão Preto, SP: USP, 2011.

MACHADO, A. F.; PAGLIOTO, B. F.; CARVALHO, T. B. Creative industries in brazil: Analysis of specifics cases for a country in development. **Theoretical Economics Letters**, v. 8, n. 07, p. 1348, 2018.

MAÑAS, P.; DE LAS HERAS, J. Phytotoxicity test applied to sewage sludge using Lactuca sativa L. and Lepidium sativum L. seeds. **International journal of environmental science and technology**, v. 15, n. 2, p. 273-280, 2018.

MARIN, P.; BERGAMASCO, R.; MODENES, A. N.; PARAISO, P. R.; HAMOUDI, S. Synthesis and characterization of graphene oxide functionalized with $MnFe_2O_4$ and supported on activated carbon for glyphosate adsorption in fixed bed column. **Process Safety and Environmental Protection**, v. 123, p. 59-71, 2019.

MEHL, H.; MATOS, C. F.; NEIVA, E. G.; DOMINGUES, S. H.; ZARBIN, A. J. Efeito da variação de parâmetros reacionais na preparação de grafeno via oxidação e redução do grafite. **Química Nova**, v. 37, p. 1639-1645, 2014.

MENDES, P. M.; BECKER, R.; CORRÊA, L. B.; BIANCHI, I.; DAI PRÁ, M. A.; LUCIA JR, T.; CORRÊA, E. K. Phytotoxicity as an indicator of stability of broiler production residues. **Journal of environmental management**, v. 167, p. 156-159, 2016.

MÓDENES, A. N.; ESPINOZA, F.R.; ALFLEN, V. L.; COLOMBO, A.; BORBA, C. E. Utilização da macrófita Egeria densa na biosorção do corante reativo 5G. **Engevista**, v. 13, n. 3, 2011.

MOHAN, S.; SINGH, D. K.; KUMAR, V.; HASAN, S. H. Effective removal of Fluoride ions by rGO/ZrO2 nanocomposite from aqueous solution: fixed bed column adsorption modelling and its adsorption mechanism. **Journal of Fluorine Chemistry**, v. 194, p. 40-50, 2017.

NASCIMENTO, B. F.; ARAUJO, C. M. B.; NASCIMENTO, A. C.; COSTA, G. R. B.; GOMES, B. F. M. L.; SILVA, M. P.; GHISLANDI, M. G.; MOTTA SOBRINHO, M. A. adsorption of reactive black 5 and basic blue 12 using biochar from gasification residues: batch tests and fixed-bed breakthrough predictions for wastewater treatment. **Bioresource Technology Reports**, v. 15, p. 100767, 2021.

NASCIMENTO, R. F.; LIMA, A. C. A.; VIDAL, C. B.; MELO, D. Q.; RAULINO, G. S. C. **Adsorção: aspectos teóricos e aplicações ambientais.** Fortaleza: Imprensa Universitária, 256p, 2020.

NAYAK, A. K.; PAL, A. Statistical modeling and performance evaluation of biosorptive removal of Nile blue A by lignocellulosic agricultural waste under the application of high-strength dye concentrations. **Journal of Environmental Chemical Engineering**, v. 8, n. 2, p. 103677, 2020.

NEHABA, S. S.; ABDULLAH, R. H.; ODA, A. M.; OMRAN, A. R.; MOTTALEB, A. S. Evaluation of the efficiency of tea waste powder to remove the Safranin O dye compared to the activated carbon as adsorbent. **Oriental Journal of Chemistry**, v. 35, n. 3, p. 1201, 2019.

NOVOSELOV, K. S.; GEIM, A. K.; MOROZOV, S. V.; JIANG, D. A.; ZHANG, Y.; DUBONOS, S. V.; GRIGORIEVA, I. V.; FIRSOV, A. A. Electric field effect in atomically thin carbon films. **Science**, v. 306, n. 5696, p. 666-669, 2004.

O SALOMÓN, Y. L.; GEORGIN, J.; DOS REIS, G. S.; LIMA, É. C.; OLIVEIRA, M. L.; FRANCO, D. S.; NETTO, M. S.; ALLASIA, D.; DOTTO, G. L. Utilization of Pacara Earpod tree (Enterolobium contortisilquum) and Ironwood (Caesalpinia leiostachya) seeds as low-cost biosorbents for removal of basic fuchsin. **Environmental Science and Pollution Research**, v. 27, n. 26, p. 33307-33320, 2020.

OLIVEIRA, G. A. R.; LEME, D. M.; LAPUENTE, J.; BRITO, L. B.; PORREDON, C.; BRITO RODRIGUES, L.; BRULL, N.; SERRET, J. T.; BORRAS, M.; DISNER, G. R. D.; CESTARI, M. M.; OLIVEIRA, D. P. A test battery for assessing the ecotoxic effects of textile dyes. **Chemico-biological interactions**, v. 291, p. 171-179, 2018.

OMOROGIE, M. O.; BABALOA, J. O.; ISMAEEL, M. O.; MCGETTRICK, J. D.; WATSON, T. M.; DAWSON, D. M.; CARTA, M.; KUEHNEL, M. F. Activated carbon from Nauclea diderrichii agricultural waste–a promising adsorbent for ibuprofen, methylene blue and CO2. **Advanced Powder Technology**, v. 32, n. 3, p. 866-874, 2021.

OOI, K.; MAKITA, Y.; SONODA, A.; CHITRAKAR, R.; TASAKI-HANDA, Y.; NAKAZATO, T. Modelling of column lithium adsorption from pH-buffered brine using surface Li+/H+ ion exchange reaction. **Chemical Engineering Journal**, v. 288, p. 137-145, 2016.

PARK, J. H.; CHO, J. S.; OK, Y. S.; KIM, S. H.; KANG, S. W.; CHOI, I. W.; HEO, J. S.; DELAUNE, R. D.; SEO, D. C. Competitive adsorption and selectivity sequence of heavy metals by chicken bone-derived biochar: batch and column experiment. **Journal of Environmental Science and Health, Part A**, v. 50, n. 11, p. 1194-1204, 2015.

PARLAYICI, Ş. Alginate-coated perlite beads for the efficient removal of methylene blue, malachite green, and methyl violet from aqueous solutions: kinetic, thermodynamic, and equilibrium studies. **Journal of Analytical Science and Technology**, v. 10, n. 1, 2019.

PEEL, R. G.; BENEDEK, A. A simplified driving force model for activated carbon adsorption. **The Canadian Journal of Chemical Engineering**, v. 59, n. 6, p. 688–692, 1981.

PENG, W.; LI, H.; LIU, Y.; SONG, S. Adsorption of methylene blue on graphene oxide prepared from amorphous graphite: Effects of ph and foreign ions. **Journal of Molecular Liquids**, v. 221, p. 82-87, 2016.

PIMENTEL, T. **Santa Cruz é sinônimo de pólo têxtil**. Diário de Pernambuco. 2017. Disponível em: http://www.impresso.diariodepernambuco.com.br/app/noticia/cadernos/economia/2017/01/14/intinte_economia,161460/santa-cruz-e-sinonimo-de-polo-textil.shtml. Acesso em: 11 nov. 2017.

QIN, J.; ZHANG, X.; YANG, C.; CAO, M.; MA, M.; LIU, R. ZnO microspheres-reduced graphene oxide nanocomposite for photocatalytic degradation of methylene blue dye. **Applied Surface Science**, v. 392, p. 196-203, 2017.

QUILAQUEO, M.; GIM-KRUMM, M.; RUBY-FIGUEROA, R.; TRONCOSO, E.; ESTAY, H. Determination of size distribution of precipitation aggregates using non-invasive microscopy and semiautomated image processing and analysis. **Minerals**, v. 9, n. 12, p. 724, 2019.

RAMÍREZ-MALULE, H.; QUINONES-MURILLO, D. H.; MANOTAS-DUQUE, D. Emerging contaminants as global environmental hazards. A bibliometric analysis. **Emerging contaminants**, v. 6, p. 179-193, 2020.

RANA, C.; MISHRA, M.; DE WIT, A. Effect of anti-Langmuir adsorption on spreading in porous media. **EPL (Europhysics Letters)**, v. 124, n. 6, p. 64003, 2019.

REYNOLDS, T. D.; RICHARDS, P. A. Unit operations and processes in environmental engineering. 2ª Edição. Boston: PWS Plublishing Company, 1995.

RHIM, J. W. Effect of clay contents on mechanical and water vapor barrier properties of agar-based nanocomposite films. **Carbohydrate polymers**, v. 86, n. 2, p. 691-699, 2011.

RIOS, A. G.; MATOS, L. C.; MANRIQUE, Y. A.; LOUREIRO, J. M.; MENDES, A.; FERREIRA, A. F. Adsorption of anionic and cationic dyes into shaped MCM-41. **Adsorption**, v. 26, n. 1, p. 75-88, 2020 b.

RIOS, A. G.; RIBEIRO, A. M.; RODRIGUES, A. E.; FERREIRA, A. F. Bovine serum albumin and myoglobin separation by size exclusion SMB. **Journal of Chromatography A**, v. 1628, p. 461431, 2020 a.

RODRIGUES, A. E.; SILVA, C. M. What's wrong with Lagergreen pseudo first order model for adsorption kinetics? **Chemical Engineering Journal**, v. 306, p. 1138–1142, 2016.

RODRIGUES, C. S. D. **Textile Dyeing Wastewater Treatment by Single and Integrated Processes of Coagulation , Chemical Oxidation and Biological Degradation**. Porto: [s.n.], 2013.

SÁ LUÍS, P. M. Dos S. DE. **REMOÇÃO DE COR EM EFLUENTES TÊXTEIS POR ADSORÇÃO EM MATERIAIS INORGÂNICOS DE ORIGEM NATURAL**. Porto: [s.n.], 2009.

SADEGH, H.; ALI, G. A.; GUPTA, V. K.; MAKHLOUF, A. S. H.; SHAHRYARI-GHOSHEKANDI, R.; NADAGOUDA, M. N.; SILLANPAA, M.; MEGIEL, E. The role of nanomaterials as effective adsorbents and their applications in wastewater treatment. **Journal of Nanostructure in Chemistry**, v. 7, n. 1, p. 1-14, 2017.

SAIM, S.; BEHIRA, B. Impact of Chloroquine as treatment of pandemic COVID-19 on environment. **Materials and Biomaterials Science**, v. 4, n. 1, p. 100-105, 2021.

SAMIEY, B.; ASHOORI, F. Adsorptive removal of methylene blue by agar: Effects of NaCl and ethanol. **Chemistry Central Journal**, v. 6, n. 1, p. 14, 2012.

SANTOS, R.; MELO, R. A. Global shortage of technical agars: back to basics (resource management). **Journal of Applied Phycology**, v. 30, n. 4, p. 2463-2473, 2018.

SARKAR, N.; SAHOO, G.; SWAIN, S. K. Nanoclay sandwiched reduced graphene oxide filled macroporous polyacrylamide-agar hybrid hydrogel as an adsorbent for dye decontamination. **Nano-Structures and Nano-Objects**, v. 23, p. 100507, 2020.

SARKER, F.; KARIM, N.; AFROJ, S.; KONCHERRY, V.; NOVOSELOV, K. S.; POTLURI, P. High-performance graphene-based natural fiber composites. **ACS applied materials & interfaces**, v. 10, n. 40, p. 34502-34512, 2018.

SASUGA, K.; YAMANASHI, T.; NAKAYAMA, S.; ONO, S.; MIKAMI, K. Discolored red seaweed Pyropia yezoensis with low commercial value is a novel resource for production of agar polysaccharides. **Marine Biotechnology**, v. 20, n. 4, p. 520-530, 2018.

SCHROEDER, R. L.; GERBER, J. P. Chloroquine and hydroxychloroquine binding to melanin: Some possible consequences for pathologies. **Toxicology Reports**, v. 1, p. 963–968, 2014.

SELVALAKSHMI, S.; VIJAYA, N.; SELVASEKARAPANDIAN, S.; PREMALATHA, M. Biopolymer agar-agar doped with NH4SCN as solid polymer electrolyte for electrochemical cell application. **Journal of Applied Polymer Science**, v. 134, n. 15, 2017.

SHAHRIARY, L.; ATHAWALE, A. A. Graphene oxide synthesized by using modified hummers approach. **Int. J. Renew. Energy Environ. Eng**, v. 2, n. 01, p. 58-63, 2014.

SHAMAILA, S.; SAJJAD, A. K. L.; IQBAL, A. Modifications in development of graphene oxide synthetic routes. **Chemical Engineering Journal**, v. 294, p. 458-477, 2016.

SHARMA, G.; THAKUR, B.; NAUSHAD, M.; KUMAR, A.; STADLER, F. J.; ALFADUL, S. M.; MOLA, G. T. Applications of nanocomposite hydrogels for biomedical engineering and environmental protection. **Environmental chemistry letters**, v. 16, n. 1, p. 113-146, 2018.

SHI, H.; LI, W.; ZHONG, L.; XU, C. Methylene blue adsorption from aqueous solution by magnetic cellulose/graphene oxide composite: equilibrium, kinetics, and thermodynamics. **Industrial & Engineering Chemistry Research**, v.53, n. 3, p. 1108-1118, 2014.

SIDDIQUI, M. F.; KHAN, E. A.; ALAM KHAN, T. Synthesis of MoO3/polypyrrole nanocomposite and its adsorptive properties toward cadmium(II) and nile blue from aqueous solution: Equilibrium isotherm and kinetics modeling. **Environmental Progress and Sustainable Energy**, 2019. v. 38, n. 6, p. 1–12.

SILVA, M. P.; SOUZA, A. C. A.; LIMA FERREIRA, L. E.; NETO, L. M. P.; NASCIMENTO, B. F.; ARAUJO, C. M. B.; FRAGA, T. J. M.; MOTTA SOBRINHO, M. A.; Ghislandi, M. G. Photodegradation of Reactive Black 5 and raw textile wastewater by heterogeneous photo-Fenton reaction using amino-Fe_3O_4-functionalized graphene oxide as nanocatalyst. **Environmental Advances**, v. 4, p. 100064, 2021.

SINHA, V.; CHAKMA, S. Advances in the preparation of hydrogel for wastewater treatment: A concise review. **Journal of Environmental Chemical Engineering**, v.7, 103295, 2019.

SIRCAR, S.; HUFTON, J. R. Why does the linear driving force model for adsorption kinetics work? **Adsorption**, 2000. v. 6, n. 2, p. 137–147.

SOBRERO, M. C.; RONCO, A. Ensayo de toxicidad aguda con semillas de lechuga (Lactuca sativa L.). Ensayos toxicologicos y metodos de evaluacion de calidad de aguas: standerizacion, intercalibracion, resultados y aplicaciones. Mexico: IMTA; 2004.

SRIVASTAVA, V.; ZARE, E. N.; MAKVANDI, P.; ZHENG, X. Q.; IFTEKHAR, S.; WU, A.; PADIL, V. V. T.; MOKHTARI, B.; VARMA, R. S.; TAY, F. R.; SILLANPAA, M. Cytotoxic aquatic pollutants and their removal by nanocomposite-based sorbents. **Chemosphere**, v. 258, p. 127324, 2020.

SUÁREZ-IGLESIAS, O.; COLLADO, S.; OULEGO, P.; DIAZ, M. Graphene-family nanomaterials in wastewater treatment plants. **Chemical Engineering Journal**, v. 313, p. 121-135, 2017.

SUMALINOG, D. A. G.; CAPAREDA, S. C.; LUNA, M. D. G. DE. Evaluation of the effectiveness and mechanisms of acetaminophen and methylene blue dye adsorption on activated biochar derived from municipal solid wastes. **Journal of Environmental Management**, v. 210, p. 255–262, 2018.

TABRIZI, N. S.; ZAMANI, S. J. W. S. Removal of Pb (II) from aqueous solutions by graphene oxide aerogels. **Water Science and Technology**, v. 74, n. 1, p. 256-265, 2016.

TANG, T.; GOOSSENS, K.; LU, S. J.; MENG, D.; BIELAWSKI, C. W. Agar-reduced graphene oxide selectively adsorbs organic dyes and strengthens double-network hydrogels. **RSC advances**, v. 10, n. 49, p. 29287-29295, 2020.

THAKUR, K.; KANDASUBRAMANIAN, B. Graphene and Graphene Oxide-Based Composites for Removal of Organic Pollutants: A Review. **Journal of Chemical and Engineering Data**, v. 64, n. 3, p. 833–867, 2019.

TIWARI, J. N.; MAHESH, K.; LE, N. H.; KEMP, K. C.; TIMILSINA, R.; TIWARI, R. N.; KIM, K. S. Reduced graphene oxide-based hydrogels for the efficient capture of dye pollutants from aqueous solutions. **Carbon**, v. 56, p. 173-182, 2013.

ULLAH, F.; OTHMAN, M. B. H.; JAVED, F.; AHMAD, Z.; AKIL, H. M. Classification, processing and application of hydrogels: A review. **Materials Science and Engineering: C**, v. 57, p. 414-433, 2015.
United States Patent Office. William S. Hummers Jr. **Preparation of graphitic acid**. U.S. Patent n. 2,798,878, 9 jul. 1957.

UPADHYAY, R. K.; SOIN, N.; ROY, S. S. Role of graphene/metal oxide composites as photocatalysts, adsorbents and disinfectants in water treatment: a review. **Rsc Advances**, v. 4, n. 8, p. 3823-3851, 2014.

VIOTTI, P. V.; MOREIRA, W. M.; DOS SANTOS, O. A. A.; BERGAMASCO, R.; VIEIRA, A. M. S.; VIEIRA, M. F. Diclofenac removal from water by adsorption on Moringa oleifera pods and activated carbon: Mechanism, kinetic and equilibrium study. **Journal of Cleaner Production**, v. 219, p. 809-817, 2019.

WALKER, G. M.; WEATHERLEY, L. R. Textile wastewater treatment using granular activated carbon adsorption in fixed beds. **Separation Science and Technology**, v. 35, n. 9, p. 1329–1341, 2000.

WANG, Q.; LI, C.; WANG, Y.; QUE, X. Phytotoxicity of graphene family nanomaterials and its mechanisms: A review. **Frontiers in chemistry**, v. 7, p. 292, 2019.

WANG, R.; LI, N.; JIANG, B.; LI, J.; HONG, W.; JIAO, T. Facile preparation of agar/polyvinyl alcohol-based triple-network composite hydrogels with excellent mechanical performances. **Colloids and Surfaces A: Physicochemical and Engineering Aspects**, v. 615, p. 126270, 2021.

WERNKE, G.; SILVA, M. F.; SILVA, E. A.; FAGUNDES-KLEN, M. R.; SUZAKI, P. Y. R.; TRIQUES, C. C.; BERGAMASCO, R. Ag and CuO nanoparticles decorated on graphene oxide/activated carbon as a novel adsorbent for the removal of cephalexin from water. **Colloids and Surfaces A: Physicochemical and Engineering Aspects**, v. 627, p. 127203, 2021.

WORSLEY, M. A.; PAUZAUSKIE, P. J.; OLSON, T. Y.; BIENER, J.; SATCHER Jr, J. H.; BAUMANN, T. F. Synthesis of graphene aerogel with high electrical conductivity. **Journal of the American Chemical Society**, v. 132, n. 40, p. 14067-14069, 2010.

YAN, H.; TAO, X.; YANG, Z.; LI, K.; YANG, H.; LI, A.; CHENG, R. Effects of the oxidation degree of graphene oxide on the adsorption of methylene blue. **Journal of hazardous materials**, v. 268, p. 191-198, 2014.

YANG, Y.; XU, L.; WANG, H.; WANG, W.; ZHANG, L. TiO_2/graphene porous composite and its photocatalytic degradation of methylene blue. **Materials & Design**, v. 108, p. 632-639, 2016.

YE, S.; LIU, Y.; FENG, J. Low-Density, Mechanical Compressible, Water-Induced Self-Recoverable Graphene Aerogels for Water Treatment. **ACS Applied Materials and Interfaces**, v. 9, n. 27, p. 22456–22464, 2017.

ZAKA, A.; IBRAHIM, T. H.; KHAMIS, M. Removal of selected non-steroidal anti-inflammatory drugs from wastewater using reduced graphene oxide magnetite. **Desalination and Water Treatment**, v. 212, p. 401–414, 2021.

ZHAO, J.; CAO, X.; WANG, Z.; DAI, Y.; XING, B. Mechanistic understanding toward the toxicity of graphene-family materials to freshwater algae. **Water Research**, v. 111, p. 18-27, 2017.

ZHENG, Y.; ZHU, Y.; WANG, A. Highly efficient and selective adsorption of malachite green onto granular composite hydrogel. **Chemical Engineering Journal**, v. 257, p. 66-73, 2014.

APPENDIX A - PUBLISHED PAPERS RELATED TO THE RESEARCH REPORTED IN THIS THESIS

A.1 NANOCOMPOSITES AND THEIR EMPLOYMENT AS SCAVENGERS OF WATER POLLUTANTS

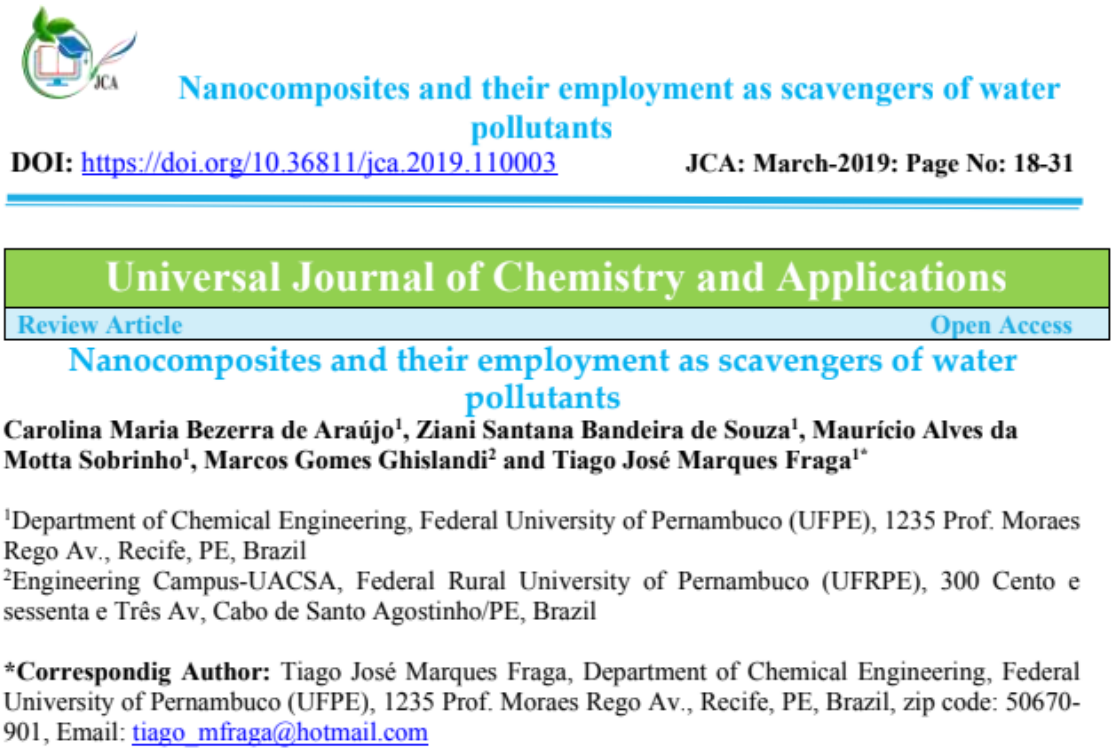

Nanocomposites and their employment as scavengers of water pollutants

DOI: https://doi.org/10.36811/jca.2019.110003 JCA: March-2019: Page No: 18-31

Universal Journal of Chemistry and Applications

Review Article Open Access

Nanocomposites and their employment as scavengers of water pollutants

Carolina Maria Bezerra de Araújo[1], Ziani Santana Bandeira de Souza[1], Maurício Alves da Motta Sobrinho[1], Marcos Gomes Ghislandi[2] and Tiago José Marques Fraga[1*]

[1]Department of Chemical Engineering, Federal University of Pernambuco (UFPE), 1235 Prof. Moraes Rego Av., Recife, PE, Brazil

[2]Engineering Campus-UACSA, Federal Rural University of Pernambuco (UFRPE), 300 Cento e sessenta e Três Av, Cabo de Santo Agostinho/PE, Brazil

***Correspondig Author:** Tiago José Marques Fraga, Department of Chemical Engineering, Federal University of Pernambuco (UFPE), 1235 Prof. Moraes Rego Av., Recife, PE, Brazil, zip code: 50670-901, Email: tiago_mfraga@hotmail.com

https://doi.org/10.36811/jca.2019.110003

Journal of Chemistry & Applications (RAFT Pubs, USA), **Impact factor: N.A.** (2019).

This mini review originated from an invitation by Dr. Tiago José Marques Fraga to write a broad min-review on the use of different nanomaterials (ceramic, nano-clays and carbon nanomaterials – GBM, carbon nanotubes, quantum dots) for wastewater treatment.

A.2 GRAPHENE-BASED MATERIALS PRODUCTION AND APPLICATION IN TEXTILE WASTEWATER TREATMENT: COLOR REMOVAL AND PHYTOTOXICITY USING *LACTUCA SATIVA* AS BIOINDICATOR

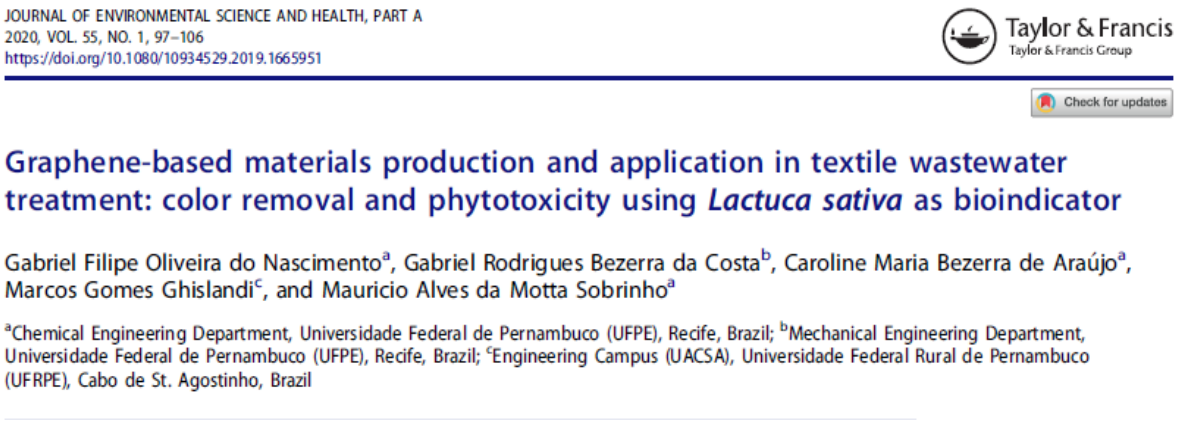

JOURNAL OF ENVIRONMENTAL SCIENCE AND HEALTH, PART A
2020, VOL. 55, NO. 1, 97–106
https://doi.org/10.1080/10934529.2019.1665951

Taylor & Francis
Taylor & Francis Group

Check for updates

Graphene-based materials production and application in textile wastewater treatment: color removal and phytotoxicity using *Lactuca sativa* as bioindicator

Gabriel Filipe Oliveira do Nascimento[a], Gabriel Rodrigues Bezerra da Costa[b], Caroline Maria Bezerra de Araújo[a], Marcos Gomes Ghislandi[c], and Mauricio Alves da Motta Sobrinho[a]

[a]Chemical Engineering Department, Universidade Federal de Pernambuco (UFPE), Recife, Brazil; [b]Mechanical Engineering Department, Universidade Federal de Pernambuco (UFPE), Recife, Brazil; [c]Engineering Campus (UACSA), Universidade Federal Rural de Pernambuco (UFRPE), Cabo de St. Agostinho, Brazil

https://doi.org/10.1080/10934529.2019.1665951

Journal of Environmental Science and Health, Part A, **Impact factor 2.582** (2021), **Qualis A2** (Eng. II)

This research paper is the first one published by my supervisors and I, as being part of the studies developed during the first year of my doctorate, which was also part of the scientific initiation research developed by the undergraduation students *Gabriel Filipe Oliveira Nasciemnto* and *Gabriel Rodrigues Bezerra da Costa*, who I was co-supervising at that time. This paper brings new perspectives on the production process of graphene oxide under different working conditions for environmental applications, as well as the phytotoxic assays to evaluate the toxicity of the treated effluent (before and after treatment) using GO as adsorbent.

A.3 CHAPTER FIVE - THE ROLE OF MULTIFUNCTIONAL NANOMATERIALS IN THE REMEDIATION OF TEXTILE WASTEWATERS

Sustainable Technologies for Textile Wastewater Treatments

The Textile Institute Book Series

2021, Pages 95-136

Chapter Five - The role of multifunctional nanomaterials in the remediation of textile wastewaters

Tiago José Marques Fraga [a], Caroline Maria Bezerra de Araújo [a, b], Maurício Alves da Motta Sobrinho [a], Marcos Gomes Ghislandi [a, c]

[a] Department of Chemical Engineering, Federal University of Pernambuco, Recife, Brazil
[b] Department of Chemical Engineering, Faculty of Engineering, University of Porto, Porto, Portugal
[c] Engineering Campus—UACSA, Federal Rural University of Pernambuco, Cabo de Santo Agostinho, Brazil

https://doi.org/10.1080/10934529.2019.1665951

Sustainable Technologies for Textile Wastewater Treatments - The Textile Institute Book Series 2021, Pages 95-136

This book chapter is the first one published by Dr. Tiago José Marques Fraga, our supervisors, and I. This chapter talks about the importance and applications of multifunctional nanomaterials in the treatment of textile wastewater. It composes the book, entitled: *Sustainable Technologies for Textile Wastewater Treatments*.

A.4 WASTEWATER TREATMENT USING RECYCLABLE AGAR-GRAPHENE OXIDE BIOCOMPOSITE HYDROGEL IN BATCH AND FIXED-BED ADSORPTION COLUMN: BENCH EXPERIMENTS AND MODELING FOR THE SELECTIVE REMOVAL OF ORGANICS

Colloids and Surfaces A: Physicochemical and Engineering Aspects 639 (2022) 128357

Contents lists available at ScienceDirect

Colloids and Surfaces A: Physicochemical and Engineering Aspects

journal homepage: www.elsevier.com/locate/colsurfa

Wastewater treatment using recyclable agar-graphene oxide biocomposite hydrogel in batch and fixed-bed adsorption column: Bench experiments and modeling for the selective removal of organics

Caroline Maria Bezerra de Araujo [a,b,*], Marcos Gomes Ghislandi [c], Albertina Gonçalves Rios [b], Gabriel Rodrigues Bezerra da Costa [d], Bruna Figueiredo do Nascimento [a], Alexandre Filipe Porfírio Ferreira [b], Mauricio Alves da Motta Sobrinho [a], Alírio Egídio Rodrigues [b]

https://doi.org/10.1016/j.colsurfa.2022.128357

Colloids and Surfaces A: Physicochemical and Engineering Aspects, **Impact factor 5.518** (2021), **Qualis A1** (Eng. II)

This research paper is the second one published by my supervisors and I, as part of the studies developed during the second and third years of my doctorate. It was partially conducted in the laboratories of the Chemical Engineering Department of the University of Porto (Porto, Portugal), being also co-advised by Prof. Alexandre Ferreira. The doctoral internship abroad was possible thanks to the sandwich scholarship granted to the student by the *Coordenação de Aperfeiçoamento de Pessoal de Nível Superior* - CAPES (PDSE-CAPES 2019-2020). This paper brings new perspectives on the production and application of an agar/ graphene oxide composite for the continuous treatment of textile wastewater in a fixed-bed adsorption system.

A.5 CONTINUOUS REMOVAL OF PHARMACEUTICAL DRUG CHLOROQUINE AND SAFRANIN-O DYE FROM WATER USING AGAR-GRAPHENE OXIDE HYDROGEL: SELECTIVE ADSORPTION IN BATCH AND FIXED-BED EXPERIMENTS

Environmental Research 216 (2023) 114425

Contents lists available at ScienceDirect

Environmental Research

journal homepage: www.elsevier.com/locate/envres

Continuous removal of pharmaceutical drug chloroquine and Safranin-O dye from water using agar-graphene oxide hydrogel: Selective adsorption in batch and fixed-bed experiments

Caroline Maria Bezerra de Araujo [a,*], Gessica Wernke [b], Marcos Gomes Ghislandi [c], Alexandre Diório [b], Marcelo Fernandes Vieira [b], Rosângela Bergamasco [b], Maurício Alves da Motta Sobrinho [a], Alírio Egídio Rodrigues [d]

https://doi.org/10.1016/j.envres.2022.114425

Environmental Research, **Impact factor 8.431** (2021), **Qualis B1** (Eng. II)

This research paper is the third one published by my supervisors and I, as part of the studies developed during the final year of my doctorate. It was partially conducted in the laboratories of the Chemical Engineering Department of the State University of Maringá - UEM (Paraná, Brazil), being co-advised by Prof. Rosângela Bergamasco and Prof. Marcelo Vieira. The short-term internship was possible thanks to the financial support provided by UFPE. This paper brings new perspectives on the application of the agar/ graphene oxide composite for the continuous removal of Safranin-O and the pharmaceutical drug chloroquine diphosphate in a fixed-bed adsorption column.

APPENDIX B - BREAKTHROUGH MODELING OF BF DYE CONSIDERING THE ABSORPTIVE CAPACITY AND EQUILIBRIUM CONCENTRATION OF THE FIXED-BED EXPERIMENT

B.1 PARTICLE SIZE DISTRIBUTION FOR AGAR-GO

The particle size distribution of the hydrogels was performed for each sample produced, placing an amount of the sample produced under a plastic surface with a white background, gently separating the wet hydrogel pieces with a spatula. With a transparent ruler next to the surface containing the sample, photographs were taken. From these photographs, the average particle sizes were estimated using statistical software - See Figure 54. As observed, the average particle size for all samples was approximately 0.3 cm.

Figure 54 - Average particle size for the hydrogel samples produced

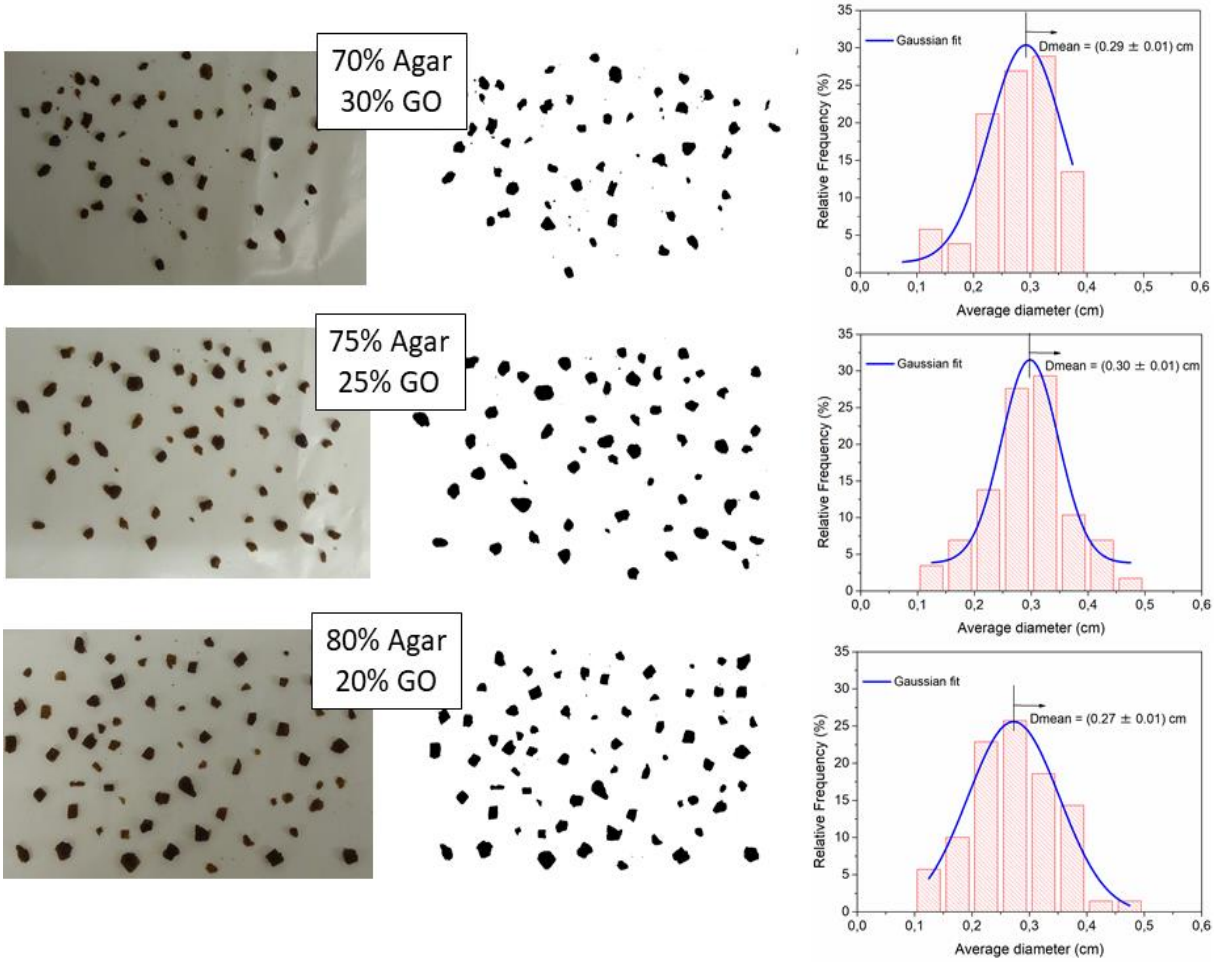

Source: The Author (2022)

APPENDIX C – BREAKTHROUGH MODELING OF BF DYE CONSIDERING THE ADSORPTIVE CAPACITY AND EQUILIBRIUM CONCENTRATION OF THE FIXED-BED EXPERIMENT

C.1 MODELING RESULTS

Considering the adsorption capacity and the equilibrium concentration of the fixed-bed experiment with basic fuchsin (BF), modeling of the breakthrough curve was performed (Figure 55), keeping the other parameters constant - k_h = 0.075 min^{-1}, *Pe* =76.28, D_{ax} =1.56 10^{-5} $m^2.min^{-1}$. In this case, R^2 value increased from 0.88 to 0.94.

Values of the parameters obtained from the Freundlich isotherm, after including the experimental point obtained in fixed-bed test to those obtained in batch were: K_F =1.74 ($mg^{1-(1/n)}$. (g^{-1}). $L^{1/n}$), *n* =0.745. With the parameters obtained from the Freundlich isotherm, after including the fixed-bed experimental point to those obtained in batch, q_e was estimated when C_e =9.28 $mg.L^{-1}$ (equilibrium concentration for fixed-bed tests). Therefore, the estimated q_e values were 29.18 $mg.g^{-1}$ (batch isotherm), and 33.20 $mg.g^{-1}$ (batch isotherm including the fixed-bed experimental point), which is closer to the fixed-bed experimental value q_e = 38.11 $mg.g^{-1}$.

Figure 55 - Experimental values and breakthrough curve predicted for BF dye (Experimental conditions: m_{bed}= 6.0g hydrogel (~0.13 g dry basis); Q =2 $mL.min^{-1}$; T =24ºC)

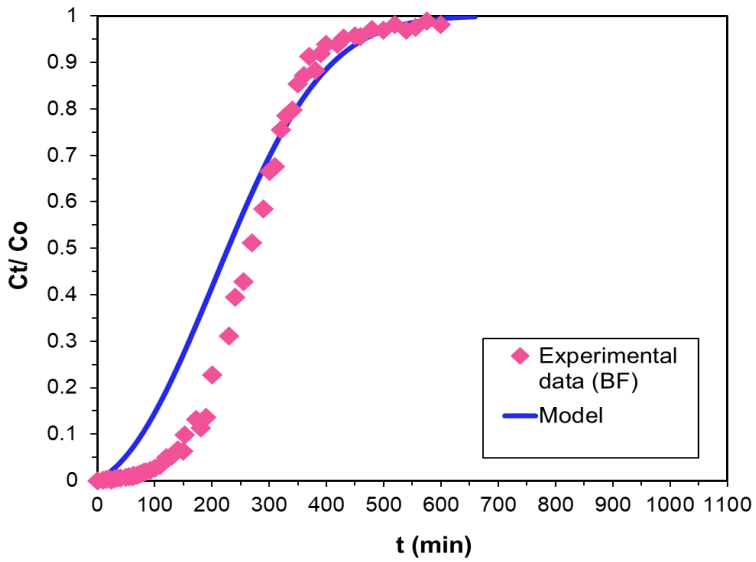

Source: The Author (2022)